Universitat Autònoma de Barcelona

Doctorat en Bioquímica, Biologia Molecular i Biomedicina

Departament de Bioquímica i Biologia Molecular – Facultat de Medicina

Nanoplasmonic Biosensors for Clinical Diagnosis at the Point of Care

Doctoral Thesis – 2015

Maria Soler Aznar

Author

Dr. M. Carmen Estévez

Prof. Laura M. Lechuga

Directors

Prof. Carles Arús

Tutor

CSIC Consejo Superior de Investigaciones Científicas

ICN2 Institut Català de Nanociència i Nanotecnologia

Excelencia Severo Ochoa

Abstract

This Doctoral Thesis focuses on the development of novel analytical methodologies in optical biosensors as alternative solutions for diagnosis or therapy monitoring of relevant diseases, such as allergy, celiac disease or cancer. In particular, we propose the use of nanoplasmonic biosensors for a rapid, sensitive and label-free detection of biomarkers present in human fluids. Both the well-known Surface Plasmon Resonance (SPR) biosensor and an innovative nanoplasmonic biosensor based on gold nanodisks surfaces have been evaluated for their real application in the clinical field.

The different biosensor methodologies make use of antibodies, either as biorecognition elements in immunoassays or as specific disease biomarkers for diagnostics. First, an in-depth study of two site-directed antibody immobilization strategies is presented for the direct immunoassay of protein biomarkers in biological fluids. In second place, a novel immunosensing strategy is proposed for the detection of gluten-derivative peptides in urine as a rapid and non-invasive technique for dietary control in celiac patients. On the other hand, two assays have been developed employing the nanoplasmonic biosensor to detect blood circulating antibodies as disease biomarkers. First, we have designed an alternative approach for drug allergy diagnosis (in particular for amoxicillin) based on dendrimer-based receptors, which enable the detection IgE antibodies directly in serum. And second, a new biosensing strategy is assessed to quantify specific tumor-related autoantibodies for the early diagnosis of colorectal cancer.

The work in this Thesis combines the wide knowledge of the research group in the design and fabrication of powerful biosensor technology with the development of surface activation chemistry and bioanalytical techniques to overcome current challenges related to costly and time-consuming clinical analysis. Besides, the strong experience of our research group in technological transfer and the established collaborations during this doctoral work with companies as Biomedal S.L. or Protein Alternatives S.L. open up interesting opportunities to facilitate the technology-transfer process for the real implementation of Point-of-Care biosensors.

Resum

Aquesta Tesi Doctoral se centra en el desenvolupament de noves metodologies analítiques en biosensors òptics com a solucions alternatives per a la diagnosi o la monitorització terapèutica de diferents malalties, com ara l'al·lèrgia, la celiaquia o el càncer. En particular, es proposa l'ús de biosensors nanoplasmònics per a la detecció de biomarcardors presents en fluids humans de manera ràpida, sensible i que no requereixi d'amplificació de senyal o de l'ús d'etiquetes. Tant el ja ben establert biosensor de Ressonància de Plasmó Superficial (SPR) com un innovador biosensor nanoplasmonic basat en nanodiscs d'or han estat avaluats per a la seva aplicació real en l'àrea clínica.

Les distintes metodologies biosensores presentades estan basades en l'ús d'anticossos, tant com a elements de bioreconeixement o com a biomarcadors específics de malalties. Primer, es presenta un estudi en profunditat de dues estratègies d'immobilització orientada d'anticossos per tal d'obtenir immunoassaigs en format directe de biomarcadors proteics en fluids biològics. En segon lloc, es proposa una nova estratègia immunosensora per a la detecció de pèptids derivats del gluten directament en orina com a tècnica ràpida i no invasiva per al control dietètic de pacients celíacs. A més, s'han desenvolupat dues metodologies utilitzant el biosensor nanoplasmònic per a detectar anticossos circulants en sang com a biomarcadors de malalties. Per una banda, s'ha dissenyat una estratègia alternativa per a la diagnosi d'al·lèrgia als medicaments (en particular a l'antibiòtic amoxicil·lina) basada en uns receptors dendrimèrics per a la detecció directa d'anticossos tipus IgE en sèrum. Finalment, s'ha avaluat una nova estratègia biosensora per a quantificar específicament autoanticossos tumorals per a la diagnosi precoç de càncer colorectal.

El treball d'aquesta Tesi combina l'experiència del grup de recerca en el disseny i fabricació de tecnologia biosensora avançada i innovadora amb el desenvolupament de tècniques bioanalítiques i de química de superfície per tal de superar els reptes actuals relacionats amb el cost i el temps requerit per a les anàlisis clíniques. A més, l'àmplia experiència del grup de recerca en transferència tecnològica i les col·laboracions establertes durant la tesi doctoral amb empreses com Biomedal S.L. o Protein Alternatives S.L. obren oportunitats interesants de cara a facilitar el procés de transferència tecnològica per a la implementació real de biosensors tipus *Point-of-Care*.

Acknowledgements

Llega el momento de compartir la gran alegría y satisfacción que significan llegar hasta aquí con todas aquellas personas que, de una forma u otra, lo habéis hecho posible. Quiero empezar agradeciéndole a Laura Lechuga haberme dado la oportunidad de empezar el doctorado en su grupo, por confiar en mí, por ayudar a que no pierda la motivación por la investigación y siga luchando por mis sueños. Por supuesto, un inmenso agradecimiento a M. Carmen Estévez: moltes gràcies per tot l'esforç i la dedicació que has posat des d'un primer moment en ajudar-me i acompanyar-me durant aquest projecte. Per endinsar-me en aquest món, per ensenyar-me tantíssimes coses i per mostrar-te sempre tant o més interessada que jo en resoldre qualsevol complicació. Has sigut una directora envejable.

Quería mostrar también un especial agradecimiento a todos aquellos investigadores que han colaborado en el desarrollo de esta Tesis. Al grupo del Dr. Ezequiel Perez-Inestrosa de la Universidad de Málaga, el Dr. Ángel Cebolla y la gente de Biomedal S.L., el Dr. Ignacio Casal y su grupo del CIB y Protein Alternatives S.L., y cómo no al Dr. Sergio Valenzuela y su familia, sin todos ellos el trabajo no hubiera sido posible. Also I want to thank to Prof. Hatice Altug for giving me the opportunity to work with her group, to actively participate in their projects and to appreciate my work and offer me the chance to continue my research career.

Pero todo esto no hubiera sido tan especial sin los inigualables NanoB2A Group. Todos y cada uno de vosotros tendréis siempre un rinconcito en mi corazón que me hará recordar mi camino hacia el doctorado con una gran sonrisa. Aquel grupo de mis comienzos en la ETSE formado por grandes como David Regatos, Laurita o Elena, y los que continuaron hasta el deseado edificio raro, como Mar o Daphné, o los creadores de mi juguete nanoplasmónico, Bert y Borja. Los que siguen en el grupo, David Fariña, Ana o Silvia, y las nuevas pero no desconocidas incorporaciones, como Rebeca o Adrián. Un particular recuerdo también para los NanoB2A temporales como Paty o Anna Serra que me ayudaron con el trabajo, y especialmente para Melissa, Adrián y su querida esposa Mane con quien compartimos tan buenos momentos. Y es que, ¿qué sería del grupo sin la comunidad mexicana? Sam, Jesús, Daniel y mi niña, Iraís, quien tanto apoyo me ha transmitido y de quien he aprendido grandes verdades como aquello de "yo conozco mis defectos y, algunos, me encantan". Gracias por dejarnos conocer un trocito de ese país extraordinario a través de tan buena gente y haberos convertido en grandes amigos. A vosotros, como a las otras nuevas y no-tan-nuevas incorporaciones, Joel, Gerardo, Jhonattan, Santos y Blanca, ¡mucha suerte y muchos

ánimos! No me olvido de mi italiana favorita, Stefiiii: imprescindibles nuestros momentos de estrés y des-estrés en el ICN2 y los mejores ratos fuera de aquel maldito edificio. Y por último pero no menos importante, mi niño, César, el mejor compañero de viaje, de aventuras (incluso de aquellas que alargan la tesis xD), de agobios y momentos duros pero sobretodo, el mejor compañero de risas, complicidades y momentos inigualables en el trabajo y fuera de allí. Porque 4 años de una amistad así solo son el principio de lo que está por venir, ¡te quiero mucho! Mil gracias por todo.

I sortint d'allà, una primera parada a Barcelona i tota la gent que ha format part de la meva vida aquestos anys a la ciutat. Als veins i veïnes del millor barri-barri, heu fet que em senta meu allò de que el Fort Pienc no és un barri, és un sentiment. No us oblidaré mai. I com no, a tots els valencians a Barcelona, en especial als meus Cérvols de la Safor, la família que totes desitgem tindre a prop quan vivim lluny de casa. Però un gràcies enorme és per tu Pau. Perquè mai oblidaré aquell dia a Benimaclet que em vas prometre que si me'n venia a Barcelona, venies amb mí. I ací has estat, éssent part imprescindible de la meua vida a Barcelona i fins i tot, part fonamental en aquesta tesi. T'estime! Baixant cap al sud, faré una primera parada a Vinaròs, per aquella gran família que em fan sentir especial i orgullosa. Al cap i casal la segona parada, per un xiquet, Lluís, amb qui vaig començar compartint la Química i que m'ha demostrat ser un company d'il·lusions i un amic per sempre, molts ànims futur doctor! I a la fí, Potries. No puc oblidar-me d'aquelles amistats, les de sempre, sobretot la meua Mà de Fàtima. Marta, Patri, Rut i Alba sabeu que sou, heu sigut i sereu imprescindibles per ajudar-me a superar qualsevol repte que em propose. Que no puc demanar més que seguir tinguent-vos al meu costat i saber que, després de tants anys, ja res pot trencar el que ens uneix. Us estime molt amigues!

Per últim, l'agraïment més gran i sincer de tots. A la meua família, la que ha confiat en mi, m'ha fet voler allò que faig i s'ha sentit orgullosa de mi. Papà i mamà, moltes gràcies per donar-ho tot per mi, per inculcar-me els valors i donar-me forces per aconseguir el que em propose, per fer-ho possible i per sentir-vos orgullosos de mi. No tinc paraules. I no m'oblide de tu, Sareta, que m'ha tocat la millor germaneta del món mundial! És impensable imaginar tot aquest camí sense tu. Vos vull molt! I per què no, vull acabar dedicant tot això que ara sóc a aquella persona que més m'ha volgut mai, allà on estigues *uela*, t'estime.

Contents

NANOPLASMONIC BIOSENSORS FOR CLINICAL DIAGNOSIS AT THE POINT OF CARE

Motivation and Objectives

Healthcare is nowadays a crucial challenge focusing the attention of the scientific community around the world. The ability to early diagnose a disease appearance or to enhance the efficacy of therapies is a main goal for biomedical research and industry. Nanotechnology promises an exceptional pathway for the accomplishment of personalized medicine and for the achievement of more affordable solutions to improve the quality of life. In particular, optical biosensors have been profiled as reliable and efficient analytical tools offering rapid, simple and highly sensitive detection of disease-related biomarkers. Besides, optical biosensors and especially photonic and nanoplasmonic platforms, show interesting miniaturization and integration capabilities, representing a potential alternative for the development of Point-of-Care (PoC) devices.

However, the great majority of innovative nanoplasmonic technology has barely reported real utility for biomedical applications, usually publishing work of a very fundamental physics nature. In order to accelerate the technology-transfer process of biosensors to the clinical field, more intensive research effort must be directed to develop and optimize biofunctionalization and assay procedures that allow reliable and accurate detection of relevant biomarkers directly in biological fluids and, importantly, avoiding any type of pretreatment of the sample. The development of versatile and fully optimized biosensor methodologies might signify a breakthrough for PoC achievement. It will be a considerable step forward in clinical decentralization and healthcare progress.

From the abovementioned, this PhD Thesis has aimed at designing and evaluating novel biosensor methodologies with views of improving the performance of nanoplasmonic biosensors in the particular field of clinical diagnosis or therapy monitoring. In particular, the main objectives outlined for this work involve:

1) Assessment and optimization of biofunctionalization strategies that enhance the analytical features of the assay in terms of sensitivity, selectivity and reproducibility;

2) Design of methodologies for prevention and minimization of interferences coming from complex biological matrices such as urine or serum;

3) Validation of the accuracy and reliability of the proposed strategies with the nanoplasmonic biosensors employing real clinical samples.

Chapter 1

INTRODUCTION

This chapter provides a general introduction to Nanomedicine, mainly focusing on the role of biosensor devices as diagnostic tools in the clinical and biomedical environment. After a brief review of biosensor technologies, plasmonic biosensors are described, pointing out their advantages and limitations for the clinical practice. Special attention is given to the properties and requirements of the biorecognition layer to achieve optimal biosensor performance. Finally, we discuss the function of antibodies in biosensor devices, either as biorecognition elements or as biomarkers for diagnosis or therapy monitoring.

1. Introduction

1.1. Nanomedicine: Novel Solutions for the Clinical Practice

Nanomedicine refers essentially to the application of Nanotechnology to the biomedical and clinical field. The European Science Foundation (ESF) defined Nanomedicine as the use of nanometer-sized tools for diagnosis, prevention and treatment of disease and for better understanding of the complex underlying pathophysiology, with the ultimate goal of the improvement of the patient's quality of life.[1] Although nanomedicine is not new and first results related to this discipline could be identified in the late 1960's,[2] the term has emerged in the last decades parallel to the exponential growth experienced by Nanotechnology. Significant advances made in fabrication and characterization of nanomaterials and nanostructures have opened up a vast field of research and application, holding important benefits for the improvement of the healthcare quality and clinical practice.

The exceptional potential of the Nanotechnology relies on the extraordinary physical and chemical properties shown by materials at the nanoscale range (~10^{-9} m). Nanomaterials consist of metallic, organic or semi-conducting structures that present high surface-volume ratio, enhanced chemical reactivity and that can be engineered to have different sizes, shapes and chemical compositions.[3, 4] Since many diseases originate from biological alterations at the nanoscale level (e.g. mutated genes, low-abundance proteins, viral or bacterial infections, etc.), nanomaterials could be designed as specific carriers to aid the transport of diagnostic or therapeutic agents through biological barriers, to gain access to molecules or to mediate in molecular interactions.[5] Furthermore, some nanostructures have proven to exhibit unique electron behavior that turns into tunable electric, magnetic and optical properties extremely useful for detection at the molecular scale.[6] On the other hand, the small dimensions of nanomaterials can be exploited for device integration and miniaturization. Smaller devices offer promising opportunities to develop compact and portable analytical platforms that contribute to the decentralization of clinical analysis or that can even be implanted inside the body.[7] Nanotechnology is also positively impacting in biomedicine related fields, such as genomics and proteomics. The implementation of ultra-sensitive analytical devices enables the design of more suitable pharmacotherapy for each individual patient and can also help in the definition of relevant biomarkers. Both aspects are harnessing new alternatives for the development of personalized medicine and improved therapy and diagnostic modalities.[8]

Generally, nanomedicine encompasses two main areas of research and development: in therapeutics, based on the design of innovative techniques and biomaterials for drug delivery, specific therapies or regenerative medicine; and in diagnostics, by the development of novel diagnostic and monitoring techniques, such as biosensors or imaging agents.

1.1.1. Nanomedicine in Therapeutics

Therapeutic nanomedicine is aimed at overcoming several drawbacks of conventional drugs and pharmaceuticals mainly related to the lack of effectiveness or potential adverse reactions, usually due to the non-specificity of their action. Nanopharmaceuticals are sophisticated systems designed to selectively accumulate only at pathological tissues or cells, to assist drug molecules in permeating biological barriers or to increase or improve the resistance to degradation and excretion.[9] Typically, nanopharmaceuticals include liposomes,[10] polymers[11] or nanoparticles[12] acting as carriers with high loading capacity. These systems are commonly decorated on their surface with chemical or biochemical compounds to enhance stability and biocompatibility and/or for site-specific targeting. Today, there are already some approved and marketed drug delivery nanosystems for the administration of different type of drugs,[10] such as Doxil™ (doxorubicin hydrochloride liposome injection) used for cancer therapy.[13] These nanopharmaceuticals are generally passive drug delivery systems, comprising the active principle and a container (usually liposomes), which can localize and permeate into the target site by means of specific physical properties of the disease environment (e.g. enhanced permeability and retention effect).[14] In recent years, increasing efforts are focused on developing therapeutic nanosystems with additional functionalities in order to overcome the biological barriers of the body, to promote active molecular recognition of the target tissue and to trigger the release of the drug at the disease site. This next-generation of nanopharmaceuticals are functionalized with targeting moieties, such as antibodies or small peptides that bind to specific surface markers expressed in the disease microenvironment, and they also include responsive systems to internal or external stimuli like pH changes, enzyme activation, light, magnetic fields or ultrasounds, allowing the controlled delivery of the drug.[15, 16] Although most representative of these nanopharmaceuticals have not been approved yet by the Food and Drug Administration (FDA) or the European Medicines Agency (EMA), on-going clinical trials involving targeting and stimuli-responsive drug delivery systems are showing potential benefits, particularly in cancer applications.[17]

Additionally, exciting applications of Nanotechnology in regenerative medicine have arisen in recent years.[18] Tissue engineering holds great promise for regenerating damage tissues and organs by stimulating the cells to repair themselves or by growing artificial tissues (i.e. implants) in the laboratory by the combination of living cells and biocompatible materials. Most significant advances have been achieved in the development of more efficient cell-based regenerative therapies. Manipulation of cells with nanoparticles and nanostructured surfaces has endorsed the understanding of cell-repair mechanisms and has provided efficient tools for the identification and manipulation of targeted adult stem cells.[19]

Another aspect to consider in the nanotherapy area relates to safety issues, that is, toxicity and biocompatibility of the nanopharmaceuticals.[20] The high reactivity arising from the large surface-to-volume ratio of nanoparticles is a latent risk for all new nanosystems that should be carefully considered. Possible incompatibility may result in generation of disorders such as inflammation, immunoreaction or even cancer. In this line, major research is directed to exploit polymeric materials, such as polyethylene glycol (PEG) derivative compounds, for nanoparticle surface coating which provides biomimetic, hydrophilic and biocompatibility properties.[21, 22] Certainly, surface functionalization has proven to be critical for the feasibility and the efficiency of therapeutic nanomedicine.

1.1.2. Nanomedicine in Diagnostics

Diagnostics play a crucial role in medicine for the successful prevention and therapy of diseases. The diagnosis process involves detection and identification of the pathology, definition of its severity and stage, and selection of the more suitable treatment. In addition, monitoring of the therapeutic response and continuous follow-up of pathologies or physiological states during and after treatments are critical in order to improve patient's health. Nanomedicine contribution to the diagnostics field has been directed to the design and development of sensor and analytical technologies for both *in vivo* (i.e. inside the body) and *in vitro* (i.e. outside the body) modalities.[23]

In vivo diagnostics or imaging techniques are designed to obtain molecular, cellular, physiological or anatomical data from inside the patient's body to detect or identify the presence and the progression of diseases. Classic imaging systems comprise computed tomography (CT), magnetic resonance imaging (MRI) or ultrasounds among others, which make use of X-rays, photons or sound waves to explore diagnosis or treatment follow-up. More recent technologies such as positron-emission tomography (PET), fluorescence-mediated tomography (FMT), laser-scanning confocal microscopy or multiphoton microscopy have gained importance and have become

indispensable diagnostic tools for numerous diseases, including cancer, cardiovascular diseases or neurological syndromes, among others.[24] However, these methods can only readily detect pathologies once they have caused a visible change to a tissue and do not provide significant information related to the cause or biochemical mechanisms involved in onset of the disease.[25-27] Therefore, advances in imaging techniques have been driven by the need of powerful tools capable of studying biological processes in different organs and of identifying pathologies at earlier stages.

Besides the improvement of imaging technologies, intense research have been addressed to develop novel contrast agents more robust and highly sensitive and selective.[28] Most representative proposed nanoparticles for clinical *in vivo* diagnosis include quantum dots (QDs) and metal nanoparticles. Especially QDs could profile the next-generation dyes for biological analysis.[29] These nanoparticles made of semiconductor materials exhibit interesting optical properties such as extraordinary brightness and stability, besides a large versatility and sensitivity for cellular and molecular analysis. However, a major limitation for their implementation is their elevated toxicity, which is encouraging the development of novel functionalization or encapsulation techniques that may allow their application for *in vivo* imaging.[30-32] Similarly, metal nanoparticles (e.g. iron oxide or gold nanoparticles) can be used to enhance contrast signaling in tomography, resonance imaging or microscopy techniques.[33-35]

Furthermore, increasing efforts in research are directed to the combination of therapeutic and imaging devices for the final development of theranostic formulations.[36] Theranostic nanosystems are designed for the diagnosis (mainly referred to the pre-selection of a suitable therapy), treatment and monitoring of a disease. The aim is to create detection agents that can also deliver the drug in the specific pathological site and to serve as imaging devices for the follow-up of the therapeutic effect. Clinical trials with radiolabeled polymers or liposomes have already proven to enable simultaneous drug delivery and quantification of nanosystems accumulation at the target tumor in a selective and non-invasive manner.[37, 38] These theranostic systems hold significant potential for personalizing nanomedicine and for improvement of patient's quality of life.

Although *in vivo* imaging is a valuable tool for rapid and accurate identification of pathologies and monitoring the therapeutic progression, *in vitro* analysis is clearly necessary for the early detection of diseases and for the fundamental study of the molecular and cellular mechanisms involved.

In vitro diagnosis is generally based on the analysis of biological fluids (i.e. blood, urine, saliva, tears, etc.) in order to detect and quantify a specific biomarker, that is, a genomic or protein biomolecule indicator of presence, severity or stage of a particular disease or physiological state. Nowadays, clinical diagnosis is based in highly sensitive and specific laboratory assays such as cell culture methods, polymerase chain reaction (PCR) or enzyme-linked immunosorbent assays (ELISA). These conventional methods involve laborious, multi-step and time-consuming techniques and the need of fully equipped laboratories and specialized technicians to perform the analysis. More recently, microarray technology is offering a highly efficient alternative for simultaneous identification and determination of a broad range of biomolecules. Microarray chips consist of regular patterns of DNA sequences or proteins attached to a solid support capable of identifying complementary nucleotide sequences, mutations or relevant protein biomarkers in a sample, typically using fluorescence labels. Although this technology arose in the 1980s, recent advances in nanomaterials and nanofabrication techniques have enabled a significant increase of the resolution and multiplexing capabilities as well as the detection sensitivity.[39-42] Nanoarray technology offers accurate and high-throughput screening in a rapid manner it is widely employed in research laboratories to explore and profile the underlying causes of numerous human disease and to design new therapeutic drugs.

However, there is a huge demand for more accessible and affordable healthcare techniques that allow decentralized analysis, which specifically involve the development of reliable point-of-care (PoC) diagnostics.[43] PoC platforms are defined as portable and user-friendly analytical systems capable of providing fast, sensitive and selective response to several biomarkers using low sample volumes. PoC diagnostics open up important opportunities for rapid screening and disease detection, especially in resource-constraint settings. Early diagnosis and monitoring of diseases would significantly improve prognosis and survival rates, reducing disease burden and helping social development, opening the door to a global healthcare access.

Development of PoC devices is typically based on two main techniques that include lateral-flow assays or biosensors (Figure 1.1). The lateral-flow assay (LFA) is the commonest commercially available PoC diagnostic format, being the home pregnancy test as the most representative example. These devices, usually based in immunochromatographic techniques, are able to detect the presence or absence of a target compound and provide analytical information without the need of specialized and costly equipment. The technology consists of capillary strips, such as pieces of porous paper or polymer, that can be directly soaked into the fluid sample. The fluid migrates through the strip till reaching a particular area with an immobilized capture molecule.

The capture molecule interacts with the specific target analyte triggering a series of physicochemical changes that are readily visible to the patient, like a change of color. LFA tests are affordable, rapid and easy to use, therefore they are interesting candidates as diagnostic tools at low-resource environments. Besides, the introduction of nanoparticles as colorimetric agents or novel materials as substrates are greatly improving the efficiency of the assay.[44, 45] However, main weaknesses of LFA tests are related to the limitation to qualitative or semiquantitative results (often aimed at yes/no response) and difficulties for accurate multiplexed assays.[46]

Most promising alternatives for clinical diagnostics are expected in the employment of biosensor devices, which hold enormous potential as technological solutions for rapid and reliable biomedical analysis.[47] Biosensor platforms can be designed to provide quantitative analytical information with elevated accuracy in few minutes, employing low sample volumes and minimum pretreatment. They are promising analytical tools for the efficient clinical diagnosis as well as for better understanding of the complex molecular mechanisms of the pathophysiology, which will build the basis to identify novel biomarkers and to design new and more suitable treatments. Moreover, the ability to miniaturize and integrate different functional components (e.g. microfluidics, electronics, etc.) in a single platform allows the fabrication of smaller, cheaper and easy-to-use devices which can accelerate the real implementation of PoC biosensors in the clinical practice.

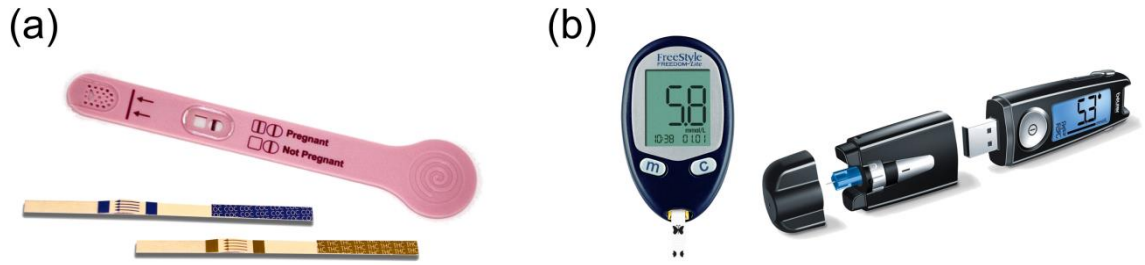

Figure 1.1 PoC devices based on **(a)** lateral-flow assays and **(b)** biosensor technology.

1.2. Biosensors

1.2.1. Definition and Classification

According to the International Union of Pure and Applied Chemistry (IUPAC), a biosensor is a self-contained integrated device capable of providing specific quantitative or semi-quantitative analytical information using a biological or biomimetic recognition element which is in direct

spatial contact with a transducer.[48] The biorecognition layer, typically composed of enzymes, antibodies or nucleic acids, is specifically designed to interact with the target compound in a sample. When the biochemical interaction occurs, a series of physicochemical changes in the medium or the surface are detected by the transducer and converted into discrete or continuous signals (Figure 1.2).

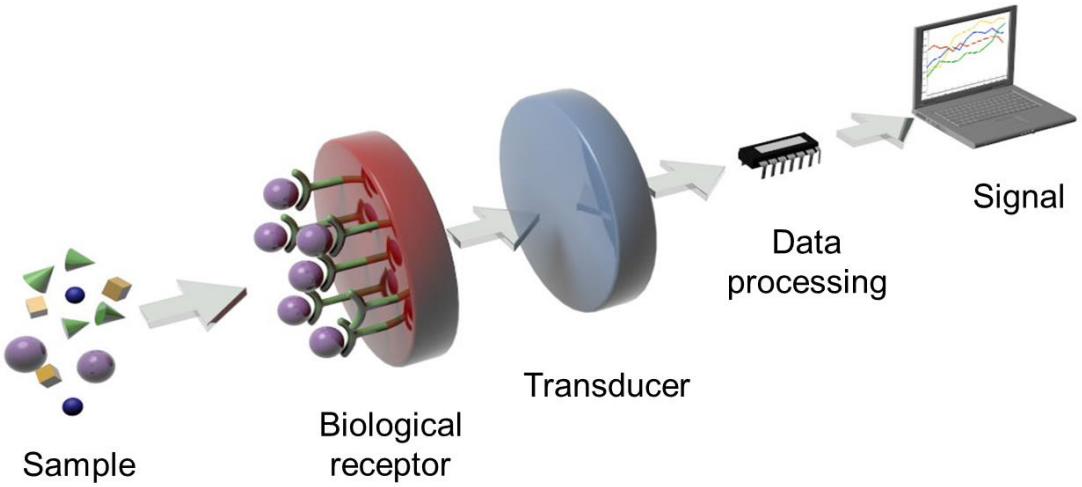

Figure 1.2 Schematic representation of a biosensor including the heterogeneous sample, the specific biological receptor, the transducer, the data processing system and the final signal.

The design and integration of biosensors offer unique features to improve current analysis. The combination of the bioreceptor layer with the transducer in a single device confers the ability to detect the target analyte with high sensitivity and selectivity in a fast way. Moreover, biosensors could ideally overcome important disadvantages of conventional techniques such as the need of analyte extraction or purification or the use of additional equipment for signal read-out (e.g. UV-VIS spectrometer, microscope, etc.) which is usually operated by specialized personnel. Biosensors can also monitor biological interactions in real time allowing the evaluation of the affinity and kinetics of the interaction and, thereby, helping in elucidating the biochemical mechanisms involved in the disease.[49] Biosensors also benefit from great versatility, being possible to measure a wide range of analytes just by selecting the appropriate biological receptor. Recent advances in nanofabrication further provide interesting opportunities for biosensor miniaturization, high-throughput and low-cost production.[50, 51] Biosensor platforms have shown exceptional capabilities to turn into portable and user-friendly devices which can be used at doctor's office or patient's home.[52, 53]

Driven by the urgent demand of PoC diagnostics, the attempt to develop highly efficient biosensors have experienced an exponential growth encompassing the interest of numerous disciplines, such as material technology, molecular biology, chemistry or biotechnology among others. The multidisciplinary nature of biosensor research has led to a vast range of biosensor platforms based on different type of transducers or biorecognition elements. Generally, biosensors are classified according to (i) the biological recognition mechanisms or, alternatively, to (ii) the physicochemical transduction of the signal.

Considering the nature and properties of the biochemical interaction, biosensors can be divided in two main types: catalytic biosensors and affinity biosensors.

In **catalytic biosensors**, the recognition event consists of a (bio)chemical reaction catalyzed by the biomolecular receptor which transforms a substrate present in the sample into a product (Figure 1.3a).[54] Most common biocatalytic elements are enzymes, cellular organelles, microorganisms or tissues. The analyte is chemically modified by the biorecognition element yielding to a product which is detected by the transducer, such as proton concentration, light or heat emission, release of ammonia or oxygen gasses, etc. Catalytic biosensors show extremely high specificity and fast response times, but present drawbacks related to the activity and stability of the biorecognition element.

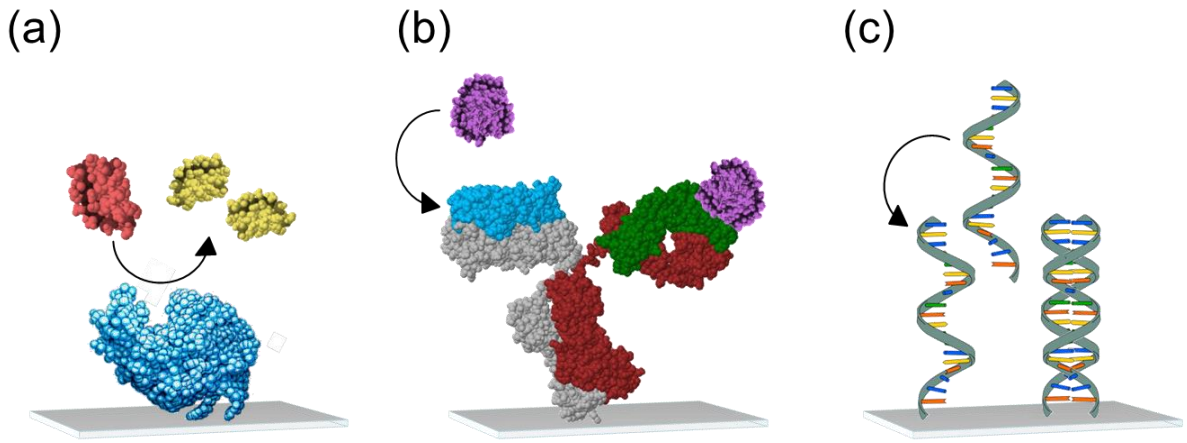

Figure 1.3 Main types of biosensors depending on the biorecognition element: **(a)** enzymatic biosensor (catalytic), **(b)** immunosensor (affinity) and **(c)** DNA biosensor (affinity).

Affinity biosensors employ the conformational recognition between an analyte and its specific bioreceptor which results in an equilibrium reaction.[55] The interaction can be determined by the change of mass or variations in optical or electrical properties detected by the transducer. Immunosensors, in which the interaction occurs between an antigen and its antibody, are the representative example of affinity biosensors (Figure 1.3b). DNA biosensors that exploit the

specific interaction between complementary oligonucleotide chains, are also increasingly used (Figure 1.3c). Cellular receptors or aptamers are other examples of affinity biorecognition elements. In most cases, the high affinity between the analyte and the bioreceptor confers increased sensitivity and specificity to the analysis.

On the other hand, biosensors can be classified depending on the type of transducer employed in the detection. Main categories are: electrochemical, mechanical and optical biosensors.

The **electrochemical biosensors** are the most employed ones in the clinical field due to their excellent analytical features, simple and efficient fabrication and unique miniaturization capabilities. In these devices the transducer measures electrochemical changes in the medium caused by the biomolecular interaction.[56] Four main types of electrochemical biosensors can be distinguished depending on the mode of operation: amperometric, potentiometric, impedimetric and conductimetric. Commonly, electrochemical biosensors employ catalytic bioreceptors (e.g. enzymes) which provide elevated sensitivity and selectivity. But the high sensitivity achieved mainly relies on amplification or labeling steps, which implies extra pretreatment or processing. Furthermore, since the detection mechanism is based on changes of the electrochemical properties, the inherent variations of biological fluids, for example pH or ionic strength, lead to important interferences, worsening the biosensor performance.[57] Among them, we should highlight the enzymatic biosensor first proposed by Clark and Lyon in 1962 for the determination of glucose in blood, which is currently used around the world for monitoring diabetic patients.[58] Recently, electrochemical biosensors have experienced an unparalleled growth with the incorporation of graphene or carbon nanotubes as transducers due to their exceptional electrical and chemical properties.[59, 60] Carbon nanotubes provide high surface area, mechanical strength, good chemical stability and excellent electrical conductivity, as well as being easily fabricated and biofunctionalized.[61]

In **mechanical biosensors** the biochemical interaction is measured as changes of mass on the surface of the transducer.[62] We can distinguish between acoustic-wave biosensors or nanomechanical biosensors. In acoustic-wave devices, also referred as piezoelectric biosensors, the transducer is a microbalance composed of a quartz crystal without center of symmetry sandwiched between two electrodes delivering an alternating electrical field.[63] Changes of mass on the surface cause variations of the acoustic wave frequency which are transduced to measurable signals. Nanomechanical biosensors detect changes of mass by employing micro or nanocantilevers as transducers.[64] The biological interaction occurring on the surface of the

cantilevers may either produce a nanomechanical deflection or changes in the vibration frequency which can be measured and quantified. Mechanical biosensors have attractive features such as label-free detection, multiplexing capabilities and thermal stability.[65] However, the mechanical nature of the sensing mechanism is a main constraint for sample handling or when working in liquid environments.[66]

Optical biosensors detect the biological interaction by measuring variations of the optical properties of the propagated light, such as intensity, wavelength, refractive index or polarization.[67, 68] Optical sensors can be divided in two types: bio-optrodes and evanescent wave sensors. In the bio-optrodes light is guided (generally with an optic fiber) to the evaluation chamber where the biomolecular interaction produces a change in the properties of the light (absorption, fluorescence, refractive index, bioluminescence or dispersion). These sensors usually employ optical labels, such as dyes or fluorescent molecules. On the other hand, evanescent wave biosensors exploit the possibility of the electromagnetic (EM) wave confinement in certain dielectric and/or metals, which can result in either a localized or propagating EM mode (Figure 1.4). Part of the EM mode penetrates into the external medium, forming a so-called evanescent field. The evanescent field acts as a probe to detect refractive index (RI) changes caused for example by a biological interaction, so that no label is required for sensing. Interferometers, resonators or plasmonic biosensors are typical examples of evanescent wave biosensors.[69, 70] These devices achieve high detection sensitivities with short response time, they do not suffer from electromagnetic or mechanical interferences and present potential miniaturization capabilities.

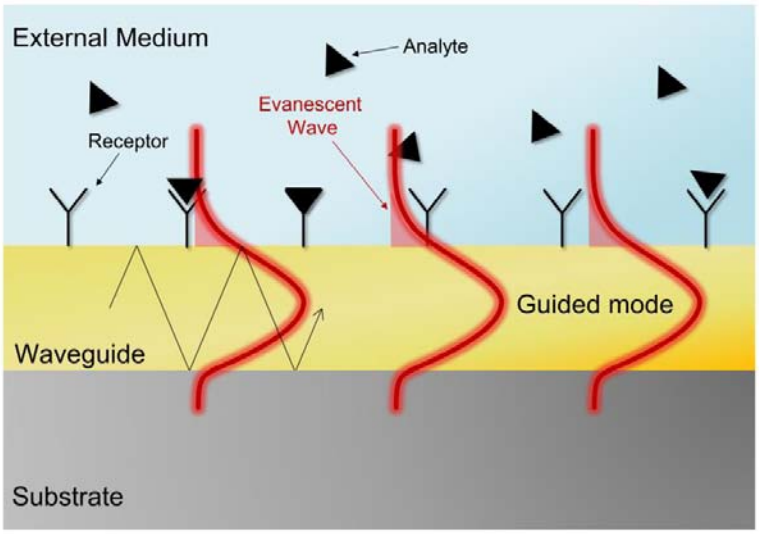

Figure 1.4 Schematics of the sensing principle of an evanescent wave biosensor.

1.2.2. Plasmonic Biosensors

Plasmonics is the field that studies the interaction of electromagnetic waves with metals and its applications. The coupling of optical waves to the free electrons of a metal can give rise to electromagnetic modes named **Surface Plasmons** (SPs). These plasmonic modes can be excited at the interface of a noble metal and a dielectric and exhibit an evanescent field that penetrates into the surrounding media. This evanescent field is extremely sensitive to refractive index (RI) changes close to the metal surface, acting as detection probe when plasmonic structures are used as refractrometric sensing platforms.[71, 72] Depending on the excitation of the SPs, we can distinguish two varieties: propagating SPs excited in thin metal films, commonly referred as Surface Plasmon Polaritons (SPPs) or **Surface Plasmon Resonance** (SPR), and **Localized Surface Plasmon Resonance** (LSPR) when SPs are excited on sub-wavelength-sized metal nanoparticles.

1.2.2.1. Surface Plasmon Resonance (SPR) Biosensor

Since the introduction of SPR-based refractometric sensors by Nylander and Liedberg[73] more than three decades ago, the interest in plasmonic sensing has increased tremendously. SPR biosensors are nowadays the most widely used and commercialized label-free optical sensors, becoming a widespread tool for the study of any type of biochemical interactions. SPR sensing shows excellent properties for its application in different fields, such as environmental monitoring, food quality and safety analysis, diagnostics and biomedicine, biological engineering, drug discovery, etc.[74]

SPR biosensor is based on propagating surface plasmon polaritons (SPP), electromagnetic waves occurring at the interface between a thin film of metal and a dielectric which behave like a quasi-free electron plasma, generating an evanescent field (Figure 1.5a). The SPP is a transverse-magnetic (TM) mode (the magnetic vector is perpendicular to the direction of propagation of the wave and parallel to the plane of the interface) and it is characterized by an evanescent field distribution and its propagation vector:

$$k_x^{SPP} = k_0 \sqrt{\frac{\varepsilon_m \varepsilon_d}{\varepsilon_d + \varepsilon_m}}$$

where k_0 is the wave vector of the light in vacuum: $k_0 = \omega/c$. In this equation, ε_m represents the frequency-dependent and complex dielectric function of the metal ($\varepsilon_m = \varepsilon_m' + i\varepsilon_m''$) and ε_d is the dielectric constant of the medium, which is directly related to the refractive index ($\varepsilon_d = n_d^2$). This constitutes the main principle of refractometric sensing platforms. Biochemical interactions

occurring in the vicinity of the interface metal-dielectric induce RI changes that alter the propagation condition of the SP. These changes can be tracked in real time providing a measurable and quantifiable signal without the need of labeling.

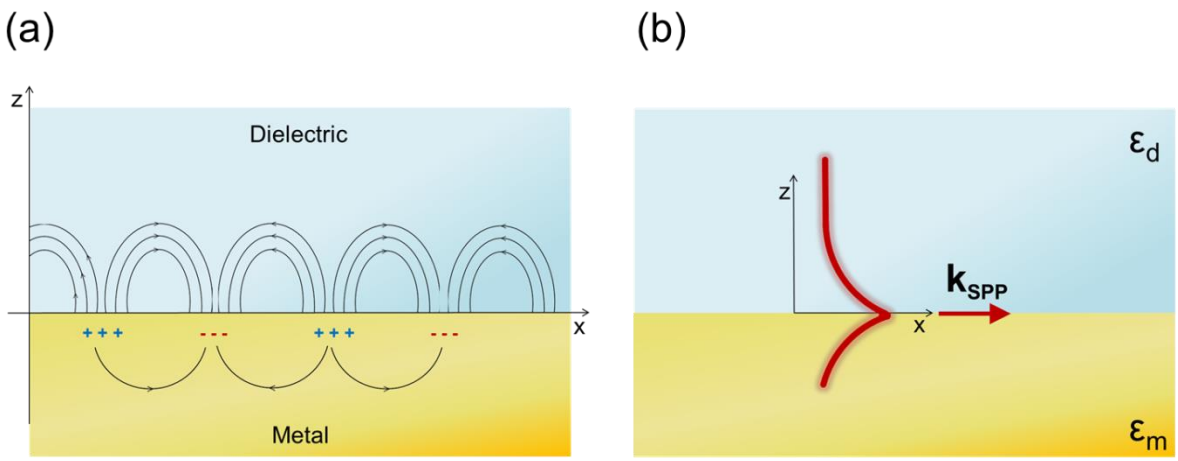

Figure 1.5 Schematics of a SPP at the interface of a metal and a dielectric showing**: (a)** the collective charge oscillation at the surface and **(b)** the transversal evanescent field distribution.

For the SPP excitation and propagation, the real part of the ε_m must be negative and its absolute value smaller than ε_d. At optical wavelengths, this condition is fulfilled for several metals, from which gold, silver or aluminum are the most commonly used in plasmonics. Further, due to the relatively small imaginary part of the refractive index of these metals, they show strongly suppressed plasmonic attenuation when compared to other materials, thus minimizing propagation losses.

The evanescent field of the SPP is confined at the metal-dielectric interface and decreases exponentially into both media (Figure 1.5b). The field is distributed in a highly asymmetric fashion and most of it is concentrated in the dielectric close to the surface, showing a typical penetration depth between 100-500 nm when working in visible (VIS) or near infrared (NIR) regions.[75] This is particularly significant for SPR sensing, as it represents the depth probe in optical sensors using SPPs. This means that only biomolecular interactions occurring in the metal surface and within the evanescent field penetration depth would produce changes in the SP and could be detected.

The excitation of the SPR is achieved by coupling a light wave to the surface plasmons only if the component of light's wave vector parallel to the interface matches the propagation vector of the SPP:

$$k_x^{Light} = \frac{2\pi}{\lambda}\sqrt{\varepsilon_d}\sin\theta = k_x^{SPP}$$

Generally, the SPP propagation vector is considerably larger than the wavenumber of the light wave in the dielectric, therefore surface plasmons cannot be excited by direct illumination. Several techniques can be employed to enhance the wave vector of the incoming light by means of a) prism coupling, b) waveguide coupling and c) grating coupling (Figure 1.6).

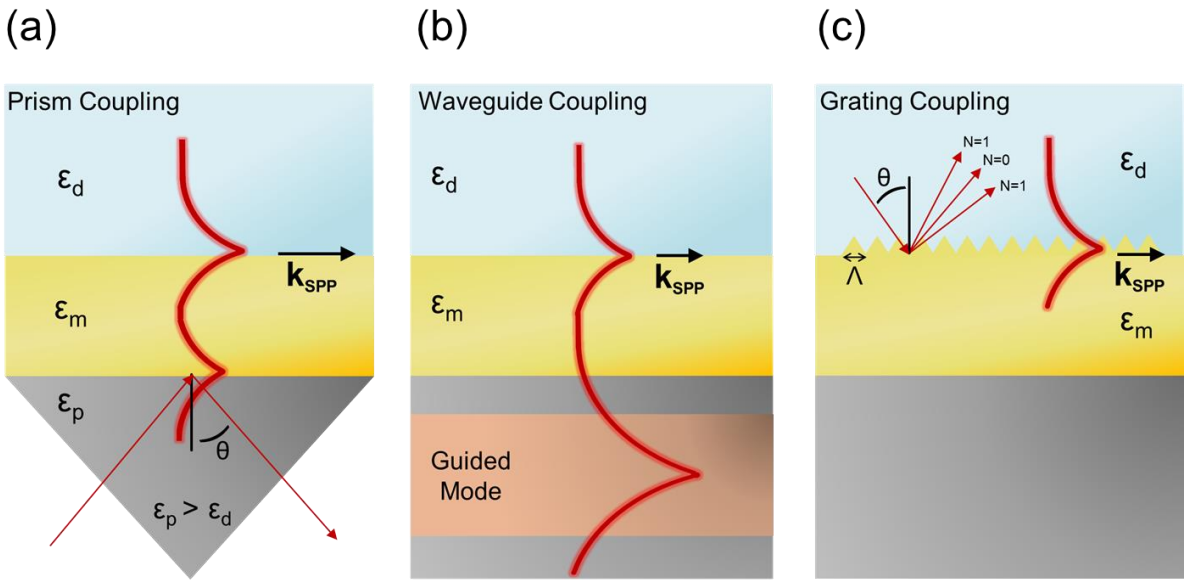

Figure 1.6 SPR coupling methods, including **(a)** a prism-coupled Kretschmann configuration, **(b)** the waveguide coupling and **(c)** grating coupling.

Prism couplers are the most common method used for the optical excitation of surface plasmons. In the well-known Kretschmann configuration (Figure 1.6a),[76] light passes through a high RI prism (ε_p) and is totally reflected at the prism base, generating an evanescent wave which penetrates the metal film. This evanescent wave propagates along the interface with a certain propagation vector which can be adjusted to match that of the SPP by controlling the angle of incidence. This method is referred to as Attenuated Total Reflection (ATR) method.[77, 78] Similarly, the process of excitation of SPP can be achieved by using an optical waveguide-based SPR structure.[79] The light wave is guided by an optical waveguide and, when entering the region with a thin metal layer, it evanescently penetrates through the metal layer exciting an SPP at its outer interface (Figure 1.6b). Excitation via grating couplers is based on the diffraction of the light wave. The component of the wave vector of the diffracted waves parallel to the interface is increased by an amount inversely proportional to the period of the grating and can be matched to that of the SPP (Figure 1.6c).[80]

The resulting SPR is characterized by the appearance of a spectral reflectivity dip, which strongly depends on the refractive index of the dielectric but also on the properties of the metal film.

Although silver has shown most efficient SPR excitation (i.e. deeper and sharper peaks) and it is quite versatile for functionalization, it is also very susceptible to surface oxidation on exposure to the atmosphere or liquid aqueous environments. Thus, the biofunctionalization and the assay performance become more complicated and require careful protection of the surface and accurate conditions of analysis to avoid or minimize degradation. On the contrary, gold is very resistant to oxidation and other atmospheric contaminants as well as it can be readily modified for surface biofunctionalization procedures (e.g. thiol-gold chemistry). This makes gold the most practical and efficient metal for SPR biosensors. The thickness of the gold film is also a determining factor. For Kretschmann configurations in particular, the thickness should be around 50 nm. Above this thickness the dip in the reflective light becomes shallow while below 50 nm the peak becomes broader, worsening the sensitivity of the biosensor.[81]

A SPR biosensor generally consists of an optical system for excitation and interrogation of propagating SPP, that is, the light source (either mono-chromatic or broadband) and the detector (intensity- or phase-based); the plasmonic transducer, which usually consists of a thin film (≈ 50 nm) of gold that incorporates the biomolecular recognition element on its surface; and a fluidic system comprising one or more flow cells for sample confinement at the sensing surface and flow delivery systems for sample injection and delivery. Figure 1.7 illustrates a typical SPR biosensor employing a Kretschmann configuration. In this particular scheme, SPP excitation can be achieved by either light wavelength (λ)-modulation or angle of incidence (θ)-modulation.[75]

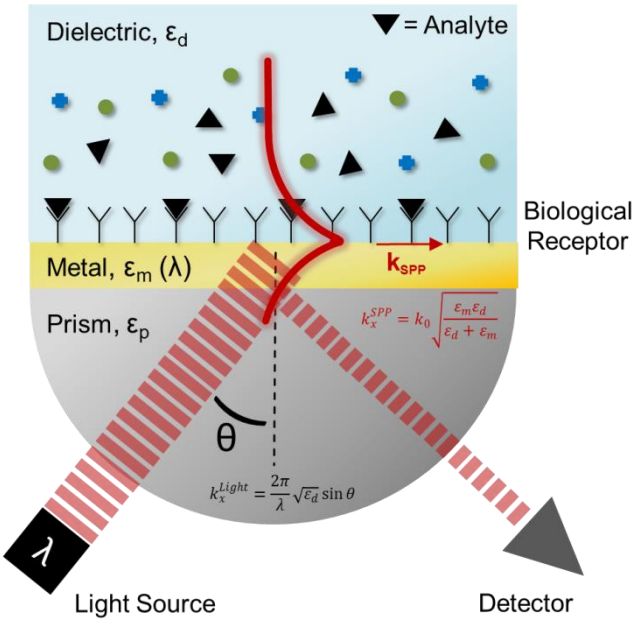

Figure 1.7 Schematics of a SPR biosensor employing a Kretschmann configuration with a monochromatic light source.

When working with a monochromatic source (i.e. fixed wavelength), the reflected light is measured as a function of θ. At certain angle denoted as θ_{TIR}, the Total Internal Reflection (TIR) sets in. As the angle increases, the reflected intensity exhibits a strong decrease, until a minimum value is reached. It is at this angle (θ_{SPP}), where the light wave vector matches the SPP wave vector, yielding to the excitation of the SPP. When a biomolecular interaction takes place within the evanescent field of the SPP, a local RI change is induced that alters the SPP wave vector and its excitation condition. Changes in the SPP can be observed as changes in the characteristics of the light. These can be detected by time-dependent monitoring of the entire curve, or by fixing θ at the point where the slope of the SPP resonance curve is maximized, after which intensity changes of the reflected light are monitored as a function of time (Figure 1.8a and c). Our research group has a strong experience in developing SPR biosensor platforms based in Kretschmann configuration which employs a monochromatic source for the excitation of the SPP and measures intensity changes of the reflected light working at fixed angle.

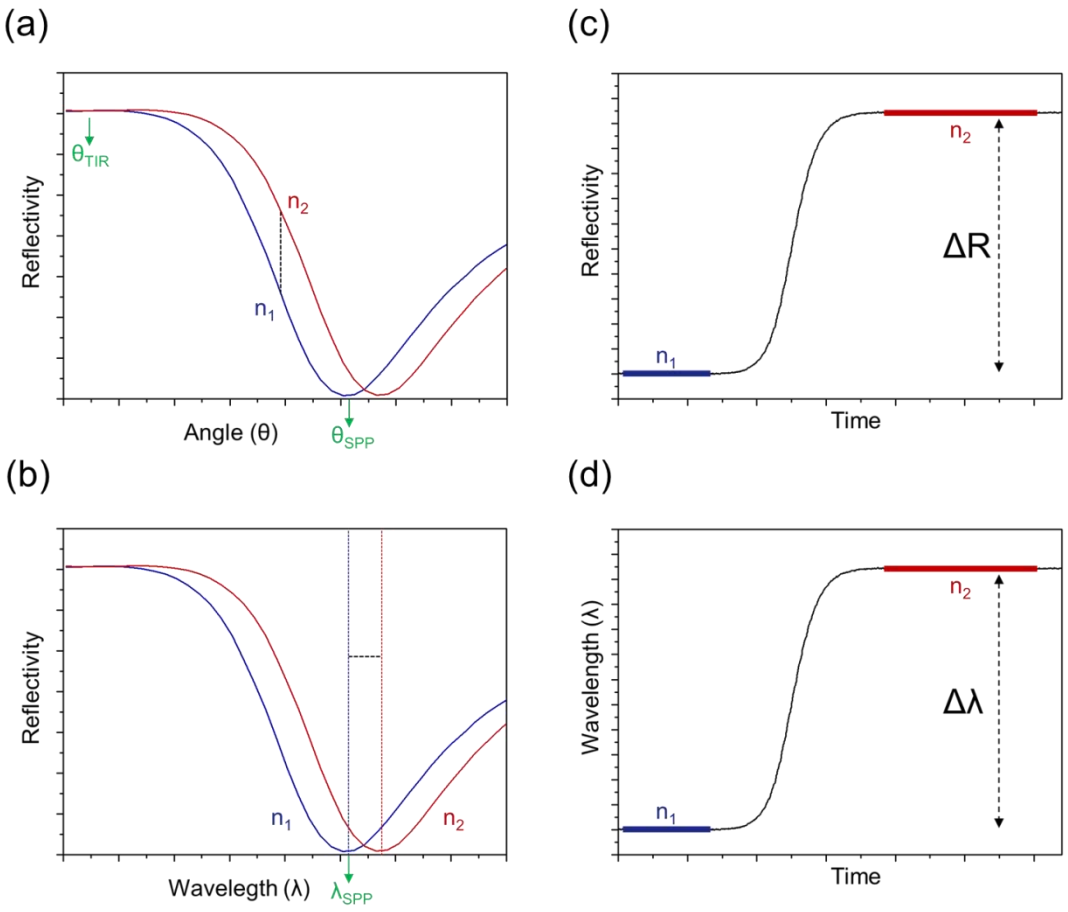

Figure 1.8 Representative SPR curves for **(a)** θ- and **(b)** λ-interrogated SPR sensors, together with their corresponding real-time tracking of curve displacements via the monitoring of **(c)** changes of the reflectivity, R, and **(d)** shifts of the resonance wavelength, λ_{SPP}.

On the other hand, when illuminating with a broadband light source at a fixed θ, the detection is performed by spectral analysis of the reflected light. The reflectivity spectrum shows a dip located at λ_{SPP}, which is subjected to lateral (spectral) displacements induced by changes of RI. Spectral interrogation of λ_{SPP} translates changes of RI into a measurable quantity that can be extracted as a function of time (Figure 1.8b and d). Working in either two schemes, biochemical interactions can be directly monitored in real time allowing the evaluation of the affinity and kinetic studies in a simple, rapid and label-free manner.

Worth mentioning is that the changes of the local RI are related to the direct mass changes on the surface (i.e. an increase or decrease of the coverage of the surface with molecules of a particular size and density, will alter the overall local RI). Therefore, the smaller the molecule bond the smaller the RI changes induced, as compared to an analyte at the same concentration but with a higher molecular weight.

1.2.2.2. Localized Surface Plasmon Resonance (LSPR) Biosensor

Accompanied by the progress of Nanotechnology, which has provided new methods to fabricate, to assemble and to characterize nanomaterials, the nanoplasmonics field (i.e. plasmonics applied to nanomaterials) has experienced an enormous boost during the last years leading to a deeper comprehension and control of the light-matter interactions at the sub-wavelength scale.[82] Nanoplasmonic sensors, such as the LSPR refractrometric biosensors, are considered as the next generation of plasmonic sensing platforms offering highly sensitive analytical tools with multiplexed capabilities and showing great potential for integration and miniaturization.[83]

Interaction of metal nanostructures with an electromagnetic (EM) field can give rise to a surface plasmon mode based on non-propagating oscillation of the conduction electrons of metal nanoparticles, known as Localized Surface Plasmon Resonance (LSPR). This effect leads to the accumulation of polarization charges on the surface of a nanoparticle, acting as a dipole (Figure 1.9a). The dipolar field is responsible for the enhanced absorption and scattering of light, as well as for the strongly enhanced EM field in close vicinity of the nanoparticle surface.

In order to simplify the theoretical description of the LSPR principle, we consider metallic spherical nanoparticles with $\emptyset \ll \lambda$, where $\emptyset$ is the diameter of the particle and λ is the wavelength of the incident light. In this limit, the external EM field appears static around the nanoparticle and the charge oscillation behaves as a single dipole with an amplitude that is strongly influenced by the distance between the surface charges. Herein, the LSPR condition is related to the polarizability (α_0) of the particle, which is given by:

$$\alpha_0 = 4\pi\emptyset^3 \frac{\varepsilon_m(\lambda) - \varepsilon_d}{\varepsilon_m(\lambda) + 2\varepsilon_d}$$

The polarizability represents the distortion of the electron cloud in response to the external EM field and basically depends on the size of the particle (ø) and the dielectric functions of the metal ($\varepsilon_m(\lambda) = \varepsilon'_m(\lambda) + i\varepsilon''_m(\lambda)$) and the surrounding medium ($\varepsilon_d = n_d^2$). The maximum polarizability is achieved when the absolute value of the denominator approaches zero, hence the LSPR is observed when $\varepsilon'_m(\lambda) = -2\varepsilon_d$. For noble metals such as gold or silver, this condition is met in the visible region of the light spectrum.

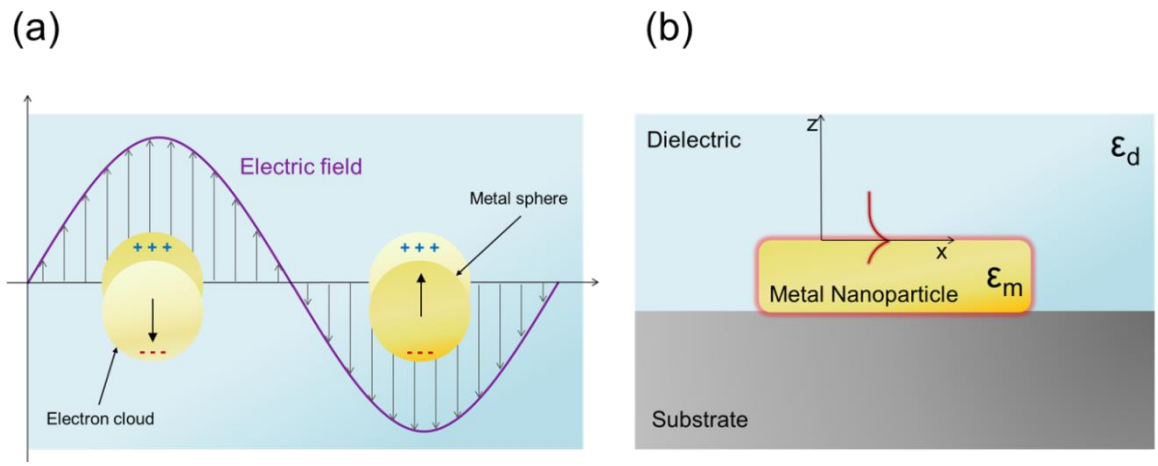

Figure 1.9 Schematic representation of **(a)** the LSPR of spherical nanoparticles positioned in a static electric field and **(b)** the evanescent field distribution of a metal nanostructured surface.

This theory can be extended to larger or nonspherical nanoparticles, revealing the appearance of LSPR modes with higher multipoles, where half of the electron cloud moves parallel and half anti-parallel to the external EM field.[84] Especially for ellipsoidal nanoparticles, such as nanorods or nanodisks, surface plasmons split into two distinct modes due to surface curvature and symmetry exhibiting strong polarization-dependent spectra, where small changes in aspect ratio result in significant changes in the absorption band. This size- and shape-dependency leads to another important property of plasmonic nanostructures: the spectral tunability. The morphology, size and distance separation between the nanostructures contribute to the spectral signature of its resonance, dictating the bandwidth and peak position of the LSPR. By varying the size and shape of the plasmonic nanostructures, the LSPR can be tailored and tuned along the entire VIS and NIR regions of the light spectrum. This property is extremely useful for many applications, among which, biosensing can be highlighted.

Besides the material, size and shape, LSPR strongly depends on the dielectric constant of the medium surrounding the nanostructures. Changes in the RI of the medium within the evanescent field lead to changes in the polarizability, which result in displacements of the LSPR peak. In contrast to propagating SPR, the LSPR evanescent field is strongly confined to the particle surface exhibiting a rapid decay in the dielectric medium (Figure 1.9b).[82] The smaller penetration depth of the evanescent field (few tens of nm) can confer to LSPR sensing high resolution detection, even at the level of single particle analysis for instance.[85, 86]

In general, LSPR biosensor schemes are based on arrays of nanostructures that can be either particle- or hole-based substrates, where the particle-based ones are the most extensively employed for nanoplasmonic biosensors. The use of nanostructured surfaces instead nanoparticles in solution avoids agglomeration and provides a better control of the interaction between LSPR of individual nanoparticles, which may affect the reproducibility of the analysis. The LSPR of the nanostructured arrays can be excited by a VIS-NIR light source, while a spectrometer or a microscope objective collects the read-out light. For high nanostructure surface densities, extinction measurements are the easiest way to characterize the optical properties (Figure 1.10a). In this case, light is shed on the plasmonic nanostructures and the transmitted light is analyzed with a spectrometer.

However, in the limit of single particle sensing, a much higher contrast is needed between the excitation light and the light absorbed by the nanoparticles. In those cases, scattering measurements are preferred. These high signal-to-background levels can be achieved by dark-field (DF) microscopy or total internal reflection (TIR) spectroscopy. In DF microscopy (transmission configuration) a DF condenser is used to focus a hollow - high numerical aperture - cone on the nanostructured surface. Then the scattered light dispersed by the nanostructures can be collected by a microscope objective with a lower numerical aperture (Figure 1.10b). In contrast, in TIR microscopy, the LSPR is excited in a prism-coupled TIR configuration (Figure 1.10c), also using a microscope objective to collect the scattered light, without any restriction on its numerical aperture. Generally, scattering measurements offer a much more control than extinction configurations and permits the study of single nanostructures. However, as the size of the particles is reduced, the scattering becomes smaller and absorption becomes dominant, making extinction measurements more suitable.

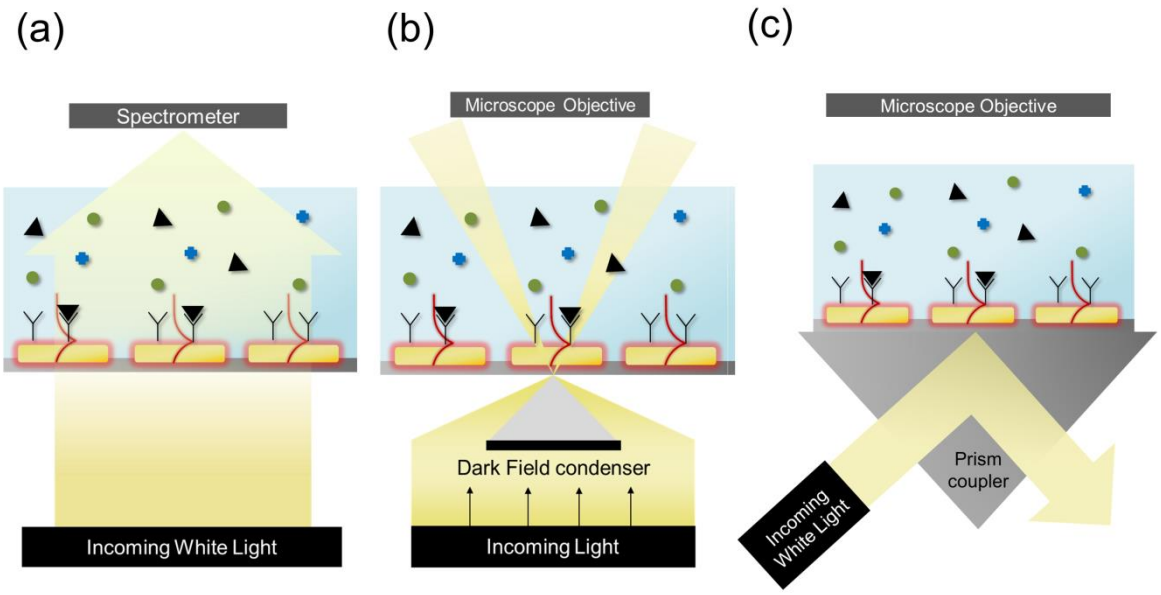

Figure 1.10 Diagrams illustrating nanostructure-based biosensor setups: **(a)** extinction measurements, **(b)** dark-field (DF) microscopy and **(c)** total internal reflection (TIR) microscopy.

Recently, our research group proposed a novel LSPR sensor scheme based on a waveguided electromagnetic mode that arises in thin monolayers of sparse and randomly distributed plasmonic nanoparticles.[87] In this scheme, the in-plane LSPR excitation in TIR strongly enhances the polarizability of the nanoparticles, creating an effective RI that is sufficiently large to support a guided electromagnetic mode. This waveguided mode has shown not only a large increase of the RI sensitivity, but also a great enhancement of the signal-to-noise ratio. Both effects provide an overall improved refractometric sensing performance that is up to an order of magnitude better than that of isolated non-interacting nanoparticles.

Previous in-house studies demonstrated that the sensing performance of these guided modes is determined by both the nanoparticle surface density (F) and the incidence angle of the light (θ).[87] The nanoparticle surface density F needs to be precisely chosen in such a way that optimal mode excitation (i.e. light coupling efficiency close to 100%) occurs at angles where the sensitivity is maximized (θ close to 90°). In our case, the nanoplasmonic surface consists of short-ordered arrays of gold nanodisks (diameter D = 100 nm, height H = 20 nm) fabricated onto a glass substrate. The LSPR-based waveguide is excited by illumination with a collimated broadband light source polarized in TE mode at the determined angle of incidence, similarly to the conventional SPR Kretschmann configuration (Figure 1.11). Due to restrictions of our measurement setup, the

largest possible incidence angle was limited to θ = 80°. For this angle, optimal mode excitation is achieved when the nanodisks surface density was approximately F = 6 - 7%. In this Thesis, we have worked with two analogous biosensor platforms with two different angles of incidence at 80° and at 70°. The later was especially designed since at this particular angle it is possible to excite either the LSPR of gold nanodisks (with TE polarization) and the propagating SPR of thin film gold surfaces (with TM polarization). This would allow us to carry out direct and reliable comparisons between the two biosensor schemes (LSPR and SPR). Reflected light is collected by a spectrometer, showing a mode-specific reflectivity dip at the LSPR wavelength (λ_{LSPR}). This LSPR peak depends on the RI of the dielectric medium in contact with the gold nanodisks. Thus, RI changes close to the nanostructures, such as the ones originating from biorecognition events, cause wavelength displacements ($\Delta\lambda_{LSPR}$) that can be monitored to extract real-time quantitative information related to the biomolecular interactions taking place. Similarly to SPR, these RI changes are closely related to the mass (molecular weight) of the molecules interacting on the nanostructure surface.

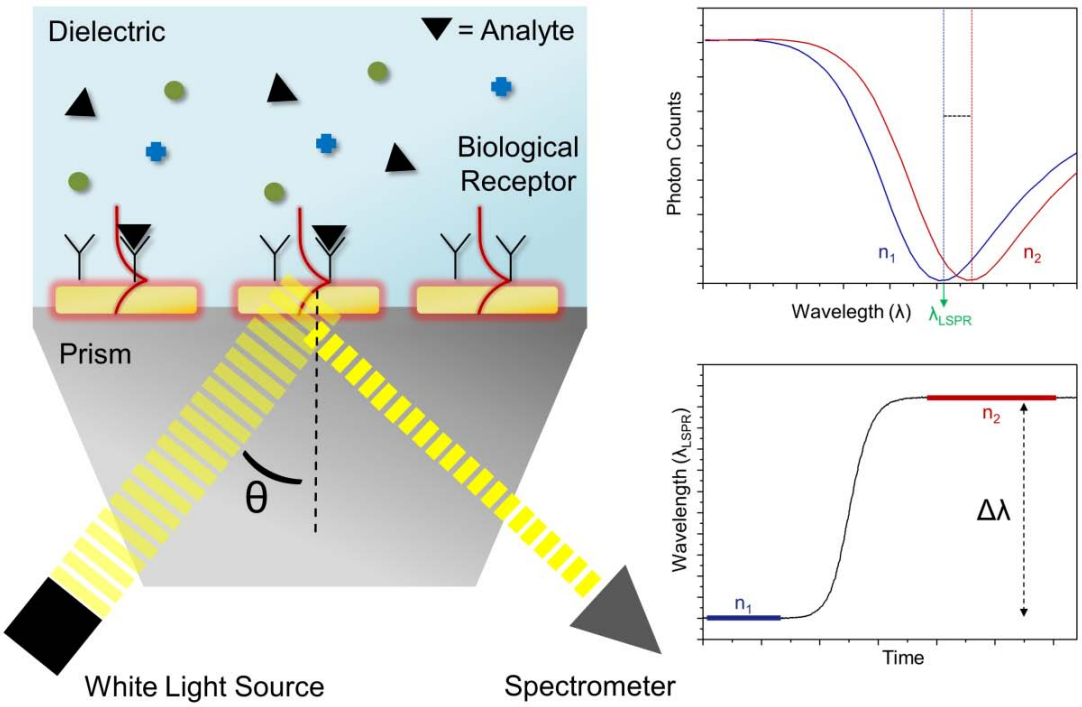

Figure 1.11 Schematic representation of the LSPR-based biosensor. Graphs illustrate spectral wavelength displacements ($\Delta\lambda_{LSPR}$) caused by RI changes (top) and the monitoring of $\Delta\lambda_{LSPR}$ in real time (bottom).

1.2.2.3. Advances and Challenges in Plasmonic Biosensors

SPR biosensor is nowadays a mature technology offering direct, rapid and systematic analysis of any type of biochemical interaction. The sensitivity of refractometric SPR sensors usually ranges between 10^{-6} and 10^{-7} refractive index units (RIUs) and a limit of detection (LoD) in the pM-nM range, if an optimal biofunctionalization has been previously achieved and high-quality biological reagents are employed.[74, 88] These sensitivities are good enough for a great variety of real diagnostic applications, but become a critical factor for the direct determination of small analytes at very low concentrations or for single-molecule detection. However due to its simplicity and versatility, SPR biosensors have profiled themselves as a routine analytical instrument whose scope of application has spread into a wide range. Furthermore, the label-free detection and the real-time monitoring of biochemical interactions allow the determination of any target analyte and the affinity or kinetic studies of the reaction in a simple and reliable way. SPR-based kinetic analysis permits the monitoring of both weak and strong interaction (K_D ranging from 1 mM to 1 pM)[89, 90] and typically requires lower amount of reagents than traditional biophysical techniques (titration calorimetry, ultracentrifugation, stopped flow or column chromatography).

Currently, SPR biosensor is a widespread technique and a large variety of instruments, from miniature SPR-based devices to robust laboratory units, are commercially available to meet special requirements of a multitude of applications.[74, 91, 92] Biacore (GE Healthcare)[93] was the first commercial system launched in 1990. Since then, more than 20 companies worldwide have been offering different SPR instruments, such as Texas Instruments,[94] XanTec Bioanalytics,[95] Horiba Scientific[96] or Biosuplar,[97] among others. Our research group also developed a portable and highly integrated SPR biosensor that was commercialized by our spin-off Sensia S.L.[98]

Research in plasmonic biosensors has been directed to develop fast, cost-effective and ease-of-use analytical platforms, primarily motivated by the urgent demand of ultra-sensitive and reliable PoC devices in the clinical field. However, miniaturization and multiplexed analysis are still important challenges in SPR biosensors. The simplest way to reach high-throughput detection is provided by Surface Plasmon Resonance Imaging (SPRi).[99] In this technique, a collimated monochromatic light beam excites the SPR in an extended area *via* prism coupling. The variations of the intensity of the reflected light due to RI changes are analyzed in a 2D charge-coupled device (CCD) camera. If various biomolecules are immobilized at different areas of the metal layer, the multianalyte evaluation can be made with the analysis of the 2D reflected intensity pattern. SPRi however presents important drawbacks related to sensitivity and channel cross-talk.[100] Although the design and development of novel multiplexed imaging platforms has greatly

progressed, their performance characteristics such as resolution or limit of detection are still behind the best spectroscopic SPR sensors and need to be further improved.[101]

At this point, continuous advances in material science and nanotechnology introduce unique opportunities to satisfy the main limitations of SPR biosensors: sensitivity, throughput capabilities and miniaturization. During last decades, nanoplasmonic biosensors have experienced a rapid development, pushed by the enormous progress in nanofabrication techniques, microfluidics and electronic technology, to offer novel solutions in biosensing. Plasmonic nanostructures have demonstrated exceptional properties to significantly enhance the sensing performance not only in refractometric LSPR biosensors but also in Surface Enhanced Raman Spectroscopy (SERS) and Metal Enhanced Fluorescence (MEF) sensors.[102, 103] Recent trends in nanoparticle SERS tags, for example, offer important opportunities for its exploitation as *in vivo* contrast agents and multiplexed analysis of cells,[104, 105] while MEF-based sensors have reported considerable advantages over conventional fluorescence- or radio-labelled assays in terms of sensitivity, cost, time and simplicity.[106, 107] In the case of LSPR biosensors, some examples have already demonstrated their potential to detect biomarkers, small analytes and cells in complex environments, exhibiting promising features for extension to PoC or mobile platforms.[108, 109] In terms of multiplexing and miniaturization, nanoplasmonic biosensors benefit from the reduced sensor area of metal nanostructures as well as the possibility of excitation with direct EM illumination. Herein, the use of simple light emitting diodes (LEDs) for excitation and small photodetectors rather than spectrometers can greatly reduce the cost and size of nanoplasmonic biosensors, even being possible their integration with portable smartphones.[110, 111] LSPR biosensors are indeed considered to be the next-generation plasmonic sensing platforms,[83] and new companies are emerging and introducing this powerful technology into the market, such as Plasmore[112] or Lamdagen.[113]

However, besides those few examples aforementioned, the use of nanoplasmonic biosensors as analytical platforms for clinical and biomedical applications has not been fully accomplished. At the state-of-the-art most effort has been directed toward the fabrication and development of the nanostructures and the evaluation of its physical and optical properties. The published work related to nanoplasmonic sensors is often of a very fundamental nature, only accompanied by standard proof-of-concept biosensing assays. The real implementation of this powerful technology necessarily requires research effort focused on one of the most underexposed aspects of the nanoplasmonics: the surface biofunctionalization. In this regard, proper surface chemistry and optimized assay methodologies are crucial to enhance the biosensor performance and to

assure reliable and accurate clinical and biomedical analysis. Nanoplasmonic biosensors are set to positively impact on the biomedical industry offering powerful analytical technology, but the development of specific bioanalytical methodologies is the key factor to provide viable solutions for the improvement of the healthcare scenario.

1.2.3. The Biorecognition Layer

In biosensors, the analytical sensitivity and selectivity depend on the biorecognition element tethered to the sensor surface. Typically, in affinity-based biosensors, the most employed biological receptors are antibodies, nucleic acids or cell membrane receptors. These biomolecules show extraordinary affinity and specificity towards certain analytes, such as the corresponding antigen or the complementary oligonucleotide chain, allowing the selective capture of the target compound with extreme sensitivity. The immobilization procedure onto the transducer must take into account several factors for an optimum biosensor: (i) the packing density and orientation of the biorecognition element, (ii) the activity and stability during the analysis time and (iii) the possible interferences or nonspecific binding coming from other substances present in the sample.

Biofunctionalization procedures have been developed since many years ago, aiming to provide the best analytical performance. **Physical adsorption** is the simplest strategy to attach the bioreceptor to the sensor surface, which takes advantage of intermolecular forces like electrostatic, hydrophobic and/or polar interactions (Figure 1.12a). Although it is a widely employed procedure in solid-based assays, such as ELISA, physical adsorption suffers from important drawbacks when dealing with biosensors. Flow-through assays or changes in the pH or buffer composition can lead to easily desorption of the biomolecules.[114] In addition, the uncontrolled interaction of the biomolecules with the surface can cause denaturation, unfolding or loss of affinity for the analyte. In order to avoid the direct contact of the biorecognition element with the sensor surface, immobilization can be performed by **physical entrapment** in a polymer matrix (Figure 1.12b). The most common polymers employed are polyaniline, polythiophen, polypyrrole or dextran-based polymers, which create uniform matrices allowing the inclusion of the bioreceptors as guest molecules in a single step. This procedure permits the immobilization without any modification of the receptor ensuring its biological activity, and provides a better environment for the preservation of the immobilized molecules during prolonged storage. However it can present important diffusion and mass transport problems of the analyte toward the entrapped bioreceptors.[115]

Due to the above-described drawbacks, biofunctionalization is usually done via **Self-Assembled Monolayers** (SAM) (Figure 1.12c). SAMs basically consist of amphiphilic molecules that self-organize onto the sensor surface creating a tight and ordered matrix. The external functional groups of the SAMs can be activated to link molecules in a covalent manner. This procedure offers important benefits like the high robustness and stability of the immobilization or the possibility to control the bioreceptor packing density by using lateral spacers. Another variant makes use of heterobifunctional polymers, such as polyethylene glycol (PEG), to create the functional layer. The use of PEGylated compounds, due to the high hydrophilicity and protein adsorption resistance, provide advantages in terms of antifouling or biocompatibility.[116]

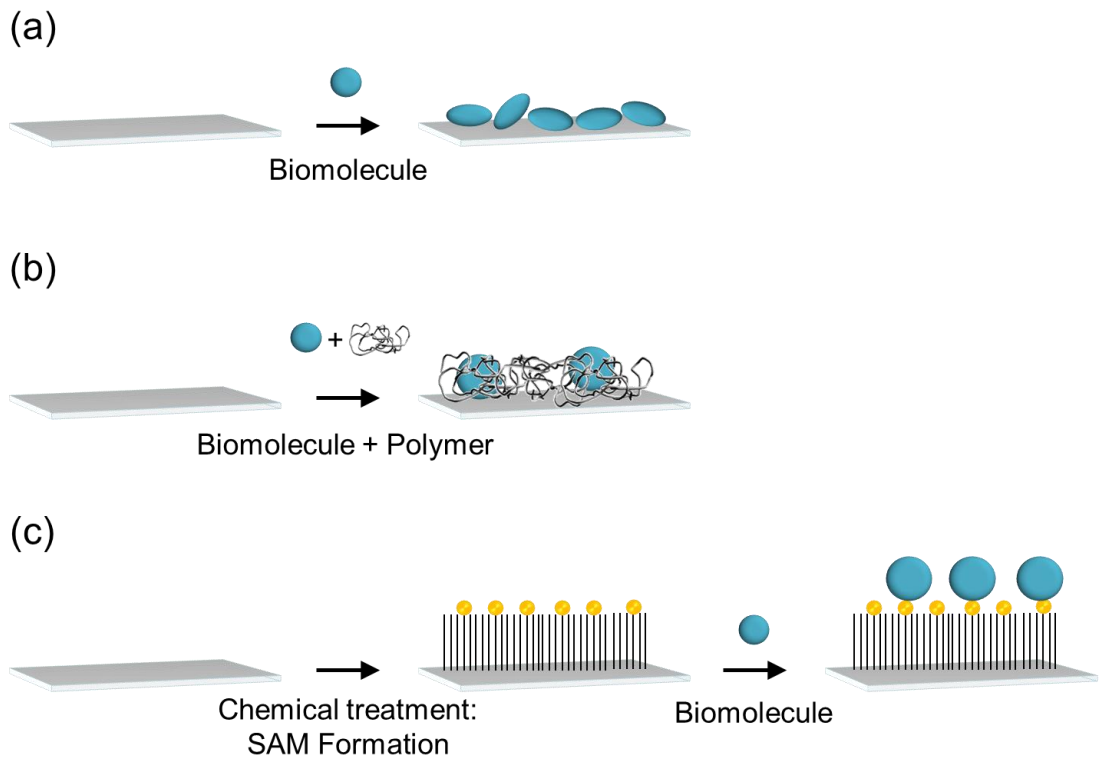

Figure 1.12 Main types of biofunctionalization processes: **(a)** physical adsorption, **(b)** polymer entrapment and **(c)** covalent binding to a self-assembled monolayer (SAM).

For protein immobilization, the covalent binding takes advantage of the aminoacid sequence of the biomolecule, mainly using the exposed amine groups of Lysine (Lys) residues. Amine groups readily react with supports bearing active esters (e.g. NHS ester) to form stable amide bonds. Besides, aldehyde groups or epoxides can also be coupled to amines resulting in a secondary amine linkage. Alternatively, carboxylic groups from aspartic (Asp) and glutamic (Glu) acids or thiol groups from cysteines (Cys) can be used as anchoring points by linker molecules such as

succinimide ester or carbodiimides, that in turn are linked to the surface previously modified with carboxyl, amine or thiol groups.

In the case of nucleic acid immobilization, the versatility of DNA synthesis allows the direct incorporation of the desired functional groups at the end of the sequence. Therefore, capture probes can be designed for any particular surface chemistry. Both approaches are universally applicable to any protein or modified-DNA sequence, but the efficiency of the attachment to the surface depends on many factors (i.e. pH, concentration, ionic strength and reaction time) that must be optimized to enhance the yield of the chemical process. In addition to the conventional covalent binding, numerous immobilization strategies have been developed for a wide variety of chemically functionalized surfaces, including photoactive reactions or *click* chemistry.[117]

The choice of the biofunctionalization strategy ultimately depends on the purpose of the study and the receptor characteristics. In some cases, for example when enzymes or antibodies are employed as biorecognition elements, the site-specific interaction with the target molecule requires an oriented immobilization avoiding the modification of the binding sites. To this end, other functionalization strategies have been developed such as the biotin-streptavidin affinity system or by using cofactors or site-directed affinity proteins.[118, 119] Although offering site-specific functionalization, these methodologies have some drawbacks related to the chemical modification of native biomolecules, the need of multi-step procedures or stability problems.

Another important aspect in biofunctionalization is related to the surface regeneration, that is, the removal of the target analyte after the detection step without altering the immobilized receptor molecule. Efficient regeneration would provide reusability of the surface, which is particularly important not only to save costs and time, but also to evaluate the stability and robustness of the bioactive surface. Typically, regeneration can be accomplished by injecting a low or high pH solution (e.g. HCl, NaOH, glycine, etc.) that disrupt the biochemical interaction between the target analyte and the bioreceptor. Other methods make use of ionic strength changes (e.g. high/low salt content buffers) or specific chemicals (e.g. formamide for DNA dehybridization) to break the interaction. Nevertheless, the regeneration procedure has to be evaluated empirically since the combination of binding forces is often unknown, and it is important to select the mildest regeneration conditions that assure the stability and integrity of the bioactive layer.

On the other hand, one of the crucial factors in biosensor functionalization nowadays is related to the selectivity and antifouling properties of the biorecognition layer. Especially for label-free

biosensors, like the nanoplasmonic ones that detect changes in the RI (and therefore changes of mass on the surface), the nonspecific binding is a major challenge for the application to real clinical scenarios. A number of strategies have been employed to reduce the adsorption of matrix components of clinical samples: (i) the use of hydrophilic compounds like polyethylene glycol (PEG) or dextran-derivatives for surface coating, (ii) the addition of surfactants or other agents to the assay buffer, (iii) to block the surface with milk, proteins or certain polymers, or (iv) diluting the sample till the background signal is minimized. However, the effects of these approaches in the label-free analysis are not totally controlled and need to be checked for each application. Therefore there is a wide interest to develop and optimize biosensing procedures that ensure the detection selectivity while minimize at the same time the nonspecific adsorptions.

In conclusion, the advances in biosensor technology inherently involve research in surface chemistry, materials science and biological engineering. The accomplishment of highly sensitive and reliable PoC biosensors relies in the achievement of optimum biofunctionalization strategies that provide specific control of the receptor immobilization, ensuring the affinity and stability, and maximizing the surface antifouling properties.

1.3. The Role of Antibodies in Biosensors

Antibodies (Ab) are glycoproteins belonging to the Immunoglobulins (Ig) family which are produced by B cells in plasma and used by the immune system of vertebrates to identify and neutralize foreign agents in the body, known as antigens. The basic structure of an antibody is outlined in Figure 1.13. An antibody is a Y-shaped molecule presenting four polypeptide chains, two heavy (H) chains with molecular weights of 50 kDa and two light (L) chains with molecular weights of 25 kDa, linked by disulfide bonds. The chains have both constant (C) and variable (V) regions. Antigen recognition is mediated by the variable light (V_L) and heavy (V_H) domains, known as the Fab (Fragment antigen-binding) region, situated at the arms of the Y. The base of the Y is composed of constant domains of the two H chains. This region is called Fc (Fragment crystallizable) region and plays a role in the immune cell activity, ensuring that each antibody generates an appropriate immune response for a given antigen, by binding to a specific class of Fc receptors and other immune molecules.

The estimated molecular dimensions of the antibodies are 15 x 7 x 3.5 nm (although the immunoglobulins are highly flexible).[120] In mammalian cells, there are five classes of immunoglobulins which are distinguished by their heavy chains: IgA, IgD, IgG, IgM and IgE. Different isotypes are generated during gene rearrangement, resulting in a series of structural

changes that confer different functions in the organism. IgA forms a dimer molecule and is mainly found in mucosal areas (e.g. gut, respiratory track or urogenital track). It prevents the colonization by foreign pathogens. IgD and IgM are related with the immunologic response mechanism: IgD acts as antigen receptor in B cells and activates basophils and mast cells; IgM in turn is secreted from B cells forming a pentameric molecule to eliminate pathogens at early stages of the humoral response. IgE is the antibody involved in allergic processes; it binds to allergens and triggers the histamine release from mast cells and basophils. Finally, IgG is the predominant class of antibody produced during mature immune response, being the only isotype able to cross the placenta to give passive immunity to the fetus. IgG provides the majority of the antibody-based immunity against pathogens and thereby it is the most studied and employed in biosciences.

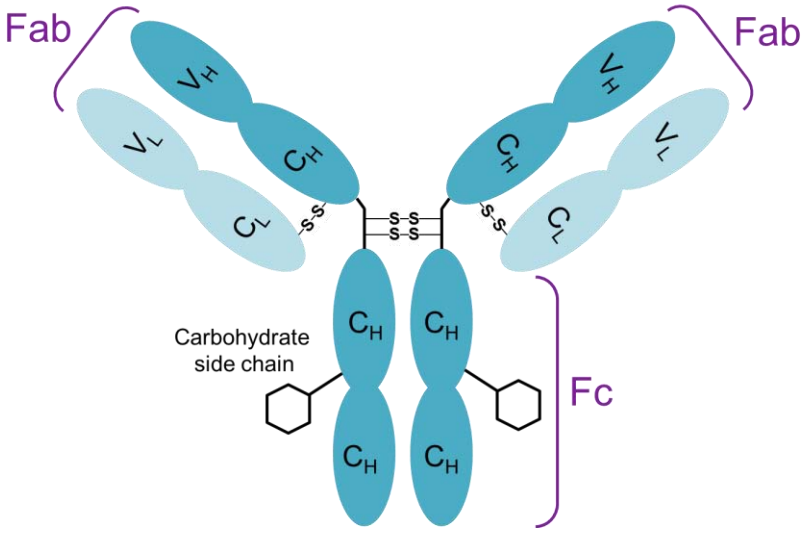

Figure 1.13 Basic structure of an antibody.

Due to the exceptional affinity and specificity for antigen binding together with the important role in the human immune response, antibodies are widely used in the biomedical field, either as biorecognition elements for immunochemical analysis or as clinical biomarkers for diagnostics.

1.3.1. Antibodies as Biorecognition Elements

Immunochemical techniques cover all those analytical methodologies that involve the interaction between a specific antibody and its target molecule. Among them, immunoassays are the most

widely used technique to determine the presence of an analyte in a sample in a qualitative, semiquantitative or quantitative way.

Antibodies can be produced in the laboratory for the specific recognition of a vast number of analytes, either biological molecules (such as hormones, proteins, peptides, etc.) or other chemical compounds of analytical interest (drugs, pollutants, etc.). Furthermore, progress in biotechnology and molecular biology is providing novel tools and techniques for more efficient and simple antibody production as well as for enhancing the affinity and specificity of the immunoglobulins. Depending on the production process, the antibodies can be polyclonal (pAb), monoclonal (mAb) or recombinant (rAb). **Polyclonal antibodies** are directly obtained from the immunized serum of an animal, therefore deriving from multiple clones of B cells.[121] Each clone recognizes different binding sites of the antigens (known as epitopes), each one showing different affinity and specificity. Thus, the polyclonal sera recognize the global structure of the immunogen. Main problems of pAb are the restricted production to limited amounts from the same specimen and the inherent variability between animals. **Monoclonal antibodies** are produced by the fusion of antibody-producing spleen cells from an immunized animal (usually mice) with mutant tumor cells derived from myelomas (a single clonal B cell hybridoma). A unique IgG molecule is obtained from a single cell clone, so each mAb is specific for one epitope.[122] Commonly, they are obtained from highly stable and immortal cell lines providing an unlimited source of antibodies with identical affinity for the antigen as long as the hybridoma line is stable. The screening process to isolate the desired clone is long and complex, the cost of production is higher than for pAbs, but they are obtained in large quantities with low variability and usually present higher specificity for the antigens.[123] Finally, **recombinant antibodies** are the result of genetic engineering, producing antibody fragments with improved or modulated affinities and specificities from simple hosts as yeast, plants, bacteria or even insect cells.[124-126] These antibodies were initially designed for therapeutic purposes, but they have also been used in immunochemical analysis. Production of rAb consists of several steps involving the isolation and cloning of encoding mRNA from immunized cells, expression in the host and screening for antigen specificity.[127] Although rAb can *a priori* provide certain advantages in terms of sensitivity and selectivity, main limitations are nowadays related to the cost and more laborious techniques involved in their production.

Generally, immunoassays are classified according to whether it is necessary to separate the immunocomplex prior to the analyte determination. *Heterogeneous* immunoassays require previous separation of the antibody-antigen complex to avoid interferences, and therefore they

are usually performed on a solid phase. In *homogeneous* immunoassays all the reagents are in solution and the detection can be directly carried out during the immunochemical reaction. Additionally, immunoassays can be distinguished by the type of label employed in the detection: radioactive, enzymatic, fluorescent or chemiluminescent.

Immunoassays can also be categorized according to two different detection formats: (i) non-competitive and (ii) competitive assays (Figure 1.14). The format is chosen on the basis of the size of the target analyte molecule, binding characteristics, dynamic range and sample matrix. In the particular case of label-free techniques, the formats are as follows: in **non-competitive immunoassays**, the antibody is immobilized on a solid support and the analyte is directly captured from the sample (Figure 1.14a). The direct immunoassay is preferred in applications where the analyte produces sufficient response by simple binding to antibody, typically because of high concentration or large size of the analyte (high molecular weight). Usually, the sensitivity and selectivity of the assay is improved by sandwich amplification (Figure 1.14b) which employs a second specific antibody to interact with the captured analyte molecules. Sandwich detection format requires large analytes presenting two different epitopes to allow the interaction with two different antibodies (a capture and a detection antibody). When analytes are not big enough to be directly detected, **competitive immunoassays** are performed. In direct competitive immunoassays (Figure 1.14c) the specific antibody is immobilized on the surface and the sample containing the target analyte is added together with a conjugated or larger analyte (competitor), thus establishing a competition between the two molecules to interact with the antibody. In this case, the labelled analyte is the one detected; hence the signal is inversely proportional to the analyte concentration. Finally, indirect competitive immunoassays (Figure 1.14d) consist of incubating a certain concentration of antibody with the analyte in solution. The mixture then is added to the surface, where an analogue or a conjugate of the analyte has been previously immobilized (coating antigen). Again, a competition is established between the three species, and the free unbound antibody interacts with the coating antigen, generating also a response inversely proportional to the analyte concentration in the sample. This competitive approach offers benefits in terms of sensitivity and stability when compared to direct immunoassay. Generally, the immobilization of antibodies on solid supports diminishes the biological activity either by alteration of the antigen binding sites or by the use of harsh conditions to regenerate the biosurface. Indirect competitive immunoassay employ native or intact antibodies for the analyte recognition and immobilized antigen, and is usually less prone to degradation or to lose

properties, ensuring the reutilization and stability of the sensor for a presumably higher number of analysis.

In biosensor research, antibodies are considered the landmark biorecognition elements, and they are used for countless applications in the clinical field, but also in environmental monitoring, drug discovery, food safety, etc. Recently, major efforts are directed not only to improve the inherent antibody recognition capabilities (i.e. affinity and specificity) but to develop novel conjugation, labelling or immobilization techniques that enhance the detectability and maximize the reproducibility and accuracy of the analysis.

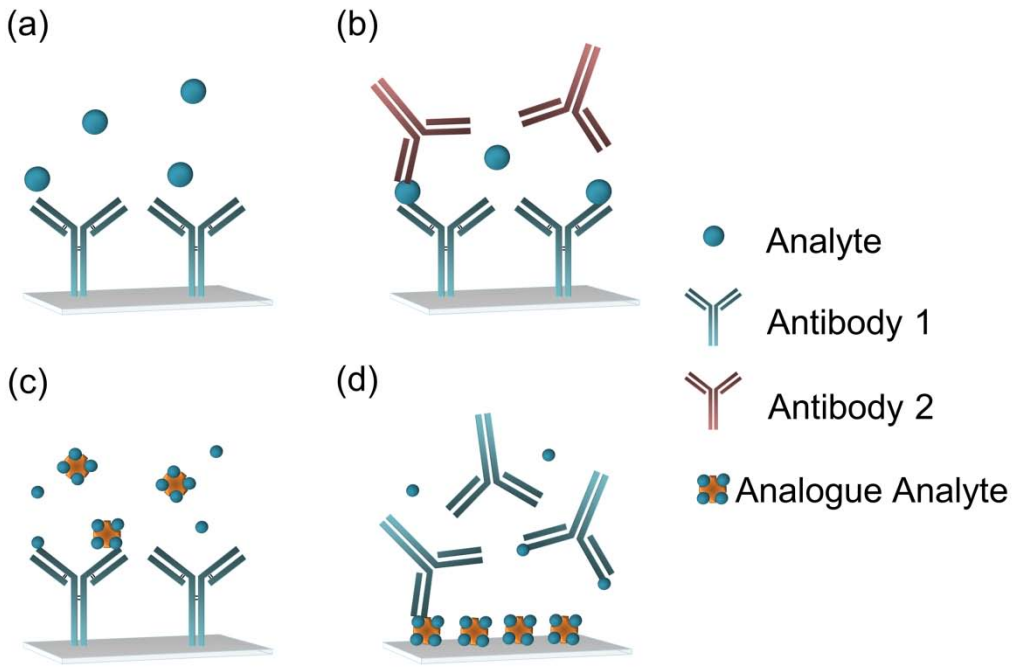

Figure 1.14 Main formats of immunoassay: **(a)** non-competitive direct detection, **(b)** sandwich amplification, **(c)** competitive direct detection and **(d)** competitive indirect detection.

1.3.2. Antibodies as Biomarkers

The immune system functions as a surveillance mechanism against foreign agents and infectious organisms. It responds to pathogens through two main defense mechanisms: the non-adaptive (innate) and the adaptive (acquired) immunity.[128] Non-adaptive immunity is a general nonspecific response to prevent penetration and spread of the infectious agents, including phagocytosis (macrophages), cell lysis (natural killer cells) and a variety of chemical molecules and

physicochemical changes. The adaptive immunity is mediated by the B lymphocytes (specific white blood cells), which synthesize cell surface receptors and secrete the specific immunoglobulins (antibodies) against the foreign molecules. Adaptive immunity has the ability to be acquired or improved after exposure to specific molecules, but it can also be modified or suppressed due to illness or medical conditions.

Antibodies are blood circulating proteins involved in several defense mechanisms such as phagocytosis, inactivation of toxic substances, the direct attack to viruses and bacteria, the activation of the complement system or helping natural killer cells to suppress infected or cancer cells. The presence or altered levels of specific antibodies in blood can be directly related to the appearance, stage or progress of diseases. For example allergies,[129, 130] autoimmune diseases[131, 132] or some infectious,[133] can be diagnosed by determination of specific antibodies in blood.

Lately, scientific interest has been focused on discovering new specific antibody patterns related to diverse human diseases, including oncological,[134] inflammatory[135] or neurological and psychiatric disorders, such as Alzheimer disease.[136] The analysis of these novel biomarkers is potentially useful along with the complete diagnosis and evolution of the disease. Before diagnosis, they can be employed for screening and risk assessment. During diagnosis, antibody levels can determine staging, grading and selection of the initial therapy. And later, they can be used for therapy follow-up, to select additional treatment or to monitor recurrent diseases. Furthermore, antibodies are usually generated in relative large amounts – compared to disease-associate antigens – and they are highly stable biomolecules in serum, representing a valuable circulating biomarker for clinical and biomedical analysis.

Chapter 2

MATERIALS AND METHODS

A description of the materials and procedures employed throughout this doctoral work is summarized. A detailed explanation of both SPR- and LSPR-based biosensor schemes is provided, followed by the nanofabrication protocol of the nanoplasmonic substrates and bulk sensitivity characterization. Also a list of all chemical reagents, buffers and biological compounds is included. Finally, the chapter describes the biofunctionalization protocols and the different assay formats employed, whose results are presented in this dissertation.

2. Materials and Methods

2.1. Biosensor platforms

2.1.1. SPR Biosensor

One of the SPR biosensors employed in this work was developed in our research group in 2004 and was commercialized by the spin-off company Sensia S.L. (www.sensia.es), which currently belongs to Mondragon Corporation (www.mondragon-corporation.com). The SENSIA SPR biosensor is integrated in a reduced platform and can be used as a portable and easy-to-use device (Figure 2.1a). The sensor platform is based on the Kretschmann configuration that allows the real-time monitoring of the intensity of the reflected light at a fixed angle of incidence. Excitation is carried out with a diode laser (RS 194-032, Amidata, Spain), emitting at 670 nm. The laser beam is divided in two identical intensity beams using a light splitter (5 mm/side cube) to enable the simultaneous evaluation in two independent channels. The laser beams pass through a glass coupling prism (n = 1.52), reaching the backside of the gold sensor chip *via* a RI matching oil (n ≈ 1.515) (Figure 2.1b).

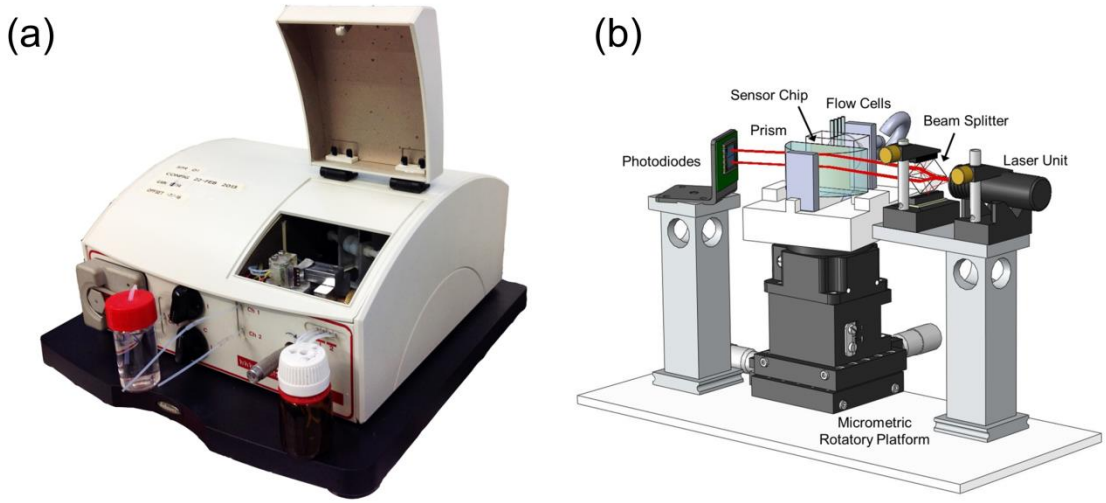

Figure 2.1 (a) SENSIA SPR Biosensor device; **(b)** Schematic representation of the sensor module of the SENSIA SPR Biosensor.

The sensor chips consist of a glass surface (10 × 10 × 0.3 mm) coated with 2 nm of chromium and 45 nm of gold (Ssens, The Netherlands). The gold sensor surface contacts two identical flow cells of approximately 300 nL volume each one, where the biomolecular interaction takes place. Biological events occurring at the sensor surface are detected as changes in the reflected light

intensity by a multielement photodiode (S5870, Hamamatsu, Japan). This part of the setup is mounted on a rotary platform in order to select the optimum incidence angle that maximizes the changes of reflected light intensity. The device also incorporates all electronics and fluidics components necessary to operate autonomously. The fluidic system consists on a peristaltic pump which keeps a continuous flow and a set of tubing and valves for the sample handling and injection to the flow cuvette.

A custom-made software in Labview controls the flow rate and injection of the sample as well as the monitoring of the binding events. Sensorgrams reproduce the interaction as an increase (or decrease in case of unbinding events) of the normalized intensity of the reflected light (%ΔR) *vs.* time. Figure 2.2 represents typical sensorgrams obtained with the SPR biosensor. Binding events lead to positive changes of the baseline while unbinding events lead to negative variations. Signals are determined by measuring the absolute value of the baseline variation after the biochemical interaction. Data analysis was carried out using OriginPro 8.0 software.

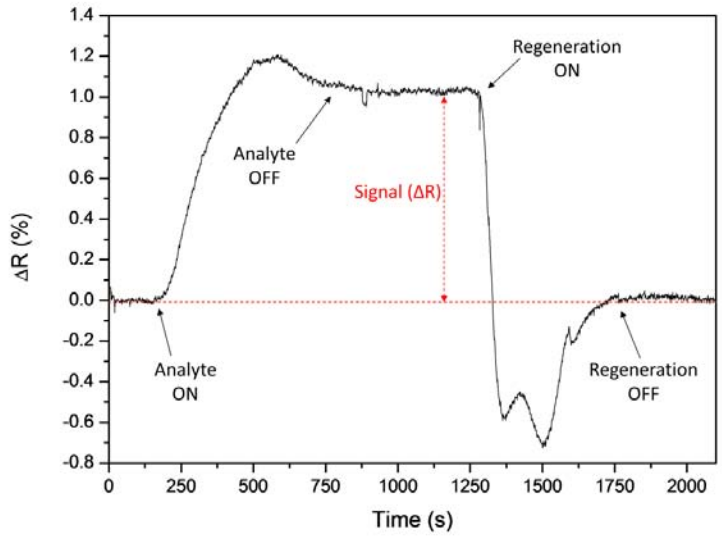

Figure 2.2 Typical SPR sensorgrams representing detection of an analyte and regeneration of the bioreceptor surface.

2.1.2. Nanoplasmonic Biosensor

The nanoplasmonic biosensor used is based on a novel in-plane waveguiding mechanism in thin layers of plasmonic nanodisks, whose excitation can be accomplished in total internal reflection.[137] The in-plane LSPR excitation leads to a strong enhancement of the polarizability of the nanodisks, creating an effective RI that is sufficiently large to support a guided mode inside a thin and sparse monolayer of nanostructures.

The nanostructured substrates are clamped between a trapezoidal glass prism (n = 1.52) contacting the sample through a RI matching oil (n ≈ 1.512) and a custom-made Delrin flow cell (volume = 4 µL), connected to a microfluidic system comprising a syringe pump (NE-1000, New Era, USA) that ensures a constant flow and a manually operated injection valve (V-451, IDEX Health and Science, USA). The LSPR is excited by a collimated halogen light source (HL-2000, Micro-Pack, Ocean Optics, USA). The light reaches the substrates through the prism and the reflected light is collected and fiber-coupled to a CCD spectrometer (Jazz Module, Ocean Optics, USA) (Figure 2.3). The setup design involves a triangular platform with lateral sides designed at certain angle with attached rails that incorporates the optical components, ensuring that incoming and outgoing optical paths remain constant.

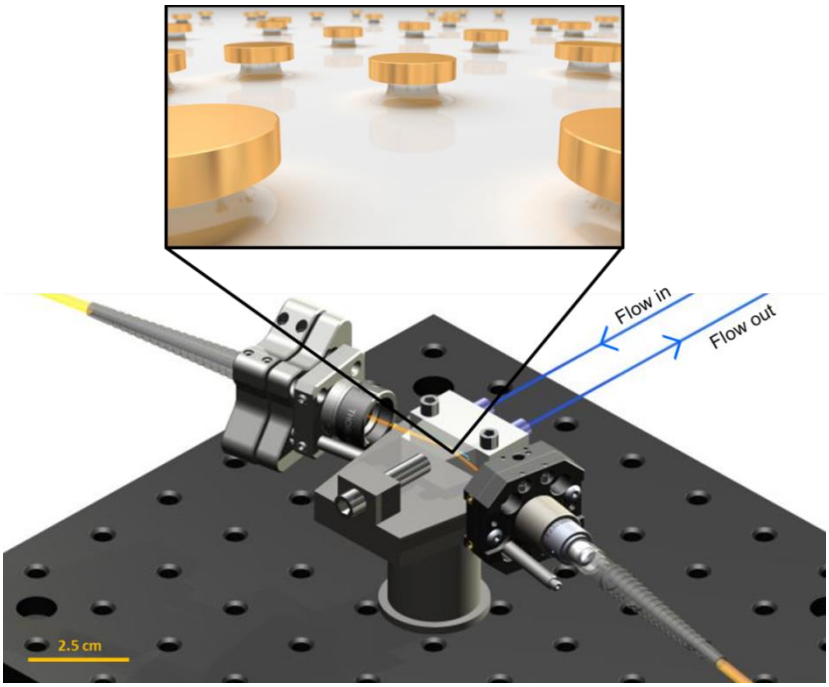

Figure 2.3 Schematic representation of the LSPR biosensor platform.

Two analogue setups were designed with different angle of incidence of the light: 70° and 80°. The 70°-setup permit the employment of the platform either for nanoplasmonic measurements, by setting the incident light in TE polarization for gold nanodisks LSPR excitation, or for conventional SPR measurements, by setting the incident light in TM polarization for thin film gold SPR excitation. The 80°-setup operates only for nanoplasmonic measurements.

Reflectivity spectra are acquired every 3 ms, and 300 consecutive spectra are averaged to provide the spectrum to be analyzed. Tracking of the real-time resonance peak position is achieved *via*

polynomial fit using a homemade readout software. Sensorgrams reproduce the biomolecular interaction by monitoring spectral displacement of the resonance peak ($\Delta\lambda_{LSPR}$) *vs.* time (Figure 2.4). Biomolecular binding events produce shifts to higher λ, while unbinding events produce shifts to lower λ. Signals are determined as the absolute value of the $\Delta\lambda_{LSPR}$ after the biochemical interaction. Data analysis was carried out using OriginPro 8.0 software.

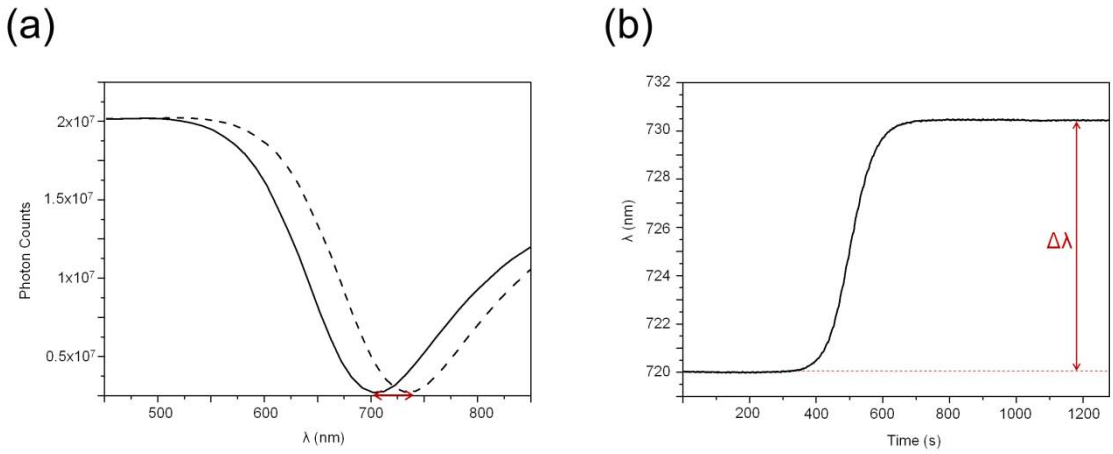

Figure 2.4 Typical sensorgrams representing a biomolecular binding event: **(a)** graph showing the spectral shift (photon counts *vs*. λ); **(b)** graph showing the shift of the resonant peak over time ($\Delta\lambda_{LSPR}$ *vs.* time).

2.1.3. Nanoplasmonic Sensor Chip Fabrication

Nanoplasmonic substrates consists of short-ordered arrays of gold nanodisks (Diameter ≈ 100 nm, Heigh ≈ 20 nm, F = 6-7%) fabricated by Hole-Mask Colloidal Lithography (HCL).[138] First, SiO_2 substrates (nr. 4, Menzel-Gläser, Germany) are cleaned by placing them 20 min in a freshly prepared piranha solution (3:1 H_2SO_4/H_2O_2). After drying with N_2, the HCL process is carried out following the next protocol (Figure 2.5):

1) Polystyrene Bead Deposition. An approximately 200 nm thick layer of 950 K PMMA (4% in Anisol) are spin-coated on clean SiO_2 substrates (4000 rpm, 1500 $r{\cdot}s^{-2}$). After a 5 min baking process at a temperature superior to 150°C, the substrates are subjected to a brief O_2 plasma (10 s, 75W, 75 mTorr and a 20% O_2-flux) in order to increase the hydrophilicity of the PMMA. Then, oppositely charged polyelectrolyte is drop coated on top of the PMMA layer to create an adhesive layer. For this purpose, surface is coated with 0.2 wt% PDDA (Sigma-Aldrich, Germany) for 1 min and thoroughly rinsed with H_2O and dried with N_2. As a last step, colloidal solution containing 0.2% D100 polystyrene beads (Invitrogen, USA) is deposited for 1 min, subsequently rinsing and

drying with H_2O and N_2, respectively. The electrostatic repulsion between the polystyrene beads, in combination with the attractive force that exists between these spheres and the PDDA layer, define a short-range ordered polystyrene particle array (Figure 2.5a).

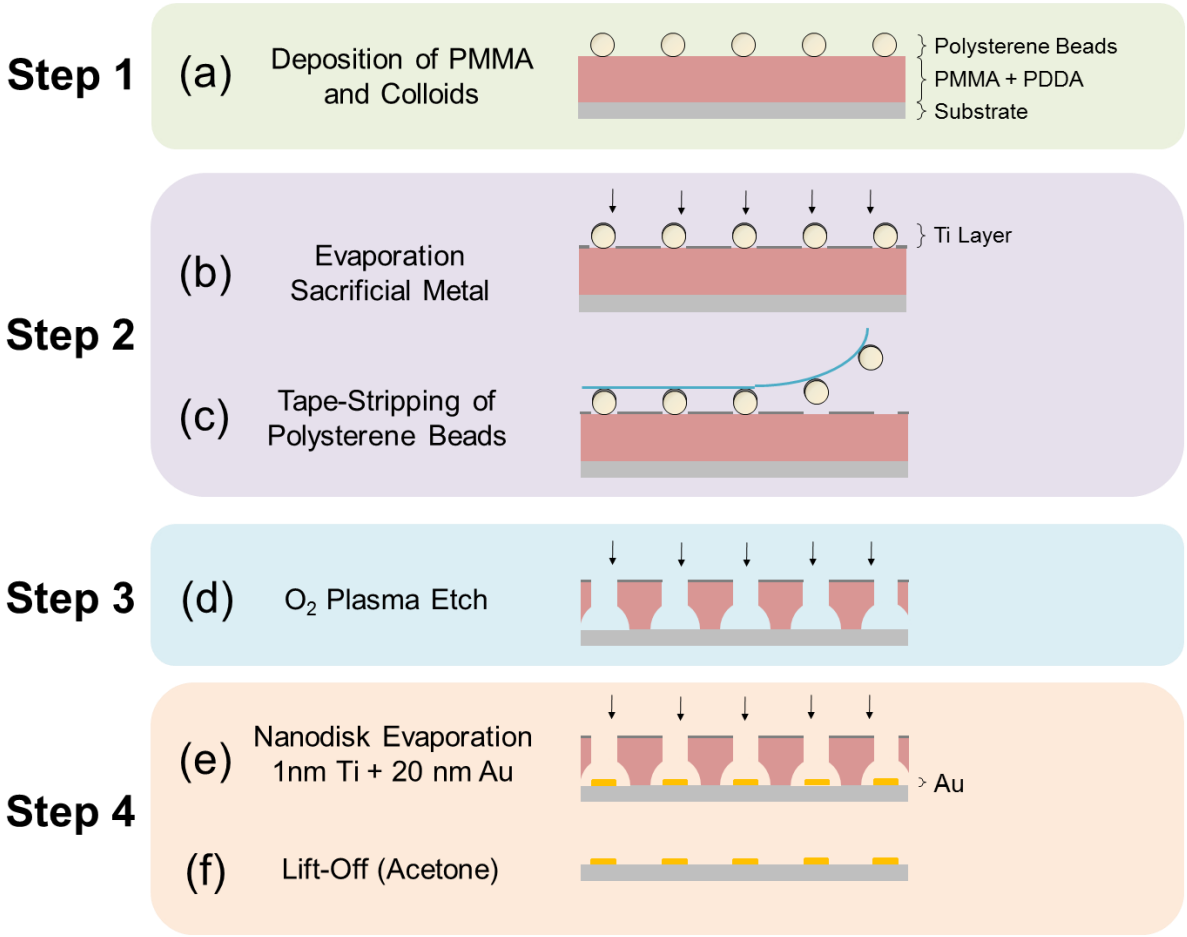

Figure 2.5 Schematic of the four steps fabrication process by hole-mask colloidal lithography These steps include: **(a)** polymer (PMMA and PDDA) deposition for the following adhesion of polystyrene beads, **(b)** evaporation of a sacrificial metal layer, **(c)** tape-stripping process of the polystyrene beads, **(d)** oxygen plasma etching for the creation of holes in the polymer layer, **(e)** evaporation of the metal adhesion layer (1 nm Ti) and the Au (typically 20 nm), and finally **(f)** removal of the remaining hole mask by a lift-off process in acetone.

2) Creation of Hole-Mask Template. The hole-mask template is created by first depositing 15 nm of Ti, as a sacrificial layer that is resistive to O_2 plasma treatments (Figure 2.5b). Secondly, the polystyrene beads are tape-stripped away, leaving a sacrificial PMMA layer with perforated Ti hole-mask on top (Figure 2.5c).

3) Oxygen Plasma Treatment. Next, an O_2 plasma treatment (180 s, 75 W, 75 mTorr and a 20% O_2-flux) is applied, removing the exposed polymer (PMMA/PDDA) underneath the holes. The

etching selectivity of the PMMA and Ti, and ion over-exposure result in under-cut features as depicted in Figure 2.5d.

4) Disk Evaporation and Lift-Off. The resulting hole-mask is used as a deposition mask for the Au nanodisks. Using electron-beam evaporation, an adhesive layer of 1 nm of Ti is deposited followed by 19 nm of Au (Figure 2.5e). The remainder of the hole-mask is removed by a lift-off process, carried out in acetone at room temperature (Figure 2.5f).

The final result is a nanostructured SiO_2 surface with Au nanodisks of approximately 20 nm of height and 100 nm of diameter (Figure 2.6). The nanodisks density (F) obtained is around 6 – 7%. Note that the nanodisks diameters and interdisk spacing are entirely governed by the properties of colloidal polystyrene bead solution (e.g. concentration, electrostatic interactions...).

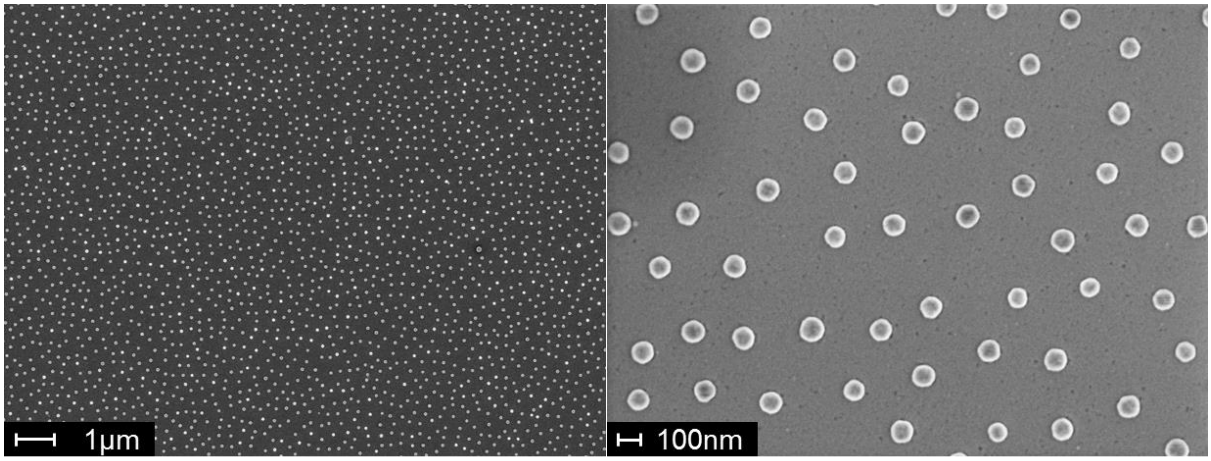

Figure 2.6 SEM images of gold nanodisks arrays fabricated on glass substrate.

2.1.4. Bulk Sensitivity Study

An evaluation of the bulk sensitivity of the two analogous nanoplasmonic biosensors (θ_1 = 70° and θ_2 = 80°) was carried out. Bulk sensitivity ($\eta_B = {}^{\Delta\lambda}/_{\Delta n}$) is defined as the variation of the resonance peak induced by RI changes of the bulk dielectric surrounding of the sensor surface. This factor is the most commonly used to quantify and compare the intrinsic sensitivities provided by plasmonic biosensor platforms. The study was performed by flowing a set of serially diluted glycerol solutions with known RI and measuring the induced $\Delta\lambda_{LSPR}$ while MilliQ water was employed as continuous running solution. Signals were plotted as a function of the RI variations ($\Delta n \approx 0.03$ RIU) showing linear dependence (Figure 2.7). Fitting to a linear regression function we can determine the η_B values for both platforms: $\eta_B(70°) \approx 100$ nm and $\eta_B(80°) \approx 375$ nm. This comparison confirmed the improved sensing performance expected at higher angles of incidence

of the light (see Introduction, section 1.2.2.2), reaching approximately 4 times better sensitivity with the 80°-setup.

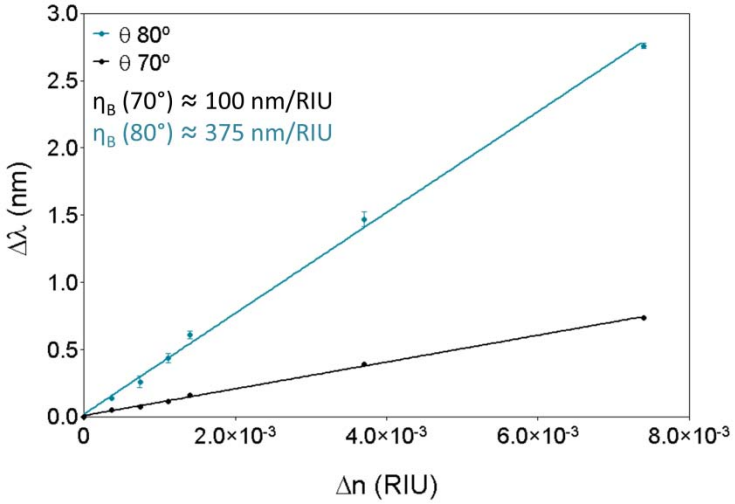

Figure 2.7 Bulk sensitivity calibration (Δn = 0.03 RIU) for the nanoplasmonic setup at different angles of incidence: 70º (black) and 80º (blue).

2.2. Chemical and Biological Reagents

2.2.1. Chemical Reagents and Buffers Composition

Main salts and chemical reagents for buffer preparation and biofunctionalization procedures were acquired from Sigma-Aldrich (Germany): alkanethiols for SAM formation (16-mercaptohexadecanoic acid (MHDA) and 11-mercaptoundecanol (MUOH)), reagents for carboxylate group activation (1-ethyl-3(3-dimethylaminopropyl)carbodiimide hydrochloride (EDC) and N-hydroxysulfosuccinimide (sulfo-NHS)), ethanolamine, crosslinking molecule (bis(sulfosuccinimidyl) suberate, BS^3), glycine, Tween 20, bovine serum albumin (BSA), sodium periodate ($NaIO_4$) and dithiothreitol (DTT). ProLinker™ B was provided by Proteogen Inc. (Korea). The copolymer poly-(L-lysine)-graft-PEG (PLL-PEG, MW~67.000 g/mol) was purchased to SuSoS (Switzerland) and diamine-PEG (NH_2-PEG-NH_2, MW 10.000 g/mol) to Laysan Bio. (USA) Amine-dextran (MW 10.000 g/mol) was obtained from Invitrogen (USA). Oligonucleotide cross-linker used for antibody conjugation (HyNic) was purchased to Solulink (USA). Commercial serum was obtained from Sigma Aldrich (Germany) and commercial plasma was purchased to Innovative Research (USA).

Several buffers have been used either for functionalization or target analysis: PBS 10 mM (10 mM phosphate, 137 mM NaCl and 2.7 mM KCl, pH 7.4), PBST (PBS buffer + 0.5% Tween 20), acetate buffer (10 mM, pH 5.0), MES buffer (0.1 M, pH 5.4) and HEPES buffer (10 mM, pH 7.0). Specific

cocktails were prepared in order to minimize nonspecific adsorptions when working with biological fluids, such as High-Blocking Buffer (HBB) (PBS buffer + 500 mM NaCl + 200 µg/mL BSA + 500 µg/mL amine-dextran + 0.5% Tween 20) or the Antifouling Buffer (AFB) (PBS buffer + 500 mM $MgCl_2$ + 2% Tween 20 + 2% commercial serum).

2.2.2. Biological Compounds

Proteins, antibodies and hormones employed for each study were obtained from different sources. For the site-specific antibody immobilization study, human Chorionic Gonadotropin (hCG) was purchased to Abcam (UK), Focal Adhesion Kinase (FAK) was obtained from OriGene (USA) and C-Reactive Protein (CRP) from AntibodyBcn (Spain). Monoclonal antibody anti-hCG was a kind gift by the Dr. Jose Miguel Rodríguez Frade from the Departamento de Immunología y Oncología, Centro Nacional de Biotecnología, CSIC (CNB-CSIC, Madrid, Spain). The antibody was purified by affinity chromatography using 1 mL HiTrap™ Protein G and PD-10 Desalting Columns (GE Healthcare, UK). Monoclonal antibody anti-FAK was supplied by BD Biosciences (USA) and monoclonal antibody anti-CRP was from AntibodyBcn (Spain). Recombinant Protein G was from Merck (Germany). Oligonucleotide used for polyA-based strategy study (d(T_{26}-A_{15}) = Amino-PolyT_{26}PolyA_{15} (C3NH_2)TTT TTT TTT TTT TTT TTT TTT TTT TTA AAA AAA AAA AAA AA) was provided by IBA Lifesciences (Germany).

For the gluten detection study, the biological material (Gliadin PWC, Gliadin-33mer-Peptide and monoclonal antibody G12) was provided by Biomedal S.L. (Spain). Gluten-free urine for the optimization and assessment study was kindly provided by a celiac patient. Urine samples with different gluten content were provided by the Hospital Virgen del Rocío (Sevilla, Spain) and from healthy volunteers. For the allergy diagnosis application, dendrimers PAMAMG2-AXO and BAPADG2-AXO were provided by the Department of Organic Chemistry (University of Malaga, Spain) and the clinical serum samples were obtained from the Hospital of Malaga (Spain). The monoclonal antibody anti-Penicillin IgG was purchased to Acris Antibodies (Germany). Finally, for the study of TAA autoantibodies detection, the recombinant TAAs (GTF2b and EDIL3) were provided by the Centro de Investigaciones Biológicas, CSIC (CIB-CSIC, Madrid, Spain) and clinical serum samples were obtained from the Hospital de Gijón (Spain). The specific antibodies anti-GTF2b and anti-EDIL3 were purchased to Santa Cruz Biotechnology (USA) and Abcam (UK), respectively.

2.3. Biofunctionalization Procedures

Prior to surface functionalization, both gold and nanodisks sensor chips are subjected to a cleaning procedure consisting of consecutive 1 min sonication cycles in acetone, ethanol and MilliQ water, respectively, dried with N_2 stream and placed in an UV/O_3 generator (BioForce Nanosciences, USA) for 20 min, after which they are rinsed with ethanol and water and dried with N_2.

In the following, we provide detailed descriptions of the different biofunctionalization procedures used in this dissertation. The chapter in which each strategy is employed is also indicated.

2.3.1. Amine-reactive Antibody Covalent Immobilization (Chapter 3)

Formation of a mixed self-assembled monolayer (SAM) of carboxylic/alcohol-ended alkanethiols was carried out *ex situ*, by coating the sensor chip overnight at room temperature (RT) with a mixed solution of MHDA/MUOH in ethanol. A molar ratio of 1:20 and total alkanethiol concentration of 250 µM was used for antibody immobilization. Once the SAM is formed, the chip was rinsed with ethanol and MilliQ water, dried with N_2 stream and mounted on the sensor platform. MilliQ water was selected as running buffer for the immobilization procedure at a constant rate of 25 µL/min approximately. Activation of carboxylic groups was performed by flowing a 0.2M EDC/0.05 M sulfo-NHS solution in MES buffer for 20 min, followed by the antibody solution in PBS buffer. Finally, 1M ethanolamine solution (pH 8.5) was used to deactivate the unreacted carboxylic groups. Figure 2.8 illustrates a standard covalent immobilization sensorgram obtained with the SPR biosensor.

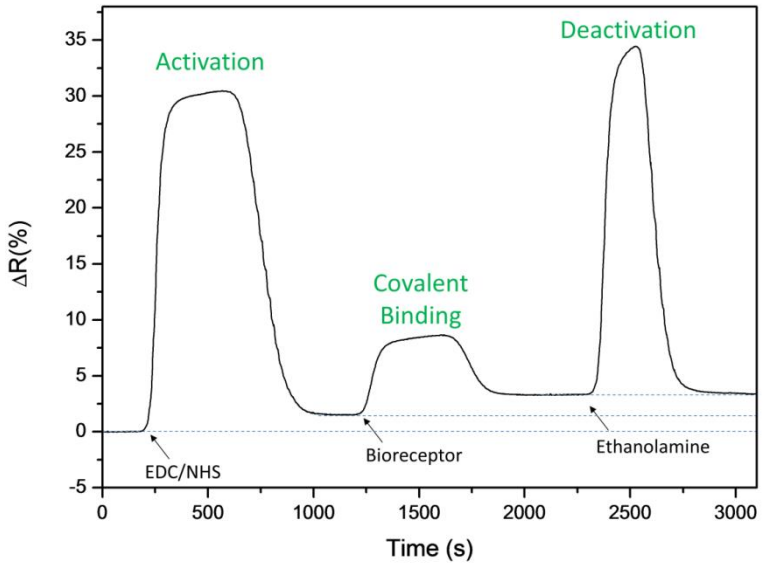

Figure 2.8 Representative SPR sensorgram of a typical covalent immobilization procedure.

2.3.2. Protein G-mediated Antibody Immobilization (Chapter 3)

Protein G diluted in PBS (50 µg/mL) was immobilized by covalent binding to the mixed alkanethiol SAM (1:20, 250 µM) formed as described above. Then, the antibody was injected in acetate buffer and once captured by Protein G, the crosslinker BS3 dissolved in PBS was flowed (1000-fold molar excess with respect to antibody concentration). In order to quench crosslinking reaction and remove unreacted molecules, 100 mM Glycine-HCl solution (pH 2.7) was injected.

2.3.3. ProLinker™ B Antibody Immobilization (Chapter 3)

ProLinker™ B layer was formed by incubating the sensor chip in a 3 mM ProLinker™ B solution in chloroform for 1 hour at RT. Next, the surface was rinsed with chloroform, acetone, ethanol and water; dried with N_2 stream and mounted on the sensor. Antibody solution in PBS buffer was injected at 25 µL/min followed by a BSA solution (100 µg/mL in PBS) to block remaining free areas. For the evaluation of the behaviour of the biological fluids, the concentration of the different blocking agents tested (BSA, amino-PEG, PLL-PEG and amino-dextran) was increased to 1 mg/mL.

For contact angle characterization, the immobilization procedure was carried out *ex situ*. After ProLinker™ B layer formation, the sensor surface was coated with the antibody solution in PBS for 30 min, then rinsed with PBS and MilliQ water and carefully dried with N_2 stream. Next, the sensor chip was coated with the BSA solution for 30 min and rinsed and dried again. Drop shape analysis was performed with Easy drop standard (Krüss, Germany), placing a 5 µL water drop onto the surface by triplicate.

2.3.4. PolyA-based Antibody Immobilization (Chapter 3)

Antibody oxidation was achieved by incubating 1 mg/mL of antibody in 10 mM $NaIO_4$ in acetate buffer for 30 min at RT in dark. Then, the antibody was purified using 30K centrifugal filter units (Amicon Ultra, Millipore, USA) and buffer was changed to Conjugation Buffer (Na_2HPO_4 100 mM, NaCl 150 mM, pH 6.0). In parallel, oligonucleotide modification with HyNic crosslinker was carried out following SoluLink instructions: 1 mM of d(T_{26}-A_{15}) was dissolved in Modification Buffer (Na_2HPO_4 100 mM, NaCl 150 mM, pH 8.0) on one hand and 200 mM succinimidyl-6-hydrazino-nicotinamide (s-HyNic) was dissolved in anhydrous dimethylformamide (DMF) on the other. 20 molar equivalents of HyNic solution were added to the oligonucleotide solution, keeping the percentage of DMF (vol/vol) in the final reaction mixture at or below 5% of the total reaction volume. The mixture was incubated for 1.5 hours at RT, purified using 3K centrifugal filter units and desalted to Conjugation Buffer. To carry out the conjugation procedure both solutions were

mixed (Ab:Oligonucleotide 1:2) and 100 mM aniline was added as catalyst. The mixture was incubated with gentle agitation for 2 hours at RT and then it was purified using 30K centrifugal filter units and buffer was changed to PBS. Characterization was carried out by spectroscopic determination using a UV Cary 4000 Spectrometer and measuring absorbance at λ = 350 nm. Final concentration of the conjugate was also determined by measuring antibody absorbance at λ = 280 nm.

Immobilization of the antibody-polyA conjugate was carried out in flow by injecting the desired concentration of antibody diluted in $CaCl_2$-TE buffer (1 M $CaCl_2$, 10 mM Tris, 1 mM EDTA, pH 7) at 20 µL/min.

2.3.5. PWG Gliadin Immobilization (Chapter 4)

PWG Gliadin was immobilized onto a carboxyalkanethiol SAM *via* the amine terminal groups of the amino acids presents in the protein, similarly to antibody immobilization. Optimized conditions for alkanethiol SAM formation resulted in 1:1 MHDA:MUOH 250 µM in ethanol for 5 hours at RT. After SAM formation, surface was rinsed with ethanol and MilliQ water and dried with N_2 stream. Activation of carboxylic groups was carried out *ex situ* by coating the chip with a 0.2M EDC/0.05M sulfo-NHS solution in MES for 20 min at RT and then rinsed with MilliQ water and dried. Rapidly, the surface was coated with PWG Gliadin solution in PBS and incubated overnight at 4°C. Finally, the biofunctionalized sensor chip was rinsed with PBS and MilliQ water, carefully dried with N_2 stream and mounted on the sensing platform.

2.3.6. d-BAPADG2-AXO Immobilization (Chapter 5)

In order to obtain the thiol functional d-BAPADG2-AXO a reduction procedure was carried out by incubating with 10 mM DDT in MilliQ water during 15 minutes and gentle agitation. Rapidly, the solution was flowed over the gold nanodisks sensor surface keeping a constant MilliQ water flow of 15 µL/min. The non-sensing glass areas were covered with PLL-PEG at 0.5 mg/mL in HEPES buffer to prevent nonspecific adsorption.

2.3.7. PAMAMG2-AXO Immobilization (Chapter 5)

For the immobilization of PAMAMG2-AXO dendrimer, gold nanodisks sensors were primarily functionalized by coating them with a 1:20 MHDA/MUOH SAM at 250 µM in ethanol overnight at RT. After rinsing with ethanol and MilliQ water and drying with N_2 stream the nanoplasmonic sensor surface was mounted on the sensing platform. PAMAMG2-AXO was covalently bound to the SAM *via* the amine group present in the peripheral AXO structure and employing the

EDC/NHS chemistry described previously. The procedure was carried out in flow at a constant rate of 25 µL/min and keeping MilliQ water as running buffer. Finally, 1M ethanolamine solution was used to deactivate unreacted carboxylic groups.

2.3.8. TAA Immobilization (Chapter 6)

Both tumor-associate antigens (TAA) (GTF2b and EDIL3) were immobilized to gold nanodisks sensor surfaces by covalent linking through the lysine groups of the proteins. A carboxylic-functional monolayer was employed as chemical matrix, coating the nanoplasmonic sensor surfaces with 250 µM MHDA in ethanol for 5h at RT. Then, surface was rinsed with ethanol and MilliQ water and dried with N_2 stream. Activation of carboxylic groups was carried out *ex situ* by coating the sensor chip with a 0.2M EDC/0.05M NHS solution in MES for 20 min at RT and then rinsed with MilliQ water and dried. Rapidly, the surface was immersed on the TAA solution in PBS and incubated overnight at 4°C. Finally, biofunctionalized sensors were carefully rinsed with PBS and MilliQ water, dried with N_2 stream and mounted in the platform.

2.4. Assay Formats

2.4.1. Direct Assay

In the direct assay approach, the receptor is immobilized onto the sensor surface, the sample is flowed and the target analyte directly detected during binding. This assay format was employed either with target proteins (as in Chapter 3) or with antibodies as target analyte (as in Chapters 5 and 6).

Generally, once the biofunctionalized procedure is completed the running buffer is changed to PBS or PBST in order to assure maximum stability of the immobilized layer and optimum conditions for the interaction. Samples containing the target were flowed over the sensor surface at 25 µL/min and the response was monitored in real-time. After each sample, regeneration of the surface was achieved by injecting a specific regeneration cocktail (e.g. HCl 5 mM or NaOH 20 mM) at 50 µL/min. Calibration curves were obtained by evaluating different analyte concentrations in triplicate. Mean and standard deviation (SD) of each signal were plotted *versus* the analyte concentration (Figure 2.9) and fitted to a one-site binding curve:

$$y = \frac{Ax}{B + x}$$

where *x* is the concentration, *y* is the response signal, *A* is the extrapolated maximum signal obtained by the specific analyte and *B* is related to the equilibrium binding constant, being the analyte concentration needed to achieve half-maximum binding at equilibrium. **Limit of Detection** (LoD) was calculated as the concentration corresponding to the blank signal plus three times its SD. **Limit of Quantitation** (LoQ) was determined as the minimum measurable signal, set as the blank signal plus 10 times its SD.

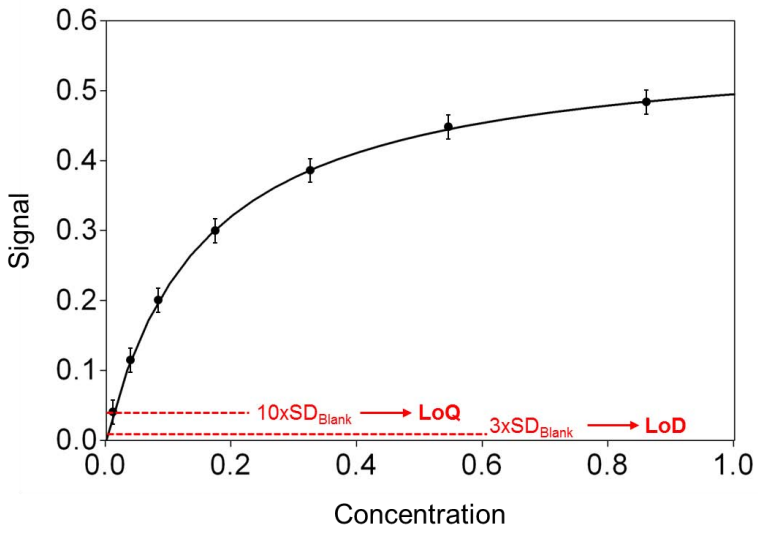

Figure 2.9 One-site specific binding curve fitting. Sensitivity parameters are defined as Limit of Detection (LoD) and Limit of Quantitation (LoQ).

2.4.2. Competitive Assay

For the competitive assay employed in Chapter 4, the sample containing the 33-mer peptide was incubated for 15 min with a fixed concentration of antibody and then flowed over the biofunctionalized sensor surface at 25 µL/min and keeping PBS or PBST as running buffer. The obtained signal resulting from the binding of the free Ab was inversely proportional to the concentration of the peptide in the sample.

Calibration curves were obtained by evaluating different concentrations of analyte in triplicate, and signals (mean ± SD) were plotted *versus* the logarithmic value of analyte concentration (Figure 2.10). Curve was fitted to a dose-response equation:

$$y = \frac{D + (A - D)}{1 + (\frac{x}{C})^B}$$

where *x* is the concentration, *y* is the response signal, *A* is the asymptotic maximum corresponding to the signal in absence of analyte, *B* is the slope at the inflection point, *C* is the inflection point, equivalent to the half inhibitory concentration IC_{50}, and *D* is the asymptotic minimum corresponding to the background signal. In this case, LoD is calculated as the analyte concentration corresponding to the 90% of the signal (IC_{90}). LoQ matches the higher limit of the dynamic range of the curve, set as the interval between the 80 – 20% of the signal (IC_{80}-IC_{20}). The IC_{50} value is commonly used in competitive assays as a measure of the sensitivity of the assay.

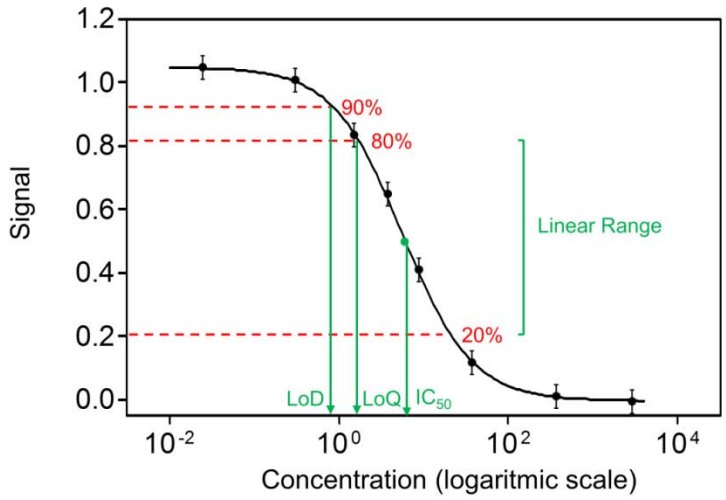

Figure 2.10 Representation of a dose-response inhibition fitting curve for different analyte concentrations. Sensitivity parameters are defined as the Limit of Detection (LoD), Limit of Quantitation (LoQ), linear range and IC_{50} value.

Chapter 3

DIRECT IMMUNOASSAY FOR PROTEIN BIOMARKERS DETECTION IN BIOLOGICAL FLUIDS

This chapter focuses on the optimization and assessment of site-specific antibody immobilization strategies for the direct detection of protein biomarkers. The biofunctionalization procedures are analyzed in terms of sensitivity, stability and selectivity. An exhaustive study for the minimization of nonspecific absorptions onto the SPR sensor surface is presented and the results are evaluated for the direct immunoassay in biological fluids. Finally, the optimum conditions have been tested with the nanoplasmonic biosensor showing promising advantages for its application in diagnosis.

3. Direct Immunoassay for Protein Biomarkers Detection in Biological Fluids

3.1. Introduction

Nowadays, main limitations for the final implementation of PoC biosensors are related to the biofunctionalization of the transducers, the stability of the biological reagents that must preserve their functionality until the biochemical interaction, and the robustness of the whole system to evaluate human samples. This challenge is particularly relevant for immunosensors in direct configuration (i.e. direct immunoassays) due to the complexity of retaining the biological activity of the antibodies during their immobilization on a solid support. This direct approach should be the preferred format for PoC diagnosis since it permits one-step analyte detection and, ideally, direct evaluation in biological fluids.

Design and optimization of proper antibody immobilization strategies is critical to maximize sensitivity, selectivity and reproducibility of the assays as well as to ensure high stability of the biofunctionalized surface. Main requirements taken into account include orientation control, minimization of random chemical modification of the antibodies and the minimization of nonspecific adsorptions. Antibodies are asymmetric biomolecules with site-specific functionalities, for example, the antigen recognition takes places exclusively at the Fab regions. Random immobilization of antibodies or arbitrary chemical modification may alter or block the antigen binding sites and hinder the analyte detection. Figure 3.1 illustrates the different orientations that antibodies can adopt when attached to a solid support: end-on (Fc closer to the surface), head-on (Fab closer to the surface), side-on (Fc and one of the Fab closer to the surface) and lying-on (Fc and the two Fab closer to the surface).

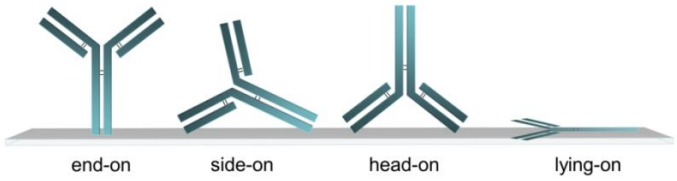

Figure 3.1 Possible orientation of antibodies immobilized on a solid surface.

Maximum detectability would be thus expected for site-directed end-on immobilization of antibodies. In addition, the size of antibodies (~150 kDa) and their surface distribution are significant factors to consider in order to avoid steric hindrance effects. Finally, the biofunctionalization strategy must also assure selective detection of the analyte in the biological

sample. This is especially relevant when working with label-free biosensors in which nonspecific adsorption onto the sensor surface may lead to false positive signals.

Many antibody immobilization strategies have been studied and developed in order to improve the overall efficiency of direct immunoassays. Table 3.1 summarizes the main advantages and drawbacks for some of the mostly employed methodologies for antibody immobilization described below.

Table 3.1 Comparison of different antibody immobilization strategies.

Immobilization Strategy	Advantages	Disadvantages
Physical adsorption	▪ Simple method ▪ No antibody modification	▪ Random orientation ▪ Antibody denaturation ▪ Poor reproducibility ▪ Nonspecific adsorptions
Amine-reactive covalent binding	▪ Stable and strong attachment ▪ Controlled distribution ▪ High reproducibility	▪ Random orientation ▪ Possible alteration of antigen binding sites
Site-directed covalent binding (e.g. carbohydrate moieties, sulfhydryl groups)	▪ Controlled orientation and distribution ▪ Stable and strong attachment	▪ Chemical modification of antibodies
Biotin/Avidin system	▪ Stable and strong attachment ▪ Controlled distribution ▪ Possible proper orientation	▪ Chemical modification of antibodies ▪ Possible alteration of antigen binding sites
DNA-mediated affinity coupling	▪ Improvements for antibody multiplexing ▪ Possible proper orientation	▪ Chemical modification of antibodies ▪ Instability under dehybridization conditions
Protein A/G-mediated Affinity Coupling	▪ Proper orientation ▪ No antibody modification	▪ Random orientation of the protein ▪ Instability under certain conditions

Physical adsorption of antibodies is the simplest methodology and it is commonly used in conventional immunoassay techniques (e.g. ELISA or antibody microarrays). It occurs *via* hydrophilic or hydrophobic interactions and can be employed to modify a wide range of solid

supports, including plastic surfaces (polystyrene and silicone), membranes (nitrocellulose and nylon) and various metallic surfaces.[139] However, antibody adsorption results in serious drawbacks such as denaturation of proteins,[140] very low stability and random orientation and distribution.

The most common methodology for antibody immobilization is the covalent coupling to the sensor surface previously modified with different reactive coatings such as self-assembled monolayers, dextran or polymers.[117] Usually, the strategy makes use of the amine groups of the exposed Lys residues of the antibodies, which react with the activated functional groups of the chemical matrix to form a stable covalent bond. Amine coupling to a SAM has shown multiple advantages such as controlled distribution of the antibodies, elevated reproducibility and stability of the bioreceptor layer, ensuring no desorption of the receptor molecules in flow-through assays. However, amine groups are randomly distributed over the antibody structure and therefore this methodology does not allow site-directed immobilization.[141, 142] In order to minimize arbitrary orientation of antibodies, several strategies have been developed for controlled covalent coupling through the carbohydrate moieties of the Fc regions or disulfide bridges of antibodies.[143, 144] These methods permit for example the direct immobilization of Fab fragments by active sulfhydryl groups improving the sensitivity up to 20 times as compared to the standard amine coupling.[145] However, they require chemical treatment of the antibodies such as carbohydrate oxidation, enzymatic digestion to obtain the IgG fragments (Fab, Fc, etc.) or disulfide bond reduction prior to the immobilization. If the experimental conditions are not accurately controlled, these approaches may influence negatively in the biological activity and the affinity of the biomolecule. In this regard, advances in biochemical engineering have enabled the production of recombinant antibodies, directly generating the desired fragments such as single chain antibody fragments (scFv) or Fab fragments.[146] Handling directly the fragments permit in a more convenient way the oriented and efficient immobilization by employing genetic fusions such as histidine (His)[147] or cysteine (Cys) tags.[148]

Other strategies for antibody immobilization employ affinity tags such as the well-known biotin/avidin system. Antibodies can be conjugated to biotin molecules by covalent crosslinking either to the amine functional groups which lead to random orientation or *via* the sulfhydryl groups[145] or carbohydrate chains[149] that allow site-specific immobilization, as commented previously. Biotinylated antibodies interact with avidin- or streptavidin-coated surfaces with extremely high affinity (K_D = 10^{-15} M) resulting in a nearly irreversible interaction. The biotin/avidin methodology provides highly efficient coverage of the sensor surface and elevated

stability and robustness, but also requires chemical manipulation of the antibodies. More recently, several reports have demonstrated DNA-directed antibody immobilization.[150] Single-stranded DNA-antibody conjugates can be captured by hybridization with the complementary DNA-functionalized surface. This strategy has proven to be very useful for multiplexing antibody immobilization, avoiding harsh spotting processes which may affect the biological activity of the antibodies. However, separate preparation of each DNA-antibody conjugate is mandatory and the immobilization must be controlled to avoid from instability due to dihybridization of DNA by temperature, pH or ionic strength changes.[151]

Another approach towards antibody orientation is to be mediated by affinity proteins able to bind the Fc region of antibodies, i.e. Protein A or Protein G. These proteins have been widely employed in affinity chromatography, especially for antibody purification,[152, 153] and numerous studies have reported their advantages for oriented capture of antibodies in bioanalytical applications.[154] Protein A and G are bacterial proteins, originated from pathogenic staphylococcal and streptococcal bacteria, respectively, and they present structural domains that recognize several IgG types with different affinities (Table 3.2).

Table 3.2 Protein A and G affinities to immunoglobulins of different species.

Specie	Immunoglobulin	Protein A affinity	Protein G affinity
Human	IgG1	++++	++++
	IgG2	++++	++++
	IgG3	-	++++
	IgG4	++++	++++
	IgM	-	-
	IgA	-	-
	IgE	-	-
Mouse	IgG1	+	++++
	IgG2a	++++	++++
	IgG2b	+++	+++
	IgG3	++	+++
Rat	IgG1	-	+
	IgG2a	-	++++
	IgG2b	-	++
	IgG2c	+	++
Goat	IgG	+/-	++
Rabbit	IgG	++++	+++
Sheep	IgG	+/-	++

Protein A or G mediated strategy allows the capture of antibodies in an end-on orientation without the need of any previous modification. The methodology can result in a significantly higher fraction of active antibodies but major concerns are related to the previous immobilization of the affinity proteins onto the sensor surface and the instability of the Protein A/G-antibody interaction under particular assay conditions.

In the last years, novel organic linkers, such as metal complexes[155] or calixarene derivatives,[156] have been designed and synthesized with the aim of orienting the immobilization of antibodies based on affinity interactions. It is the case of molecular derivatives of calixarene molecules, for example, which have demonstrated their usefulness to capture antibodies in an oriented arrangement avoiding chemical modification of the biomolecule.[156, 157] Unfortunately, in many cases these strategies are not optimized and assessed in depth for the direct and label-free immunoassays in biological fluids.

In this chapter we have focused on the development and optimization of two oriented antibody immobilization strategies in terms of sensitivity, selectivity and stability, paying special attention to the prevention and minimization of undesired nonspecific events in complex matrices, such as serum or urine. We have first dedicated our attention on a calixarene-based antibody immobilization strategy (ProLinker^{TM} B) which mediates the binding of proteins in a uniform and tight manner. Moreover, it has shown the ability to efficiently orientate and immobilize antibodies.[157] Further, we have proposed a novel immobilization methodology based on the high affinity of poly-adenine (polyA) chains for gold surfaces.[158] Site-specific conjugation of antibodies to polyA-containing oligonucleotides might lead the oriented immobilization onto the sensor surface in a fast and efficient way. A SPR biosensor has been employed for this study. Besides, the biofunctionalization methodology has been later applied for the evaluation of the LSPR biosensor platform based on gold nanodisks sensors in order to demonstrate the capabilities of nanoplasmonic biosensors for the development of reliable PoC devices.

3.2. Calixarene-based Immobilization Strategy

3.2.1. Description of the Calixarene-based Strategy

Calix[n]arenes are cyclic oligomers consisting of *n* phenol units bridged by methylene groups in *ortho*-position to the phenolic hydroxyl group. Calixarenes are cup-shaped molecules, where the cavity can serve as a binding site for numerous guest species, including ions and molecules.[159] The formation of variable, stable and separable conformers with different reactivity and binding capabilities make calixarenes unique molecular receptor for numerous applications.[160] In this

research, the calixarene-derivative employed is the 1,3-dimethoxy-2,4-dithiol-Calix[4]crown-5-ether (ProLinker™ B) (Figure 3.2), a bifunctional molecular linker with a crown moiety designed for protein immobilization and two thiol-functional arms that allow stable attachment onto gold surfaces by direct chemisorption.

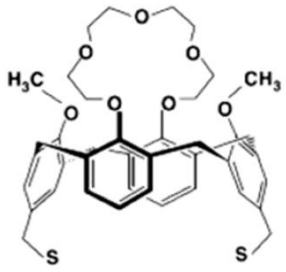

Figure 3.2 Structure of ProLinker™ B.

The proposed mechanism for antibody immobilization attributes the major coupling force to a host-guest interaction between ionized amine groups of the protein and the crown-ether moiety of the linker (Figure 3.3). [157] In fact, the interaction of the ProLinker™ B with several α-aminoacids has been reported[161] indicating that Ala and Val establish strong interactions due to spherical effects. Also strong complexes are formed with Arg and Lys, by electrostatic interactions. These interactions ensure the formation of stable complexes with aminated proteins such as antibodies. In this particular case, hydrophobic interaction between the hydrophobic residues of the immunoglobulin, present in the Fc region, and methoxy groups of the ProLinker™ B layer may also be involved in the immobilization, inducing a vertically oriented capture.

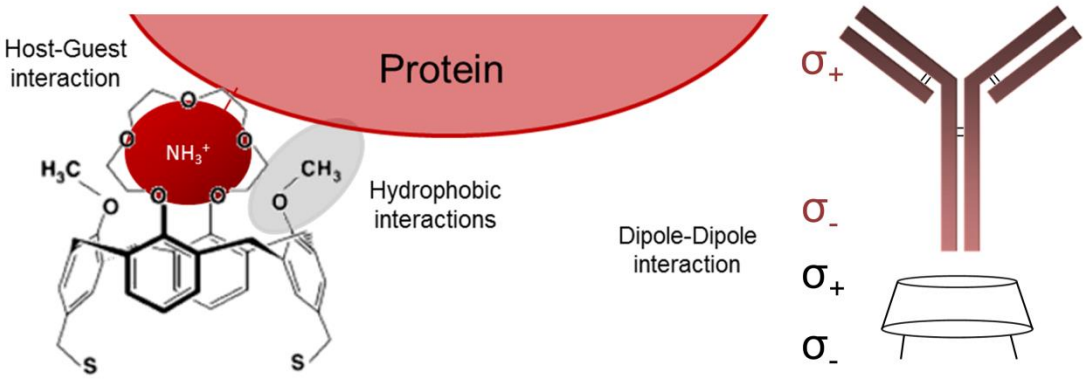

Figure 3.3 Proposed mechanism for antibody capture by ProLinker™ B molecule. Main contribution to coupling is attributed to the host-guest interaction between ionized amine groups and the crown-ether moiety. Hydrophobic interactions between methoxy group of the linker and hydrophobic residues of the protein are also involved. End-on orientation is induced by dipole-dipole interactions.

A possible mechanism for the orientation of the antibodies onto the ProLinker™ B layer was given by Chen *et al.*[157] It is generally assumed that antibodies present a dipole momentum pointing from Fc to $(Fab)_2$ due to differences in the isoelectric point between the two regions.[162] According to the direction of the ProLinker™ B dipole and antibody dipole, the immobilized antibody in an end-on orientation can interact with the ProLinker™ B layer with lower energy than with other orientations (Figure 3.3). Conclusively, the sum of hydrophobic, host-guest and dipole-dipole interaction participating in the antibody coupling will predictably confer both highly stable attachment and proper orientation.

Furthermore, another variant of the ProLinker molecule is also commercially available (ProLinker™ A), which incorporates aldehyde (-CHO) instead of thiol groups to the functional arms. This way, the immobilization onto glass or silicon-derivative surfaces is also possible.[156] This strategy should be quite versatile to be used not only with plasmonic biosensors but also with other type of transducers and biosensor configurations.

The calixarene-mediated immobilization procedure involves few steps: (i) formation of the ProLinker™ B layer onto the gold surface *via* thiol chemisorption, (ii) antibody capture due to the host-guest interaction and (iii) blocking of the free areas by using bovine serum albumin (BSA) or other blocking agent (Figure 3.4). BSA is a common protein widely used in bioanalytical applications to prevent nonspecific adsorptions onto surfaces. In this case, the amine groups of the Lys residues in the BSA can interact with the fraction of ProLinker™ B that remains free, avoiding nonspecific adsorption of analyte molecules or other proteins present in the sample.

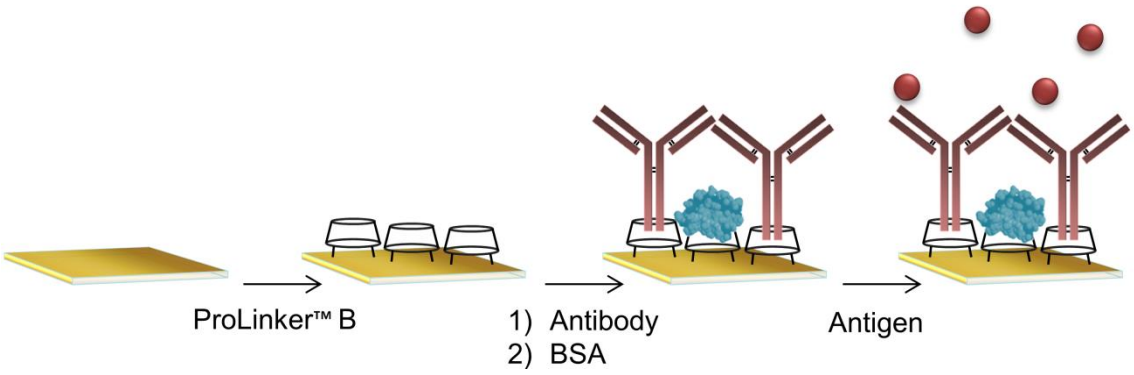

Figure 3.4 ProLinker™ B-based biosensing strategy: (i) surface coating with ProLinker™ B, (ii) antibody immobilization and blocking step with bovine serum albumin (BSA), and (iii) specific antigen detection.

3.2.2. Optimization and Assessment of the Calixarene-based Strategy

An optimization and assessment study was performed with the SPR biosensor and using the human Chorionic Gonadotropin (hCG) hormone and its complementary anti-hCG antibody as standard antibody/antigen pair. The hCG is a reported tumor biomarker in some types of cancer such as prostate, testicular, breast or ovarian cancer,[163] besides being the main diagnostic biomarker for most pregnancy tests.

First of all, the efficiency of ProLinker™ B strategy to capture antibodies was evaluated by monitoring the immobilization of several concentration of anti-hCG (5, 10, 20, 50 and 100 µg/mL). Figure 3.5a illustrates a model sensorgram (anti-hCG 10 µg/mL) of the antibody capture followed by the BSA blocking step. The sensorgram represents changes of the intensity of the reflected light due to variations of the refractive index in the medium close to the gold sensor surface. It can be observed a change of the baseline corresponding to the RI of running water after the injection of the antibody, indicating adsorption of biomolecules onto the ProLinker™ B functionalized surface. Immobilization signals gradually increased with the antibody concentration (Figure 3.5b).

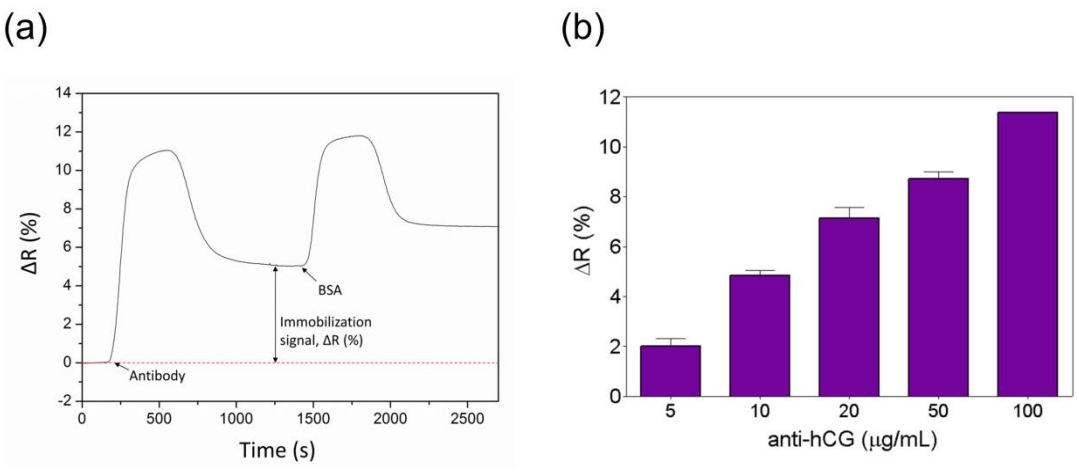

Figure 3.5 (a) SPR sensorgram of the immobilization procedure of anti-hCG antibody at 10 µg/mL and subsequent blocking step with BSA at 0.5 µg/mL; **(b)** Immobilization signals for anti-hCG immobilization onto ProLinker™ B at different concentration (5, 10, 20, 50, 100 µg/mL).

The immobilization procedure was characterized by measuring variations in the contact angle of the sensor surface. This characterization technique is based on the evaluation of the angle formed when a drop of liquid (usually H_2O) meets a solid surface, which is directly related to the wetting properties of the surface. When the contact angle of a drop on a surface is over 90° the surface is referred as hydrophobic, and when the angle is below 90° the surface is referred as

hydrophilic. Thus, contact angle characterization can provide information about the cleanliness, roughness or surface heterogeneity among other properties. It can also be useful to characterize or evaluate the progress of a reaction on a surface, in cases that the added layers cause changes in the surface polarity and its lipophilia. Table 3.3 lists the contact angle values obtained for the different layers during the ProLinker™ B mediated antibody immobilization.

Table 3.3 Contact angle values of the sensor surface at different stages of the ProLinker™ B biofunctionalization strategy.

Functionalized Surface	Contact Angle
Au (after piranha cleaning)	30.6 ± 0.51
Au + ProLinker™ B	64.0 ± 0.20
Au + ProLinker™ B + anti-hCG	47.0 ± 0.16
Au + ProLinker™ B + anti-hCG + BSA	56.1 ± 0.21

As can be appreciated, the gold surface presents high hydrophilicity after the cleaning procedure with piranha solution, which is reduced after ProLinker™ B functionalization. The increase of the contact angle can be attributed to the presence of the ProLinker™ B layer. Once the antibody is immobilized, the surface becomes more hydrophilic, mainly due to the functional groups (CO_2H and NH_2) distributed around the immunoglobulin structure. Finally, after the BSA blocking step the contact angle increases again due to the general hydrophobic behavior of albumins. This preliminary characterization seems to indicate a correct performance of each step of the biofunctionalization strategy.

Next, in order to evaluate the efficacy of the calixarene-mediated strategy, we performed a comparative test with other conventional strategies: amine-based covalent binding to an alkanethiol SAM and affinity capture by Protein G layer. Particularly, the comparison study was focused on analyzing not only the improvement that can be achieved when appropriately orienting the antibody layer but also on evaluating the simplicity and the potential of the methodologies to generate stable and robust biofunctionalized sensor surfaces.

Covalent immobilization strategy was selected as reference of a standard and commonly used procedure that generally leads to random oriented layer of antibodies. The covalent coupling consists of an amide bond formed between the primary amine ($-NH_2$) groups of the Lys amino acids of the antibodies and carboxylic functional groups ($-CO_2H$) of long-chain alkanethiols (Figure

3.6a). The use of long-chain alkanethiols (i.e. more than 10 atoms of carbon) leads to dense and ordered SAMs similar to crystalline structures. We selected a mixed monolayer of mercaptohexadecanoic acid (MHDA) and mercaptoundecanol (MUOH) in a molar ratio 1:20. This specific mixed SAM has been previously evaluated in our group for antibody immobilization, resulting in minimum steric hindrance effects and, therefore, enhancing the antigen detection.[164] For protein immobilization, carboxylic groups of the SAM were activated by using the well-known EDC/NHS chemistry, which results in a NHS-ester intermediate highly reactive to primary amines of antibodies. This chemical procedure is well established and it generates highly stable amide bonds. The strategy allows the control of the packing density, however it does not result in proper orientation and usually requires high concentration of antibody, between 0.1 and 1 mg/mL.[165, 166]

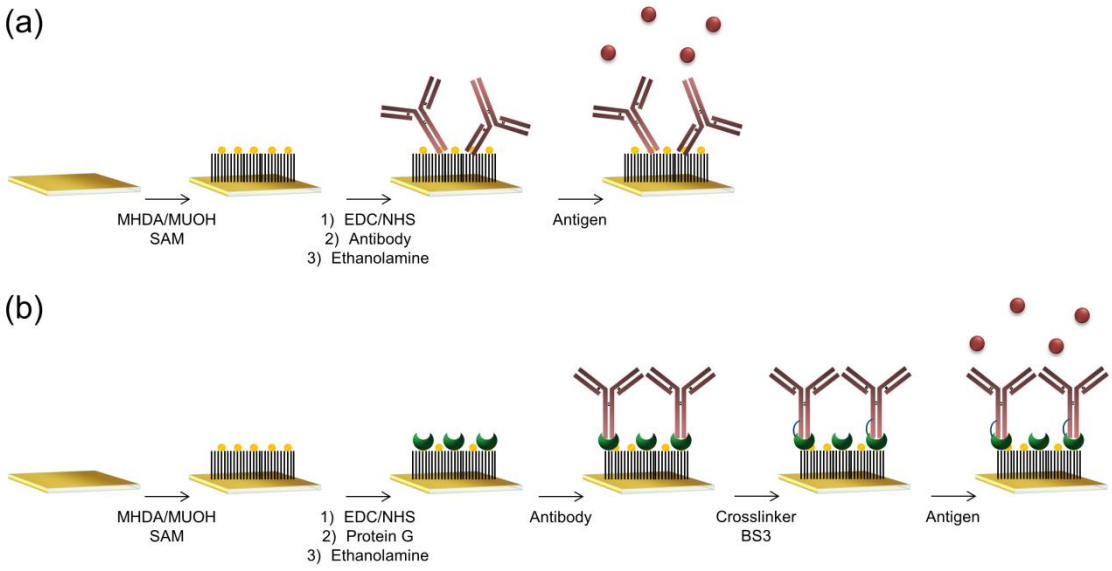

Figure 3.6 Schematic representation of biosensing strategies based on: **(a)** Covalent coupling: mixed alkanethiol SAM formation, covalent attachment of antibodies and antigen detection; and **(b)** protein G strategy: mixed alkanethiol SAM formation, covalent attachment of protein G, antibody affinity-capture, crosslinking with BS3 and antigen detection.

Protein G-mediated immobilization is also a widely employed methodology which provides uniform and oriented layer of antibodies. Protein G in its native form is expressed in group C and G *Streptococci* and it presents 3 antibody-binding domains that recognize both Fc and Fab regions of immunoglobulins of all human IgG subclasses, rabbit, mouse and goat IgGs (Table 3.1).[154] Although native protein G shows approximately 10-fold higher affinity for Fc than for Fab regions, some nonspecific binding to Fab domains could occur. Currently, recombinant protein G, usually expressed in *Escherichia coli*, presents improved specificity for site-directed capture of antibodies

as well as enhanced affinity.[167] The immobilization strategy is based on the covalent coupling of the protein G to a mixed SAM in a similar way than covalent immobilization described previously and subsequent capture of antibodies in end-on orientation (Figure 3.6b). The affinity capture of antibodies is mainly attributed to electrostatic and hydrophobic interactions, therefore the process is highly dependent of the isoelectric point (pI) of the protein and the ionic strength and pH of the medium.[168] For this reason, a previous optimization of the immobilization buffer was done in order to ensure maximum capture efficiency. The optimal affinity for the particular case of protein G binding takes place at pH < 6.0. According to that, a considerably higher amount of immobilized antibodies was achieved when using sodium acetate buffer at pH 5.0 instead of the standard PBS buffer at pH 7.4 (Figure 3.7).

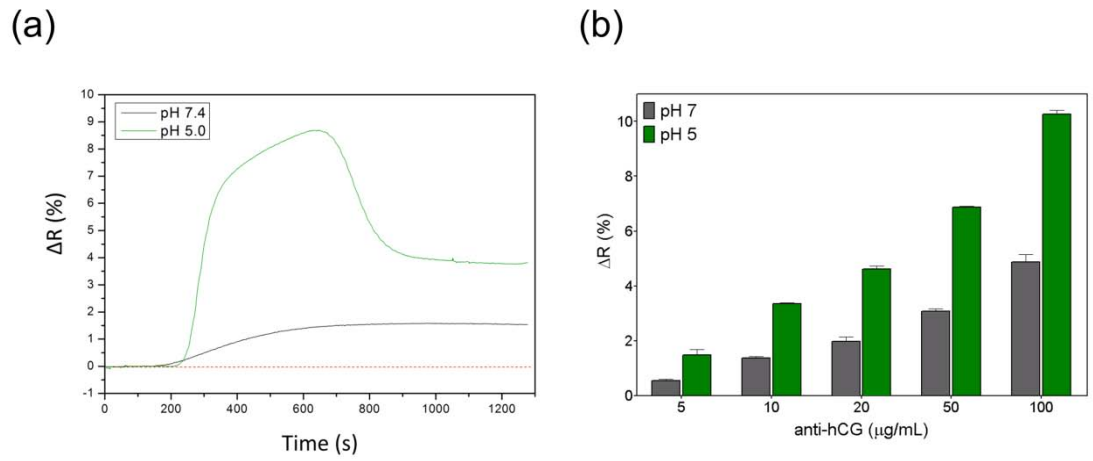

Figure 3.7 (a) SPR sensorgram of the affinity capture of anti-hCG antibody at 10 μg/mL in different buffer conditions: standard PBS at pH 7.4 (black) and sodium acetate buffer at pH 5.0 (green); **(b)** Immobilization signals for anti-hCG immobilization onto protein G at different concentrations (5, 10, 20, 50, 100 μg/mL) using two immobilization buffers: PBS at pH 7 (grey) and sodium acetate buffer at pH 5.0 (green).

Despite the affinity is quite good,[169, 170] the dissociation of Protein G/A-antibody occurs at extreme pH values, which are usually the conditions also required in regeneration steps to remove target from antibody. In order to generate a bioactive surface with potential for reusability, an additional crosslinking step may be considered. For that purpose we selected the bis(sulfosuccinimidyl)suberate (BS3), a homobifunctional molecule containing two sulfo-N-hydroxysulfosuccinimide (s-NHS) ester at each end of an 8-carbon spacer arm (Figure 3.8). This crosslinker is able to readily react with primary amines of both proteins at pH 7 – 9, resulting in stable amide bonds.

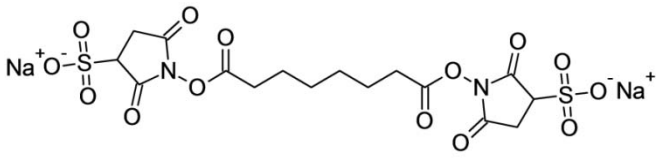

Figure 3.8 Structure of bis(sulfosuccinimidyl)suberate (BS3).

The three strategies were primarily compared in terms of antibody immobilization efficiency. Several concentrations of antibody ranging between 5 and 100 µg/mL were tested, which can be considered between low and moderate values for label-free biosensors. As can be seen in Figure 3.9, Protein G and ProLinker™ B strategies showed higher signal response, even 10 times higher with ProLinker™ B coating, than covalent coupling method, which indicates a significant better antibody binding. It is noteworthy that conventional covalent attachment resulted in very low amount of antibody on the surface (according to the low signals obtained). An antibody concentration of 10 µg/mL was initially selected. Although this concentration is low as compared with the regular concentrations employed in direct immunoassays (around 100 µg/mL[171] or even higher[166]) we obtained significant binding responses both for Protein G and ProLinker™ B strategies.

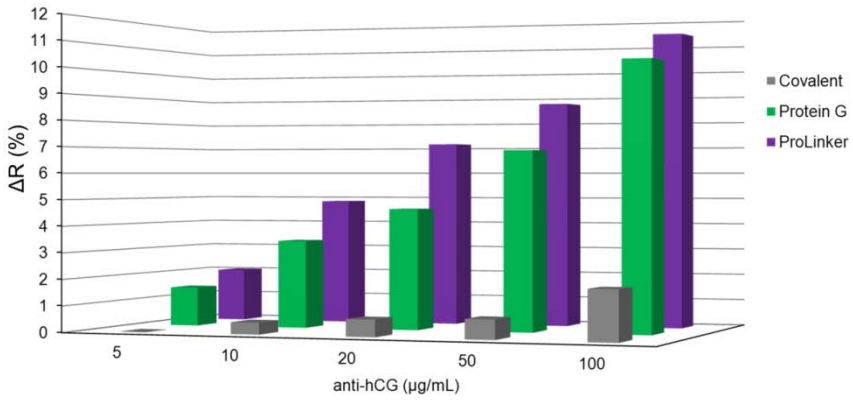

Figure 3.9 Comparison of antibody immobilization at different antibody concentration (5, 10, 20, 50, 100 µg/mL) using different strategies. Grey: covalent strategy; green: protein G strategy; purple ProLinker™ B strategy.

Sensitivity and specificity for the target detection were assessed. As can be seen in Figure 3.10, the target binding (hCG protein) using ProLinker™ B strategy was considerably higher as compared with Protein G and covalent approaches. It is however worth mentioning the lower signal observed with the Protein G-based methodology, with similar detection signals than

covalent binding, even having ~11 times more amount of antibody (as can be deduced from the signals obtained in the immobilization step) and, in theory, with a more oriented distribution. This might be due to the crosslinking step introduced to stabilize the antibody-Protein G interaction. The crosslinking procedure consists of the formation of covalent bonds between the free amine groups that are in close contact by BS3, which contains two succinimidyl groups at each end. However, the reaction involves a high excess of BS3 which could result also in undesirable side reactions, for instance, between amine groups in the Fab regions of the antibody which are in close proximity. This eventually could lead to an alteration of the binding sites responsible for recognition, reducing their biological activity.[172] On the other hand, target recognition performed using ProLinker™ B strategy resulted in relatively higher signals (Figure 3.10) reaching Limits of Detection (LoD) of 0.1 µg/mL for hCG. These results seem to confirm that ProLinker™ B strategy provides a tight and right oriented antibody layer with presumably good accessibility to the active binding sites.

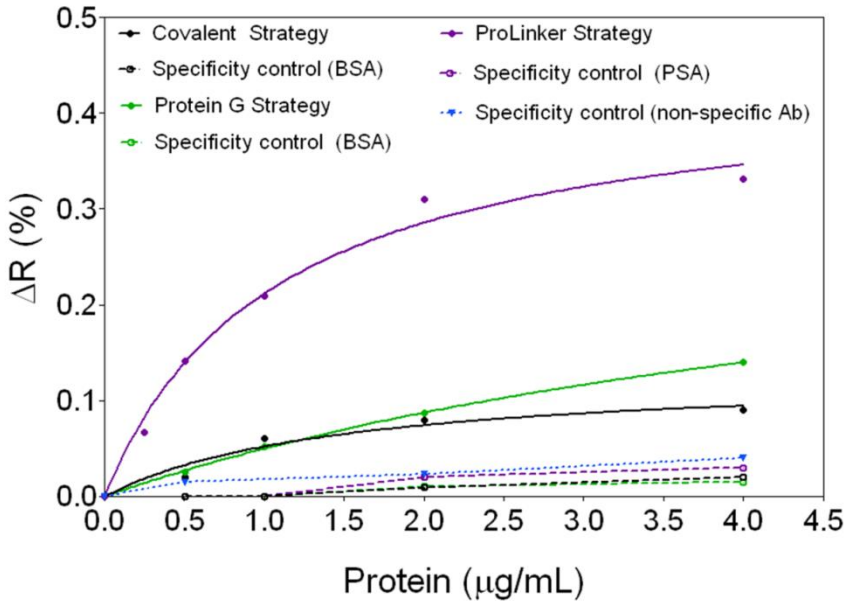

Figure 3.10 Evaluation of hCG/anti-hCG interaction using covalent strategy (black), protein G strategy (green) and ProLinker™ B strategy (purple). Concentration of anti-hCG was 10 µg/mL in all cases. Dashed lines represent adsorption of nonspecific proteins onto antibody functionalized surfaces for covalent strategy (black), protein G strategy (green) and ProLinker™ B strategy (purple). Blue dotted line indicates additional control for ProLinker™ B strategy, based on the detection of hCG onto a nonspecific antibody (also at 10 µg/mL) immobilized over ProLinker™ B layer (same experimental conditions as with specific antibody).

The specificity of the antigen detection was evaluated by performing assays with non-target control proteins (BSA and prostate specific antigen (PSA)) at different concentration (Figure 3.10).

Results showed negligible binding of these proteins onto the biofunctionalized surfaces with any of the three strategies, ProLinker™ B, Protein G or covalent binding and confirmed that signal contribution comes only from specific detection of the corresponding target by the antibody. In the particular case of ProLinker™ B strategy, an additional specificity test was performed, considering the type of interaction established between the molecules and the antibody. As described before, the crown-ether moiety present in the structure couples proteins via free amine groups and, in fact, a blocking step with amine-containing molecules such as BSA is necessary to cover free ProLinker™ B spaces on the surface (Figure 3.4). In order to discard a direct binding of the target molecules onto the ProLinker™ B itself, an evaluation of the cross-reactivity of the target protein to a nonspecific antibody previously immobilized was performed. Results depicted in Figure 3.10 confirmed the high specificity of the assay. As can be observed, protein (hCG) does not bind to any component on the surface unless its specific antibody is present, showing a decrease in the response of up to 8 times compared with the response from the corresponding specific layer.

Immobilization strategies were further assessed for the direct detection of protein biomarkers, such as focal adhesion kinase (FAK) and C-Reactive Protein (CRP). FAK is an intracellular protein which plays an important role in cell growth and regulation. It is known that FAK overexpression contributes to the development of malignancy in many tumors and its early detection has become a key factor in cancer diagnosis and therapy.[173] CRP is a widely studied biomarker indicative of inflammation and infection and it is also used in heart disease risk assessment, progression and treatment effectiveness.[174] It has been also reported that detection of low levels of CRP in urine may be useful for the diagnosis of lower urinary tract symptoms (LUTS).[175] Thus, detection of both biomarkers can be relevant and exemplifies two useful applications where direct detection in serum or urine is necessary.

Under same assay conditions (i.e. [Antibody]=10 µg/mL) ProLinker™ B strategy showed higher antibody immobilization for both antibodies (%ΔR(CRP)=5.18 and %ΔR(FAK)=7.17), compared with Protein G approach (%ΔR(CRP)=2.08 and %ΔR(FAK)=1.95), being very similar to the results observed with anti-hCG. As can be seen in Figure 3.11, calibration curves for CRP and FAK biomarkers clearly showed also better sensitivities using ProLinker™ B with Limits of Detection (LoDs) of 85.93 ng/mL and 23.14 ng/mL for FAK and CRP respectively, when compared with the ones achieved with the Protein G strategy using the same concentration of antibody (208.4 ng/mL and 42.25 ng/mL for FAK and CRP respectively).

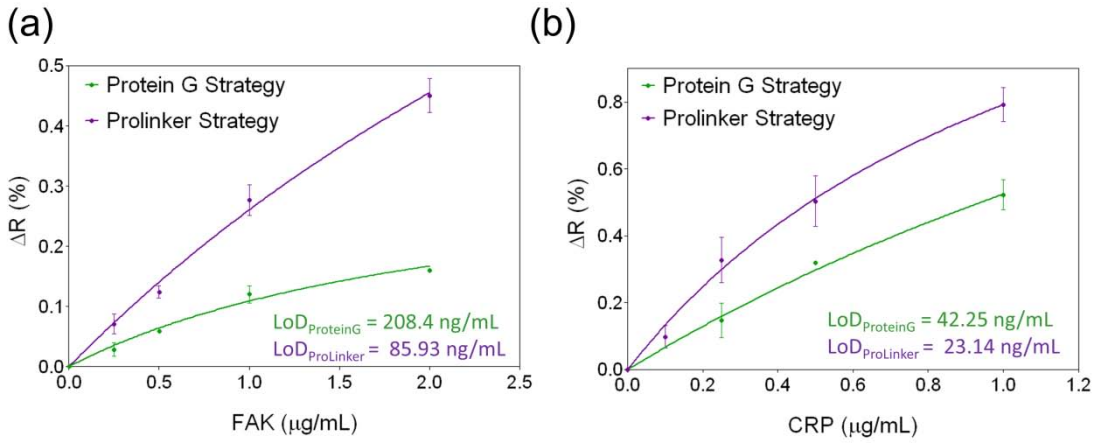

Figure 3.11 Calibration curves for **(a)** FAK and **(b)** CRP, using 10 μg/mL of specific antibody and following both protein G strategy (green) and ProLinker™ B strategy (purple). Limit of Detection (LoD) is determined as the minimum measurable signal corresponding to three-times the standard deviation of the blank.

The stability and robustness of the bioactive surface was also assessed for the ProLinker™ B strategy. This is particularly important to ensure the reusability of the sensor if needed, either to lengthen the surface life-time, to save costs or to study reproducibility and optimization of protocols. The regeneration of the surface was evaluated by removing target proteins from the antibody-immobilized layer, using acidic conditions (HCl 5 mM) (Figure 3.12).

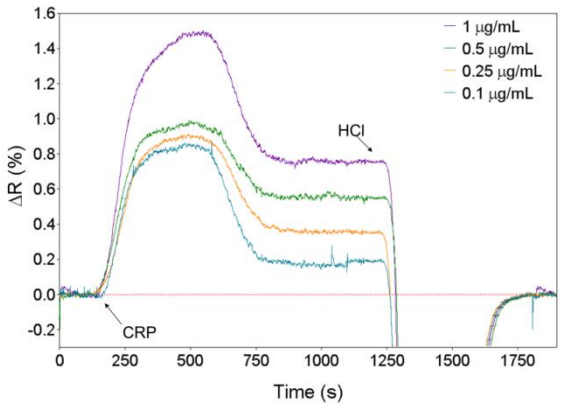

Figure 3.12 SPR sensorgrams corresponding to detection of different concentrations of CRP and subsequent regeneration of the biosurface with HCl 5 mM.

Considering that antibody coupling to ProLinker™ B layer does not involve any covalent bond but host-guest interaction (i.e. high affinity electrostatic interaction), a partial loss of antibody on the surface under extreme pH conditions could not *a priori* be discarded. Remarkably, we observed complete removal of target protein without altering the amount of antibody on the surface. Sensorgrams depicted in Figure 3.12 show how the baseline after regeneration comes back to the same level than before CRP detection at different concentrations.

Also a certain decrease of activity of the remaining bound antibody would be likely. Assays with PBS as running buffer resulted in good stability and reproducibility until the seventh cycle (Figure 3.13a); then a loss around 60% of the detection signal was observed and kept decreasing exponentially in subsequent experiments. These results are considered usual in solid-based direct immunoassays,[176, 177] due to the limited stability of antibodies in aggressive mediums such as acidic or basic pH. Same experiments were carried out with PBS buffer containing Tween 20. This additive is a widely used surfactant for reducing nonspecific binding events[178] and is usually added in conditions where detection in biological samples is the final purpose. Surprisingly, when assays were performed over ProLinker™ B-based surfaces with PBST (PBS with a 0.5% of Tween 20) the stability of the biosurface was greatly increased and was possible to perform up to 20 direct detection cycles with high reproducibility before reaching a loss of 40% of the signal (Figure 3.13b).

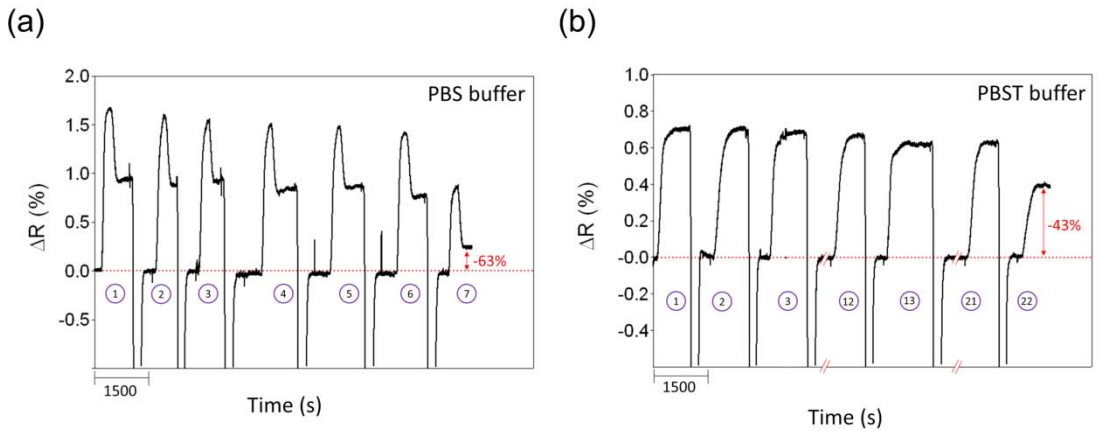

Figure 3.13 Detection cycles performed by consecutive interaction of specific target at 1 µg/mL and regeneration with HCl 5 mM **(a)** using PBS in flow, and **(b)** using PBST in flow.

From above results, we can conclude that ProLinker™ B strategy has demonstrated to provide efficient antibody immobilization with proper orientation and without the need of chemical manipulation of the biomolecule, yielding high specificity and better sensitivity for direct target detection when compared to other conventional immobilization procedures. Besides, the strong host-guest interaction between the calixarene and antibodies confers unexpected stability and robustness to the biosurface, while optimized regeneration conditions under acid conditions allow the reusability of the antibody layer with good reproducibility during several experiments.

3.2.3. Analysis in Biological Fluids

Protein biomarker analysis is crucial in clinical diagnosis and their direct detection from biological fluids is a required demand. This analysis may become especially complex due to the presence of interferences and undesired nonspecific adsorption of matrix components present in urine, serum or whole blood (Figure 3.14). In the case of label-free detection and in particular for evanescent wave optical biosensors where signals are directly related with mass changes on the sensor surface, this must be minimized as much as possible.

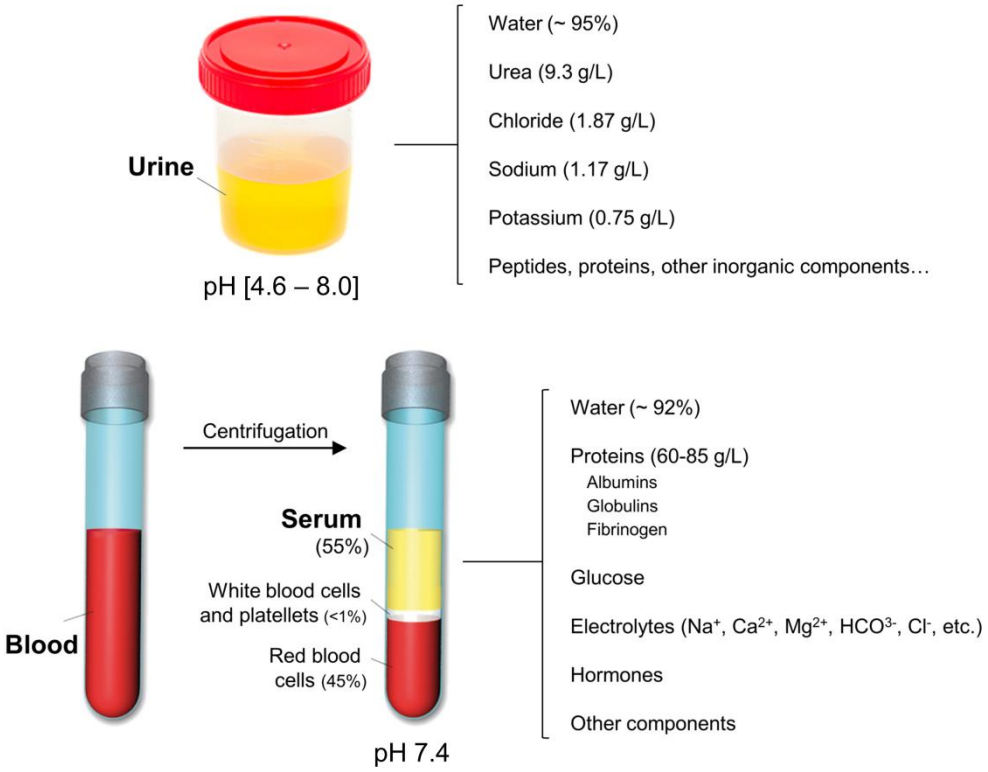

Figure 3.14 General composition of the most commonly used human clinical samples for diagnostics: urine, blood and serum.

Urine is an ideal sample for disease biomarker determination as it can be obtained in large amounts with non-invasive methods. Human urine consists primarily of water with organic solutes, such as urea or creatinine, inorganic ions to a much less extent, also small organic substances and metabolites, enzymes or proteins.[179] The urine matrix effect in direct analysis of proteins might be less severe than serum or plasma, where considerably higher concentrations of proteins are present (Figure 3.14). However, a high salt content like the one in urine samples may interfere in the immunochemical interaction and also other potential nonspecific adsorptions cannot be discarded.[180] On the other hand, most protein biomarkers are not excreted in the urine but appear in blood and in those cases analysis of serum, plasma or whole blood is the best non-

invasive method. Direct evaluation of undiluted serum (and especially whole blood) still remains a not well-solved problem in direct label-free evaluation. The high amounts of proteins and lipids present in blood (Figure 3.14), which can adsorb onto the sensor surface usually lead to high background signal and in the case of immunochemical interactions can also hamper the antigen recognition.

Generally, nonspecific adsorptions are mainly due to electrostatic and hydrophobic interactions between the surface and matrix components. Several antifouling compounds can be employed as blocking agents to prevent or reduce nonspecific binding onto the sensor surfaces, such as PEGylated or dextran derivatives. These polymers are widely used in biomedicine because of their high hydrophilicity, which confers extraordinary protein adsorption resistance and biomimetic properties.[181] Besides, buffer composition can also be modified by adding blocking compounds (e.g. BSA) or surfactants (e.g. Tween 20) that reduce nonspecific adsorptions onto the surface.

Based on this, we studied the behavior of different biological fluids (i.e. urine and serum) onto ProLinker™ B biofunctionalized SPR surface for the direct detection of protein biomarkers. For the assessment of undiluted urine, ProLinker™ B layer was blocked with BSA and CRP immunoassays were carried out with PBST 0.5% as running buffer, which provides high stability to the bioactive surface as its elevated concentration of surfactant might minimize nonspecific interaction. Calibration curves for CRP-spiked urine showed comparable sensitivities to the ones obtained with standard buffer conditions (PBS and PBST) demonstrating that urine components did not hinder the immunochemical reaction (Figure 3.15a).

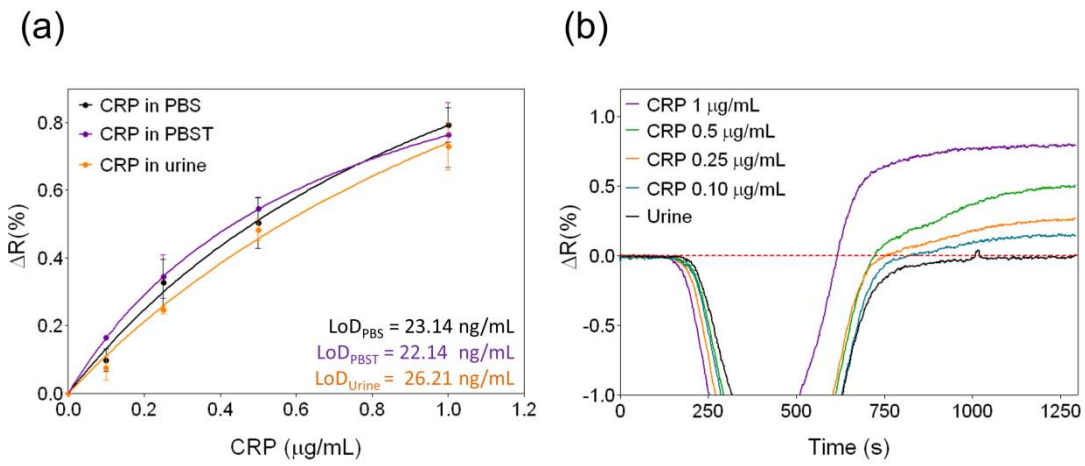

Figure 3.15 (a) Calibration curves for CRP detection using ProLinker™ B strategy with 10 μg/mL of specific antibody performed in PBS (black), PBST 0.5% (purple) and undiluted urine (orange); **(b)** SPR sensorgrams for pure urine spiked with different CRP concentrations.

Pure urine injected on the surface without spiked protein resulted also in no background signals as can be observed in Figure 3.15b (black line). We can observe how the baseline remains at the same level after all the urine has flowed through the fluidic cell. This confirms the absence of nonspecific binding onto the biofunctionalized surface. Furthermore, regeneration with the previously selected conditions resulted in a similar number of cycles (up to 20 measurements) without losing signal, confirming the robustness of the assay using the ProLinker™ B strategy for antibody immobilization.

On the other hand, when undiluted serum was tested over a ProLinker™ B-based bioactive surface, we observed a significant increase of signal coming from nonspecific binding. In order to minimize the undesired adsorption, an optimization study was carried out, initially with diluted serum, consisting of: (i) evaluating surface blocking with different antifouling compounds and (ii) changing the buffer composition employed to dilute the serum. In the ProLinker™ B strategy, BSA is used as a conventional blocking agent to cover the remaining free ProLinker™ B groups (free crown moiety of ProLinker™ B will interact with amine groups present in the protein). BSA is a globular protein with a molecular weight of approximately 66.5 kDa that shows a slightly hydrophobic behavior. By substituting BSA with other amine-containing compounds with more biocompatibility and hydrophilic properties such as PEG (diamine-PEG and poly-L-lysine PEG, PLL-PEG) (Figure 3.16a,b) or dextran (amine-dextran) (Figure 3.16c), we would expect an improved behavior of the sensor surface against serum.

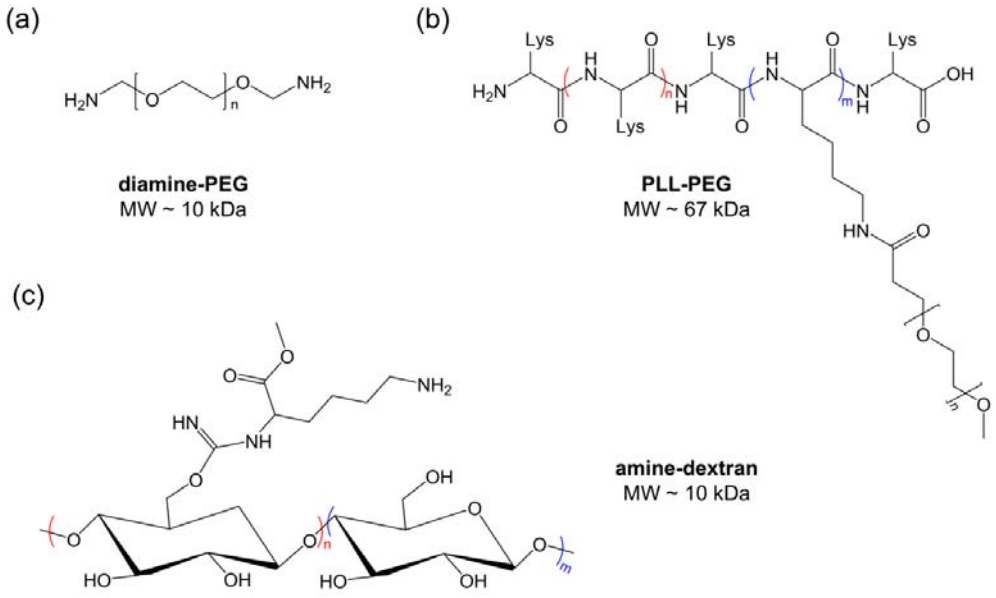

Figure 3.16 Blocking agent compounds: **(a)** diamine polyethylene glycol (diamine-PEG), **(b)** poly-L-lysine polyethylene glycol (PLL-PEG), and **(c)** amine-dextran.

Different buffer compositions were tested based on the blocking effect of compounds as BSA or dextran, and on the presence of Tween 20 as surfactant. Figure 3.17 summarizes the results when these parameters were tested using serum diluted at 10%.

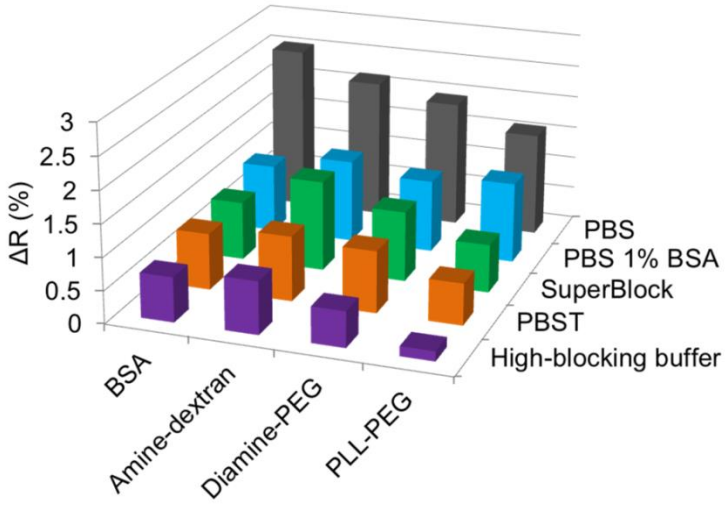

Figure 3.17 Serum nonspecific adsorption onto sensor surface blocked with different agents (BSA, amine-dextran, diamine-PEG and PLL-PEG) diluted 1:10 with different buffers (PBS, PBS+1%BSA, SuperBlock®, PBST 0.5% and HBB buffer).

As it can be observed the presence of surfactants in the dilution buffer helps to reduce the adsorption of serum components onto the sensor surface (i.e. PBST and High-Blocking Buffer, HBB) while the use of PLL-PEG offers a significant improvement of the antifouling resistance. A possible reason for this better behavior as compared with diamine-PEG may lie in the higher molecular weight and the relative high ratio of amine groups present in the poly-lysine chains of the PLL-PEG that could more efficiently cover free ProLinker™ B molecules and, at the same time, could confer high hydrophilicity to the bioactive layer. The combination of HBB buffer, which contains a high salt and Tween 20 concentration and blocking agents such as BSA and dextran, with PLL-PEG for surface blocking, produced a reduction of the nonspecific binding of diluted serum of 94% with respect to standard conditions (BSA as blocking agent and PBS buffer) and around 76% when using PBST 0.5% instead of PBS. However, these changes can also affect to the antibody-antigen recognition, especially in cases involving extra-components in the buffer composition. Thus the antigen binding efficiency was evaluated with these new conditions by performing the assays with CRP/anti-CRP in serum diluted with HBB (10%) and with the surface blocked with PLL-PEG. No specific detection of the target protein was achieved with these new

assay conditions, indicating that this buffer somehow hindered accessibility of the protein to interact with the immobilized antibodies.

However, the use of PLL-PEG was not discarded, since the optimization study seemed to highlight its role as a promising candidate in substitution of BSA as blocking agent. The influence of PLL-PEG in the antigen recognition was evaluated in serum diluted ten times in PBST buffer. The recognition of target protein was observed (Figure 3.18a), while leading at the same time to a lower nonspecific binding as compared to a BSA-blocked surface. Overall a reproducible and constant background signal of %ΔR = 0.31 ± 0.02 with PLL-PEG was observed, 50% lower than with BSA (%ΔR = 0.60 ± 0.08). Taking as reference the constant background signal, a calibration curve for the CRP detection in serum was performed (Figure 3.18b), resulting in a slight loss of sensitivity (i.e. higher LoDs) compared with pure PBST. These promising results were considered as the first approach in order to improve the conditions to work with more concentrated serum, or ideally with pure serum samples.

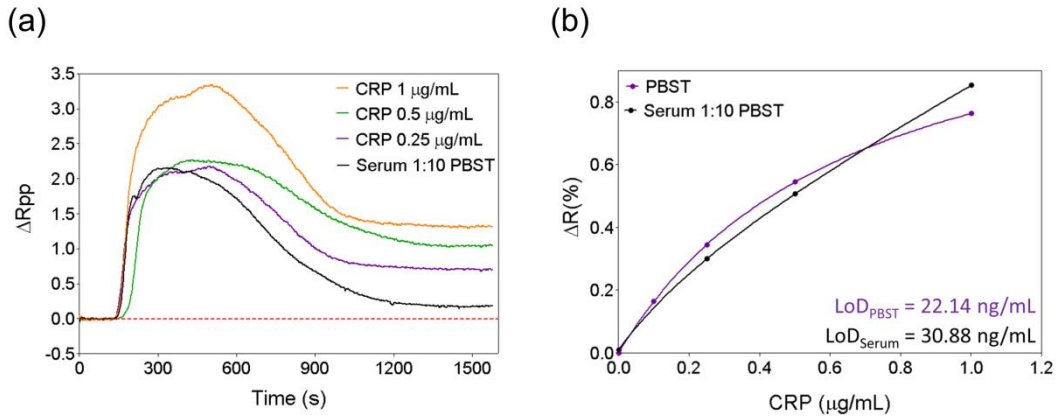

Figure 3.18 **(a)** SPR sensorgrams for diluted serum (1:10 PBST 0.5%) spiked with different CRP concentrations; **(b)** Calibration curves for CRP detection using ProLinker™ B strategy (using 10 µg/mL of specific antibody) performed in PBST and BSA as blocking agent (purple) and serum-PBST 1:10 and PLL-PEG as blocking agent (black).

3.2.4. Application to the Nanoplasmonic Biosensor

A key factor on the final development of LSPR biosensors is related to the surface biofunctionalization. Nanoplasmonic sensor configurations can offer important benefits in terms of sensitivity and selectivity, but the transfer of conventional gold surface chemistry to nanostructured surfaces implies additional factors such as the material heterogeneity of the

surfaces, which must be taken into account when optimizing the overall performance of the biosensor.

ProLinker™ B was evaluated for the antibody immobilization on gold nanodisks surface. Nanoplasmonic surfaces were fabricated by the hole-mask colloidal lithography (HCL)[138] process explained in Chapter 2, which is a simple and large-scale production technique that leads to short-ordered arrays of gold nanodisks (diameter 100 nm, height 20 nm) onto glass substrates. We employed our homemade nanoplasmonic biosensor based on the LSPR arising on gold nanodisks when illuminated at a fixed angle of incidence. The 70° angle of incidence setup was selected for this study since this scheme allows working in both SPR and LSPR configuration by simply changing the sensor surface and the polarization of the light (i.e. TM for gold film and TE for gold nanodisks). In this way, a reliable comparison between both biosensing approaches could be done. The nanoplasmonic biosensor allows the real time monitoring of biochemical interactions by tracking the shift of the LSPR/SPR wavelength induced by changes in the RI of the medium near the sensor surface (See Introduction and Materials and Methods sections).

We have implemented the ProLinker™ B strategy to functionalize nanoplasmonic sensors based on the initial results obtained with thin gold films in SPR (Figure 3.19).

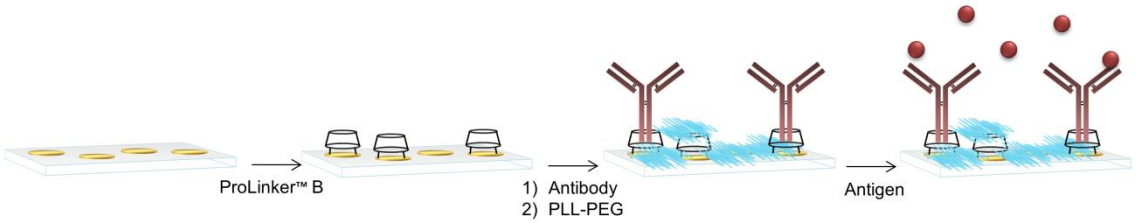

Figure 3.19 ProLinker™ B-based immobilization procedure for gold nanodisks surfaces: (i) ProLinker™ B layer formation, (ii) antibody immobilization and blocking step with PLL-PEG, and (iii) antigen detection.

Gold nanodisks sensors offer a reduced active sensor surface when compared to the thin gold films of SPR biosensors (nanodisks sensors have an approximate surface occupation of 6%-7%).[87] Therefore, one would expect an increase of the required antibody concentration in order to obtain minimum antigen detection signals comparable with SPR. Different anti-CRP antibody concentrations (10, 20 and 50 µg/mL) were immobilized following the same experimental procedure previously used in the SPR device. The antigen detection curves showed increasing signals when higher amount of receptor was immobilized (Figure 3.20a). Whereas an antibody

concentration of 10 µg/mL showed efficient capture of antibodies (Figure 3.11b), in the case of nanodisks it was necessary to increase to at least 20 µg/mL to obtain better signals. In views of that, an accurate comparison with SPR-biosensor was performed by carrying out the analysis under the same circumstances ([anti-CRP] = 20 µg/mL) and with the same biosensor (setup with 70° of angle of incidence of light). As seen in Figure 3.20b, standard SPR sensor chips showed a slightly better recognition capacity at high analyte concentration, probably due to higher amount of antibodies immobilized on the gold film with respect to the gold nanodisks surface. However, at lower concentrations of antigen, the detection with the gold nanodisks provided better sensitivity (i.e. a more pronounced slope for LSPR curve than for SPR), resulting in two-times better detectability (LoD(SPR) = 30.8 ng/mL and LoD(LSPR) = 16.2 ng/mL). This result could be partially ascribed to the strong LSPR field confinement of the nanodisks (as compared to SPR), which becomes more evident at low target concentrations.

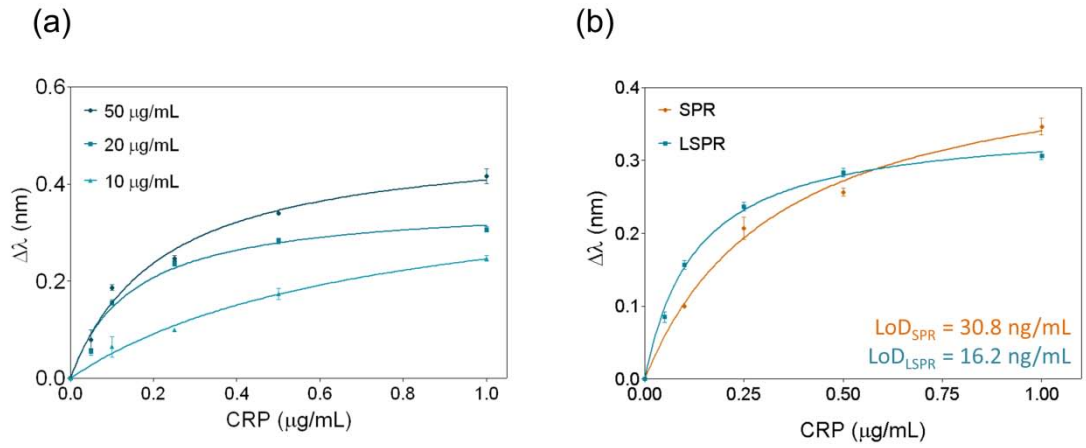

Figure 3.20 (a) CRP detection curves obtained with the nanoplasmonic biosensor at different concentrations of immobilized antibody (10, 20, 50 µg/mL) with ProLinker™ B strategy; **(b)** Calibration curves for CRP detection on SPR gold film (orange) and LSPR gold nanodisks (blue). Antibody concentration was 20 µg/mL and PLL-PEG was employed as blocking agent for both sensors.

Furthermore, taking into account the dual nature of the LSPR sensor surface (gold nanodisks on a glass substrate) we attempted a material-selective functionalization by exploiting the use of PLL-PEG as blocking agent. This compound has high affinity for glass surfaces.[182] Coating with PLL-PEG allowed us both the passivation of the glass surrounding the gold nanodisks and the additional blocking process of free ProLinker™ B molecules (as previously observed on gold). In this way we can generate a highly hydrophilic layer onto the sensor surface, increasing the resistance to nonspecific adsorption.

To evaluate the benefits of the nanostructured surfaces to reduce undesired matrix adsorptions from biological fluids we tested different serum dilutions and pure serum, using the two buffers with better output in SPR (PBST 0.5% and HBB) (Figure 3.21). In comparison with the thin gold surface, a high reduction of the nonspecific adsorption was observed for gold nanodisks in all the serum dilutions, even also in serum 100%, when using HBB buffer. Indeed, a 90% less nonspecific binding with undiluted serum was achieved when HBB was the running buffer. This result definitely brings out the exceptional advantages of nanoplasmonic biosensors for the direct detection of protein biomarkers. Material-selective functionalization can strongly minimize nonspecific fouling, guaranteeing reliable label-free analysis in biological samples.

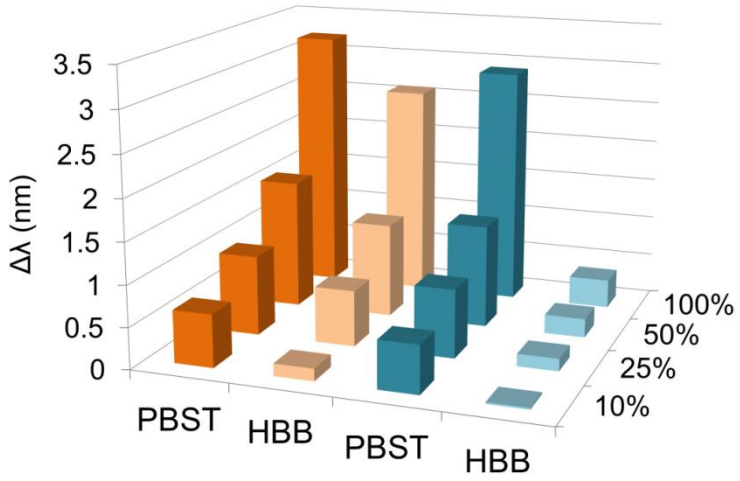

Figure 3.21 Nonspecific adsorption study of serum at different concentrations (10%, 25%, 50%, 100%) using different buffers in flow (PBST 0.5% and HBB) performed for both substrates: SPR gold film (orange) and LSPR gold nanodisks (blue).

3.2.5. Conclusions

The use of ProLinker™ B as orienting molecule for antibody immobilization has been optimized for SPR biosensor and afterwards was implemented on a novel nanoplasmonic biosensor showing great potential for direct immunoassay of protein biomarkers in biological fluids.

This strategy turned out to be highly efficient for antibody coupling in an oriented manner with a relatively low consumption of reagents, resulting in higher analysis sensitivity with respect to more conventional methodologies. The bioactive surface is stable enough to allow reusability to a quite remarkable extent (up to 20 detection cycles) without the need of extra stabilization steps. The strategy offers the same results regardless the antibody/antigen considered, providing its

versatility for different targets. Moreover, ProLinker™ B-based layer allows direct immunoassay in undiluted urine samples avoiding nonspecific adsorption while retaining same sensitivity than in standard buffer conditions. These results demonstrate the robustness of the strategy even in more complex matrices and including also regeneration of the bioreceptor layer.

A new approach based on the use of antifouling PEGylated compounds, particularly the copolymer PLL-PEG, instead of BSA as blocking agents, has shown encouraging results addressed to reduce undesired nonspecific binding events with serum, while retaining target detection's capability. This has been particularly remarkable with gold nanodisks surfaces. The high immobilization efficiency together with the high reproducibility and stability of the bioactive surface fulfill important requirements for label-free biosensor-based immunoassays. Overall, the implementation of the ProLinker™ B strategy to gold nanodisks also highlights its exceptional potential for nanoplasmonic biosensors, additionally benefiting from the sensitivity improvements that LSPR can offer.

3.3. PolyA-based Immobilization Strategy

3.3.1. Description of the PolyA-based Strategy

Antibody conjugation to single-stranded DNA probes (ssDNA) is a common method for antibody immobilization to solid supports. The strategy generally exploits the extreme affinity interaction occurring between two complementary DNA chains, one attached to the surface and one conjugated to the antibody.[150] This methodology has some drawbacks related to the random modification of the antibodies, which could alter the antigen binding sites, or the instability of the DNA helix under certain conditions that might hinder the regeneration and reusability of the biosurface. On the other hand, formation of optimum DNA brushes layer onto gold surfaces still remains challenging. In general, direct functionalization with thiolated DNA strands provides high grafting density of receptors, which usually results in efficient and reproducible hybridization of complementary DNA target. However, when aiming at immobilizing antibodies through DNA functionalization, large spaces between DNA strands and upright orientation are critically required.[183] Low grafting density of DNA may yield to nonspecific adsorption of the biomolecules in a flat conformation. Thus, competitive thiolated molecules, such as mercaptohexanol (MCH), or covalent binding of DNA receptors to a SAM are common strategies to control the lateral spacing and to ensure proper orientation.

Oligonucleotides have shown singular affinities for gold surfaces providing promise alternatives for surface biofunctionalization. Particularly, the adsorption of adenine (A) on gold surfaces has been a subject of interest in recent years due to its biological relevance and also to its potential application in biosensors or for the development of biocompatible materials. Although the interaction mechanism between adenine and gold still remains unclear, an adsorption model has been proposed consisting of adenine coordination to the metal by the NH_2 group and most likely with the contribution of the N_7 ring atom (Figure 3.22).[184, 185] This mechanism attributes major coupling forces to electrostatic interactions with the surface, stacking interaction between adenine molecules and hydrogen bonding, leading to nearly flat and relatively strong interaction with gold.

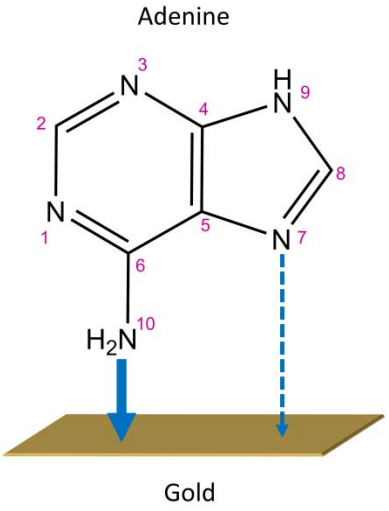

Figure 3.22 Proposed mechanism for adenine adsorption on gold surfaces. Major interaction is attributed to coordination to the metal by the N atoms of the amine group and by the N_7 atom.

Furthermore, affinity of poly-Adenine (polyA) chains was demonstrated to be significantly higher when compared to other nucleotides (polyA > polyC ≥ polyG > polyT).[158] Actually, several gold functionalization strategies have been proposed, especially for DNA immobilization, taking advantage of the base-dependent competitive affinity of homo-oligonucleotides. In this regard, d(T_m-A_n) block-oligonucleotides (i.e. thymine d(T) and adenine d(A) blocks consisting of m and n nucleotides, respectively) can be adsorbed onto gold surfaces adopting a L-shape conformation, where polyA tail binds completely flat to the surface while the polyT chain extends away from the surface, vertically oriented (Figure 3.23).[183, 186] Contrary to what might be expected, the hairpin conformation of self-complementary d(T_m-A_n) oligonucleotides in solution is disrupted in presence of Au, resulting in close-saturation coverage of the metal surface by the polyA blocks.

This unique property of $d(T_m\text{-}A_n)$ oligonucleotides can be exploited to form density-controlled DNA brushes on gold surfaces with proper conformation.

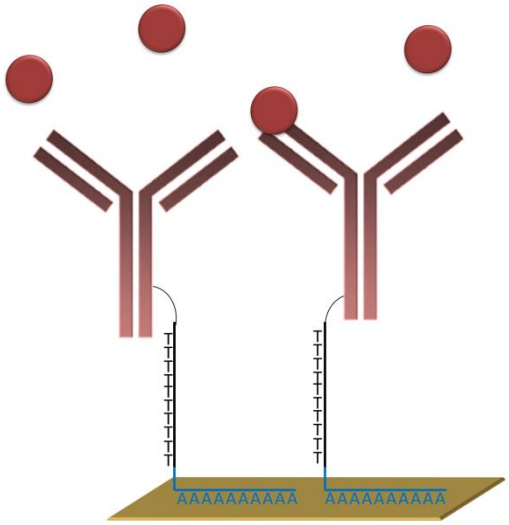

Figure 3.23 Design of polyA-based antibody immobilization strategy: site-directed conjugation of antibodies to $d(T_m\text{-}A_n)$ oligonucleotides, which are adsorbed onto the gold surface adopting L-shape conformation.

We propose a novel strategy for direct immobilization of antibodies based on site-directed conjugation of antibodies to amine-functional $d(T_{26}\text{-}A_{15})$ oligonucleotides (Figure 3.23). The specific oligonucleotide sequence (26xT + 15xA) was selected according to previous studies[183] indicating that 15 A bases ensured stable immobilization onto gold surfaces whereas a high amount of T nucleotides would provide enough vertical spacing (in our case necessary to move the antibodies away from the surface). The methodology has been designed to provide proper orientation of the antibody layer by carrying out the conjugation through the carbohydrates residues on the Fc part of the immunoglobulin. This approach should be performed in mild conditions in order to allow the chemical modification of the antibodies with minimum alteration of the antigen binding sites, so that its biological activity remains unaltered.

The polyA-mediated strategy involves basically two steps: (i) antibody conjugation to the $d(T_{26}\text{-}A_{15})$ oligonucleotide and (ii) direct adsorption onto the gold sensor surface.

3.3.2. Antibody-Oligonucleotide Conjugation

Most methods of antibody-DNA conjugation rely on nonspecific amide bond formation with lysine residues, resulting in heterogeneous mixtures that can alter antigen binding sites and lead to

antibody aggregation.[187] Several site-directed antibody modification techniques have been developed taking advantage of the different functional groups present in the immunoglobulins. Chemical modification through the carbohydrate moieties, predominantly found in the Fc region, is known to yield high efficient conjugation without significantly affecting the recognition capabilities. Carbohydrates including *cis*-diols can be oxidized to create active aldehydes (-CHO) for direct coupling to primary amines (R-CH_2-NH_2) or hydrazide groups (-NH-NH_2). Direct binding of primary amines to activated-aldehydes leads to weak and unstable linkage; instead, the terminal amine group of hydrazide is strongly nucleophilic and spontaneously reacts with aldehydes to form stable bonds (Figure 3.24).

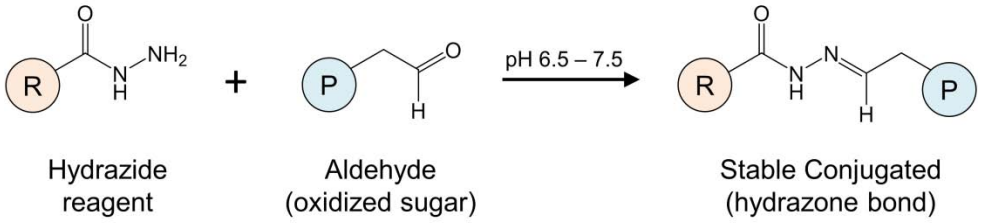

Figure 3.24 Reaction scheme between a hydrazide reagent and an aldehyde-functional compound to form a stable conjugate based on a hydrazone bond.

The conjugation procedure described in this work is schematically represented in Figure 3.25. Aldehyde-activation of the antibody is carried out via mild oxidation with sodium periodate ($NaIO_4$). This oxidation agent is known for effectively creating reactive aldehyde groups from vicinal diols, by cleaving the carbon-carbon bond between adjacent hydroxyl groups (Figure 3.25a, inset scheme). Although the carbohydrate residues affected by this procedure are distant from the antigen's binding regions, it is important to avoid harsh oxidation conditions, which may result in excessive damage to carbohydrate chains or the oxidation of amino acid residues within the antibody structure.[188, 189] On the other hand, amine-functional d(T_{26}-A_{15}) oligonucleotides are modified with succinimidyl-6-hydrazino-nicotinamide (s-HyNic), a heterobifunctional crosslinker which reacts with primary amines and introduces a hydrazine-terminal unit (Figure 3.25b). For conjugation, modified oligonucleotides are incubated with purified antibodies presenting activated aldehyde groups in a molar ratio 2:1, to ensure the complete conjugation of antibodies. Reaction can be traced and quantified by UV-spectrometry of the bis-arylhydrazone group, which exhibits a characteristic absorbance peak at 354 nm (Figure 3.25c). Determination of the absorbance of the bis-arylhydrazone group in the final conjugate allows calculating the molar substitution ratio (MSR), set as the relative concentration of bis-arylhydrazone group per total antibody concentration. In our case, MSR resulted to be 1.84 for conjugation reaction, which

means a total yield of the reaction of 74.46%. The applied procedure resulted in high efficient DNA-antibody conjugation, providing modified antibodies ready to be immobilized onto gold sensor surfaces.

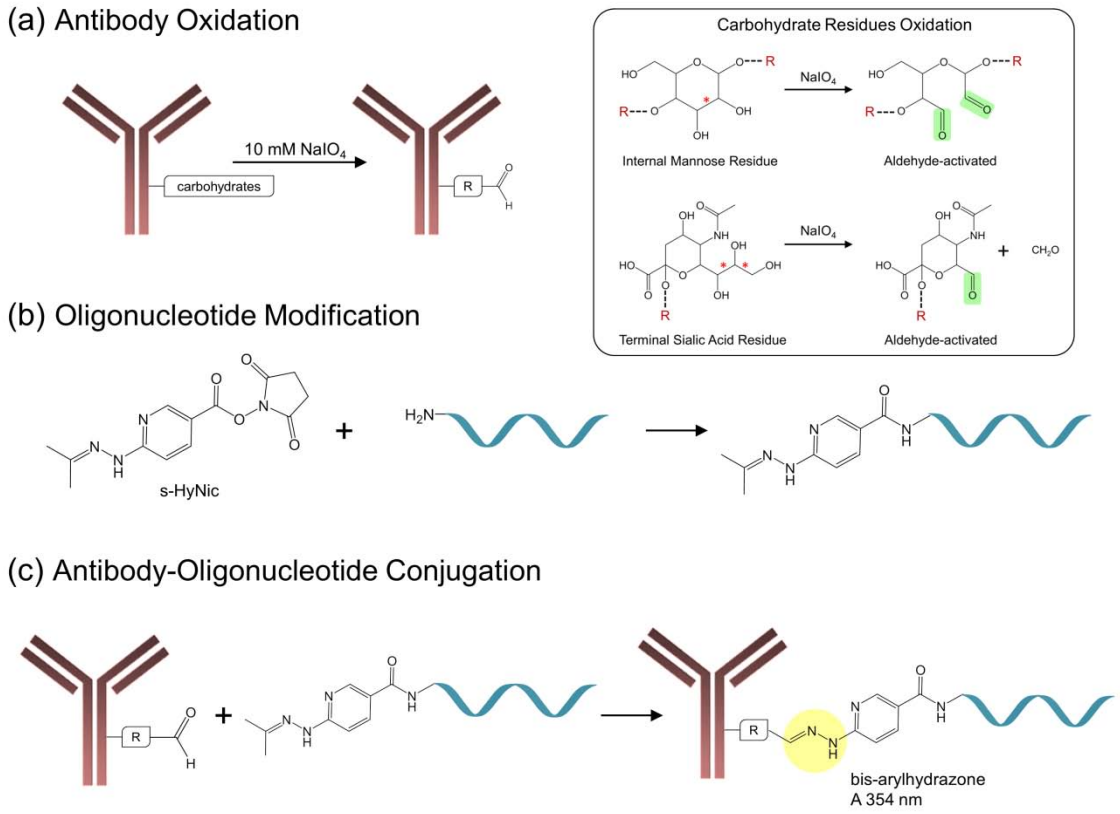

Figure 3.25 Antibody-oligonucleotide conjugation procedure: **(a)** Oxidation of the carbohydrate moieties of antibodies using $NaIO_4$ as oxidation agent, leading to aldehyde groups. Detailed oxidation reactions of sugar residues are represented in the inset scheme; **(b)** Amine-modified oligonucleotide reaction with s-HyNic crosslinker, resulting in hydrazide-functional oligonucleotide; **(c)** Conjugation procedure via direct reaction of hydrazide-modified oligonucleotide to the aldehyde groups of the Fc part of the antibody.

3.3.3. Optimization and Assessment of the PolyA-based Strategy

To assess the polyA-based strategy, d(T_{26}-A_{15}) oligonucleotides were conjugated to anti-CRP monoclonal antibodies as described in the section 3.3.2., and the immobilization efficiency, sensitivity and selectivity were evaluated for the detection of CRP. The study was performed using the SPR biosensor. Anchoring of the conjugated to the gold sensor surface was performed in-flow and results were compared to the ones obtained for direct physical adsorption of non-conjugated antibodies. In this case, comparison with simple physical adsorption is useful to test

the contribution of the polyA conjugated chain to the antibodies in the behavior of the assay which *a priori* should provide orientation, higher immobilization efficiency and stability.

Results displayed in Figure 3.26 show a higher amount of antibodies immobilized (i.e. higher immobilization signals) with the PolyA strategy, demonstrating how the high affinity of the sequence helps to bind to the gold surfaces.

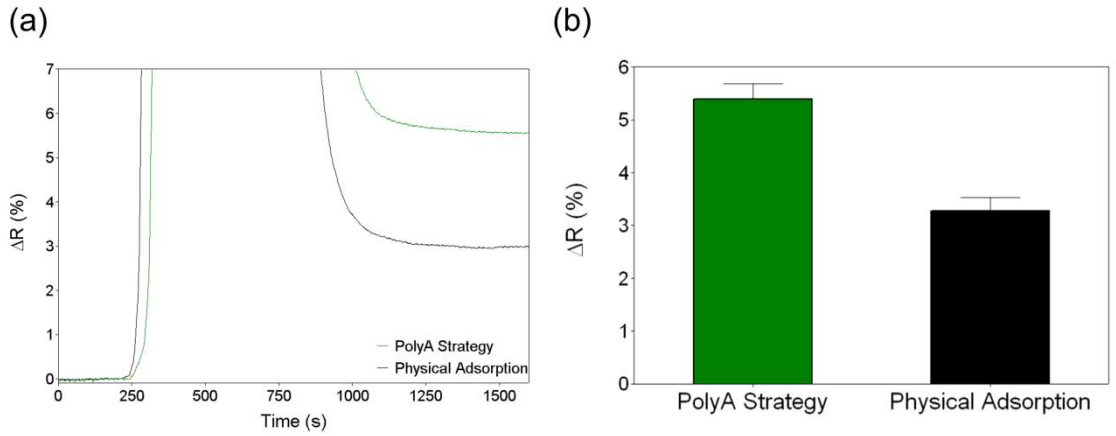

Figure 3.26 (a) SPR sensorgrams of the immobilization of anti-CRP at 50 µg/mL by physical adsorption (black) and using polyA-mediated strategy (green); **(b)** Immobilization signals obtained for the immobilization of anti-CRP at 50 µg/mL by physical adsorption (black) and using polyA-mediated strategy (green). Columns represent signal mean and standard deviation of three different immobilization procedures.

Antigen recognition curves showed significantly improved sensitivity with polyA-mediated strategy as compared to simple adsorption of antibodies (Figure 3.27), which can be attributed to a more efficient distribution of the antibody onto the surface. Random adsorption of antibodies does not offer any control over the density or orientation and may lead to losses of the biological activity or denaturation, on the contrary, the polyA-based strategy provides uniform layer of antibodies, well-oriented and highly accessible for target binding reaching a LoD = 18 ng/mL. It is worth to mention also the role of the PolyT block,[183] which might confer vertical spacing and exceptional mobility to antibodies, enhancing their capability to bind target molecules in the sample.

The achieved LoD was comparable to the one obtained with the ProLinker™ B strategy (LoD = 22.14 ng/mL) in standard buffer PBST. However, in the case of PolyA strategy, the study has been performed employing a concentration of antibody 5 times higher than the one used with the ProLinker™ B ($[anti\text{-}CRP]_{PolyA}$ = 50 µg/mL *vs* $[anti\text{-}CRP]_{ProLinker}$ = 10 µg/mL). In this regard, current work in our laboratory is directed to further optimize the PolyA-based strategy. A more in-depth

study of immobilization conditions, such as antibody concentration or dilution buffer, could enhance the efficiency of this novel procedure, improving the sensitivity of the immunoassay.

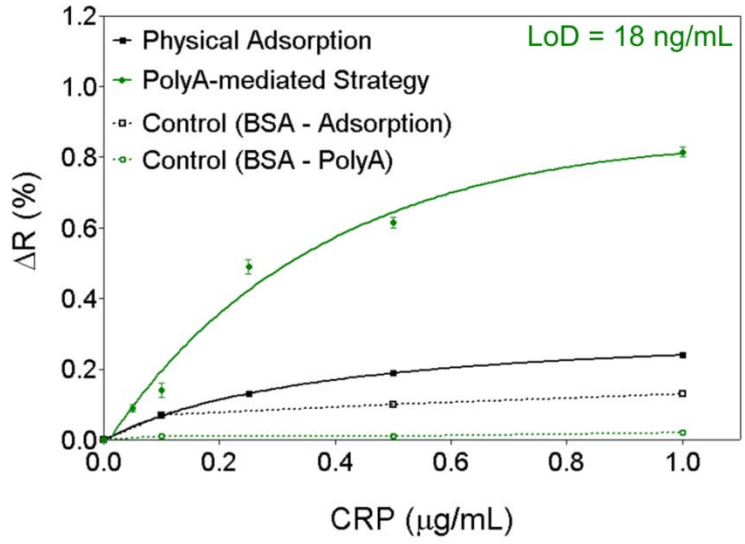

Figure 3.27 CRP detection curves in PBST buffer using 50 μg/mL of anti-CRP using the polyA-mediated immobilization strategy (green) and the physical adsorption strategy (black). Dotted lines represent adsorption of a control nonspecific protein (BSA) onto the antibody immobilized surfaces for polyA strategy (green) and physical adsorption (black).

Specificity of the detection was also examined by performing assays with non-target proteins, such as BSA, at different concentrations. As can be observed in Figure 3.27, nonspecific adsorption of BSA onto the biofunctionalized surface with polyA-based strategy was negligible while relatively significant signal was obtained for the adsorbed antibody biosurface. Main reason for these results relies on the high efficient surface coverage of the polyA blocks, which passivates the gold surface avoiding electrostatic interactions with nonspecific proteins and ensuring selective detection of the target analyte.

Despite polyA oligonucleotides present extreme affinity for gold surfaces, the stability of the interaction needs to be evaluated also under regeneration conditions (i.e. low or high pH) to ensure the robustness and reusability of the biosurface. Serial measurements of the same concentration of CRP were performed including a regeneration step (i.e. removing the target protein from the antibody-immobilized layer) using acidic conditions (HCl 5 mM). Similar detection signals were obtained up to 15 cycles, after then a decrease close to 60% was observed (Figure 3.28). The high reproducibility indicates no desorption of the antibody, whereas the signal decrease may be due to a loss of antibody activity under detection conditions. This confirms the

strong attachment of the polyA-conjugated antibody to the gold surface ensuring the stability and robustness of the strategy for biosensing applications.

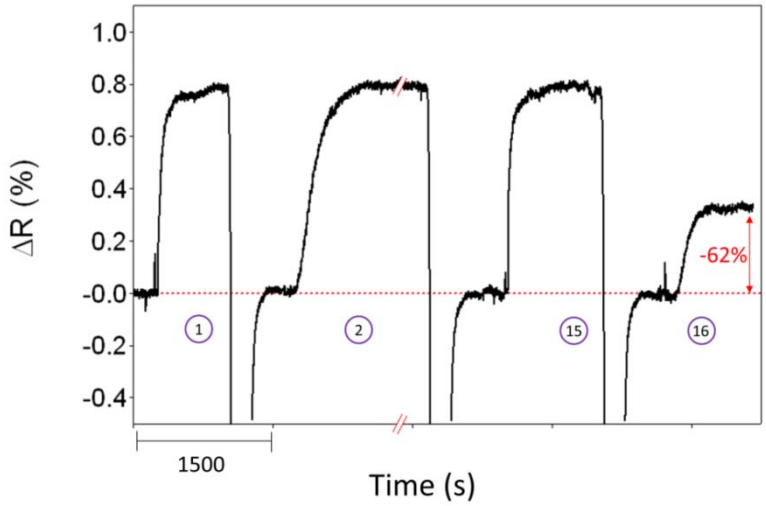

Figure 3.28 Detection cycles performed by consecutive interaction of specific target at 1 µg/mL and regeneration with HCl 5 mM using PBST as buffer.

3.3.4. Conclusions and Future Perspectives

We have proposed a novel immobilization strategy that provides uniform and oriented antibody bioreceptor layer in a simple one-step functionalization procedure. The site-directed conjugation to d(T_{26}-A_{15}) oligonucleotide minimizes possible alteration of antigen binding sites during modification process resulting in antibody conjugates with high biological activity. Furthermore, the extraordinary affinity of adenine nucleotides for gold substrates offers stable and robust immobilization, allowing the reusability of the biosurface. The d(T_{26}-A_{15}) oligonucleotides adopting a L-shape conformation lead to highly accessible antibodies with enhanced detection capabilities while providing maximum coverage of the surface that ensures the specificity.

The detection sensitivity for the direct immunoassay of protein biomarkers resulted comparable to the one achieved with other antibody oriented immobilization procedures, such as the ProLinker™ B strategy. These promising results could be further improved by performing a more in-depth optimization of the PolyA-based methodology. On-going experiments in our laboratory focus as well on the evaluation of the feasibility of this methodology to be employed for the analysis in biological fluids and the transfer to nanoplasmonic biosensor devices.

Chapter 4

ANALYSIS OF GLUTEN IMMUNOGENIC PEPTIDE IN URINE FOR CELIAC DISEASE FOLLOW-UP

We describe the application of the plasmonic biosensor for the therapy control of gluten-free diet in celiac patients. A novel methodology based on the analysis of a digestion-resistant gluten peptide (gliadin 33-mer) present in the human urine has been optimized and assessed. Direct and rapid quantification of gliadin 33-mer peptide can help in the dietary control of celiac patients in a non-invasive manner. Analysis of real clinical samples was attempted to test the feasibility of the methodology as a first approach towards the achievement of a reliable PoC device.

4. Analysis of Gluten Immunogenic Peptide in Urine for Celiac Disease Follow-up

4.1. Introduction

Celiac disease (CD) is a chronic autoimmune disorder induced in genetically susceptible individuals by the ingestion of gluten proteins contained in wheat, barley, rye or oats. The disease is triggered by the presence of not completely digested peptides in the gastrointestinal tract, which are highly reactive to celiac T cells causing inflammation of the small intestine.[190] So far the only effective treatment for CD is a lifelong gluten-free diet (GFD). The strict adherence to a GFD is essential to resolve symptoms and nutritional deficiencies, and also to avoid clinical complications associated with long-term gluten intake in celiac patients, such as osteoporosis, anemia or malignancy.[191] The dietary transgression, which is relatively frequent in celiac population (32.6 – 55.4%),[192] involuntary infringement or hypersensitivity to minute amounts of gluten are the most probable causes for these increased clinical manifestations associated to the disease. Also a part of celiac population (1 - 2%) develops refractory celiac disease (RCD), which is defined as a persistent malabsorption and intestinal damage despite an assumed GFD compliance.[193, 194] Patients with RCD show severe symptoms and they usually require additional therapeutic intervention besides the abstinence of gluten ingestion.

It is generally recommended that individuals suffering CD have a careful therapy follow-up and dietary control. Extensive clinical guidelines have been reported about the importance of a long-term monitoring of the CD patients.[195] However, the current methods or biomarkers for an efficient dietary control still remain unclear or they are risky and costly procedures.[192] Serological analysis of IgA antibodies involved in CD immunopathogenesis (e.g. tissue transglutaminase antibodies) has shown poor specificity and sensitivity for detecting either adherence to a GFD or intestinal damage recovery.[194] The use of serial endoscopies or biopsies is neither useful since it is not considered an ethical practice. Other suggested dietary controls, such as the fecal calprotectine or intestinal permeability tests, can measure the consequences of gluten intake but they do not avoid the harmful aftermaths, they require expensive laboratory analysis and they are not concluding about the adherence to a GFD.[196, 197] A more direct evaluation of the ingestion of gluten could provide a specific and reliable tool for the continued follow-up of GFD compliance, for the assessment of the adherence to treatment and, probably, for an accurate diagnosis of refractory CD.

Previous studies in the field highlight the α2-gliadin 33-mer peptide as a valuable biomarker for gluten detection.[198] The 33-mer gliadin peptide is the main immunotoxic component in wheat

gluten and is resistant toward breakdown by gastrointestinal enzymes. The identification of the 33-mer peptide (residues 57 to 89: LQLQPFPQPQLPYPQPQLPYPQPQLPYPQPQPF), together with other peptides, contributed to demonstrate that gluten epitopes with high antigenicity are located in gliadin regions rich in proline and glutamine residues.[199] This peptide persists in the gut where can interact with the antigen presenting cells (APC) *via* specific HLA-DQ2 and HLA-DQ8 recognition. These complexes activate T cells in the mucosa and, subsequently, trigger the immune response of the body, causing chronic inflammation of the small intestine (Figure 4.1).[200] Part of the 33-mer gliadin peptide is excreted from the human body; thereby the detection of this compound either in feces or urine can be an indicator of gluten ingestion.[201]

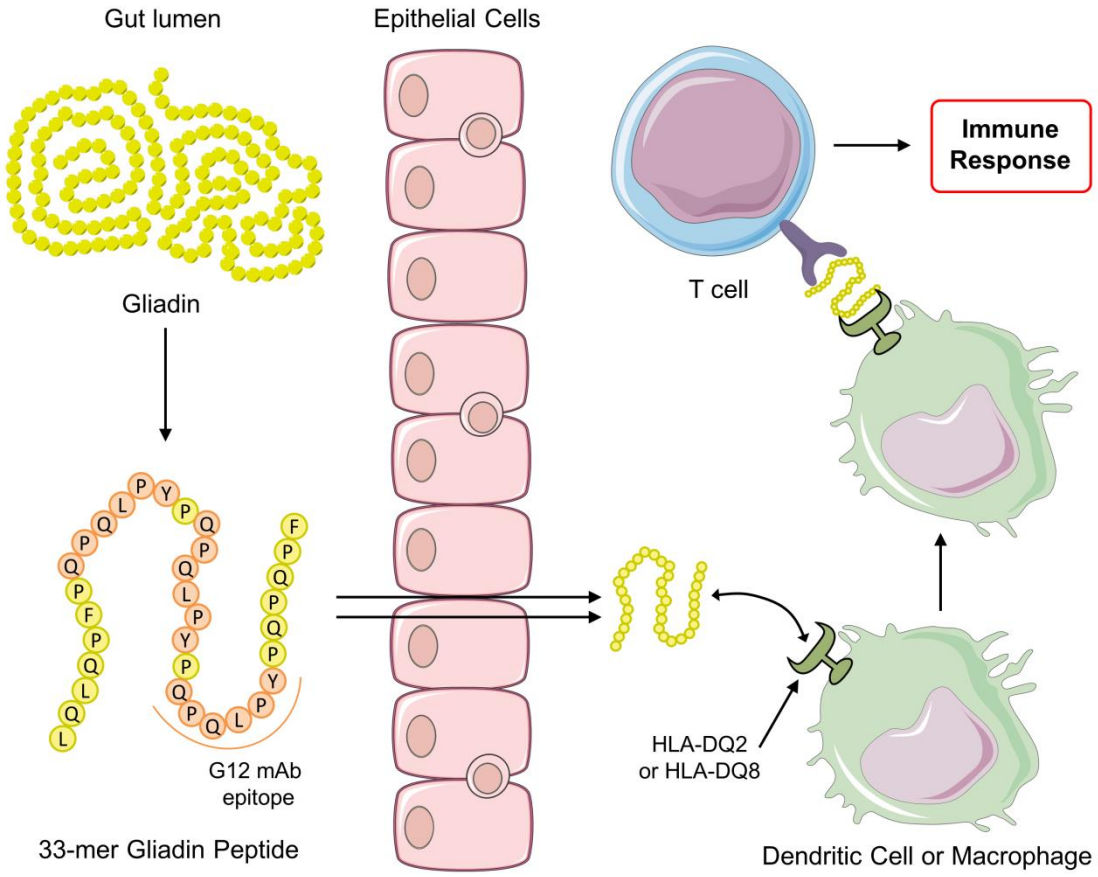

Figure 4.1 Schematic representation of the CD immunopathogenesis mechanism generated by the 33-mer gliadin peptide.

Recently, a monoclonal antibody against this toxic peptide of α-gliadin was obtained (G12 mAb).[202] The G12 mAb specifically recognizes the main immunogenic peptide, in particular the epitope QPQLPY that is repeated 3 times within the 33-mer peptide sequence (Figure 4.1). The antibody also recognizes other immunoreactive peptides in toxic prolamines.[203] The G12 mAb has demonstrated to detect gluten toxic peptides in food samples and has also been assessed in

clinical research to help in the development of novel therapies based on gluten enzymatic detoxification.[201, 204, 205] The ability of the G12 mAb to detect peptides resistant to gastrointestinal digestion makes it ideal for the development of sensitive and specific immunoanalytical methods for the GFD monitoring and evaluation. Comino *et al.* proved the feasibility of monitoring gluten in feces by the detection of epitopes associated with the 33-mer peptide. This approach could be used in clinical studies and dietary monitoring.[201] However, feces analysis requires protein extraction and sample pretreatment which must be performed in laboratory infrastructures that restrict the final implementation as point-of-care instruments. The combination of more easy-to-handle samples such as urine, if possible, and highly sensitive and easy-to-use biosensors can be extremely useful for the development of PoC devices for the dietary control of celiac patients.

In this work, we aimed to develop and evaluate a reliable methodology for the detection of the 33-mer gliadin peptide in urine samples using plasmonic biosensors. The fast and quantitative sensing of the 33-mer peptide might signify a new non-invasive and label-free analytical technique which could be performed at the doctor's office or directly by the patient at home.

4.2. Design and Optimization of the Biosensor Methodology

In order to evaluate the ability of G12 mAb to detect the 33-mer toxic peptide, we designed a competitive label-free immunoassay strategy. The optimization and assessment study was performed using conventional SPR biosensing. With views of subsequently transfer the methodology to the nanoplasmonic sensor, we employed the 70° optical setup described previously in Materials and Methods and in Chapter 3, as it allows direct and reliable comparison between the two biosensor schemes (SPR and LSPR). This biosensor measures the SPR-wavelength displacements caused by the biochemical interaction occurring at the gold sensor surface. Competitive immunoassay was chosen over direct immunoassay because of the relatively small size of the peptide (MW ~ 3.9 kDa). As it was commented in the Introduction (Section 1.2.2.1), low molecular weight analytes induce minute RI changes of the dielectric therefore hindering the direct detection at low concentrations. Instead, competitive immunoassay approach permit the analysis of small compounds usually with high sensitivity, since we monitor the changes in RI resulting from the binding of different amounts of antibody, which is considerably larger.

To carry out the competitive immunoassay, also known as inhibition immunoassay, the antigen or an analogous is immobilized on the sensor surface and a certain concentration of antibody is incubated with the sample. Then, the mixture is flowed onto the functionalized surface where free unbound antibodies (i.e. the antibodies that have not interacted with the analyte in the sample) are captured by the immobilized antigen layer generating a signal inversely proportional to the analyte concentration in the sample (Figure 4.2).

For the optimization of the surface biofunctionalization, several parameters were taken into account. Selection of the proper antigen, concentration and grafting density are crucial to enhance the efficiency of the immunoassay, along with ensuring the maximum surface coverage to prevent nonspecific adsorptions. As it has been previously commented, the use of SAMs provides tight and uniform chemical matrices onto the gold surface that can be chemically activated for the covalent coupling of biomolecules through their functional terminal groups. One of the most commonly used group is the free amine of terminal Lys residues due to its reactivity.

The 33-mer gliadin peptide does not contain any Lys (K) residue within its amino acid sequence (LQLQPFPQPQLPYPQPQLPYPQPQLPYPQPQPF). In fact, cereals in general have a very low content of Lys (K) in their structure.[206, 207] We discarded the use of the peptide as immobilized antigen due to the lack of adequate functionality to provide an easy attachment to the surface. We instead selected the whole prolamin working group (PWG) gliadin as immobilization antigen for the assay.[208] PWG gliadin is considered an international reference reagent in gluten analysis. It is a reference material obtained from the extraction of different wheat cultivars. The mixture (MW ~ 33–45 kDa) has a high content of gliadins and possesses a good solubility, homogeneity and stability.[208] As the specific epitopes for G12 mAb recognition are present in the structure, it was considered a good alternative to 33-mer peptide as competitor antigen. Moreover, PWG gliadin was also used as immobilized antigen for the development of the ELISA.[201] The attachment of the PWG gliadin to the surface was carried out *via* amide formation between those free Lys and a carboxylic acid-alkanethiol SAM making use of the EDC/NHS chemistry (Figure 4.2). The grafting density of the antigen molecules on the surface can be controlled by using mixed alkanethiol SAMs (MHDA/MUOH), varying the ratio of carboxylic/hydroxyl groups. The optimum density strongly depends of the size and nature of the biomolecule. It is difficult to set it *a priori* and it is usually selected in an empirical process for each particular case.

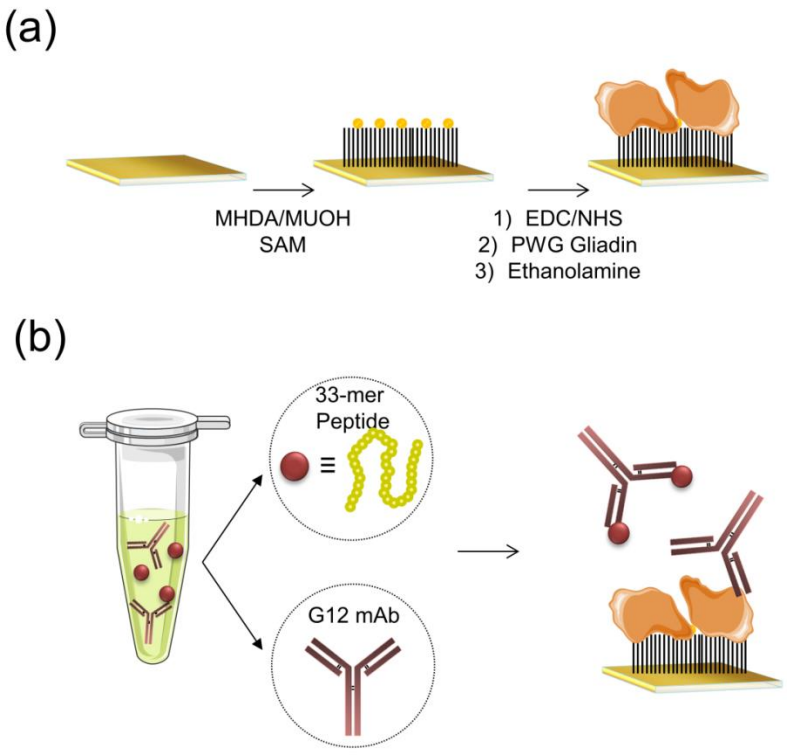

Figure 4.2 Competitive immunoassay strategy for the detection of 33-mer gliadin peptide: **(a)** Gold biofunctionalization *via* covalent binding of PWG gliadin amine terminal groups to a mixed alkanethiol SAM; **(b)** Incubation of the 33EP containing sample with certain concentration of the specific G12 mAb and subsequent detection of unreacted antibodies by the PWG gliadin.

We tested different carboxylic/hydroxyl ratios in the SAM for the immobilization of PWG gliadin by evaluating the ability to detect the G12 mAb. In the case of MHDA/MUOH monolayers, low percentage of MHDA implies low amount of antigen molecules immobilized while elevated ratio of MHDA can result in excessive antigen density, leading to steric hindrance effects. Figure 4.3 shows the signal response of a particular antibody concentration ([G12] = 2 µg/mL) for the same concentration of PWG gliadin ([PWG gliadin] = 20 µg/mL), previously immobilized onto distinct molar ratio of a mixed SAM (MHDA:MUOH = 1:0, 1:1, 1:5, 1:20) at a fixed alkanethiol total concentration of 250 µM. Maximum response was obtained when using 1:1 MHDA:MUOH SAM. As can be observed, the lateral spacing of the reactive carboxylic groups in the SAM provides a significant increase of the capture efficiency as compared to 100% MHDA. As the amount of carboxylic groups decreases also a gradual decrease in the amount of antigen on the surface would be expected, and, as a consequence, also a proportional lower signal resulting from antibody binding. According to these results, we initially set the MHDA:MUOH ratio to 1:1.

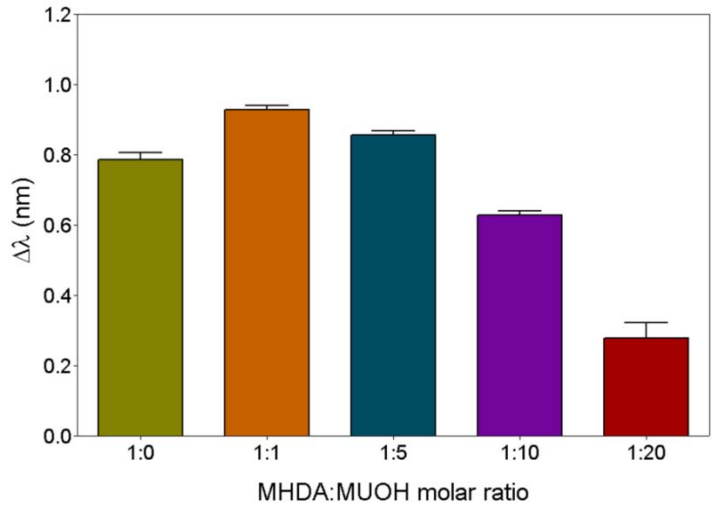

Figure 4.3 Signals obtained for G12 mAb (at 2 µg/mL in PBS) over a surface coated with PWG gliadin (20 µg/mL) with different mixed SAM (MHDA:MUOH molar ratios of 1:0, 1:1, 1:5, 1:10 and 1:20). Signals represent mean and SD of three replicates.

Different PWG gliadin concentrations ([PWG gliadin] = 10, 20, 50 and 100 µg/mL) were immobilized over this selected SAM and several concentrations of G12 antibody were injected ([G12 mAb] between 0.125 and 2 µg/mL). Figure 4.4 shows increasing signals when higher amount of antigen was immobilized. Similar curves were obtained with 50 and 100 µg/mL, which indicated that already using a concentration of 50 µg/mL a complete coverage of the surface was achieved being unnecessary to use higher amount of antigen for the composition of the formed SAM (1:1 MHDA:MUOH). We selected this concentration of PWG gliadin for the next steps.

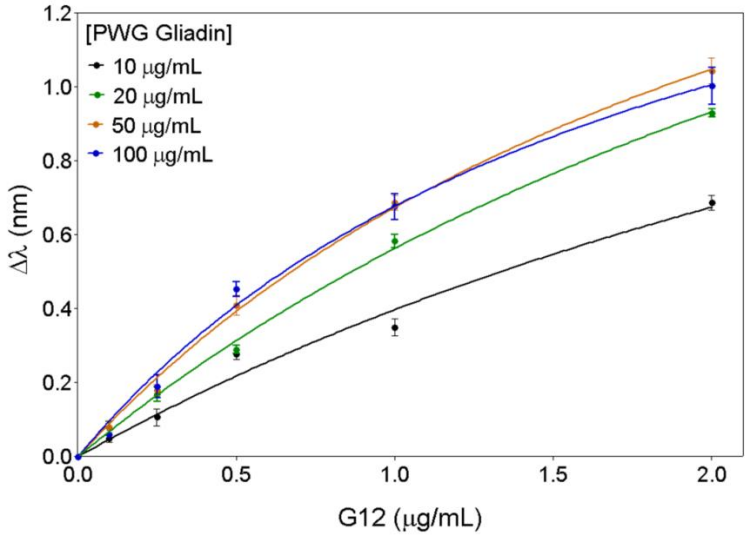

Figure 4.4 Detection curves obtained for G12 antibody in PBS with different concentration of PWG gliadin immobilized onto a 1:1 MHDA:MUOH SAM. Signals correspond to the mean value and SD of three replicates.

In inhibition assays, where a competition is established among three species (antibody against both the antigen on the surface and free analyte in the solution) it is highly relevant the employed concentration of the all three species and the affinity of the antibody towards both the immobilized antigen and the analyte. Analytical characteristics of the immunoassay such as detection limit or dynamic working range are influenced by the fixed antibody concentration incubated with the analyte. Low antibody concentration can be saturated with low amount of analyte, leading to prompt inhibition and, therefore, resulting in a reduced working range. Instead, large antibody concentration may leave high amounts of free antibody accessible to bind to the surface, especially for small quantities of analyte. This eventually leads to worst limits of detection. Proper antibody concentration should provide a measurable signal high enough to allow a wide working range but under saturation conditions, in order to ensure the detection of low concentration of analytes. Therefore a more complete saturation curve (i.e. including higher antibody concentrations between 0.5 – 8 µg/mL) was carried out onto the PWG gliadin layer (at 50 µg/mL) prior to performing the competitive assay (Figure 4.5). According to these requirements, we initially selected an antibody concentration of 2 µg/mL.

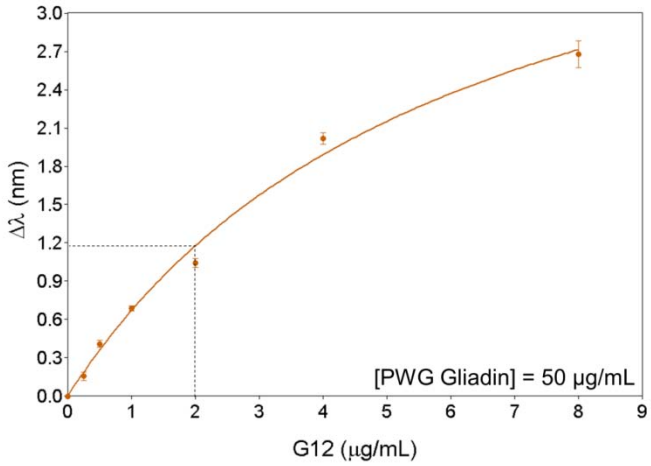

Figure 4.5 Non-competitive saturation curve obtained for G12 mAb in PBS at different concentrations (0 – 8 µg/mL) with 50 µg/mL of PWG gliadin immobilized onto a 1:1 MHDA:MUOH SAM. Signals correspond to the mean value and SD of three replicates.

Also, in competitive assays, an initial preincubation of the antibody with the analyte is often considered for the formation of the immunochemical complex before competing with the antigen at the surface. This step may be necessary depending on the affinity of the antibody for both analyte and immobilized antigen and it is usually empirically evaluated. In order to select the most appropriate time, a concentration relatively high of 33-mer gliadin (1 µg/mL) was incubated with the antibody (2 µg/mL) for different periods of time (t = 0, 5, 15, and 30 min) and then

flowed through the antigen-coated surface. As can be seen in Figure 4.6a, after 15 minutes of preincubation, complete inhibition signal was achieved. This period was enough to ensure the formation of the immunocomplex in solution and was fixed for further experiments. Additionally, we evaluated the specificity of the assay by measuring either a non-target protein which could also be found in the urine, the human Chorionic Gonadotropin, hCG, and a nonspecific antibody (anti-CRP) (Figure 4.6b). Incubation of G12 mAb with hCG at high concentration ([hCG] = 2 µg/mL) led to no inhibition, as signal matched to the one corresponding to maximum signal (zero analyte). The use of a control antibody resulted in a negligible signal, indicating no binding to the surface, which confirms that the signal we obtain in the assay corresponds exclusively to the specific recognition of gliadin by G12 mAb.

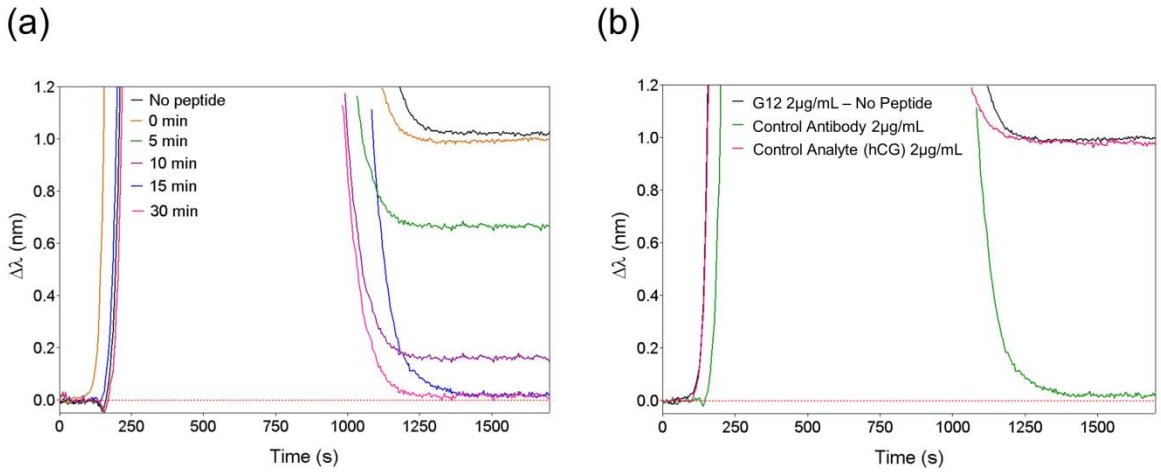

Figure 4.6 (a) SPR sensorgrams obtained for the detection of anti-gliadin G12 mAb (2 µg/mL) incubated with of 33-mer peptide (1 µg/mL) during different times (0 – 30 min) and G12 mAb as zero signal in the absence of 33-mer peptide (black line); **(b)** Specificity study performed by incubating the G12 mAb with hCG as control analyte (pink) or incubating the sample with anti-CRP as control antibody (green). Black line corresponds to maximum signal (G12 mAb signal in absence of 33-mer peptide). All measurements were done in PBS.

The possibility to reuse the biofunctionalized surface by removing completely the captured antibody was also evaluated. Although covalent binding of PWG gliadin to a SAM provides a highly stable antigen layer, it is crucial to determine the optimum regeneration conditions to dissociate the protein-antibody interaction while maintaining the antigen integrity. In our case, regeneration of the surface was accomplished with 5 mM HCl solution (Figure 4.7a). The regeneration procedure leads to complete dissociation of the PWG gliadin/anti-gliadin G12 mAb interaction (the λ_{SPR} after the measurement recovers the same value than before the antibody capture). The high stability of the PWG gliadin functionalized surface allowed more than 100 measurements cycles during more than 10 days with good repeatability and reproducibility levels.

Figure 4.7b illustrates the high reproducible signals obtained with the same biofunctionalized sensor chip during different analysis cycles.

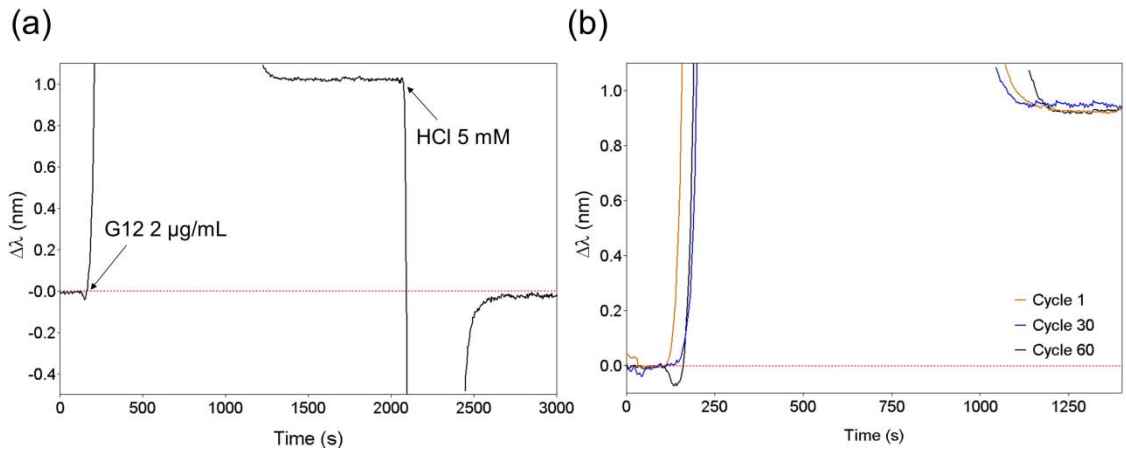

Figure 4.7 (a) SPR sensorgram showing G12 mAb (2 µg/mL in PBS) detection and subsequent regeneration of the biosurface with HCl 5 mM; **(b)** SPR sensorgrams at different lifetimes of the biofunctionalized sensor chip: cycle 1, cycle 30 and cycle 60.

With all the above selected conditions a calibration curve for the 33-mer gliadin was obtained. Different concentrations of 33-mer peptide ranging between 0 – 4000 ng/mL were incubated for 15 min with a fixed concentration of G12 antibody (2 µg/mL) and then flowed over the biofunctionalized sensor surface. Figure 4.8 shows the results obtained as a function of the 33-mer peptide concentration in logarithmic scale.

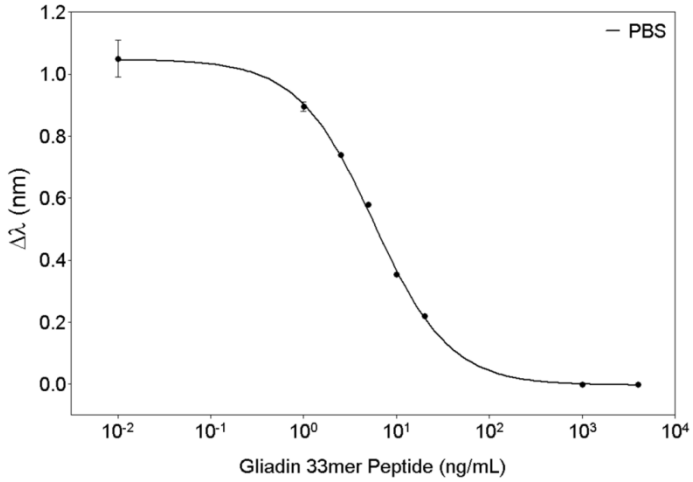

Figure 4.8 Calibration curve for the competitive immunoassay of 33-mer gliadin peptide in PBS.

Fitting to a dose-response inhibition curve, an IC_{50} value of 5.64 ng/mL was obtained. The limit of detection (LoD) (corresponding to the 90% of inhibition - IC_{90}) was 0.33 ng/mL and the linear working range was found between 1.12 – 19.20 ng/mL, being 1.12 ng/mL the limit of quantification (LoQ, corresponding to the 80% of signal inhibition – IC_{80}) (Table 4.1). The achieved sensitivity for the SPR-based detection of 33-mer gliadin peptide was comparable to the LoD determined for 33-mer peptide detection using G12 mAb in different configurations of ELISA (< 1 ng/mL).[202]

Furthermore, we studied the possible influence of the addition of surfactants (e.g. Tween 20) to the dilution buffer. This compound is usually added to prevent nonspecific adsorptions when dealing with biological fluids but can alter the immunoassay performance (the IC_{50} of the analysis). Calibration curves were done in buffers with different concentration of Tween 20: PBS, PBST 0.25% and PBST 0.5% (Figure 4.9).

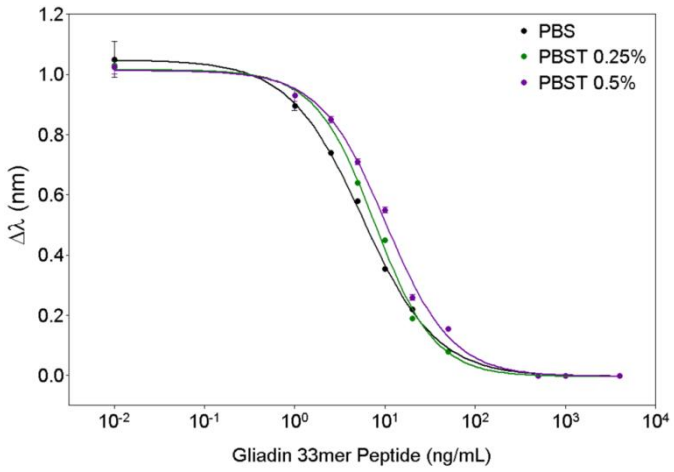

Figure 4.9 Calibration curves for the competitive immunoassay of 33-mer gliadin peptide in PBS (black), PBST 0.25% (green) and PBST 0.5% (purple).

A significant shift of the curve was observed at increasing percentages of Tween 20 in the buffer. The shift leads to an increase of the IC_{50} parameter: IC_{50}(PBS) = 5.64 ng/mL < IC_{50}(PBST 0.25%) = 7.68 ng/mL < IC_{50}(PBST 0.5%) = 10.23 ng/mL (Table 4.1). As the hillslope is similar in the three curves (between -1.22 and -1.07), the higher IC_{50} could be directly related to a higher limit of detection (LoD) and therefore lower sensitivity. According to this, the presence of Tween 20 seems to affect the sensitivity features of the assay but not to a great extent, being possible to perform the assay under these conditions in case of being necessary.

Table 4.1 SPR-based competitive immunoassay parameters for 33-mer gliadin detection.

	Immunoassay Parameters		
[G12 mAb]	2 µg/mL		
[PWG Gliadin]	50 µg/mL		
Incubation Time	15 min		
Regeneration Solution	HCl 5 mM		
Buffer	PBS	PBST 0.25%	PBST 0.5%
Analytical Parameters:			
IC_{50} (ng/mL)	5.62 ± 0.02*	7.83 ± 0.14	10.1 ± 0.3
LoD (IC_{90}) (ng/mL)	0.323 ± 0.007	1.13 ± 0.12	1.85 ± 0.07
Linear Range (IC_{80} – IC_{20}) (ng/mL)	[1.12 – 19.20]	[2.51 – 21.5]	[2.70 – 31.1]
Hillslope	-1.22 ± 0.02	-1.23 ± 0.04	-1.07 ± 0.05
Signal max (nm)	1.05 ± 0.02	1.02 ± 0.02	1.013 ± 0.016
R^2	0.9944	0.9978	0.9954

*Mean ± SD of a minimum of 2 replicate curves with the same sensor chip

Besides sensitivity and selectivity, reproducibility and robustness are key parameters to design a reliable methodology for clinical PoC. For evaluation of the reproducibility both intra- and inter-assay Coefficient of Variability (CV) of the main analytical parameters were calculated for the immunoassay done in standard PBS buffer (Table 4.2). The intra-assay CV represents the variability of the analysis within the same biofunctionalized sensor surface and inter-assay CV determines the variability of the measurements done with different sensor chips. The mean values for the intra- and inter-assay CV obtained were well-below the maximum variability recommended for clinical analysis (~15%).[209] These results proved the excellent reproducibility of the immunoassay and demonstrated the great efficiency and robustness of the biofunctionalization strategy.

Table 4.2 Intra- and inter-assay variability of the main analytical parameters for the immunoassay curve in PBS.

	Intra-assay [a]		**Inter-assay** [b]	
	Mean ± SD	**%CV**	Mean ± SD	**%CV**
IC_{50}	5.62 ± 0.02	**0.35**	5.64 ± 0.04	**0.63**
LoD (IC_{90})	0.323 ± 0.007	**2.17**	0.33 ± 0.01	**3.41**
Signal max	1.05 ± 0.02	**1.9**	1.07 ± 0.06	**5.81**
Hillslope	-1.22 ± 0.02	**1.64**	-1.15 ± 0.04	**3.32**

[a] 3 replicates with the same biofunctionalized chip
[b] 3 replicates with 3 different biofunctionalized chips

4.3. Analysis of 33-mer Gliadin Peptide in Urine

The possibility to collect urine samples repeatedly during long periods makes it one of most attractive biological fluids for dietary control analysis or therapy monitoring. However, there are several limitations for the urinary analysis mainly related to the low concentration of proteins which are usually excreted, the high levels of salts or other interfering compounds and, more importantly, the elevated variability between different samples. Several parameters like pH, osmolality, specific gravity or the concentration of certain components vary over a wide range between different subjects, the diet or the collection time (Table 4.3).[210] The big variability of urine samples represents an important barrier for the reliable detection and quantification of clinical biomarkers.

Table 4.3 Normal range levels of most important parameters for healthy individual urine.

Parameters	**Normal Range**
pH	4.6 - 8
Osmolality	300 – 900 mOsm/kg
Specific Gravity	1.003 – 1.035 g/cm^3
Protein Concentration	50 – 100 µg/mL

So far, to our knowledge, hardly any studies have been reported for the label-free biosensing of small digestive peptides in urine. Current analytical methods are based in mass-spectrometry techniques which require laborious pretreatment and extraction processes, and are expensive and time-consuming.[211] SPR-based biosensing of peptides in urine can offer a potential alternative for rapid and efficient clinical assays as well as for biomarker discovery, enabling simple and sensitive detection in few minutes. However the influence of matrix interferences and the variability among samples needs always to be assessed to provide accurate and reliable analysis.

The feasibility of the direct detection of 33-mer peptide in urine using the SPR biosensor was evaluated by studying the influence of the urine components in the performance of the competitive assay. Although protein concentration in urine is relatively low as compared to other biological fluids like serum or plasma, normal healthy urine contains a total protein concentration between 50 – 100 µg/mL (with albumin representing up to 20 µg/mL).[212] As already discussed in previous chapters, this amount of proteins can be adsorbed onto the sensor surface leading to undesired nonspecific signals. In the previous chapters, we evidenced the extraordinary resistance to protein fouling provided by PLL-PEG copolymer as blocking additive, due to its high hydrophilicity. Therefore a blocking step with PLL-PEG (0.5 mg/mL) after PWG-gliadin immobilization was carried out to prevent undesired adsorptions of urine components. Moreover, the running buffer was changed to PBST 0.5%, which has demonstrated to effectively reduce the nonspecific adsorption onto the sensor surface (see Chapter 3). Sensorgrams depicted in Figure 4.10 compare the signals obtained for undiluted urine onto a PLL-PEG blocked and a non-blocked surface. As can be observed, the use of the antifouling copolymer significantly minimized nonspecific adsorption onto the surface (55% reduction of background signal).

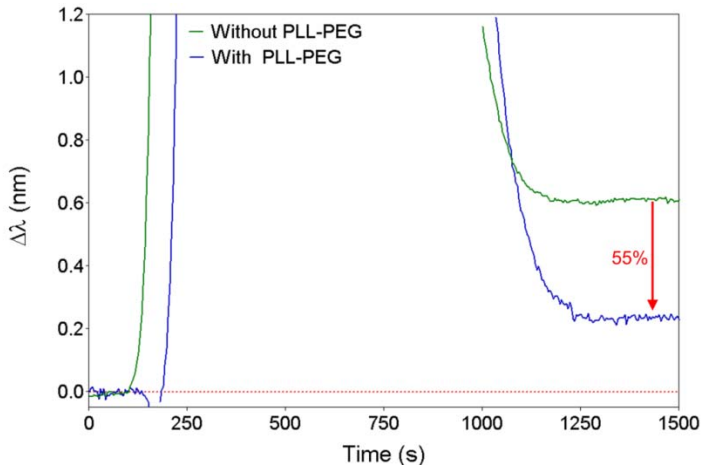

Figure 4.10 SPR sensorgrams of the background signal obtained with undiluted urine over non-blocked (green) and blocked (blue) surfaces with PLL-PEG.

On the other hand, the presence of proteins, the high salt concentration or the pH value may affect the interaction between the antibody and the biofunctionalized surface, leading to important variations of the immunoassay. The anti-gliadin G12 mAb was diluted in different GF urine samples collected from several individuals following strict gluten-free diet, and the detection signals were compared (Figure 4.11a). A clear and significant variability of the antibody signal could be observed (CV = 23.08%), which is attributed to the composition variability of the urine samples. According to this, and in order to stabilize the behavior of the assay, urine samples were buffered by diluting them with PBST 0.5% (1:1). Figure 4.11b shows the antibody detection signals obtained for the different urine samples diluted in PBST. The variability (CV) was reduced to 2.6%, which assures the reproducibility and accuracy of the immunoassay. Moreover, the nonspecific signal obtained in all cases was highly reproducible (SD < 0.01) and then it can be considered as a reference background.

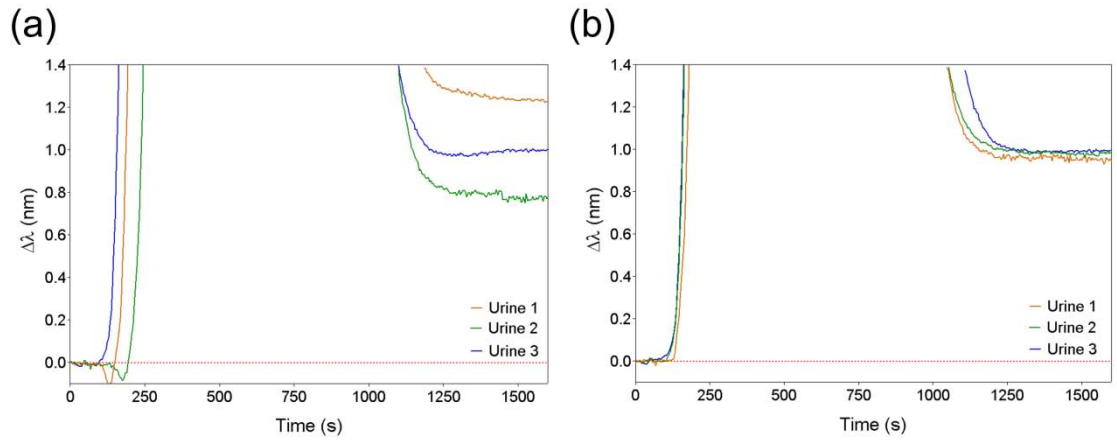

Figure 4.11 Urine variability study performed by measuring G12 mAb (2 µg/mL) in urine from different subjects: **(a)** undiluted urine; **(b)** urine diluted 1:1 with PBST 0.5%.

Finally, a calibration curve of the 33-mer gliadin competitive immunoassay in urine diluted 1:1 with PBST 0.5% was carried out. Different concentrations of 33-mer gliadin peptide (0.1 – 4000 ng/mL) spiked in urine samples were incubated with a fixed concentration of G12 antibody (2 µg/mL) for 15 minutes and then flowed over the biofunctionalized sensor surface. Figure 4.12 shows and compares the inhibition curves obtained for spiked diluted urine and three curves in buffers: PBS, PBST 0.25%, PBST 0.5%. Matrix constituents of normal urine did not produce significant interferences in the competitive immunoassay under those conditions, leading to nearly identical analytical sensitivity than the one obtained in standard PBS buffer. The IC_{50} value was determined at 5.06 ng/mL, reaching a LoD of 0.46 ng/mL and linear range between 1.20 – 21.55 ng/mL.

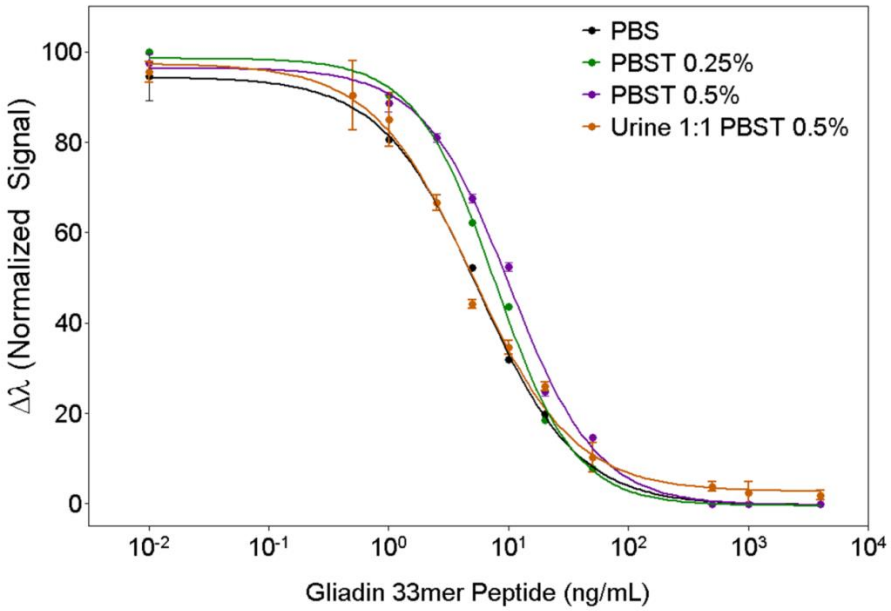

Figure 4.12 Calibration curves for the competitive assay of 33-mer gliadin peptide performed in PBS (black), PBST 0.25% (green), PBST 0.5% (purple) and in gluten-free urine diluted 1:1 with PBST 0.5%.

At this point, the analysis of real samples was attempted. Although the 33-mer peptide is highly resistant to degradation, it is involved in numerous metabolic processes, which should be considered in order to evaluate the feasibility of measuring real human urine samples. We first evaluated urine from a healthy individual following a gluten containing diet with a known concentration of 33-mer gliadin peptide (20 ng/mL), determined by Biomedal S.L. using lateral-flow immunochromatographic strips.[213] Sample was diluted with gluten-free urine and then mixed 1:1 with PBST leading to a final peptide concentration of 5 ng/mL. After incubation with G12 mAb (2 µg/mL), the sample was flowed over the biofunctionalized SPR chip. Figure 4.13 compares the signals obtained with urine samples containing the digested 33-mer peptide (green solid line) and the synthetic 33-mer peptide spiked in gluten-free urine at same concentration (5 ng/mL) (orange solid line). As can be observed, the resulting signals were significantly different, despite the 33-mer gliadin concentration being theoretically identical in both cases. Reference background signals for both samples (positive and negative urine without G12 mAb) were also evaluated in order to discard possible variability due to matrix components (dashed lines). This first result suggested that the detection of the digested peptide might be hampered by either interfering substances (e.g. formation of complexes with some protein or other peptides) or possible structural changes in the amino acid sequence happening during the metabolic process,

such as deamidation of glutamine (Q) residues. Both situations would eventually lead to higher signals (less inhibition) as observed in Figure 4.13.

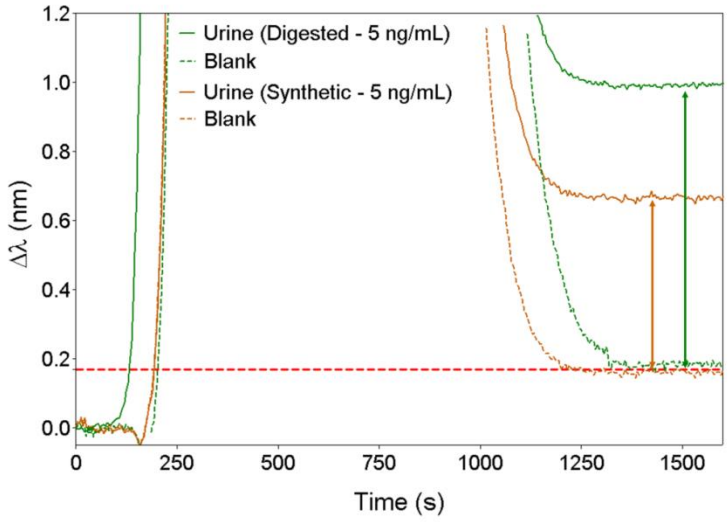

Figure 4.13 SPR sensorgrams of real gluten-containing urine (green) and gluten-free urine spiked with synthetic 33-mer gliadin peptide (orange), both at 5 ng/mL. Signals were obtained after incubation with G12 mAb and diluted 1:1 in PBST. Dashed lines represent background signal obtained by injecting urine samples (1:1 PBST) without G12 mAb.

Glutamine deamidation is a reaction carried out by the tissue transglutaminase (tTg), an enzyme present in the intestinal mucosa that converts the neutral glutamine residues to negatively charged glutamic acid (E) (Figure 4.14).[214, 215]

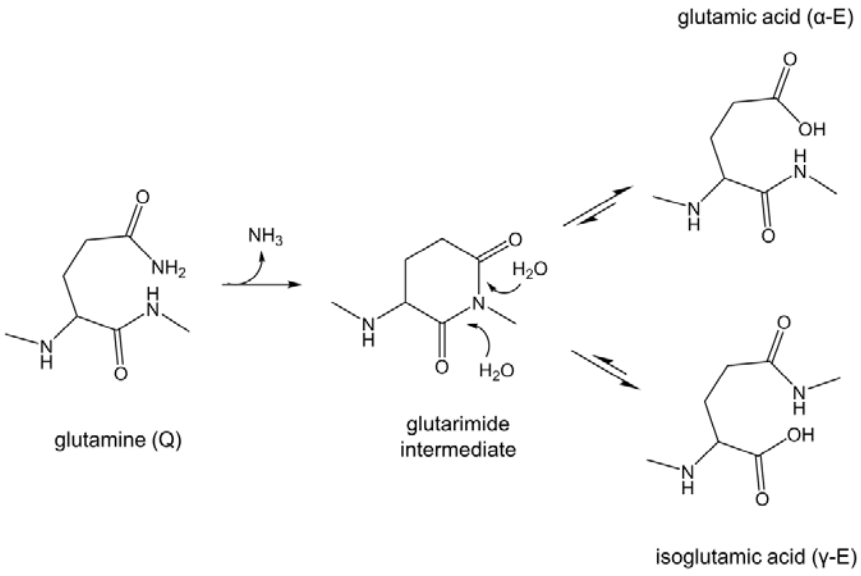

Figure 4.14 General mechanism for glutamine (Q) deamidation to form glutamic acid and isoglutamic acid via glutarimide intermediate.

This process occurs to gliadin peptides, as an essential step to trigger the immune response.[200] Celiac disease is associated to the formation of complexes between gluten peptides and HLA-DQ2 or HLA-DQ8 heterodimers, involved in antigen presenting mechanisms. Binding mechanisms of these systems require the presence of negatively charged amino acid residues at key anchor positions, and such amino acids are largely absent in native gluten peptides generated in gastrointestinal tract.[200] The main function of tTG involves the crosslinking of proteins by forming bonds between glutamine (Q) and lysine (K) residues. But the enzyme has a high avidity for gliadin peptides and in the absence of lysines can deamidate the glutamine. The 33-mer gliadin peptide in particular is considered a preferred substrate to the tTg as it contains a relatively large proportion of Q residues susceptible to turn into E residues.

Although it is not clear whether the 33-mer gliadin excreted in the urine have been either partially or totally deamidated, modification of numerous Q residues present in the G12 epitopes (QPQLPY) could be expected, which could eventually affect the antibody affinity. In fact, previous studies reported the relative affinity of the G12 mAb for different peptide versions (deamidated and native sequences). In that case, synthetic short-chain peptides were designed to represent both peptide sequences: native (QP**Q**LPYPQP) and deamidated (QP**E**LPYPQP), and the relative sensitivity of G12 was evaluated by competitive ELISA (Figure 4.15).

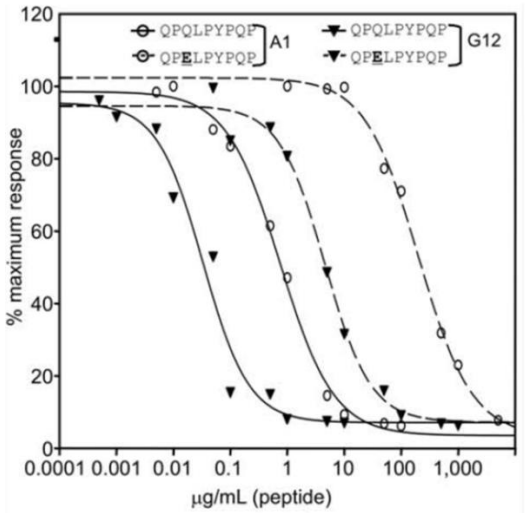

	G12		A1	
	IC50 (µg/mL)	CR (%)	IC50 (µg/mL)	CR (%)
QPQLPYPQP	0.03	100	0.75	100
QPELPYPQP	4.60	0.72	202.69	0.37

Figure 4.15 Competitive ELISA for evaluation of the affinity of G12 mAb (triangles and solid line) (and A1 mAb – circles and dashed line) for a peptide containing recognition epitope (QPQLPYPQ) and its deamidated analogue (QPELPYPQP). IC_{50} and cross-reactivity (CR) values are indicated. Figure extracted from Moron *et al.*[203]

Although G12 mAb did recognize the deamidated sequence (deamidation of just one Q residue), detection sensitivity resulted in more than 100-fold lower than it did for the non-deamidated peptide (IC_{50}(non-deamidated) = 0.03 µg/mL, IC_{50}(deamidated) = 4.60 µg/mL). Although this result suggests a decrease in the affinity of the antibody against deamidated versions of the peptide, we cannot a priori conclude and quantify what effect on the final affinity will take place when naturally metabolized 33-mer gliadin (either completely or partially deamidated 33-mer peptide) is evaluated.

To elucidate the possible reasons for the immunoassay behavior with the digested gliadin peptide observed in the Figure 4.15, part of the gluten containing urine sample was subjected to an extraction and purification procedure. The process was performed by Biomedal S.L. using their proprietary technology. After the procedure, it is expected to obtain a standard PBS sample containing the isolated digested 33-mer gliadin peptide exclusively. Concentration of the 33-mer peptide in the sample was adjusted to 20 ng/mL, considering a correction factor provided by Biomedal S.L. according to their protocol. This purified sample was considered as a standard solution of the digested 33-mer peptide.

We carried out competitive immunoassays for the digested 33-mer peptide: one preparing the standard curve in PBS using the corresponding purified sample in PBS, and the other one in human urine (gluten free diet urine) using the same sample but unpurified. We compared the results with those obtained with the synthetic peptide in both PBS and spiked in urine. As the initial concentration of the digested peptide in both PBS and urine was 20 ng/mL, samples were pre-concentrated and then, serially diluted in buffer and gluten-free urine respectively, in order to cover the concentration range necessary to define the assay. Competitive immunoassays were performed applying the optimized conditions described before (i.e. the urine was diluted with PBST 0.5%). Figure 4.16 shows the calibration curves (blue and green curves) which were compared with those obtained with the synthetic 33-mer peptide (black and orange line).

If we first compare the results obtained for the digested peptide in both PBS and urine (blue and green lines) we can observe a good correlation between both curves, suggesting that probably the peptide is not forming any complex or interacting with other compounds of the urine which could hinder its detection. This, together with all our previous experiments, would confirm the lack of interference coming from urine components.

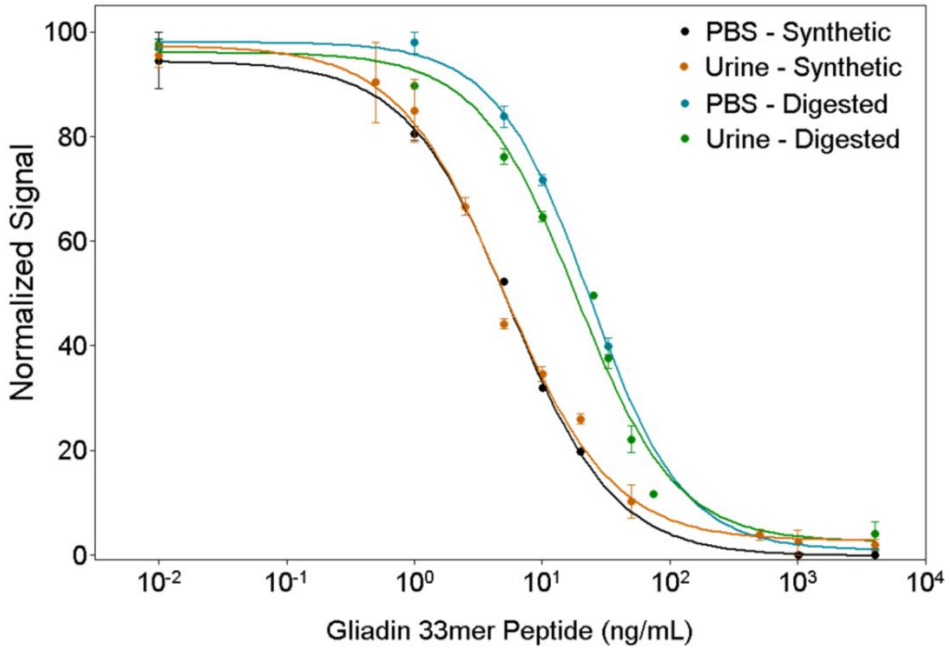

Figure 4.16 Calibration curves obtained for the competitive immunoassay of: (i) synthetic 33-mer peptide diluted in PBS (black); (ii) synthetic 33-mer peptide spiked in GF urine (orange); (iii) digested 33-mer peptide diluted in PBS (blue) – purified positive urine – and (iv) digested 33-mer peptide in urine – untreated positive urine – (green). Curves with urine samples were performed by diluting 1:1 in PBST 0.5% buffer. Values correspond to the mean value and SD of three replicates.

If we then compare the results obtained in urine with the synthetic and the digested peptide (orange and green lines) we can see a significant shift in sensitivity with the digested peptide. The IC_{50} values determined for these curves (IC_{50}(digested) = 18.58 ng/mL, IC_{50}(synthetic) = 5.06 ng/mL) revealed a cross-reactivity (%CR = IC_{50}(synthetic) / IC_{50}(digested)) around 27.2%, (Table 4.4). Similarly, if we compare the curves obtained in PBS (black and blue curves) an analogous shift revealing a CR around 24% was observed. As we have discarded a lower effective concentration of accessible peptide we could conclude that these results are a consequence of a lower affinity of the G12 mAb for the digested peptide in comparison with the synthetic one.

Combining all the above conclusions, we can preliminary suggest a structural modification of the 33-mer gliadin peptide during its metabolic route as main hypothesis for these results, possibly via transglutaminase-mediated deamidation. These results must be interpreted with caution and further studies should be carried out aimed at confirming the peptide conformation and structure in the digested urine or to find out any other reason for the unexpected behavior of the competitive immunoassay in real urine samples.

Table 4.4 Analytical parameters for synthetic and digested 33-mer peptide detection.

	PBS		Urine[a]	
	Synthetic	**Digested**	**Synthetic**	**Digested**
IC_{50} (ng/mL)	5.64	23.37	5.06	18.58
LoD (IC_{90}) (ng/mL)	0.33	3.03	0.46	1.72
Linear Range (IC_{80} – IC_{20}) (ng/mL)	1.12 – 19.20	6.65 – 76.87	1.20 – 21.55	4.57 – 68.88
Hillslope	-1.063	-1.179	-1.033	-1.121
CR (%)	100	24.1	100	27.2

[a] Urine diluted 1:1 PBST 0.5%

Although quantification was at this stage not entirely reliable, we attempted a preliminary qualitative evaluation of real samples. We measured several urine samples containing different concentration of gluten in order to test the feasibility of the biosensing methodology to identify gluten ingestion. Urine samples were collected from celiac patients of the Hospital Virgen del Rocío (Sevilla, Spain) and volunteer healthy individuals with different diet conditions: (i) gluten-free diet, (ii) low consumption of gluten and (iii) moderate/normal consumption of gluten. Four samples of each group were measured. Each sample was only diluted 1:1 with PBST and incubated with G12 mAb for 15 min. The samples were then flowed over the functionalized sensor surface and measured in real time. Samples were interpolated in the calibration curve (Figure 4.16, green curve). Figure 4.17 compares the results obtained for each diet condition based on the determined statistical median of the interpolated concentration. Concentrations for every sample qualitatively correlate with the expected amount of gluten present in the urine. Besides, it can be observed a significant statistical difference between the individual populations.

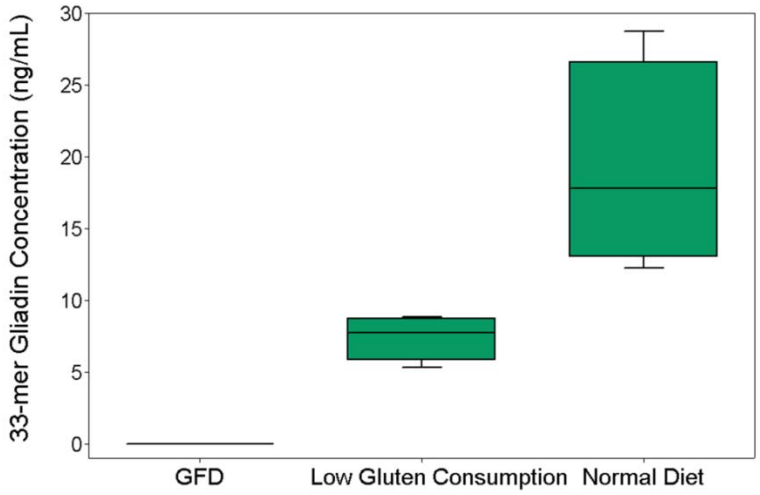

Figure 4.17 Analysis of patient's urine samples from individuals following a (i) gluten free diet (n = 4), (ii) low gluten consumption diet (n = 4) and (iii) normal diet with high/moderate consumption of gluten (n = 4). Median, maximum and minimum values are shown.

4.4. Application to the Nanoplasmonic Biosensor

The transfer of this analytical methodology to the nanoplasmonic biosensor was subsequently attempted. The nanoplasmonic chips were functionalized taking into account the previously optimized conditions with the SPR biosensor (50 µg/mL PWG gliadin over a 250 µM alkanethiol SAM). We employed the same biosensor platform than before with an angle of incidence θ = 70° but in this case using TE polarized light instead of TM polarization which is required for LSPR excitation.

Several G12 mAb concentration were measured under non-competitive conditions and a similar profile to the one obtained for SPR detection (see Figure 4.5) was obtained. As with SPR, an antibody concentration of 2 µg/mL was selected and a calibration curve was done in standard PBS buffer, applying analogous experimental conditions. Different concentrations of 33-mer peptide ranging between 0 – 4000 ng/mL were incubated for 15 min with 2 µg/mL of anti-gliadin G12 mAb and then flowed over the biofunctionalized nanoplasmonic sensor surface (Figure 4.18). A limit of detection of 0.40 ng/mL was reached, with a linear dynamic range between 1.87 – 21.95 ng/mL. The IC_{50} value was 5.80 ng/mL. The achieved sensitivity was highly comparable to SPR biosensor results (LoD = 0.33 ng/mL, IC_{50} = 5.64 ng/mL). It is worth mentioning that although our nanoplasmonic biosensor has shown a better sensitivity than the SPR (according to our previously discussed results), this improvement was observed in direct assays and particularly at low concentrations of analyte. In competitive immunoassays, a three-species system is present and

the affinity of the antibody towards both the analyte and the antigen immobilized plays a decisive role in the final sensitivity, which might be more relevant than the sensitivity gained with the sensing configuration. Moreover, we cannot indeed discard a better outcome using the nanoplasmonic biosensor set at 80º of angle of light incidence according to its better performance in terms of sensitivity (see section 2.1.4 in Materials and Methods).

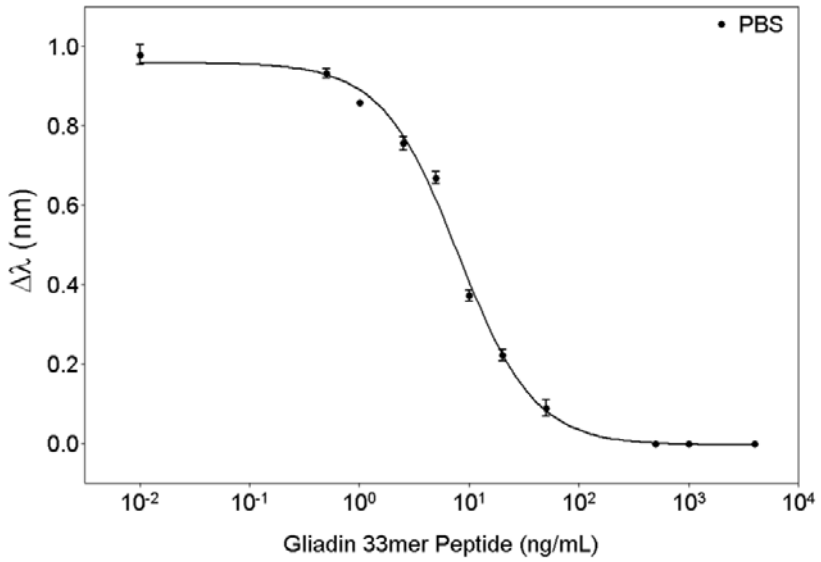

Figure 4.18 Calibration curve for the competitive immunoassay of 33-mer gliadin peptide in PBS employing the nanoplasmonic biosensor.

Besides sensitivity, we also previously observed a better assay performance with gold nanodisks compared to gold chips when dealing with complex matrices (i.e. serum samples in Chapter 3). Thus, the nanoplasmonic biosensor was further evaluated for the detection of the 33-mer gliadin peptide in urine samples. The sensor was also coated with PLL-PEG (0.5 mg/mL) in order to prevent and minimize nonspecific adsorptions of urine components. Undiluted urine samples as well as samples diluted 1:1 in PBST 0.5% were flowed over the functionalized surface and signals were compared to those obtained with the SPR biosensor (Figure 4.19). Remarkably, background signals obtained for the nanoplasmonic surface were negligible in either diluted and undiluted samples (pink and black lines), suggesting that nonspecific bindings of urine components to the sensor surface were more efficiently prevented with the nanodisks sensor chip. This confirms the benefits of the material-selective surface functionalization for the analysis of biological fluids compared to conventional gold surfaces.

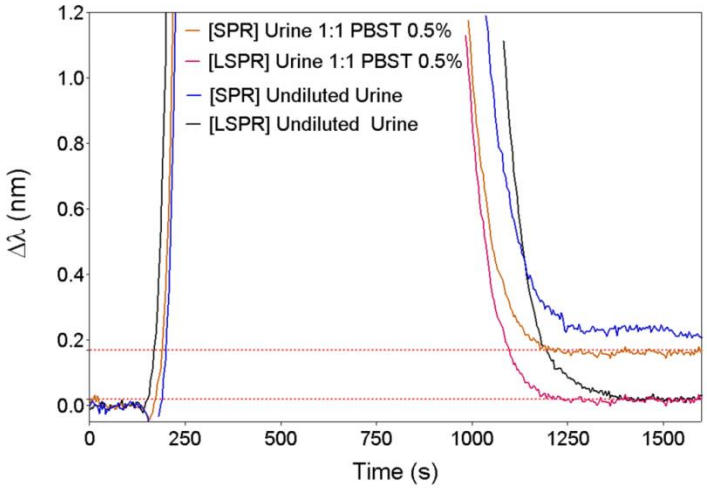

Figure 4.19 Sensorgrams showing the background signal obtained with SPR and LSPR biosensors of undiluted urine (blue and black) and urine diluted 1:1 with PBST 0.5% (orange and pink).

Unfortunately, the matrix components and the huge variability between different urine samples kept affecting the behavior of the immunoassay (variations in maximum signal at zero concentration of analyte) regardless of the chip used (either gold for SPR or nanodisks for LSPR). Therefore, also in the case of gold nanodisks it is necessary to dilute the samples with PBST 0.5% in order to assure the reproducibility and accuracy of the assay. According to this, we carried out a calibration curve in urine diluted 1:1 PBST 0.5%. Figure 4.20 shows both curves performed in standard buffer conditions (PBS) and diluted urine. The limit of detection was found at 0.30 ng/mL and a linear working range between 1.37 – 24.47 ng/mL, being the IC_{50} 5.13 ng/mL. The analytical sensitivity was nearly identical to the results obtained in standard conditions.

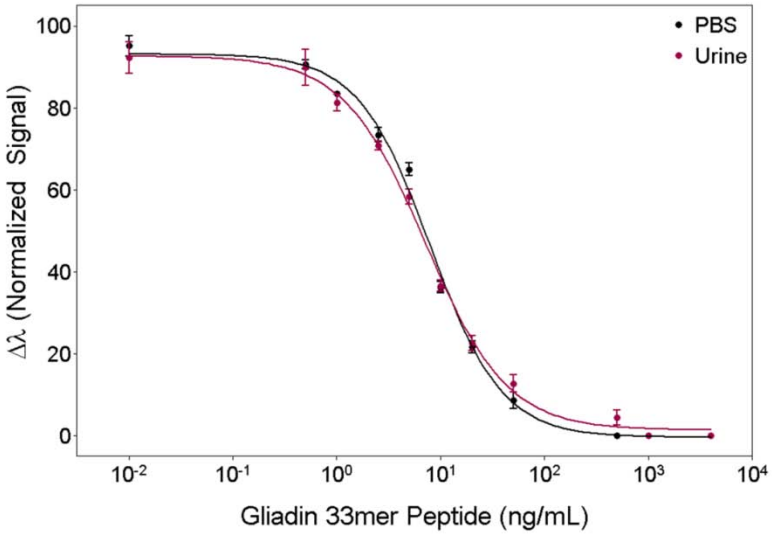

Figure 4.20 Calibration curves for the competitive immunoassay of 33-mer gliadin peptide in PBS (black) and in urine diluted 1:1 with PBST 0.5% (pink) performed with the nanoplasmonic biosensor (70°-setup).

Table 4.5 lists and compares the analytical parameters determined for the detection of the 33-mer gliadin either in PBS and urine samples when employing the nanoplasmonic biosensor.

Table 4.5 Main analytical parameters determined for 33-mer gliadin detection using the nanoplasmonic biosensor.

	PBS buffer	**Urine[a]**
IC_{50} (ng/mL)	5.80 ± 0.03*	5.13 ± 0.21
LoD (IC_{90}) (ng/mL)	0.40 ± 0.01	0.302 ± 0.009
Linear Range (IC_{80} – IC_{20}) (ng/mL)	[1.87 – 21.95]	[1.37 – 24.47]
Hillslope	-1.25 ± 0.03	-1.11 ± 0.02
Signal max (nm)	0.98 ± 0.04	1.03 ± 0.03
R^2	0.9918	0.9984

*Mean value and standard deviation for 3 replicates
[a] Urine diluted 1:1 PBST 0.5%

4.5. Conclusions and Future Perspectives

In this study we have proposed a novel analytical technique employing label-free (nano)plasmonic biosensors for the direct and simple detection of gluten in the urine of celiac patients. The methodology is based on the determination of a digestion-resistant gliadin peptide (33-mer gliadin peptide) by using a specific monoclonal antibody as biorecognition element.

The overall performance of the label-free competitive immunoassay was deeply optimized in terms of sensitivity, selectivity and stability employing a SPR biosensor. Covalent immobilization of PWG gliadin to an alkanethiol SAM functionalized gold sensor surface led to a highly stable and robust receptor layer, which allowed the reuse of the sensor for more than 100 measurement cycles, in continuous work during 10 days with elevated repeatability and reproducibility. The efficiency of G12 mAb to selectively recognize the intact 33-mer gliadin peptide was demonstrated, resulting in a highly sensitive detection with a LoD of 0.33 ng/mL, in standard buffer conditions. Furthermore, the biosensor strategy was optimized for the detection of the 33-mer peptide in urine. The use of PLL-PEG as blocking agent together with the addition of Tween 20 to the dilution buffer significantly minimized the matrix interferences, allowing the detection of the gluten-derivative peptide in urine, achieving a detection limit of 0.46 ng/mL. The analysis of

real samples revealed lower sensitivities for the digested peptide compared to the synthetic one. This fact could be attributed to possible structural variations of the 33-mer gliadin peptide occurred during the metabolic route, that lead to lower G12 affinity, athough further studies should be performed to confirm this However, the feasibility to detect the digested peptide was proved by performing a competitive immunoassay with real human urine. The limit of detection in this case was slightly worst (LoD=1.72 ng/mL), but it still represents an exceptional level of sensitivity for the direct and label-free evaluation of small peptides in urine. A preliminary qualitative assay of several real samples was also carried out, showing significant statistical differences between individuals with different diet conditions (GFD, low gluten consumption, normal diet) as well as good correlation between the calculated concentration and the expected amount of gluten-peptides in the urine.

The optimized strategy was transferred to the nanoplasmonic biosensor resulting in comparable analytical sensitivity to the one obtained with the SPR biosensor although a dilution with PBST buffer was unavoidable. Nevertheless, the nanoplasmonic surfaces showed a more efficient minimization of the nonspecific binding of urine matrix components to the sensor surface, leading to negligible background signals. On-going experiments are addressed to confirm the feasibility to directly quantify the gluten-derivative peptide in the urine and to carry out a clinical validation of the methodology.

So far, the designed methodology for the label-free detection of the gliadin peptide in human urine may constitute a first approach for the real-time monitoring of gluten ingestion in a simple and non-invasive manner. This biosensor-based immunoassay shows high potential for the direct detection of small peptides in urine without any kind of extraction or purification procedure, contrary to what is usually required by the current analytical methods (e.g. mass spectrometry). The resistance of 33-mer gliadin peptide to gastrointestinal digestion and the use of G12 mAb may be useful for monitoring dietary compliance in CD patients due to its sensitivity and significant correlation with consumed gluten. Moreover, the rapid and non-invasive determination of gliadin makes the proposed strategy a promising candidate for the development of point-of-care biosensor devices that could overcome some unresolved clinical limitations in celiac patient follow-up, including the monitoring of short- and long-term gluten-free diet compliance, the assessment of the efficacy of enzymatic therapies or the accurate diagnosis of refractory symptoms in celiac disease patients.

Chapter 5

ANALYSIS OF ANTI-AMOXICILLIN IgE ANTIBODIES IN SERUM FOR ALLERGY DIAGNOSIS

A label-free biosensor strategy for amoxicillin allergy diagnosis based on the combination of novel dendrimer-based conjugates as specific receptors and the nanoplasmonic sensor technology is reported in this chapter. The functionalization of gold nanodisks with a custom-designed thiol-ending polyamido-based dendron peripherally decorated with amoxicilloyl groups (d-BAPADG2-AXO) is optimized and assessed for the detection of specific IgE generated in patient's serum during an allergy outbreak. The methodology allows direct quantification of anti-amoxicillin antibodies in undiluted serum samples, with exceptional levels of sensitivity, specificity and reproducibility. Results have been compared and validated with clinical samples confirming the excellent accuracy and reliability of our methodology.

5. Analysis of Anti-Amoxicillin IgE Antibodies in Serum for Allergy Diagnosis

5.1. Introduction

Penicillin adverse reaction is one of most commonly reported allergies to medication, affecting 10% of the world population.[218] Allergic reactions to drugs like amoxicillin or other β-lactam derivatives are mediated by specific immunological mechanisms (Figure 5.1). The β-lactam ring present in penicillin-derivative antibiotics reacts irreversibly with free amine groups on proteins in a process called haptenization. In some patients, this leads to an immune response against the penicillin-protein adduct resulting in an increase of circulating IgE antibodies in blood. If the antibody response generates sufficient IgE antibodies, a severe allergic reaction such as anaphylaxis can happen.

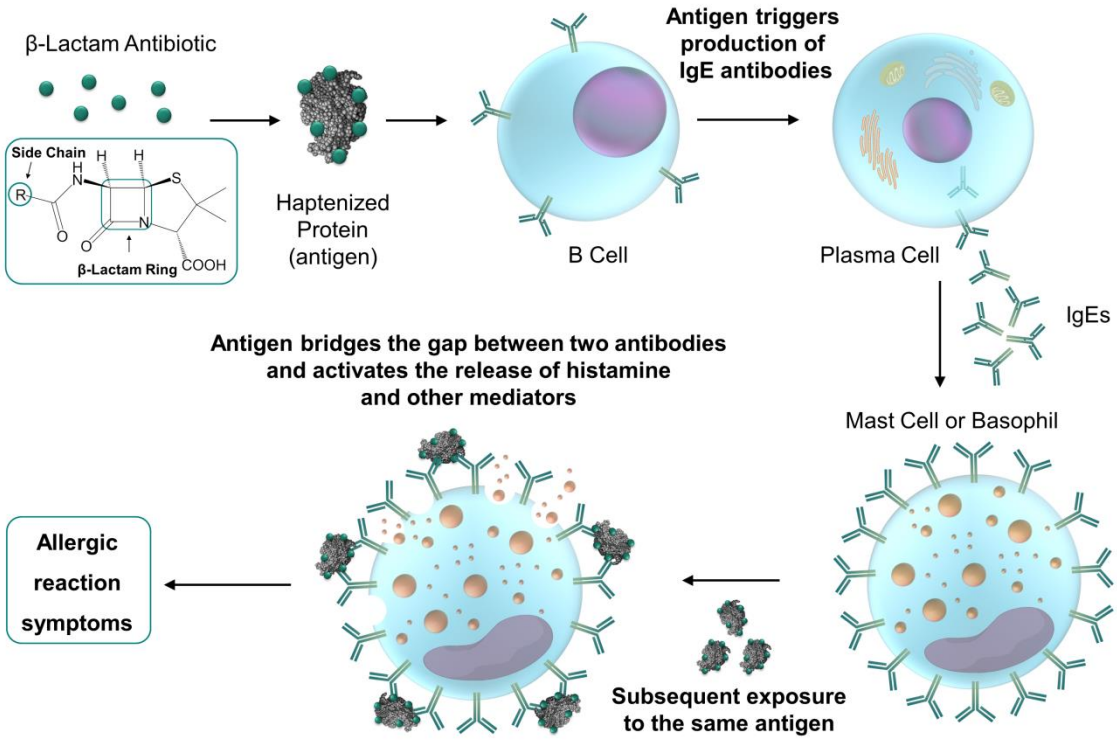

Figure 5.1 Schematic representation of the immunologic mechanism of drug allergy reaction.

The current available diagnostic methods used to assess subjects with an immediate allergic reaction include a complete clinical history plus the performance of *in vivo* skin tests or/and *in vitro* determination of specific IgE,[219] whose production is triggered by the organism during an allergic outburst. Skin testing has been the most generalized approach due to its simplicity and reliability. However it is an invasive technique, it requires the patient to stop medication, and results can be affected by skin condition. Moreover this is not always the appropriate choice

when the patient has suffered a severe allergic reaction. *In vitro* tests which only requires blood sample are attractive alternatives.[220] Radioallergosorbent test (RAST) was for many years the standard gold technique as complementary to skin prick test. The test is based on solid-phase immunoassays and requires the use of radiolabels. It is more a qualitative test and the results are usually given on a numerical scoring system (RAST scale from 0 to 6). However, and despite of being typically less sensitive that *in vivo* skin tests,[221] it has been very useful not only as diagnostic method but also in clinical studies, by investigating critical aspects such as what metabolites are involved in the induction of antibodies[222] or the specificity and activity of serum IgE.[223]

Nowadays RAST has been replaced by the ImmunoCAP tests, based on fluorescent enzyme-labeled immunoassay (FEIA).[224] Basically the methodology is analogous to RAST but substituting the use of radiolabels by fluorescent ones. It shows improved performance resulting from the high-binding capacity of the solid phase used to keep the allergen bound. This technology has been cleared by the Food and Drug Administration (FDA) to provide quantitative measurements of IgE concentration in blood, and it is a standard of sensitivity, accuracy and reliability. It is currently a well validated method which has a working range of 0.35 – 100 kU_A/L, and a cutoff value 0.35 kU_A/L (being A the allergen-specific antibody).[225, 226] In fact, RAST scores have been correlated with IgE concentration determined with ImmunoCAP tests (Table 5.1).

Table 5.1 Interpretation guidelines for allergy diagnosis

Class	IgE Concentration (kU_A/L)	Level	Clinical Correlation
0	< 0.35	Undetectable	Consider non-allergic causes
1	0.35 – 0.69	Low	Uncertain clinical relevance: weak IgE antibody response may be a risk factor for future sensitization
2	0.70 – 3.49	Moderate	Probably contributing factor to total allergic load
3	3.50 – 17.49	High	Clinically relevant
4	17.50 – 49.99	Very High	Highly clinically relevant
5	50.00 – 100.0	Very High	Highly clinically relevant
6	> 100	Very High	Highly clinically relevant

For the determination of antibodies by immunoassay, the hapten molecule or drug (with a molecular weight below 1000 Da) are often bound to a carrier molecule to facilitate the immobilization on the solid support. The nature of both the carrier and the hapten influence the overall performance of the assay (e.g. sensitivity, specificity).[227] Typically, carriers are proteins or macromolecules such as the bovine serum albumin (BSA) or the poly-Lysine (PLL) polymer. Conjugation to BSA and PLL lead to uncontrolled hapten density and a random distribution. BSA has been traditionally considered the natural globular carrier, but depending on the hapten nature (hydrophobicity, size, etc.) the conjugation procedure can alter certain properties, such as the protein solubility, necessary for further handling and use. PLL polymers consist of an average of heterogeneous molecular weight peptides, thereby this type of conjugates can lead to low reproducibility in hapten density and therefore in the subsequent immunoassay. The design of new carriers, such as dendrimers, opens up interesting alternatives for hapten conjugation and for the overall improvement of the immunoassay performance.

Dendrimers are highly branched polymeric macromolecules with a regular treelike structure. The dendritic structure is composed of a central core, the inner shell formed by repetitive monomers, and the outer shell containing the terminal groups (Figure 5.2). Generally, they are classified by generation (G0, G1, G2…), which refers to the number of branching cycles performed during their synthesis.

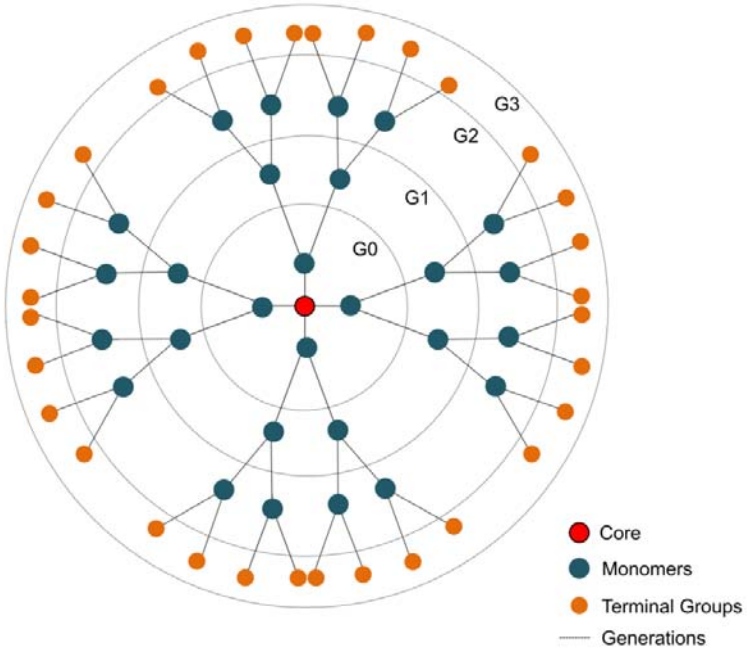

Figure 5.2 Basic structure of a dendrimer.

Contrary to other synthetic polymers (i.e. linear, cross-linked or branched polymers) which are produced by largely statistical polymerization processes and result in polydispersed compounds of many different molecular weights, dendrimers are synthesized in a controlled manner to generate monodisperse and symmetric compounds with specific physical and chemical properties.[228] The synthesis of dendrimers can be carried out through two main strategies: divergent and convergent. In the divergent strategy, the dendrimer is built from the central core towards the outer surface. A polyfunctional nucleus reacts with the branching monomer and subsequently, the monomer terminal groups are activated to react with other monomers. The successive repetition produces the simultaneous growing of the branches, leading to the different generations. In the convergent strategy, the dendrimer is synthesized from the periphery to the core. First step consists in obtaining a series of dendrons or branches of the desired generation having a reactive focal point in one end. The formation of the dendrimer is completed through the assembly of the dendrons to the polyfunctional central core by chemical coupling.

The structural precision and multifunctionality of dendrimers afford important benefits for the development of novel solutions in the biomedical field. Both the internal cavities of their structure and the high-density multidentate terminal groups have been exploited for applications in drug or gene delivery, biomedical imaging, microelectronic and biomimetic systems, detoxication agents for hydrophobic endogenous toxins and also as sensors.[229-231] Especially in biosensors, the use of dendrimers has substantially increased in the last years due to their interesting properties for the immobilization of biomolecules. The regular geometry, stability and high surface functionality provide better control over the thickness of the surface matrix and the spacing of the immobilized molecules. Several reports have demonstrated that the three-dimensional architecture of dendrimers together with the hydrophilicity can provide enhanced sensitivity, greater accessibility, reduced nonspecific binding, high stability and low variability in their response.[232]

The poly(amido amine) PAMAM dendrimers have been the first and most extensively studied family of dendrimers since their synthesis in 1985.[228] PAMAM dendrimers are globular-shaped molecules synthesized by repetitively branched subunits carrying amide and amine functionalities (Figure 5.3). The combination of amide bonds and amine functional groups in their structure is highly reminiscent to the innate biological chemistry and confers to PAMAM dendrimers exceptional biocompatibility and similarity to globular proteins. However, whereas globular proteins are tertiary structures susceptible to denaturing or unfolding conditions (e.g. pH, temperature, light) and generally present unpredictable heterogeneous domains of functionality,

dendrimers are known to be robust and stable structures with homogeneous and well-defined surface functionality. Besides, the relative easy and low-cost synthesis as well as the low toxicity of PAMAM dendrimers have made them viable candidates as biochemical scaffolds.

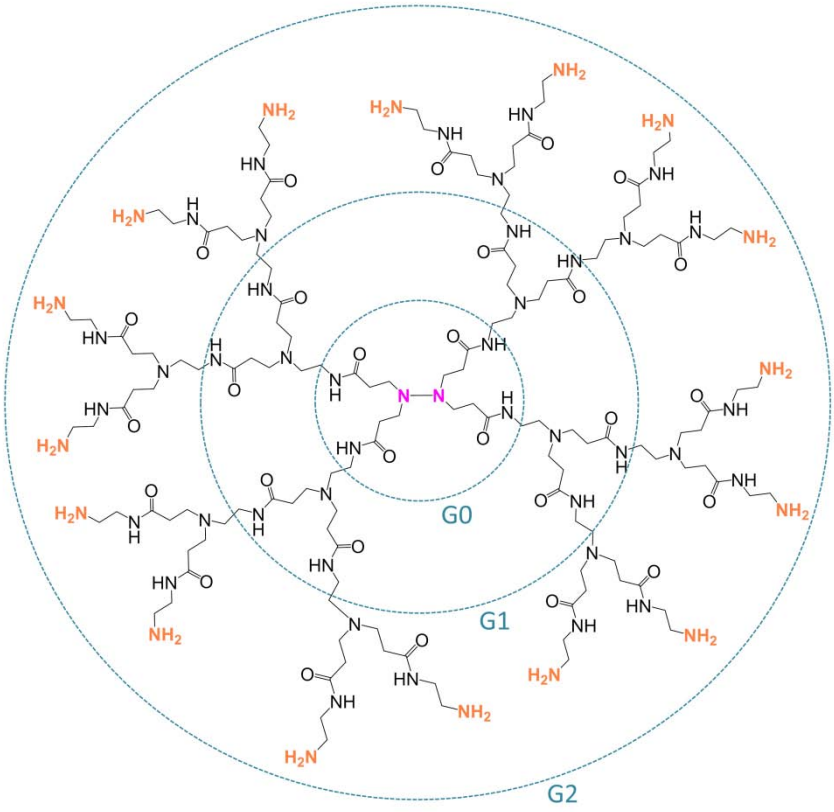

Figure 5.3 Structure of PAMAMG2 dendrimer

PAMAM dendrimers have been successfully employed as carrier molecules to conjugate β-lactam antibiotics, mimicking the behavior of protein-hapten conjugates and showing efficient recognition of IgE antibodies.[233] Further, PAMAM-based conjugates have been attached to cellulose disks[234] or to silica nanoparticles[235] and used as solid phase in RAST assays of serum patient samples. However, none of these studies provided quantitative information of IgE concentration.

In this chapter, we propose the use of a novel dendritic structure, a polyamide-based dendron (BAPAD), as receptor molecules for label-free biosensing. Particularly, we aim to develop an innovative biosensor methodology for the direct quantitation of anti-amoxicillin IgE antibodies in serum taking advantage of the potential of nanoplasmonic biosensors in combination with the exceptional properties of dendrimers for hapten-conjugation and immunoassay performance.

This approach based on the detection of blood circulating antibodies constitutes a good example of a diagnosis application where antibodies are considered disease-related biomarkers.

5.2. Design and Optimization of the BAPAD-based Methodology

Nanoplasmonic-based biosensors have previously demonstrated to provide exceptional features for the direct analysis of clinical biomarkers in biological fluids, such as urine or serum (see Chapter 3). Besides the good sensitivity for label-free analysis in real time, gold nanodisks structured sensors offer extraordinary potential for minimizing the undesired nonspecific adsorptions. However, the achievement of an efficient functionalization strategy onto the gold nanodisks is the most critical factor to define optimum sensitivity, selectivity and stability for the sensing assay.

In general, surface modification of gold patterned substrates requires conditions that assure specific and oriented binding onto the sensing areas (gold nanodisks) while avoiding nonspecific binding of molecules to the substrate (glass). This can be achieved via a stepwise selective surface modification protocol with appropriate reagents, thereby exploiting the strong selectivity of gold for thiol-based compounds. For this reason, we designed a dendrimer structure containing a spacer arm bearing a disulfide group on the core and amoxicilloyl groups (AXO) in its outer shell. Furthermore, the dendritic structure belong to the family of BisAminoalkyl PolyAmide Dendrimers (BAPAD), which is based exclusively on amide coupling emulating protein-like structures (Figure 5.4).

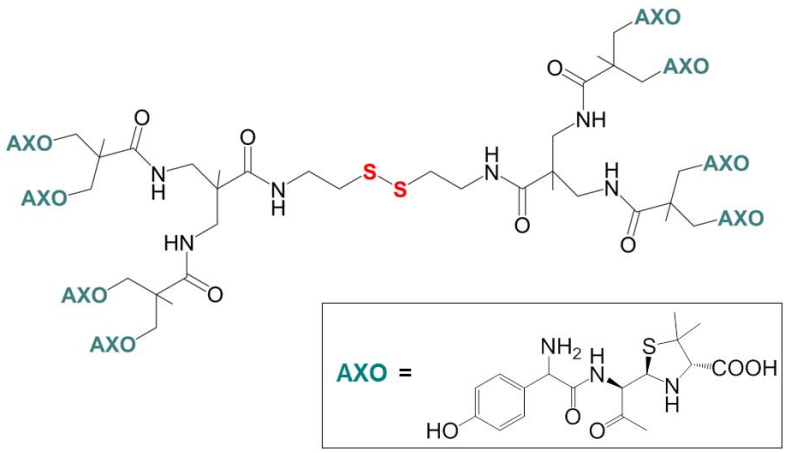

Figure 5.4 Structure of BAPADG2-AXO.

This design allows a fast and simple functionalization onto gold surfaces in only two steps: (i) the reduction of the disulfide-core of the dendrimer to create two thiol-functional symmetric

dendrons, and (ii) their direct immobilization on the gold nanodisks by thiol chemisorption (Figure 5.5). Using the d-BAPADG2-AXO dendron, which incorporates a short thiol linker, a well-ordered receptor layer is formed in a single-step chemisorption procedure. In a separate step, SiO_2 was independently modified by using PLL-PEG. This copolymer creates a brushed coating on SiO_2 surfaces which has proven to successfully prevent and reduce nonspecific adsorptions of proteins due to its hydrophilic properties (see previous chapters).[182]

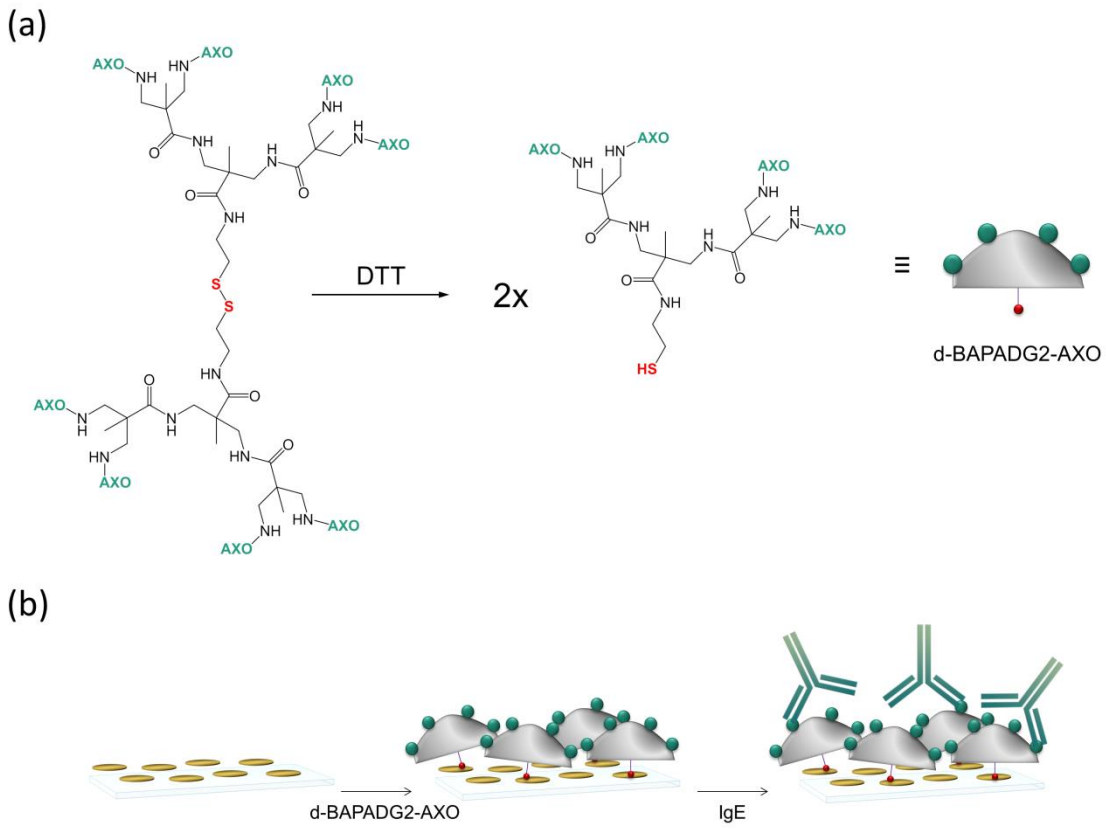

Figure 5.5 Schematic representation of the d-BAPADG2-AXO based biosensing strategy: **(a)** disulfide bond reduction with DTT and **(b)** direct immobilization on gold nanodisks by chemisorption and subsequent detection of specific IgE antibodies.

The synthesis of BAPADG2-AXO conjugates was carried out by Dr. Ezequiel Perez-Inestrosa's group from the Department of Organic Chemistry at the University of Málaga (Spain). The complete synthetic pathway is detailed in our recent article[217] and it can be summarized in Figure 5.6. Following a divergent strategy, it is based on iterative reactions for the growth of the dendrimer structure, in this case, up to generation 2. The strategy includes two steps: (i) condensation between the core (cystamine) and the 3,3'-diazidopivalic acid (1) to obtain amide linker multi-azides; (ii) reduction of the multi-azide structure to obtain the multi-amines, which then will be the reactive groups for the next generation of dendrimer. The strategy was repeated

two times, in such a way that generation 2 (G2) dendrimers were obtained, having 8 amine groups in the outer shell. Then, with the aim of obtaining the dendrimeric-antigen functionalized with the allergenic determinant responsible of the allergic reaction to amoxicillin, this epitope was covalently bound to the periphery of the dendrimer. D-BAPADG2 was reacted with amoxicillin at high pH, to ensure that the amine groups at its periphery were unprotonated, acting as nucleophilic positions that efficiently attack the electrophilic carbonyl group of the β-lactam antibiotic. Reaction conditions were optimized to obtain d-BAPADG2-AXO with amoxicillin in all the reactive positions (8 antigenic determinants per structure) (Figure 5.4). The structure of the amoxicillin-conjugated dendrimer d-BAPADG2-AXO was designed for the detection of IgE antibodies specific for this antibody. The AX was coupled via the β-lactam ring opening, in such a way that the rest of the structure particular to this penicillin (the thiazolidine ring and the variable side chain characteristic for AX) would remain exposed.

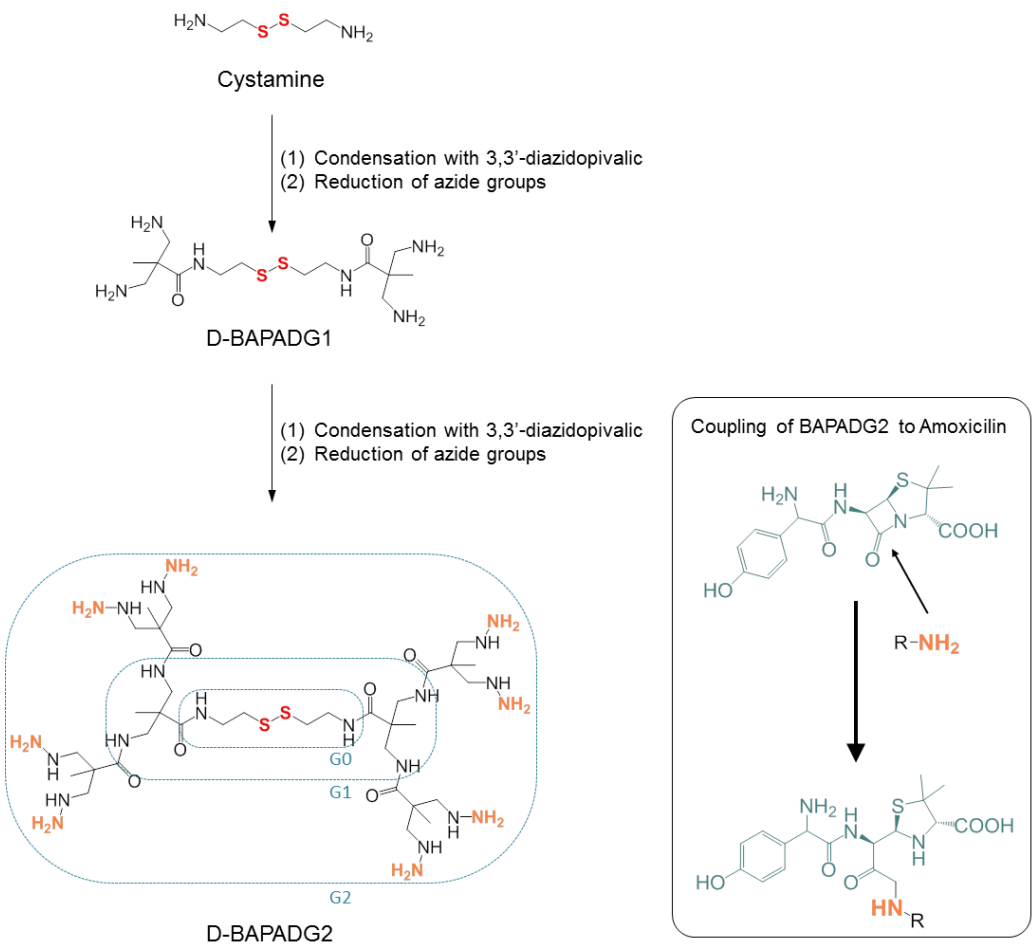

Figure 5.6 D-BAPADG2 synthetic pathway and coupling of amoxicillin.

Ideally, in order to develop the assay (i.e. generate and optimize a calibration curve) the appropriate target should be IgEs obtained from patients, or alternatively, IgE obtained after an external intended production process. However, the standard antibody production protocols are usually directed towards the mechanisms based on IgG generation, which are the most abundant type in serum. Given the difficulty of having specific IgE antibodies for amoxicillin, the evaluation and optimization of our biosensor approach was carried out with commercial anti-penicillin IgG antibodies. Although not exclusively specific for amoxicillin, but also for other β-lactam penicillins, these generic IgG antibodies are very useful to evaluate the behavior of the d-BAPADG2-AXO coated surface and the viability of our proposed approach for detecting IgEs in serum.

To evaluate the BAPAD-based biosensor strategy, we first carried out an optimization of the biofunctionalization procedure of gold nanodisks surfaces. We employed the nanoplasmonic biosensor with an angle of incidence of 80°. The reduction procedure of the disulfide bond of the dendrimer must provide maximum amount of thiol-functional d-BAPADG2-AXO dendrons able to be immobilized onto the gold nanodisks. Among the large variety of reducing agents, dithiothreitol (DTT) is one of the most commonly employed in biochemistry for cleavage of disulfide bridges. This reagent is usually used in high excess over the number of cystamines, showing an optimum pH working range between 7 and 8. A 10 mM DTT concentration was selected to reduce the BAPADG2-AXO dendrimers, which represents between 20 and 200-fold molar excess with respect to the different dendrimer concentrations tested (0.05 – 0.5 mM). The immobilization of the several concentration of d-BAPADG2-AXO onto the gold nanodisks surfaces was monitored (Figure 5.7).

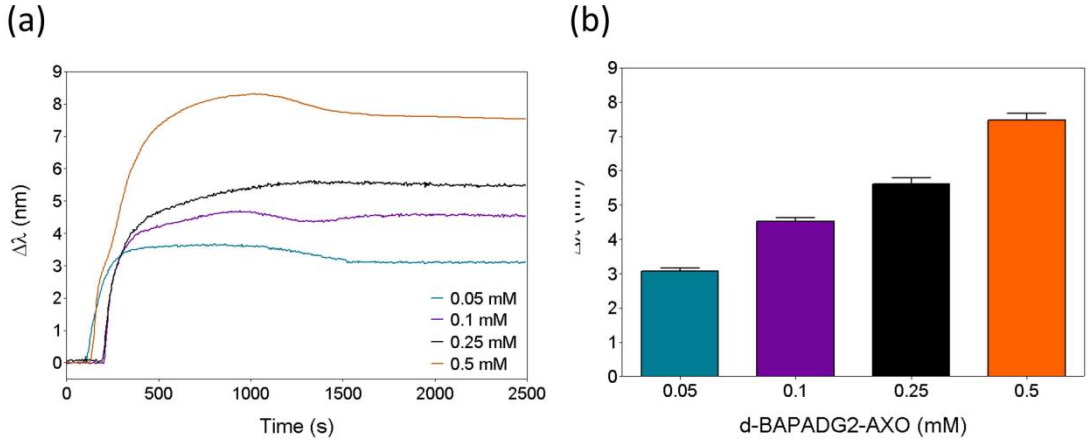

Figure 5.7 d-BAPADG2-AXO immobilization onto the gold nanodisks: **(a)** Sensorgrams of the immobilization step at different dendron concentration (0.05, 0.1, 0.25, 0.5 mM), and **(b)** Immobilization signals of the different concentrations (average signal for 4 replicates).

As can be observed, the immobilization step was concentration dependent and showed high reproducibility (CV ≈ 5-6 %) (Table 5.2).

Table 5.2 d-BAPADG2-AXO immobilization signals measured with the nanoplasmonic biosensor.

Concentration (mM)	Δλ (nm) [a]	% CV
0.05	3.07 ± 0.17	5.53
0.1	4.53 ± 0.21	4.73
0.25	5.61 ± 0.37	6.65
0.5	7.47 ± 0.40	5.33

[a] Mean value ± standard deviation for 4 replicates

Selection of the optimum concentration of receptor must assure maximum surface coverage without affecting antigen accessibility by steric hindrance. Figure 5.8a shows the antibody detection curves performed over the d-BAPADG2-AXO functionalized surfaces at different concentrations. Higher sensitivity was reached at a concentration of 0.25 mM, which resulted in a limit of detection (LoD) of 4 ng/mL. Specificity studies done with other IgGs and control proteins (such as BSA) resulted in negligible binding onto the d-BAPADG2-AXO layer (Figure 5.8b), indicating a high degree of selectivity of the active surface.

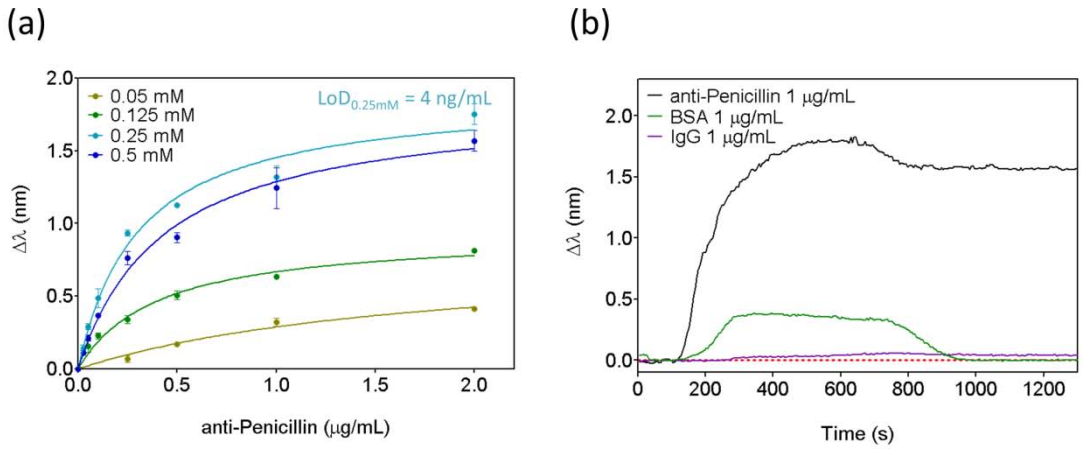

Figure 5.8 (a) Calibration curves for anti-penicillin detection at different d-BAPADG2-AXO concentrations (0.05 – 0.5 mM) performed with the nanoplasmonic biosensor; **(b)** Specificity study for the d-BAPADG2-AXO based strategy: sensorgrams for the detection of specific anti-penicillin antibody (black), nonspecific IgG antibody (purple) and bovine serum albumin (green) at 1 μg/mL; red dashed line indicates reference (background signal).

The direct chemisorption of thiol-functional dendrons onto the gold nanodisks surface offers strong attachment and highly reproducible surface modification. However, the functionalization

strategy may provide long-term stability to assure reproducibility and robustness of the assay. Regeneration of the d-BAPADG2-AXO layer with basic conditions (NaOH 20 mM) led to complete removal of the recognized antibodies after each assay while retaining the integrity of the receptor with good repeatability for more than 40 cycles (Figure 5.9).

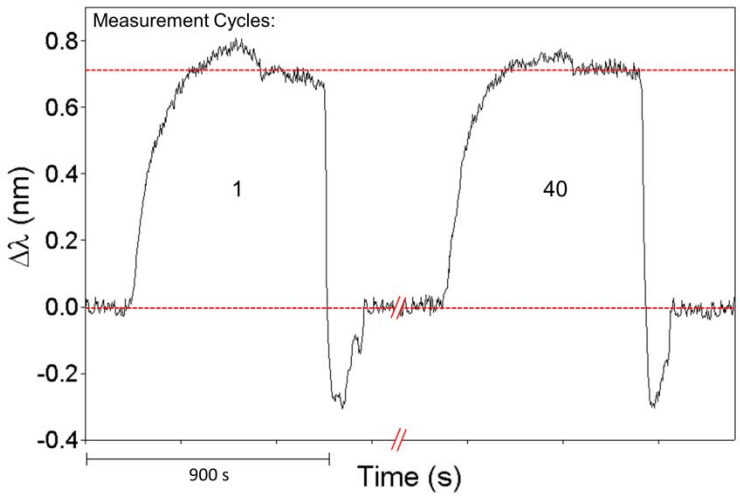

Figure 5.9 Detection cycles consisting of antibody injection (0.2 µg/mL) and subsequent regeneration with NaOH 20 mM using PBST 0.5% as running buffer.

The reproducibility was further evaluated by calculating the variability of the measurements within the same functionalized surface (intra-assay CV) and the measurements performed with distinct sensor chips (inter-assay CV). Table 5.3 lists the CV values determined for the LoD and the maximum signal (Smax) obtained with different analysis. The great reproducibility of the assay ($CV_{intra\text{-}assay}$ = 1.83% and $CV_{inter\text{-}assay}$ = 9.36%) proves the reliability of the methodology.

Table 5.3 Intra- and inter-assay variability of the LoD for the d-BAPADG2-AXO strategy

	Intra-assay		**Inter-assay**	
	Mean ± SD	**% CV**	**Mean ± SD**	**% CV**
LOD (ng/mL)	4.02 ± 0.07	1.74	3.98 ± 0.13	3.17
Smax (nm)	1.67 ± 0.03	1.83	1.66 ± 0.16	9.36

*Mean value and standard deviation for 3 replicates

As previously mentioned, this work was carried out using a nanoplasmonic biosensor with an angle of incidence of 80°. According to our previous studies, the best performance in terms of

sensitivity for our nanostructures would be at incidence angles approaching 90°.[87] In fact bulk sensitivity studies performed for both 70° and 80°- setups proved this better outcome at higher angles of incidence (see 2.1.4 section in Materials and Methods). In order to confirm this, we compared the performance of the BAPAD-based assay obtained with the 80°-setup (θ_1 = 80°) with the analogous platform at 70° angle of incidence (θ_2 = 70°, previously used in Chapter 3 and 4). We also compared both nanoplasmonic configurations with conventional SPR biosensor (70°-setup working with TE polarization) (Figure 5.10). Calibration curves were carried out with the three setups under the same assay conditions ([d-BAPADG2-AXO] = 0.25 mM). As expected, the sensitivity achieved with either the SPR and the 70° scheme were lower than the one determined for the 80° nanoplasmonic biosensor (LoD_{SPR} = 10 ng/mL, $LoD_{70°}$ = 7 ng/mL and $LoD_{80°}$ = 4 ng/mL). The better performance achieved with the 80°-setup can be explained on the basis of the nanoplasmonic sensing principle. Illumination at higher angles of incidence leads to lower energy LSPR wavelengths (λ_{LSPR} is displaced to the right in the spectra) and the light confinement is smaller and the evanescent wave is larger. For the particular angle of 80°, the λ_{LSPR} is found approximately at 750 nm. As a consequence, at these wavelengths, the sensitivity to RI changes is higher and, more importantly, also the signal-to-noise ratio is higher, overall enabling the detection of lower concentrations and improving the performance of the analysis.

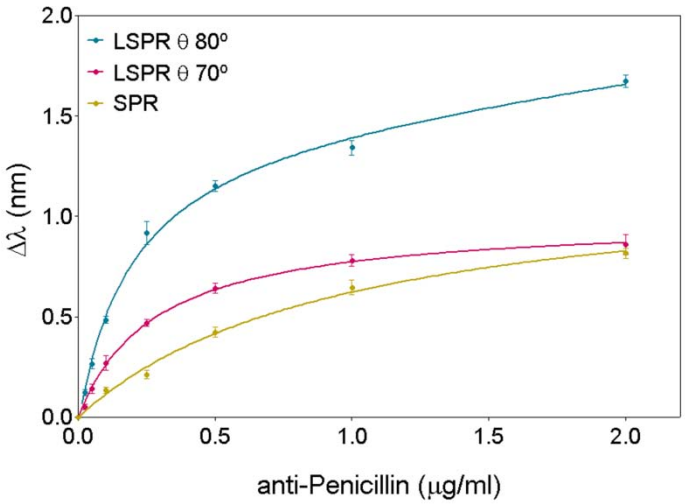

Figure 5.10 Calibration curves of d-BAPADG2-AXO / anti-Penicillin (IgG) based assay performed with 3 different biosensing schemes: conventional SPR (golden), nanoplasmonic biosensing with an angle of incidence θ = 70° (pink) and nanoplasmonic biosensing with an angle of incidence θ = 80° (blue).

5.3. Comparison to Conventional PAMAM Conjugated Dendrimers

PAMAM dendrimers have been widely employed in biomedicine due to their exceptional biomimetic properties along with the precision and stability of the dendritic structure. Especially in optical biosensors, PAMAM dendrimers have been used as functionalization scaffolds with the idea of increasing the immobilization capacity and enhancing the efficiency and stability of the modified surface.[232]

Therefore, the results obtained with the novel BAPAD-dendron approach were compared with those obtained using a conventional PAMAM dendrimer. In particular, we performed a comparison using a PAMAMG2 peripherally decorated with AX hapten, leading to a conjugate with 16 AXO molecules on the amine ends (100% amine modification) (Figure 5.11). This conjugate was also synthesized by the collaborator research group following a similar mechanism (i.e. same coupling to amoxicillin through β-lactam ring opening by the $–NH_2$ groups) to the one used for BAPAD-AXO synthesis described before.

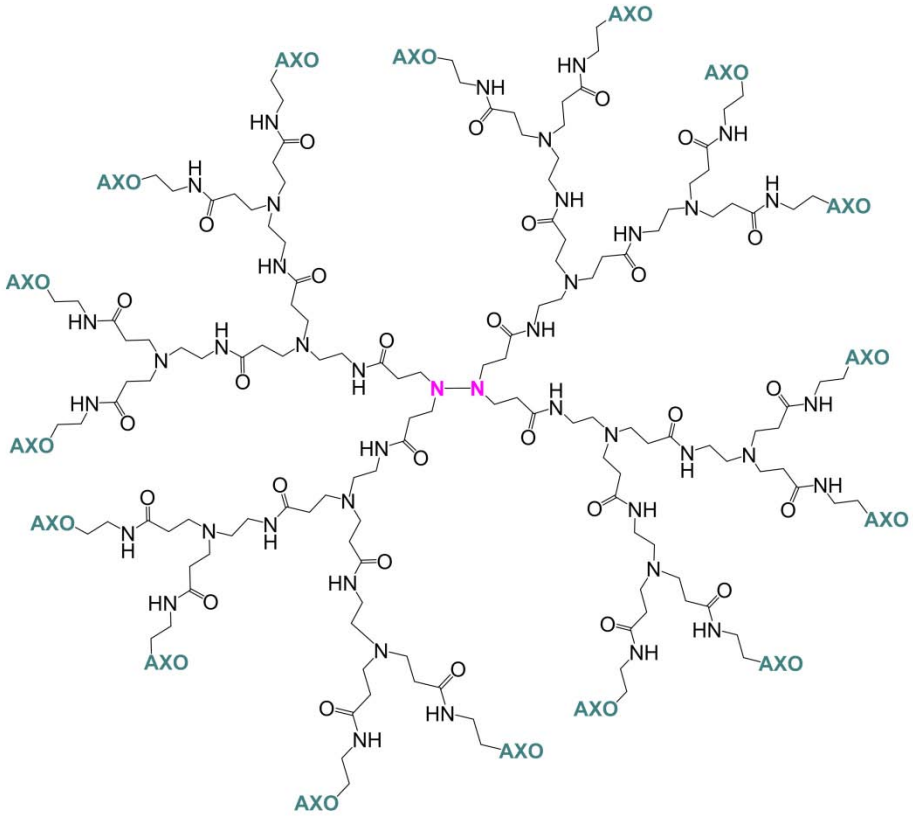

Figure 5.11 Structure of PAMAMG2-AXO dendrimer.

According to this structure, in order to create the receptor layer over the gold nanodisks, a more elaborate coupling strategy had to be used. A covalent immobilization strategy to a SAM was

selected in order to obtain highly stable and reproducible surface as well as maximum detectability of IgE antibodies. PAMAMG2-AXO was covalently coupled to a mixed alkanethiol-based SAM (carboxylic/hydroxyl groups) by using the free primary amine present in the AX molecules (see Figure 5.1 for AX structure) (Figure 5.12). A MHDA/MUOH SAM with a molar ratio of 1:20 was chosen (total SH concentration 250 µM), taking into account the size and structure of the conjugated dendrimers. PAMAMG2 dendrimers have an average diameter of approximately 3 nm presenting AX groups evenly distributed around the globular periphery. This relatively large spacing between immobilized receptors may benefit the accessibility of IgE antibodies and can minimize steric hindrance effects.

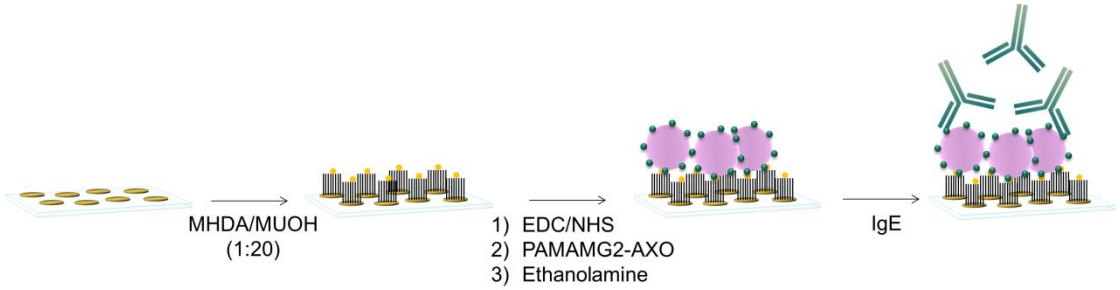

Figure 5.12 PAMAM-based biosensing strategy: (i) mixed MHDA/MUOH SAM formation, (ii) EDC/NHS activation, PAMAMG2-AXO covalent coupling and ethanolamine deactivation, (iii) IgE antibody detection.

First, several PAMAMG2-AXO concentrations were immobilized (0.05, 0.1 and 0.25 mM) obtaining similar response to d-BAPADG2-AXO (Table 5.4). However, PAMAMG2-AXO is a bigger structure than d-BAPADG2-AXO ($MW_{PAMAMG2\text{-}AXO}$ ≈ 8854 Da vs $MW_{d\text{-}BAPADG2\text{-}AXO}$ ≈ 3936 Da). This reveals an overall lower efficiency in the immobilization process as compared with the thiol binding one. The variability was also significantly higher with PAMAMG2-AXO conjugates (CV > 13% compared with CV ≈ 5-6%).

Table 5.4 d-BAPADG2-AXO and PAMAMG2-AXO immobilization signals measured with the nanoplasmonic biosensor.

Concentration (mM)	d-BAPADG2-AXO		PAMAMG2-AXO	
	Δλ (nm) [a]	**% CV**	**Δλ (nm) [a]**	**% CV**
0.05	3.07 ± 0.17	5.53	3.02 ± 0.44	14.49
0.1	4.53 ± 0.21	4.73	4.60 ± 0.62	13.43
0.25	5.61 ± 0.37	6.65	5.21 ± 1.20	15.99
0.5	7.47 ± 0.40	5.33	--	--

[a] Mean value ± standard deviation for 4 replicates

A calibration curve using anti-penicillin IgG antibodies was performed with PAMAMG2-AXO (at a fixed immobilization concentration of 0.25 mM) and compared with the one obtained for the d-BAPADG2-AXO under the same experimental conditions (Figure 5.13). A significant worse sensitivity was observed for the PAMAMG2-AXO strategy (almost 6 times higher LoD). This result can be attributed to structural differences between the dendrimeric molecules. Although PAMAMG2-AXO dendrimer contain 4 times more AX receptor groups in its structure (i.e. 4 AXO per d-BAPADG2-AXO vs 16 AXO per PAMAMG2-AXO), the accessibility of the antigens may be hindered due to an excessive number of AX coupled to the carboxylic-modified surface, leading to a deformation, flattening or collapse of the dendrimer structure. In the case of d-BAPADG2-AXO dendron, the thiol-directed and oriented attachment allows site-directed immobilization leaving exposed the AX groups and hence maximizing the antibody binding.

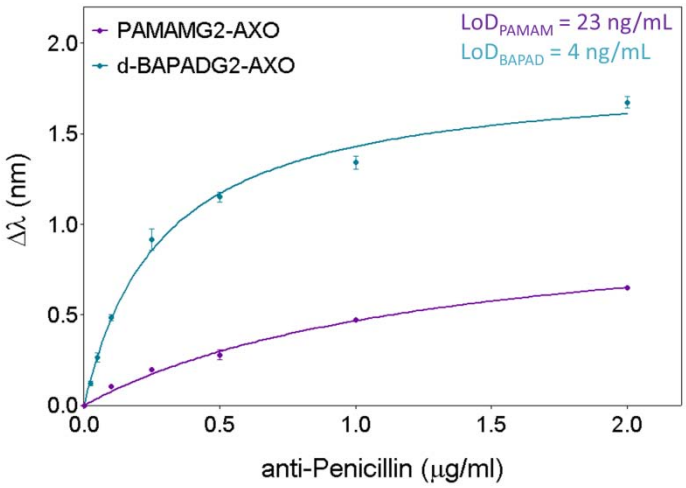

Figure 5.13 Calibration curves for anti-Penicillin (IgG) detection performed with PAMAM-AXO functionalized surface (purple) and d-BAPAD-AXO functionalized surface (blue) using the 80° nanoplasmonic setup.

Conclusively, the design of the dendron structure represents a substantial step forward compared with the strategies used so far based on conventional dendrimers. In those cases, whole PAMAM dendrimers require extra steps to be coupled to the transducer surface (i.e. surface modification with a SAM and subsequent covalent attachment of the dendrimers) which considerably stretches on the whole process and can in turn affect the overall reproducibility of the assay. The d-BAPADG2-AXO conjugate offers a much simpler and more robust functionalization approach, which at the same time facilitates a good exposure of the recognizing element (AX), enhancing its accessibility and improving the overall sensitivity for the specific antibodies.

5.4. Analysis of Anti-Amoxicillin Antibodies in Serum

The main goal of any biosensor is the demonstration of its applicability for the detection of a substance of interest in real samples, and if the intended use is in the clinical field, the purpose would be the direct analysis of human fluids. Blood serum is a valuable analytical fluid since it contains many disease biomarkers extremely useful for diagnosis or therapy monitoring. However, the 90% of the protein content (60 – 80 mg/mL) is composed of a few highly abundant proteins of scarce clinical interest which hinders the proteomic analysis. As already commented, in the case of label-free optical biosensors where the signal comes indirectly from the mass adsorbed on the surface, the main challenge is to avoid nonspecific adsorption that can lead to false positive signals.

The use of PEGylated compounds together with the addition of surfactants to the buffer have proven to reduce the adsorption of protein on different substrates.[216] In this work, our goal was the analysis of serum samples from patients with allergy. We combined the use of PLL-PEG, that selectively binds to the glass and creates a hydrophilic layer which passivates the non-sensitive areas of the nanostructured sensors,[182] with the use of an antifouling running solution that minimizes the nonspecific surface fouling.

Most common additives in antifouling cocktails are non-ionic detergents (e.g. Tween 20), due to their ability to disrupt ionic and hydrophilic biomolecule-surface bonds, or blocking agents such as BSA, non-fat dry milk, fish gelatin or whole serum. We performed a study of different buffer formulations in order to minimize the background signal produced by undiluted human serum, testing several concentrations of Tween 20 and different additives (BSA and common control serum). Best results were obtained when combining PLL-PEG coated surfaces and an antifouling cocktail consisting of PBS with 2% of Tween 20 and 2% of commercial serum as running fluid (Figure 5.14). The background signal observed under these conditions was low enough and highly reproducible (standard deviation below 0.01 nm) to permit reliable detection of antibodies in whole serum, assuming a constant background for all measurements.

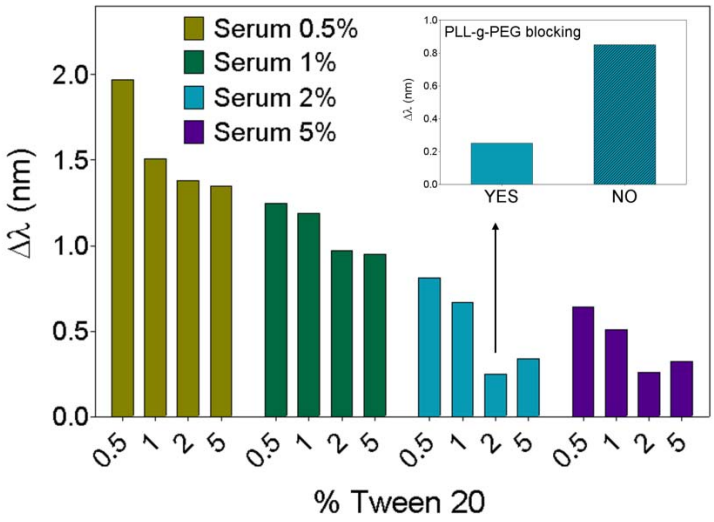

Figure 5.14 Background signal of whole serum onto the sensor surface blocked with PLL-PEG at different composition of running buffer: PBS + Tween 20 (0.5 – 2%) + serum (0.5% - 2%). Inset graph shows the influence of the PLL-PEG on the background signal by representing the nonspecific adsorption for the best running buffer conditions (PBS 2% Tween 20 and 2% serum) on surfaces lacking PLL-PEG.

The calibration curve was obtained by injecting undiluted commercial serum spiked with anti-penicillin IgG antibodies at different concentration (0.025 – 2 μg/mL) (Figure 5.15). A LoD of 8 ng/mL was achieved, while the limit of quantitation (LoQ) was set at 16 ng/mL. The LoD was slightly higher than for standard buffer conditions due to the contribution of the constant background. However, the profile of the curve was analogous, proving that serum matrix does not significantly affect the analysis performance as long as the background nonspecific signal is kept constant.

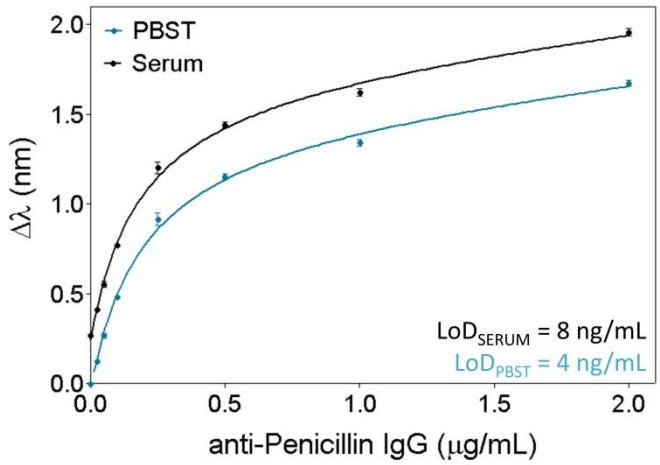

Figure 5.15 Anti-penicillin IgG calibration curves in PBST (blue) and whole serum (black).

5.5. Analysis of Clinical Serum Samples

With the optimal conditions previously selected for the evaluation of whole serum, direct detection of real samples from patients was attempted. Due to inherent differences between the IgGs used in the optimization study and the real target to measure (i.e. human specific IgE produced by the organism towards amoxicillin) we decided to perform a calibration curve directly with a serum sample from a patient, whose specific IgE concentration was known ([IgE] = 47.19 ng/mL determined with the ImmunoCAP assay).

The sample was serially diluted with commercial serum and the curve was obtained using the optimized conditions for nonspecific adsorption minimization (Figure 5.16). Using IgEs as standard, a LoD of 0.6 ng/mL was achieved (more than one order of magnitude lower) and the LoQ resulted in 2.2 ng/mL. This enhancement of the analytical sensitivity as compared to the previous values obtained with the anti-pencillin IgG (Figure 5.15) can be due to: (i) structural differences between IgG and IgE. IgE antibodies have a molecular weight that is approximately 1.3 times higher than IgGs (i.e. $MW_{IgE} \approx 200$ kDa, $MW_{IgG} \approx 150$ kDa), and since in plasmonic biosensors the mass plays a determinant role in the response, the output signal may be different; and (ii) a higher affinity for the antibodies produced by the human body against amoxicillin would be expected, as compared to the IgGs produced in mouse. Moreover, the IgG used as standard has a broad specificity towards the thiazolidine ring and, therefore, for several penicillins (i.e. it was produced using a conjugate of benzylpenicillin, presumably through β-lactam ring opening). Therefore, a lower affinity compared to the IgEs directly generated against amoxicillin would probably lead to lower signals at the same concentration. Overall, the improvement of the sensitivity when using the appropriate target clearly confirmed the higher natural affinity of the IgE against amoxicillin than the one of commercially produced IgG.

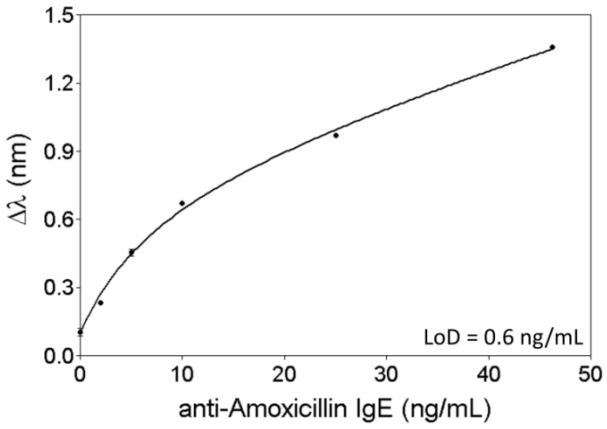

Figure 5.16 Amoxicillin-specific IgE calibration curve in serum samples

The viability of the proposed biosensor methodology for allergy diagnosis was then assessed by evaluating clinical samples from allergic patients and quantified them using the IgE calibration curve. Clinical samples were provided by the Hospital of Málaga (Spain). Non-pretreated and undiluted serum samples from amoxicillin allergic patients (S1, S3 and S5) and healthy donors (S2, S4 and S6) were directly flowed over the functionalized sensor surface by duplicate. Quantitation of the specific IgE antibodies was carried out by interpolating the values of the signals in the calibration curve (Figure 5.16). Table 5.5 lists and compares the results of the analysis obtained with the nanoplasmonic biosensor (mean ± SD) and with the ImmunoCAP test done at the hospital.

Table 5.5 Clinical serum samples analysis determined by ImmunoCAP assay and the nanoplasmonic biosensor.

Sample		anti-AX IgE Concentration			% Recovery
		ImmunoCAP (kU_{IgE}/L)[a]	ImmunoCAP (ng/mL)*	Nanobiosensor (ng/mL)	
S1	215F11	14.5	35.09	40.39 ± 1.3	115
S2	768F10	ND[b]	ND (< 0.84)	0.95 ± 0.35	113
S3	1103F09	3.53	8.54	9.00 ± 0.58	105
S4	1732F09	ND	ND (< 0.84)	0.69 ± 0.16	100
S5	29F04	3.4	8.23	7.87 ± 0.27	96
S6	2F06	ND	ND (< 0.84)	ND (< 0.6)	100

[a] 1 kU_{IgE}/L = 2.42 ng/mL[236]

[b] ND: not detected (below detection limit of the assay of 0.35 kU_{IgE}/L)

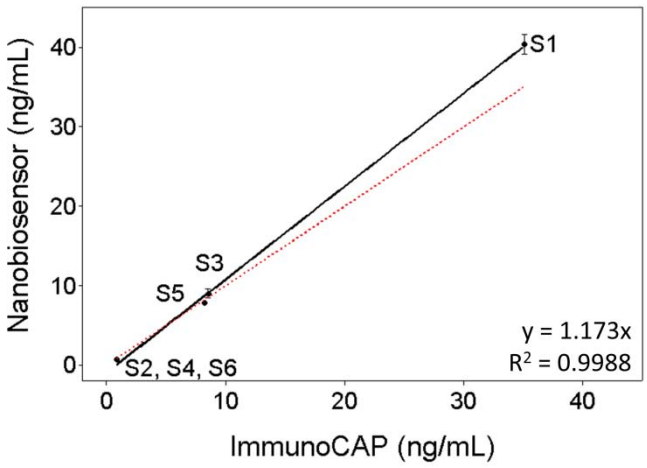

Figure 5.17 Accuracy studies performed with the nanoplasmonic biosensor. The graph shows the correlation between the values obtained with the sensing platform and the ImmunoCAP assay. Data shown correspond to the average of 2 replicates. Dotted line corresponds to a perfect correlation (slope = 1).

All recoveries ranged between 96 – 115% evidencing a good correlation between both diagnostic techniques. The concentration values obtained for each samples were also plotted and fitted to a linear regression function (Figure 5.17). As it can be observed, the excellent linearity (R^2 = 0.9988) and correlation between both approaches (slope = 1.173) corroborate the accuracy of dendrimer-based nanoplasmonic biosensor to quantify IgE antibodies in whole serum.

5.6. Conclusions

We have presented an innovative methodology for drug allergy diagnosis by direct quantification of amoxicillin specific IgE antibodies in serum using a novel nanoplasmonic biosensor device. We have designed and developed a complete biosensing strategy by combining specifically synthesized dendron-based amoxicillin conjugates with gold nanostructured sensor surfaces leading to a fast, reliable, highly sensitive and label-free analysis.

The thiol functional dendron (d-BAPADG2) allows simple and robust gold functionalization creating a regular and reproducible recognition layer. The d-BAPADG2-AXO dendron shows improved analytical features as compared to PAMAM dendrimers in terms of sensitivity and surface reproducibility, achieving 6 times lower limits of detection. Moreover, the use of PLL-PEG to block the inert areas provides an antifouling coating that reduces the nonspecific adsorptions and minimizes the background signal when evaluating whole serum. The selectivity and reliability have been demonstrated by performing a calibration curve with undiluted serum samples spiked with anti-penicillin IgG antibodies. Results showed that the serum components did not interfere in the antibody recognition process as a similar sensitivity was achieved.

To validate the proposed methodology a calibration curve was carried out with human specific amoxicillin IgE antibodies, revealing a notable increase of the sensitivity associated to the extremely high affinity of IgEs for the specific allergen. LoD was set at 0.6 ng/mL in whole serum. Finally, clinical samples from allergic patients and negative control samples were tested with the nanoplasmonic biosensor and the results were compared to those determined with the ImmunoCAP assay. An excellent accuracy was observed after obtaining recoveries in the range 96 – 115%, with an exceptional linear correlation with the conventional immunoassay.

The outstanding levels of sensitivity of the nanoplamonic biosensor (specially the setup at 80° of angle of incidence of the light) open the door to the direct measurement of human samples without any kind of pretreatment or preconcentration of the sample with a total analysis time of 15 min. The excellent features of the nanoplasmonic biosensor and the dendron-based

conjugates represent an attractive alternative as a fast and user-friendly diagnostic tool for clinical analysis and for obtaining quantitative data of amoxicillin allergy. Moreover, the overall strategy can be virtually adapted to detect other clinical biomarkers or any kind of target, simply by conjugating them to the dendron structure. The presented methodology holds great promise to improve biomarkers detection directly in human samples and constitutes a potentially useful tool for clinical diagnosis practice and for the development of point-of-care devices.

Chapter 6

ANALYSIS OF TAA AUTOANTIBODIES IN SERUM FOR EARLY DIAGNOSIS OF COLORECTAL CANCER

In this chapter, a label-free nanoplasmonic-based biosensor methodology for the determination of tumor-associate antibodies in serum is addressed. The strategy has been optimized and evaluated for two main specific autoantibodies expressed at early stages of colorectal cancer development, allowing their direct and rapid quantification. Besides, analysis in serum and plasma samples has been possible after introducing a necessary dilution step, achieving good sensitivity and selectivity. Finally, accuracy and reliability of the methodology has also been demonstrated evaluating clinical serum samples.

6. Analysis of TAA Autoantibodies in Serum for Early Diagnosis of Colorectal Cancer

6.1. Introduction

Colorectal cancer (CRC) is a worldwide health problem with an incidence over 1 million annual cases and being a major cause of morbidity and mortality in developed countries.[237] It is the third most common cancer and the fourth most common cause of death around the world. Despite that the exact cause for CRC is not known, several risk factors have been established, including genetic and epigenetic parameters.[238] Family history of colon cancer or inflammatory diseases, age, lifestyle and environmental conditions are strongly associated to CRC development. Thereby, prevention and regular screening play crucial roles in the fight against this type of cancer. Certainly, during the last years advances in screening and diagnostic techniques and the introduction of novel therapies have substantially increased patient survival rates.[239]

Colorectal cancer results from the abnormal growth of epithelial cells in the inner lining of colon or rectum, often generating polyps (Figure 6.1). Although most polyps found in the bowel are virtually benign (small hyperplastic or inflammatory polyps) and do not carry risk of developing cancer, large sized polyps or adenomas are considered highly precancerous.[240]

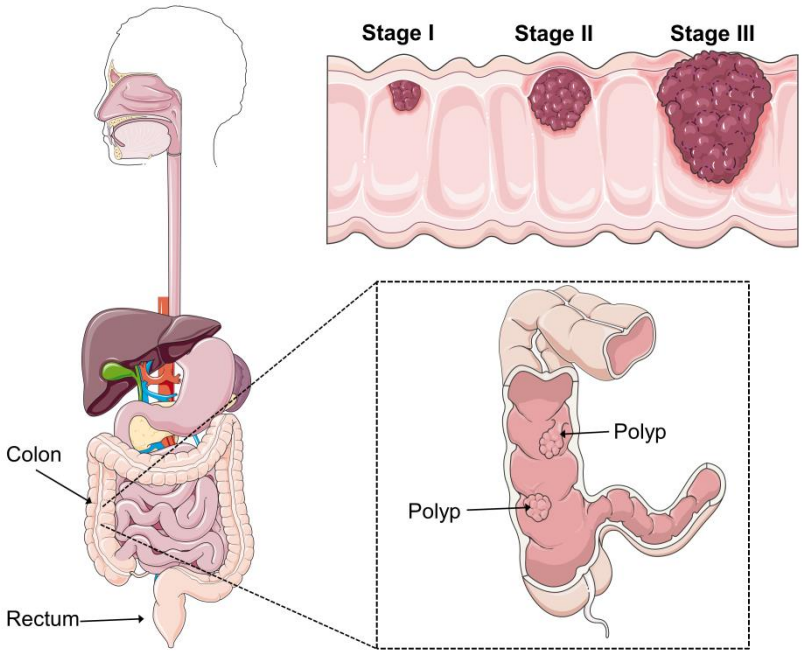

Figure 6.1 Representation of tumor polyps formed in the human colon or rectum and adenoma progression in different stages of colorectal cancer.

Adenomatous polyps generally arise from a failure in one or more steps of the normal cell proliferation and cell maturation process. Accumulation of many genetic alterations or inactivated tumor suppressor genes can cause adenoma progression to carcinoma. Fortunately, CRC is highly treatable when discovered early. At present, polyps surgery and complementary radiation therapy or chemotherapy show successful elimination of CRC when treated at beginning stages.[238]

However, CRC diagnosis is particularly challenging. Most reliable diagnosis technique is *via* sampling of colon areas suspicious for possible tumor development, which is typically done during colonoscopy, or sigmoidoscopy for the distal colon and rectum.[241] However, these procedures are highly invasive and present important limitations in terms of costs, available resources or low compliance. On the other hand, established noninvasive tests such as the guaiac-based fecal occult blood test (gFOBT) suffer from low sensitivity and inaccurate diagnosis results.[242] Therefore, there is an evident need for novel noninvasive screening tools, ideally, analytical techniques based on blood analysis, which permit the early and reliable identification and diagnosis of CRC. Development of blood biomarker assays that could indicate that a cancerous processes is triggered would be a great benefit. However, despite a few serum proteins have been described as biomarkers in CRC (carcinoembryonic antigen (CEA), CA19.9 or CA125), none of them are recommended for early clinical diagnosis but for advanced stages and for monitoring of the recurrence of the disease.[243]

Over the past decade, cancer research has made major advances in understanding the causes of developing CRC as well as the molecular mechanisms involved in the disease.[244] It has been demonstrated that many solid tumors such as breast, lung or colon cancer are immunogenic. These tumors express aberrant levels of mutated or modified proteins associated with the malignant growth, known as tumor-associate antigens (TAA). Such proteins can stimulate cellular and humoral immune response, triggering specific autoantibody production (Figure 6.2).[245, 246] The role of autoantibodies in cancer is still unclear. It is unknown if they play a cancer-promoting role, an anti-tumor effect or they are an epiphenomenon associated to inflammation and tumor progression.[247] However, autoantibody responses to TAAs hold promising characteristics to be used as blood biomarkers for cancer detection and they are currently being investigated as potential diagnostic tools in multiple cancer types.

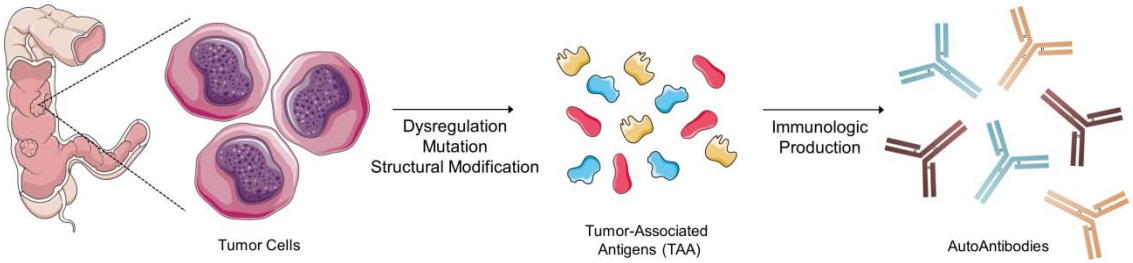

Figure 6.2 Schematics of the immunopathological mechanism of colorectal cancer representing the dysregulation, mutation or modification of tumor-associate antigens (TAA) and subsequent production of anti-TAA autoantibodies.

The utility of autoantibodies for early detection of cancer has been questioned for a long time, as the access to preclinical collection of serum is difficult. Sample collection from the same patient before and after tumor development and during all tumor stages is not generally available, making almost impossible to determine the exact moment when the autoantibodies appear and their correlation with tumor progression. However, some reports have described the use of autoantibodies for early and preclinical detection of cancer. Autoantibodies to annexin I, 14-3-3 Theta and LAMR1 were detected in prediagnostic lung cancer, using serum collected 1 year before the diagnosis of the lung cancer.[248, 249] Also, antibodies to p53, c-myc and MUC1 were detected in women between 7 and 27 months before breast cancer was diagnosed.[250] The analysis of autoantibodies offers significant benefits when compared to the direct determination of protein autoantigens associated to the tumor. Whereas detection of directly tumor-shed proteins in serum may be challenging due to their low abundance or to the difficulty of identifying simple mutations or structural modifications, serum autoantibodies are highly stable biomolecules and are produced in large amount even after stimulation by a minimal amount of tumor antigen. As a result, TAA-specific serum autoantibodies could constitute an excellent circulating reporters for early and preclinical cancer diagnosis.[251]

In the particular case of colorectal cancer, over 100 individual TAAs have been identified as target for autoantibody production, including full-length proteins, peptides, phage-peptides or glyco-peptides.[252] Although none of these TAAs are exclusively expressed in CRC, the humoral response profiling of CRC patients can enable the definition of specific autoantibody detection panels with potential value for prognosis and diagnosis of the cancer.[253]

Currently, increasing efforts in CRC research are directed not only to define specific TAA panels but also to develop efficient and highly sensitive analytical methods capable of detecting the TAA

autoantibodies in serum with optimum accuracy and reliability. Multiplexed biosensing strategies could offer a valuable alternative for diagnosis of colorectal cancer. Particularly optical biosensors have shown great promise for the development of high-throughput and miniaturized lab-on-a-chip platforms capable to carry out label-free and highly sensitive analysis of biomarkers in biological fluids. Thereby, here we aimed to design and optimize a nanoplasmonic biosensor for the direct detection and quantification of specific CRC-related TAA autoantibodies. Rapid and simple analysis of these biomarkers could provide a unique and innovative tool for CRC diagnosis. Besides, the possibility of quantifying autoantibody concentration in serum samples may allow further comprehension of the humoral response triggered by the tumor and harness the basis for the improvement of prognosis of the disease.

6.2. Design and Optimization of the Biosensor Methodology

Among the numerous defined TAAs for colorectal cancer, we selected two specific proteins because of their particular characteristics for the early and preclinical diagnosis: the general transcription factor IIB (GTF2b) and the EGF-Like Repeats and Discoidin I-Like Domains 3 protein (EDIL3).

GTF2b is one of the several factors required by RNA polymerase II for transcription initiation, that is, for promoting the transcription of genetic information from DNA to messenger RNA. Transcription factors play a crucial role in development, intercellular signaling and cell cycle, thereby aberrant regulation or mutation of these proteins are usually associated to specific diseases like cancer.[254-256] On the other hand, EDIL3 is an extracellular matrix protein acting as integrin ligand. It plays an important role mediating angiogenesis and influences significantly in endothelial cell behavior and in vessel wall remodeling and development. A large percentage of endothelial cells in primary breast carcinomas, melanomas or colon cancer in humans have reported dysregulation of EDIL3 expression.[257-261]

These two proteins have been evaluated as possible TAA targets for autoantibody production in colorectal cancer. Recently, a study in murine models has provided evidences of immediate production of anti-GTF2b and anti-EDIL3, among other autoantibodies, in cancer-induced animals.[262] The presence of autoantibodies was detectable at a very early stage in tumor development, even before adenoma formation. Particularly, GTF2b could be detected at day 21 after cellular neoplastic transformation. Furthermore, the analysis of TAAs at protein and mRNA level showed a clear overexpression for EDIL3 as expected, but almost no alterations in the expression of GTF2b, suggesting that GTF2b autoantibody response might be triggered by

possible mutations, wrong conformations or other post-translational modifications. This confirms the exquisite sensitivity of the immune system and proves the potential value of GTF2b and EDIL3 autoantibodies as serum biomarkers for the early diagnosis of CRC.

To develop our methodology, we took advantage of the previously demonstrated benefits offered by the nanoplasmonic-based biosensor in terms of sensitivity and selectivity (especially at the highest angle of 80°). The material-selective biofunctionalization of gold nanodisks surfaces has shown exceptional sensitivities and significant minimization of nonspecific adsorptions for a label-free and accurate detection of biomarkers in serum (see Chapter 5). Nanoplasmonic sensor chips were independently biofunctionalized with recombinant human GTF2b and EDIL3 proteins to detect the specific human anti-GTF2b and anti-EDIL3 autoantibodies. Both GTF2b and EDIL3 proteins possess a relatively high MW (35 kDa and 52 kDa, respectively), which makes less relevant the use of a carrier that help space them out on the surface. An ultimate goal of the study is the development of a multiplexed biosensor platform for the simultaneous detection of a panel of CRC specific autoantibodies. Therefore, although each TAA is inherently different in structure and conformation, similar biofunctionalization conditions should ideally provide efficient immobilization for both of them (or eventually to additional TAAs). A covalent binding between amine terminal groups of the Lys residues in the proteins to a carboxyl-terminated SAM was selected as functionalization technique due to its simplicity and elevated stability and reproducibility (Figure 6.3). The overall methodology was optimized and assessed for the analysis of autoantibodies in serum and plasma.

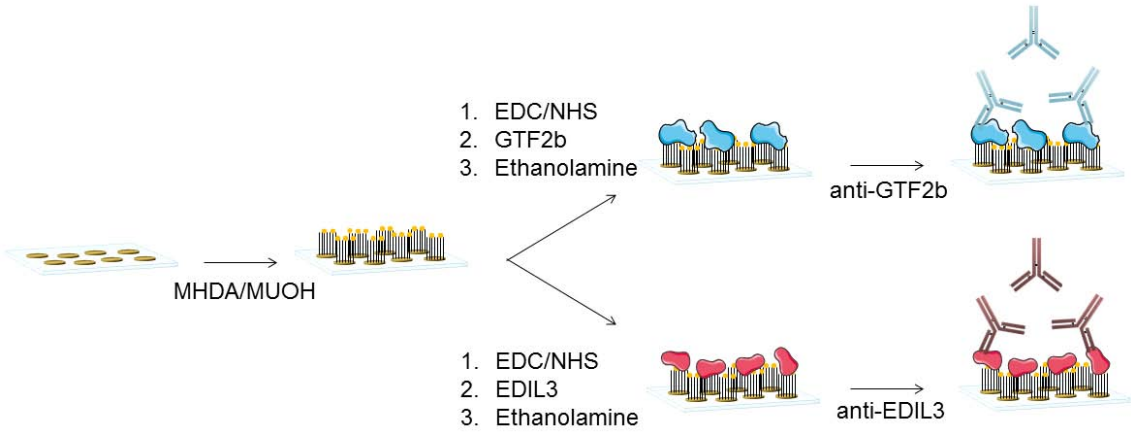

Figure 6.3 Schematic representation of the biosensing strategy for TAA autoantibodies detection: (i) mixed MHDA/MUOH SAM formation, (ii) EDC/NHS activation, GTF2b (blue protein) and EDIL3 (red protein) covalent coupling and ethanolamine deactivation, (iii) anti-GTF2b and anti-EDIL3 detection, respectively.

In order to create optimum layer of bioreceptors onto the gold nanodisks sensors, several immobilization conditions were studied. Different molar ratios of mixed alkanethiol SAM (MHDA/MUOH 1:0, 1:1, 1:10, total SH concentration of 250 µM) were tested since, as previously described, a control of the grafting density can *a priori* modulate possible steric hindrance effects, improving the ability to detect the autoantibodies. In addition, TAAs immobilization procedure was performed either *in situ*, by flowing the protein solution over the sensor chip and monitoring the covalent coupling process, and *ex situ*, by performing the reaction in three consecutive steps (EDC/NHS incubation for 20 min, covalent coupling of protein overnight at 4**°**C, and deactivation of unreacted carboxylic groups for 10 min). In all cases, the non-sensing glass areas were subsequently coated with PLL-PEG (0.5 mg/mL) to prevent nonspecific adsorptions.

Figure 6.4 shows the TAA immobilization signals (concentration 50 µg/mL) for the *in situ* procedure carried out over alkanethiol SAMs at different molar ratios using the 80**°** nanoplasmonic biosensor setup.

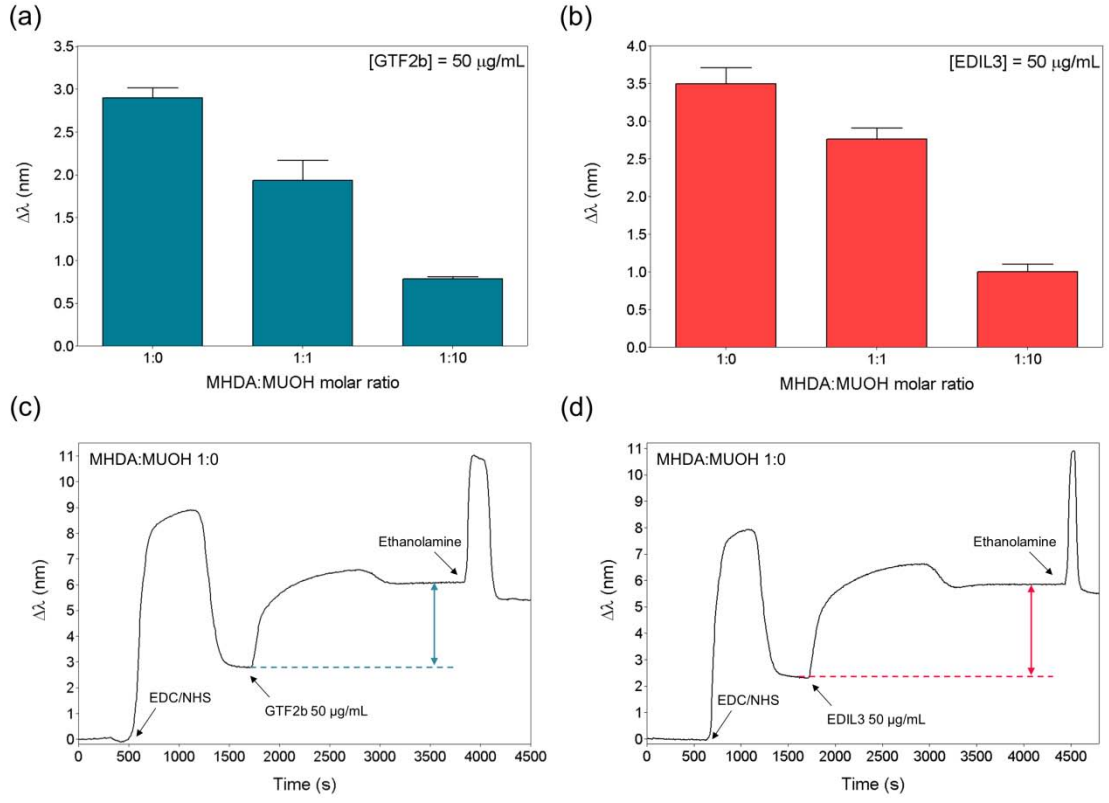

Figure 6.4 Immobilization signals performed *in situ* over alkanethiol SAMs at different molar ratios (MHDA:MUOH 1:0, 1:1, 1:10) for 50 µg/mL of **(a)** GTF2b protein and **(b)** EDIL3 protein. LSPR sensorgrams showing covalent immobilization procedure of **(c)** GTF2b and **(d)** EDIL3 over a mixed SAM (MHDA:MUOH 1:0).

As can be observed, in both cases maximum amount of protein was attached to the sensor surface when maximum carboxylic density was used, inducing wavelengths displacements of around 3 nm. Introduction of spacer molecules (MUOH) to the SAM resulted in lower signals, thereby, lower amount of protein immobilized.

However, optimum TAA layer not only depends of a sufficient amount of immobilized proteins but also of the grafting density and the subsequent accessibility of the antibodies. To evaluate the efficiency of the immobilization, we did a comparison of the responses for a constant concentration of specific antibody (1 µg/mL) over the corresponding GTF2b and EDIL3-coated surface prepared with the different conditions (Figure 6.5). No steric hindrance effects were observed as maximum detection was achieved in all cases when maximum carboxylic density was used. This suggests that immobilization of TAAs on alkanethiol SAMs formed exclusively with MHDA actually provides high efficient bioactive layer. Furthermore, it can be seen that *ex situ* immobilization resulted in significant higher antibody signals for the same concentration of immunoreagents. This can be attributed to longer reaction times (protein coupling overnight *vs.* 30 min when it is performed *in situ*) that may improve coupling yield and probably the protein arrangement on the surface. From the above results, overnight immobilization of TAA over a 100% MHDA SAM was selected as the optimum biofunctionalization strategy.

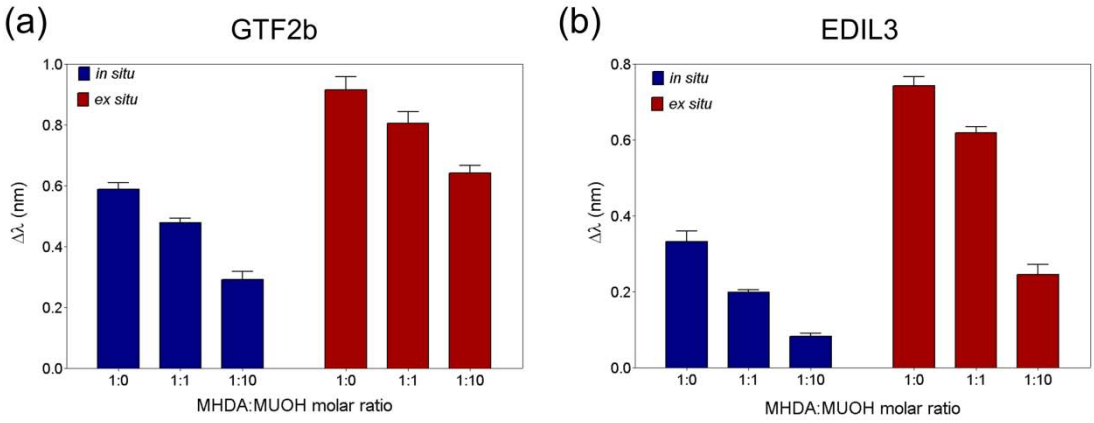

Figure 6.5 Resonance shifts obtained for the detection of **(a)** anti-GTF2b and **(b)** anti-EDIL3 antibody under different conditions for the protein immobilization. Blue columns: *in situ* immobilization onto alkanethiol SAM with different MHDA:MUOH molar ratios (1:0, 1:1, 1:10); red columns: *ex situ* immobilization onto alkanethiol SAM with different MHDA:MUOH molar ratios (1:0, 1:1, 1:10).

Regeneration and potential reutilization of the TAAs functionalized surfaces were also evaluated. In this case, regeneration of both surfaces - GTF2b and EDIL3 – was achieved by flowing a 20 mM NaOH solution (Figure 6.6). Basic conditions allowed to disrupt TAA-antibody interaction without

altering or modifying the immobilized proteins, in such a way that it was possible to reuse both functionalized surfaces. Good repeatability was observed up to 50 cycles and working for 3 days before progressive decrease of the antibody detection signals were observed

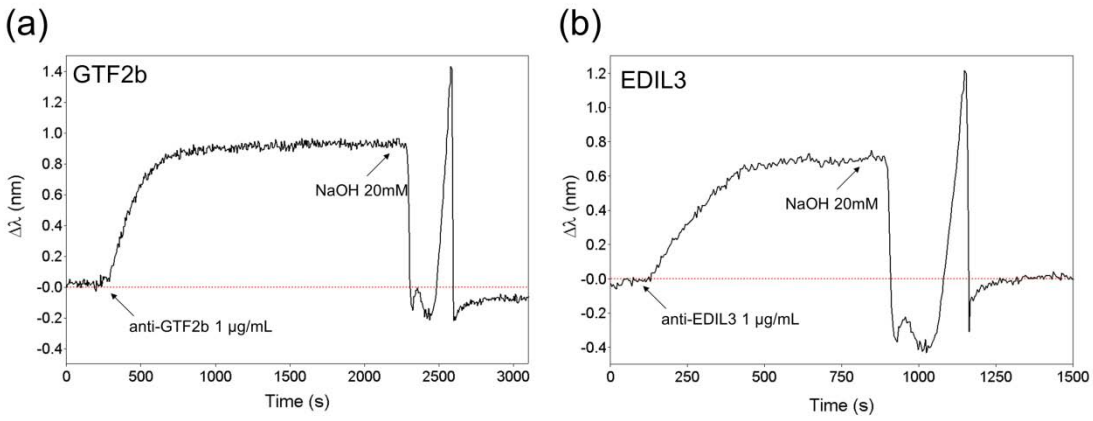

Figure 6.6 Sensorgrams showing **(a)** anti-GTF2b and **(b)** anti-EDIL3 detection at 1 µg/mL and subsequent regeneration with NaOH 20 mM.

Calibration curves for the detection of anti-GTF2b and anti-EDIL3 were then performed (Figure 6.7) in standard buffer conditions (PBST). Furthermore, nonspecific antibodies were used as control to ensure the specificity of the assays. Measurement of anti-GTF2b over an EDIL3-functionalized surface and *vice versa* led to negligible signals, which confirms that signal contribution solely comes from the specific antibody recognition. Analytical parameters were calculated for each calibration curve: LoDs were determined as 10 ng/mL for GTF2b and 5 ng/mL for EDIL3, while LoQs resulted in 34 ng/mL and 19 ng/mL for GTF2b and EDIL3, respectively.

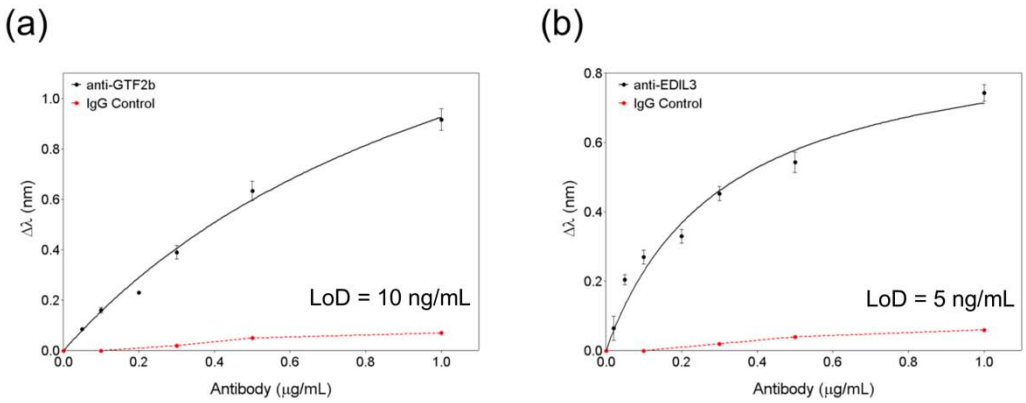

Figure 6.7 (a) Calibration curve for anti-GTF2b detection performed over GTF2b-biofunctionalized nanodisks (black). Red dashed line indicates nonspecific adsorption of an antibody control (anti-EDIL3); **(b)** Calibration curve for anti-EDIL detection performed over GTF2b-biofunctionalized nanodisks (black). Red dashed line indicates nonspecific adsorption of an antibody control (anti-GTF2b).

To assess the reproducibility and accuracy of the overall methodology, the variability of the measurements was calculated for the same functionalized surfaces (intra-assay CV) and for measurements done with distinct nanoplasmonic chips (inter-assay CV). Table 6.1 lists the CV values determined for the LoD and the maximum signal (Smax at [Ab] = 1 μg/mL) obtained for the analysis of both GTF2b and EDIL3 antibodies. These results confirm the excellent stability and reproducibility of the biofunctionalization strategy as well as the good accuracy and robustness of the biosensor assays.

Table 6.1 Inter and intra-assay features for GTF2b and EDIL3 antibodies detection with the nanoplasmonic biosensor.

		GTF2b antibody		EDIL3 antibody	
		Mean ± SD	**% CV**	**Mean ± SD**	**% CV**
Intra-assay	**LOD (ng/mL)**	9.7 ± 0.5	5.15	5.2 ± 0.2	3.77
	Smax (nm)	0.937 ± 0.0015	1.63	0.733 ± 0.016	2.08
Inter-assay	**LOD (ng/mL)**	10.1 ± 1.2	11.9	4.9 ± 0.4	8.16
	Smax (nm)	0.917 ± 0.07	8.19	0.743 ± 0.04	5.60

[a] Mean and standard deviation of 3 replicates

6.3. Analysis of TAA Antibodies in Serum and Plasma

Serum and plasma are the most usually employed biological fluids for clinical biomarker analysis since they content practically all the circulating proteins of the body. In this dissertation we previously demonstrated the exceptional properties of nanoplasmonic biosensor surfaces to minimize undesired nonspecific protein adsorptions. Combination of the PLL-PEG blocking with the use of dilution buffers with elevated percentage of surfactant (Tween 20) showed considerable minimization of the background signal enabling the evaluation of biomarkers in serum with high accuracy and reliability (see Chapter 5). In our previous work the receptor layer over the nanodisks consisted of a conjugate (dendrimers structure) incorporating small molecule to be recognized (amoxicillin). But here, the nanodisks surface is completely covered with proteins (to be recognized at a whole). Therefore the different nature of both layers might lead to different outcome when dealing with serum and plasma (i.e. hydrophilic behavior, antifouling

resistance or possible hampering of antibody-TAA interaction due to the biological matrix components).

PLL-PEG modified nanoplasmonic surfaces biofunctionalized with TAA proteins were evaluated in terms of nonspecific adsorptions by flowing either commercial serum (undiluted, diluted 1:1 and 1:10 in PBST 0.5%) (Figure 6.8a) or commercial plasma (undiluted, diluted 1:1 and 1:10 in PBST 0.5%) (Figure 6.8b). As can be seen in the sensorgrams, in both cases a significant background signal was observed with undiluted fluid, being slightly higher for plasma (it contains fibrinogen). A 1:1 dilution in PBST was not enough to remove being necessary a 1:10 dilution to achieve complete reduction of nonspecific adsorptions for both cases, resulting in virtually null background signals. We decided to apply these optimized conditions (PLL-PEG blocking and dilution 1:10 in PBST) for subsequent evaluations. It is worth mentioning the different behavior observed in comparison with the results obtained in Chapter 5, with the dendrimer-based immobilization strategy, where we were able to directly measure undiluted serum with very low nonspecific binding. Again, a highly plausible explanation for this different outcome might related to the more hydrophobic nature of the protein-coated surface.

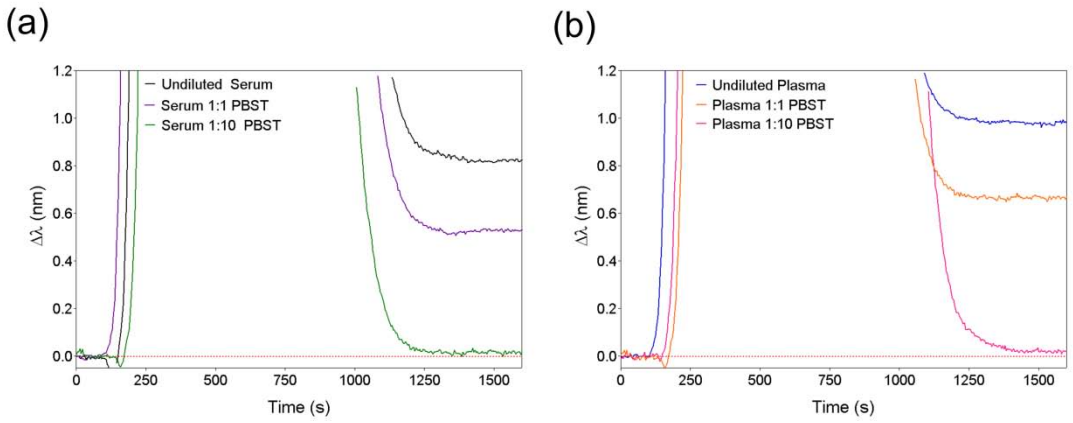

Figure 6.8 (a) Background signal corresponding to matrix nonspecific adsorption of undiluted serum (black), serum diluted 1:1 in PBST 0.5% (purple) and serum diluted 1:10 in PBST 0.5% (green); **(b)** Background signal corresponding to matrix nonspecific adsorption of undiluted plasma (blue), plasma diluted 1:1 in PBST 0.5% (orange) and plasma diluted 1:10 in PBST 0.5% (pink).

Calibration curves for both GTF2b and EDIL3 were carried out by spiking serum or plasma with several concentrations of antibodies and then diluting it in PBST (1:10) (Figure 6.9). The LoDs for the GTF2b antibody detection was 16 ng/mL in diluted serum and 15 ng/mL in diluted plasma. In the case of EDIL3 antibody detection, LoDs were 12 ng/mL in diluted serum and 11 ng/mL in

diluted plasma. These differences with buffer conditions (LoD of 5 and 10 ng/mL for GTF2b and EDIL3 respectively) might be attributed to matrix effects in the antibody/antigen interaction even after diluting the sample. However, besides this, the effective sensitivity has essentially gotten worse up to one order of magnitude (with detectabilities around 150-160 ng/mL for GTF2b and around 110-120 ng/mL for EDIL3, depending on the fluid). Despite this unavoidable dilution, the obtained calibration curves in both diluted serum and plasma could still offer a highly reliable analysis method to quantify these specific TAA autoantibodies with elevated selectivity and reproducibility.

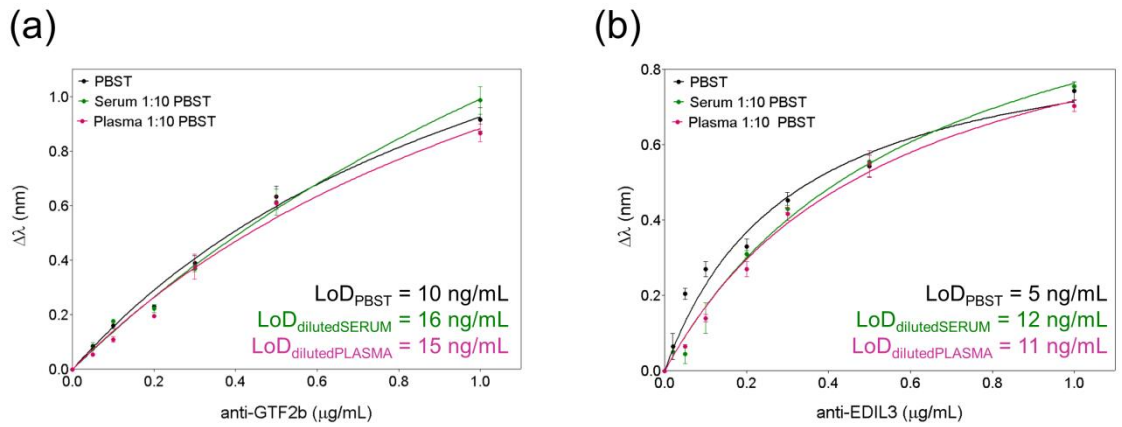

Figure 6.9 (a) Calibration curves for anti-GTF2b antibody detection in PBST buffer (black), serum diluted 1:10 in PBST (green) and plasma diluted 1:10 in PBST (pink); **(b)** Calibration curves for anti-EDIL3 antibody detection in PBST buffer (black), serum diluted 1:10 in PBST (green) and plasma diluted 1:10 in PBST (pink).

6.4. Analysis of Clinical Serum Samples

To our knowledge, not a single study has so far reported specific quantification of autoantibody concentration levels in human serum from CRC patients, as most research articles in the field focus on the identification and assessment of these novel biomarkers. A diagnostic cut-off value of 30 ng/mL was proposed by Lu *et al.*[263] based on semi-quantitative ELISA assays carried out for several CRC associated autoantibodies. Although first results achieved with the nanoplasmonic biosensor are still far from this cut-off limit, we attempted the analysis of real samples.

Clinical serum samples of CRC patients were analyzed as a preliminary evaluation of the viability of our biosensor approach . Serum samples collected from patients from the Hospital of Gijón (Spain) with diagnosed CRC together with samples from healthy individuals were evaluated employing the optimal conditions selected before. All samples had been previously analyzed for

the presence of GTF2b autoantibodies using semi-quantitative ELISA, so the exact concentration of the target biomarker was unknown. Thus, only a qualitative validation of the biosensor methodology was possible. In Table 6.2 we list and compare the concentration values obtained from interpolation of the acquired LSPR signal (in µg/mL) to absorbance measurements from ELISA (in optical density, OD, units). Interpolation of the biosensor signals was carried out in the calibration curve obtained for GTF2b spiked serum (Figure 6.9a, green curve) and applying the 10-fold dilution factor to extract the final concentration value in the sample.

Table 6.2 Clinical serum samples analysis determined by ELISA and by the nanoplasmonic biosensor.

Sample		GTF2b Analysis Results	
		ELISA (OD)	**Nanobiosensor (µg/mL)***
G30	Negative	0.18	ND [a]
G42	Positive	0.48	0.175 ± 0.008
G56	Positive	0.56	0.254 ± 0.010
G101	Negative	0.13	ND [a]

* Mean ± SD for 3 replicates

[a] ND: No Detected (below limit of detection: 160 ng/mL)

High concentration of autoantibodies was found in this case, which made possible its quantification given the detection limit of the assay. Although we cannot validate these results so far, we can observe a good correlation in terms of relative signals. Concentration values obtained for GTF2b autoantibodies qualitatively correlate with the absorbance measurements of the same serum samples. Signals obtained for negative samples from healthy subjects resulted below the limit of detection established for our biosensor technique (160 ng/mL), while positive samples lead to relatively high signals and, therefore, elevated concentration of GTF2b antibodies.

These results highlight the unique potential of the nanoplasmonic-based technology and corroborate the value of TAA autoantibodies detection for CRC diagnosis. However, further studies are pending mainly addressing two aspects: 1) to improve assay conditions in order to achieve better sensitivities, basically minimizing as far as possible the dilution ratio. If that is not possible we will contemplate other immobilization strategies that help both improving detectability and avoiding dilution of samples. And 2) to perform a clinical validation of the methodology.

6.5. Conclusions and Future Perspectives

We have proposed a new analytical methodology for the early diagnosis of colorectal cancer. The strategy is based on the direct and label-free determination of TAA autoantibodies using our innovative nanoplasmonic biosensor. The overall performance of the biosensing assay has been optimized and evaluated for the detection of two CRC specific autoantibodies: GTF2b and EDIL3, whose high value for pre-clinical diagnosis of cancer has been previously evidenced.

The use of nanoplasmonic biosensors offers rapid and reliable quantification of TAA antibodies with excellent selectivity and robustness. The biosensing strategy allows performing more than 100 measurements with good reproducibility. We have also demonstrated the feasibility to detect both GTF2b and EDIL3 antibodies in blood serum and plasma in a label-free manner, although a dilution step is necessary. Further optimization of the methodology will be required to enhance the analytical sensitivity in biological fluids. In this regard, on-going work focuses on the improvement of biofunctionalization strategies and the use of antifouling agents that permit direct measurements of undiluted serum and plasma. Besides, higher sensitivity could be achieved in case of being necessary by using amplification techniques, such as secondary antibodies.

This biosensor methodology is a first approach for the future development of a highly sensitive multiplexed biosensor platform, capable of simultaneously detecting a specific panel of CRC autoantibodies. The direct and label-free detection of CRC-related blood-circulating biomarkers could become a valuable tool for rapid and efficient population screening and early diagnosis of cancer. Besides, the use of biosensors in clinical research might provide further understanding of the immunopathological mechanisms involved in cancer disease and enable the establishment of accurate correlations between autoantibody levels and tumor progression and disease prognosis.

General Conclusions

The work described in this PhD Thesis demonstrates the potential value of plasmonic and nanoplasmonic biosensors for their application in the clinical and biomedical field. Multidisciplinary combination of surface chemistry, biochemistry and immunology with the recent advances in nanotechnology and biosensor research has enabled the development of efficient analytical methodologies as novel solutions for diagnosis and therapy.

Main goals proposed in this dissertation involved the design of several biosensing strategies for specific clinical applications, employing both the well-known SPR biosensor and a recently developed nanoplasmonic biosensor based on the LSPR phenomenon occurring on gold nanodisks surfaces. These biosensor platforms, which offer simple, label-free and fast detection of biomarkers, have been profiled as promising candidates for point-of-care analysis. Furthermore, the in-depth optimization and assessment of the sensor surface biofunctionalization has allowed an overall improvement of the bioanalytical performances, leading to direct and reliable quantitation of protein biomarkers with elevated sensitivity, selectivity and reproducibility.

The main general conclusions that can be drawn from the work done during this Thesis are the following:

- The use of antifouling PEGylated compounds as blocking agents, particularly the copolymer PLL-PEG, has demonstrated to extremely reduce protein adsorptions from biological fluids, such as urine, serum or plasma. Nanoplasmonic surfaces showed significant advantages compared to the conventional SPR biosensor. Material-selective functionalization of gold nanodisks sensors guarantees the specific biorecognition interactions to take place solely on the sensor hotspots (i.e. gold nanodisks) while the antifouling coverage of inert areas (i.e. glass substrate) provides exceptional resistance to nonspecific adsorptions in comparison to conventional gold films.

- Two innovative methodologies for the oriented immobilization of antibodies have been studied and optimized, in order to develop direct immunoassay of protein biomarkers in biological fluids. They are based on: (i) host-guest interactions with a calixarene-derivative linker (ProLinker^{TM} B) and (ii) site-specific conjugation to a poly-Adenine oligonucleotide, which presents high adsorption affinity for gold substrates. Both

strategies turned out to be highly efficient in terms of sensitivity and robustness, providing optimum coverage of the sensor surface with a remarkable stability in a simple procedure. The calixarene-based methodology has been further optimized for the direct evaluation in biological fluids (urine and serum) showing encouraging results to reduce nonspecific adsorptions while retaining the biological activity of antibodies. Besides, the implementation of this novel approach in gold nanodisks sensors has demonstrated efficient reduction of nonspecific adsorptions and slight sensitivity improvements, which highlights the exceptional potential of nanoplasmonic biosensors for the development of clinical PoC devices.

- A novel immunosensing strategy has been proposed for the detection of gluten peptides in urine as an alternative approach for the dietary control and celiac disease therapy monitoring. The methodology, based on a competitive immunoassay approach, allows simple and reliable quantification of the main immunotoxic gluten peptide (33-mer gliadin peptide) directly in diluted urine, without requiring any purification or extraction procedure. The limit of detection achieved is 1.72 ng/mL, which can be currently considered as an excellent sensitivity for the direct and label-free detection of small peptides in biological fluids. Although further studies are necessary to attempt reliable quantification, the robustness and reproducibility achieved for the analysis of clinical samples represents a step forward in the achievement of a PoC device for celiac disease follow-up. The methodology has also been transferred to the nanoplasmonic biosensor, showing considerable improvements in prevention and minimization of nonspecific adsorptions that might enhance the reliability of the analysis.

- An innovative methodology for drug allergy diagnosis by direct quantification of amoxicillin specific IgE antibodies in serum using the nanoplasmonic biosensor has been developed. The biosensing strategy combined a specifically synthesized dendron-based amoxicillin conjugate (d-BAPADG2-AXO) with the exceptional features of nanostructured sensors for highly sensitive and reliable analysis. The novel dendritic conjugate permits simple and robust gold functionalization, showing improved analytical features in terms of sensitivity and surface reproducibility when compared to more conventional dendrimers. Besides, the use of PLL-PEG blocking has provided an efficient antifouling coating for the direct detection of IgE antibodies in whole serum samples, resulting in an exceptional limit of detection set at 0.6 ng/mL. The methodology has been clinically

validated obtaining recoveries in the range 96 – 115% and an excellent correlation with conventional immunoassay results.

- The nanoplasmonic biosensor has been finally applied for the development of a new and highly demanded early diagnostics technique of colorectal cancer. In this study we have designed a rapid and label-free methodology for the detection of blood circulating CRC-specific autoantibodies. Calibration curves in diluted serum and plasma allowed the direct quantification of these autoantibodies with good sensitivity and selectivity, with detectabilities around 110 - 160 ng/mL depending on the protein. Although it requires improvements, the methodology could serve as a first efficient approach both to assist in the understanding of the immunological mechanisms involved in cancer and to develop a multiplexed PoC biosensor for efficient population screening and early diagnosis of colorectal cancer.

Future perspectives may be focused towards implementing the analytical methodologies developed in this work in innovative biosensor platforms that offer rapid and multiplexed detection and also in miniaturized and integrated PoC systems. On-going advances in photonic technology and microfluidics are further facilitating the achievement of truly lab-on-a-chip systems with enormous potential for highly efficient and decentralized diagnosis in the near future.

This doctoral work has involved a close collaboration with several SMEs companies (as Biomedal S.L. or ProAlt S.L.) and public Hospitals, which open a direct route for the commercialization of our PoC optical biosensors for therapy and diagnostic applications, such as the dietary control of celiac patients or the early detection of colorectal cancer, among others.

This PhD Thesis represents a significant contribution to the progress in Nanomedicine in general and in Nanodiagnostics in particular, for the accomplishment of improved diagnostics solutions that can help in the near future to open the door to a global health access.

Annex

ANALYSIS OF T CELL ACTIVITY FOR CANCER IMMUNOTHERAPY

The work described in this annex was carried out during a PhD stay in the École Polytechnique Fédérale de Lausanne (EPFL) (Switzerland). Here, a novel analytical technique for the identification of specific antitumor T cells is proposed. The strategy consists of the detection of the major histocompatibility complex peptide (pMHC) released by living T lymphocytes using a high-throughput nanoplasmonic biosensor based on nanohole arrays. Both the biofunctionalization strategy of the nanohole structured substrates and the cell immobilization into a microfluidic chamber have been assessed and optimized. The highly sensitive and selective detection of pMHC achieved for the analysis of living cells represents a promising proof of principle of the proposed technique for its application in cancer immunotherapy.

A. Analysis of T Cell Activity for Cancer Immunotherapy

A.1. Introduction

Cancer immunotherapy has emerged in last decades as the most promising treatment for cancer, especially for metastatic and advanced stages.[264, 265] Immunotherapy is based on the use or stimulation of the own immune system to eradicate tumors and restrain/contain cancer progression, taking advantage of the high specificity and efficacy of immunological agents and therefore reducing side-effect toxicities. Different immunotherapeutic treatments include the use of monoclonal antibodies for targeting tumor cells or their microenvironment,[266, 267] the development of cancer vaccines that stimulate the immune response in the body[268] or the adoptive transfer of antitumor T cells.[269] Among them, the adoptive T cell transfer (ACT) immunotherapy stands out due to the extraordinary effectiveness showed recently in clinical trials for patients with metastatic cancer.[270]

Adoptive cell transfer therapy involves extraction and isolation of tumor-reactive T lymphocytes and posterior reinfusion into patients. Although ACT-based immunotherapy was first described 60 years ago,[271] the decisive improvement in efficacy came in the last decade facilitated by the depth understanding of T cell biology, including the mechanisms for T cell activation and target recognition, as well as the advances in cell culture techniques that enabled the *ex vivo* cloning of large number of T cells.[272]

The efficiency of ACT therapy relies on the exceptional ability of T cells to target and kill cancer cells, especially $CD8^+$ cytotoxic T lymphocytes. These T cells move through tissues, scanning and sensing a variety of signals that can alert them from the presence of foreign pathogens or malignant cells. Activation generally occur when their T cell receptor (TCR) specifically interact with the peptide major histocompatibility complex (pMHC) of antigen-presenting cells (APC), including dendritic cells (DC). MHC is a set of cell surface peptides that are able to bind internalized peptide fractions derived from pathogens or other antigens, and then expose them on the surface of the cells for TCR recognition. Tumor-specific T cells are probably activated through encounters with the tumor-associate antigens (TAA) expressed by cancer cells and presented via pMHC complexes. The TAA-specific T lymphocytes migration is rapidly arrested after interaction with their cognate antigens, leading to tumor-infiltrating lymphocyte (TIL) populations.[273] TILs can be extracted either from tumor tissues by biopsy or from peripheral blood and they are usually expanded *ex vivo* using cell culture techniques based on the continued

exposure to IL-2, a cytokine that is known to simultaneously promote T cell proliferation and differentiation.[274] T lymphocytes presenting antitumoral activity are isolated, cloned and infused back into patients, previously subjected to a preparative lymphodepletion (i.e. a temporary ablation of the corrupted immune system of the cancer patient) (Figure A.1). Then, cancer-reactive T cells readily trigger a potent immune response to mediate tumor destruction.

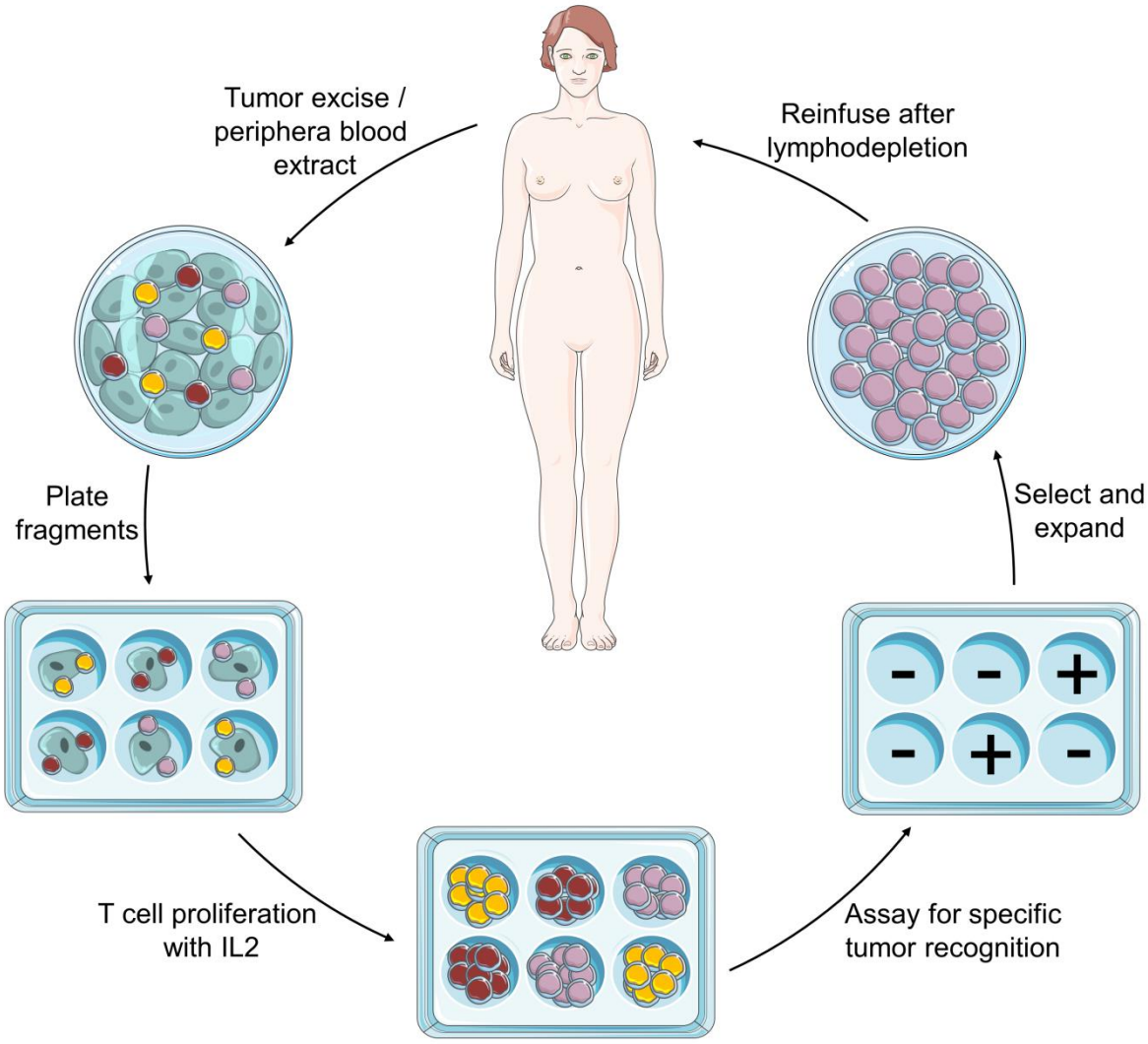

Figure A.1 Schematic representation of adoptive cell transfer immunotherapy procedure.

Several studies have demonstrated that T cell activation critically depends on TCR-pMHC binding affinity.[275, 276] Since the great majority of TAAs are typically self-proteins, TAA-specific T lymphocytes bearing high-avidity TCR are restricted to a relative central immune tolerance and can be deleted by negative selection in the thymus. Even those T cells that escape central tolerance and have potential to respond to the self-target antigens typically manifest suboptimal activation.[277, 278] In this regard, advances in biotechnology and cellular engineering have provided

efficient solutions to overcome the consequences of immunosuppression and to improve the specificity and activity of TILs. The use of transgenic TCR or chimeric antigen receptors (CAR) composed of antibody binding domains are most commonly employed strategies to induce tumor specificity to T cells and boost the immune response in cancer patients.[279-282] Additionally, engineered T cells offer promising advantages such as the ability to insert genes that encode the transduction of molecules involved in immune co-stimulation[283] or T cell survival,[284] for example.

Nowadays, major challenges in ACT-based immunotherapy are related to both the need of depleting the corrupt host microenvironment before T lymphocyte transfer and the difficulties to isolate, identify and control the activity of highly functional TAA-specific T cells. Regarding the former, immunodepletion with chemoradiotherapy has demonstrated to positively impact on the efficacy of the ACT treatment.[285] However, in the future it will be important to explore methods to improve the efficacy of immune ablation and to ensure the survival and proliferation of adoptively transferred T lymphocytes.[286, 287] On the other hand, an important obstacle for ACT therapy is the limited efficiency of the current *ex vivo* TIL expansion and analysis protocols.[288] Besides of the relatively low availability and expensive costs, cell culture techniques for T lymphocytes growth, proliferation and analysis have shown to cause efficacy losses on antitumor activity of T cells. In particular, emerging findings from both animal studies and clinical trials indicate that intrinsic properties acquired during $CD8^+$ T cells differentiation under the effect of IL-2 decline their reactivity to specific tumor antigens, which means that only young or naive T cells present high efficacy in ACT for cancer.[272, 289] Recent approaches have been reported to speed up the cloning process (often taking 4-5 weeks) and avoid terminal differentiation of T cells based on a more immediate isolation of TILs from tumor by enzymatic digestion, rather than simply waiting for them to migrate out from tumor fragments in culture.[290, 291] This strategy led to more TILs being more immediately accessible for expansion. However, clinical trial results with this approach did not show significant antitumor improvements over the previous long-term culture methods.[290, 292] Thus, additional factors or novel techniques should be developed to further enhance ACT immunotherapy efficiency against cancer.

Herein, a novel and high-throughput biosensor technology has been proposed in order to identify and isolate high avidity T cells in a rapid and efficient manner. The technique exploits the high sensitivity and multiplexing capabilities of a powerful nanoplasmonic biosensor platform to measure and evaluate TCR-pMHC interaction affinity and kinetics at clonal level simultaneously on a vast number of TAA-specific $CD8^+$ T lymphocytes and subsequent recover of candidate cells. This nanoplasmonic biosensor is based on the extraordinary optical transmission (EOT) effect in

suspended plasmonic nanohole arrays (Figure A.2).[293, 294] EOT arises as consequence of transmission of light through a subwavelength aperture in a metallic film patterned with a regularly repeating periodic structure, as the nanohole arrays. The phenomenon is generally attributed to the coupling of the EM field with plasmons generated on the surface of the periodically patterned metal film.[295] EOT is characterized by the appearance of sharp peaks and dips in the transmission spectrum, extremely sensitive to changes in the near-field refractive index of the nanoholes. Therefore, biomolecular interactions taking place on the surface of the nanoplasmonic sensor can be monitored by tracking the wavelength displacements of a particular EOT peak.[111, 294] The possibility of real-time monitoring biochemical interactions enables the study of affinity and kinetic parameters in a rapid and label-free manner. Additionally, the grating configuration allows excitation light to be coupled to surface plasmon waves even at normal incidence.[111] This scheme is compatible for imaging configuration and makes it a competitive candidate for high-throughput sensing in clinical applications. The use of this powerful nanoplasmonic biosensor offers promising opportunities to design and develop an innovative methodology for the isolation and analysis of T lymphocytes for their application in cancer immunotherapy.

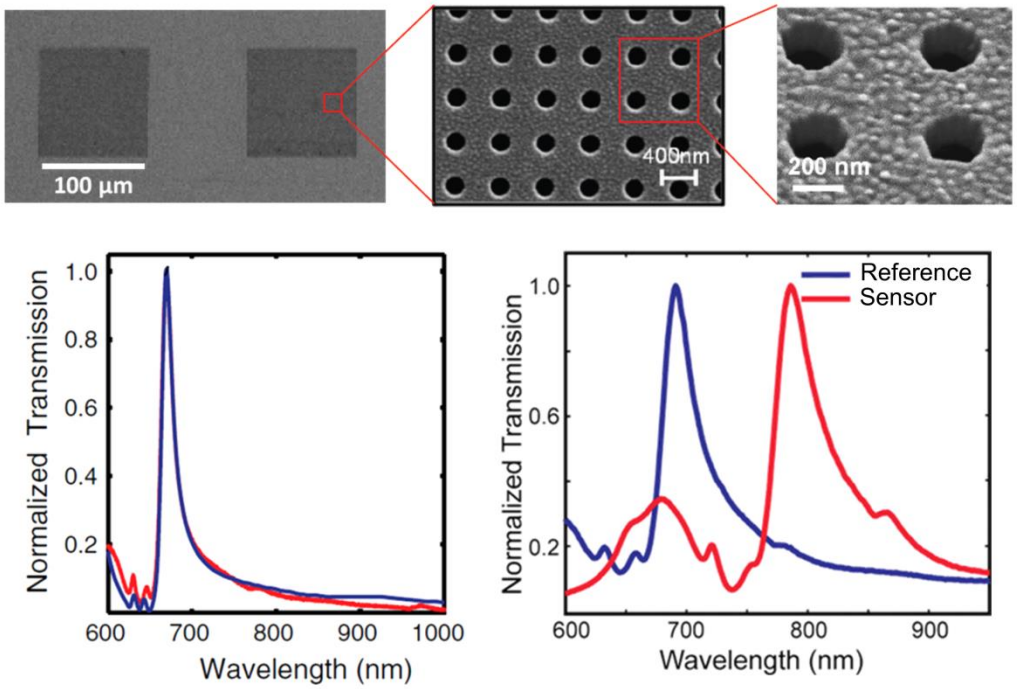

Figure A.2 SEM images of the nanohole array sensor surface (top) and EOT-wavelength displacements due to a RI change in the medium (bottom).

A.2. Design and Optimization of the Biosensor Methodology

The main goal of the study was the identification of rare TAA-specific T lymphocytes presenting high antitumor activity based on the functional avidity of the TCR for pMHC. For that purpose, we focused on determining the kinetic parameters of TCR-pMHC binding, strongly related to the protective capacity of $CD8^+$ T cells for adoptive transfer.[275, 296] Multimeric pMHC dissociation experiments are nowadays considered a gold standard technique to assess the structural avidity of antigen-specific T cells. However, pMHC multimer dissociation can be influenced by the nature or concentration of blocking reagents used to prevent rebinding of dissociated MHC to TCR and can lead to inaccurate results due to the variability in the degree of pMHC multimerization or low correlation between pMHC detection and TCR binding avidity.

In this study, we employed a recently developed pMHC multimeric complex that can be attached to surface-expressed TCRs leading to stably stained $CD8^+$ T cells.[297] The pMHC multimers were built on reversible chelate complexes (NTAmers) by affinity interaction between the MHC oligohistidine chain with Ni^{2+}-nitrilotriacetic acid (NTA) moieties conjugated to a linear peptide (PE) (Figure A.3a). $CD8^+$ T cells stained with NTAmers resulted highly stable in the absence of any chelator, but upon addition of imidazole, it complexes the NTA releasing the pMHC monomers (Figure A.3b) that will start natural dissociation in a diffusion controlled manner (Figure A.3c).[297] The use of NTAmers containing fluorescent labeled pMHC monomers was recently proved for the assessment of TCR-pMHC monomer dissociation kinetics on living cells by flow cytometry.[297] Using $CD8^+$ T lymphocytes expressing affinity engineered TCR they showed that within a wide range, TCR-pMHC monomer dissociation rates correlate with cell activation.

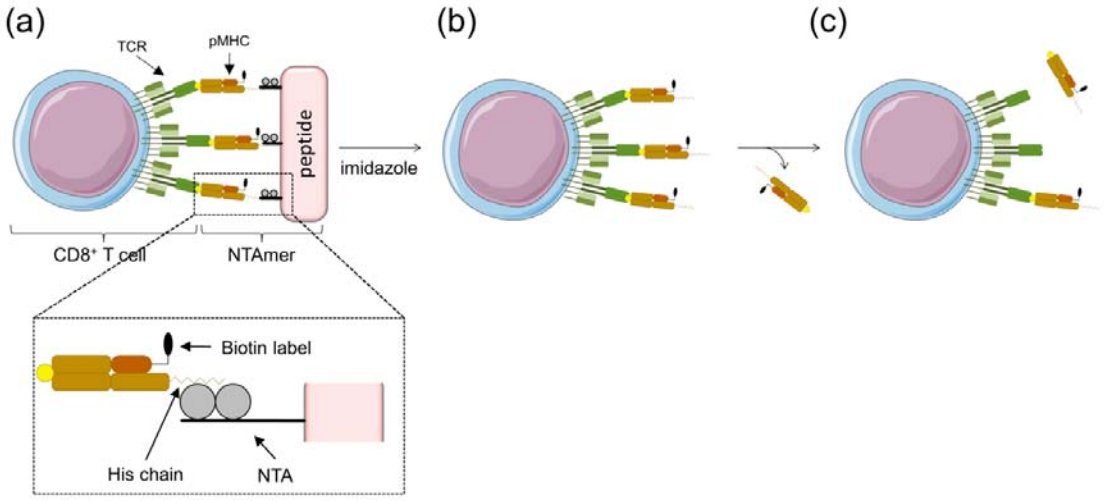

Figure A.3 Principle of TCR-pMHC monomer dissociation kinetic measurements: CD8+ are stained with NTAmers containing biotinylated pMHC; upon addition of imidazole NTAmer disintegrates, leaving TCR-associated pMHC monomers, which starts natural dissociation from cells.

In this case, NTAmers containing biotinylated pMHC monomers were designed in order to be detected over a streptavidin (SA) functionalized sensor surface. The analytical platform consisted of a nanoplasmonic sensor that enables the label-free and real-time detection of the pMHC monomers directly released from living T cells immobilized within an integrated microfluidic chamber (Figure A.4). The whole system was composed of two main parts: (i) the *nanoplasmonic chip* based on several nanohole array sensors (diameter = 200 nm and period = 600 nm) functionalized with a SA layer that specifically detect/capture the released biotinylated-pMHC monomers, and (ii) the *cell chip*, where living NTAmer stained $CD8^+$ T cells were immobilized. With the addition of imidazole through integrated microfluidic connections, NTAmers disintegrate and T cells release the pMHC monomers, being progressively captured onto the plasmonic surface. Binding of biotinylated-pMHC monomers to SA surface could be monitored in real time by tracking the EOT-wavelength displacements, which would allow the determination of the kinetic parameters of the pMHC-TCR dissociation by simply mathematical relation. Furthermore, the compact microfluidic chamber, by dramatically reducing the volume, would permit the direct analysis from low number of cells (5 – 10 cells) or even reach single-cell measurements.

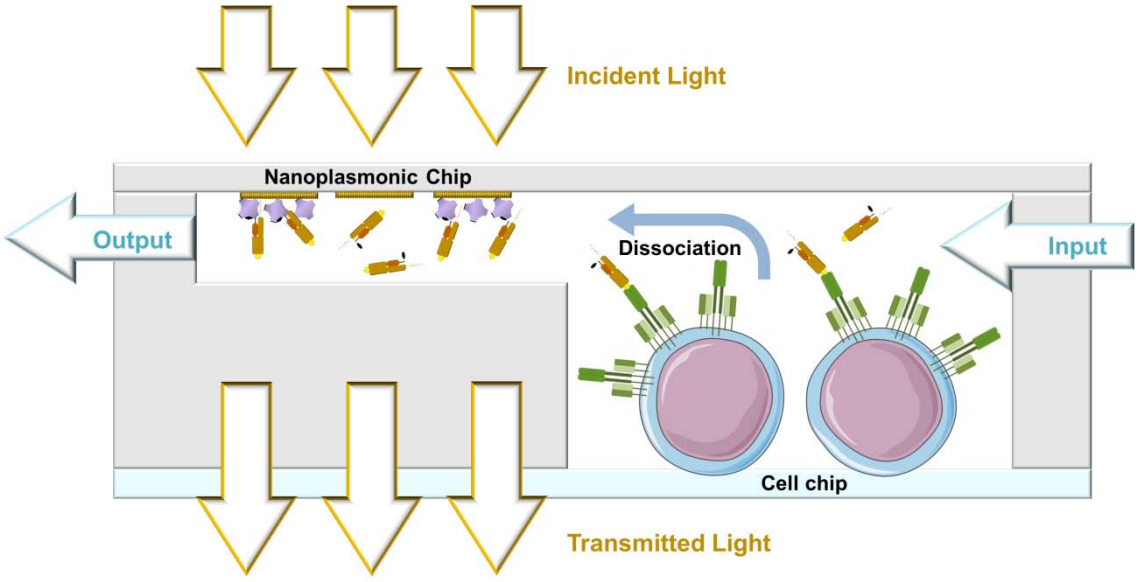

Figure A.4 Schematic representation of the biosensor platform for the analysis of T cell activity.

In order to assess the biosensing strategy, we first carried out an optimization of the nanoplasmonic surface biofunctionalization. SA modification of the sensor substrate might assure maximum coverage of the nanohole array surfaces and optimum biotinylated-pMHC detection. To that end, an additive assay of biotinylated-pMHC over the SA layer was proposed as analysis methodology, which consists of successive detection of several dilutions of analyte without any

regeneration step of the recognition layer. Additive assay was selected since biotin-streptavidin interaction is extremely strong (K_D < 1x10^{-13} M) being necessary really harsh conditions to disrupt the binding.

Prior to attempt the functionalization of the nanoplasmonic surfaces, the feasibility to detect biotinylated-pMHC was evaluated by employing a commercial SPR biosensor (Biacore X100). Conventional thin gold film chips were functionalized to obtain a stable and robust SA layer, *via* the covalent binding of amine groups in SA to the functional carboxylic acids of MHDA SAM (Figure A.5a). In order to assure maximum coverage of SA, we selected a 500 µM MHDA SAM and 50 µg/mL of SA, carrying out the overall functionalization procedure *ex situ* (see Experimental Details).

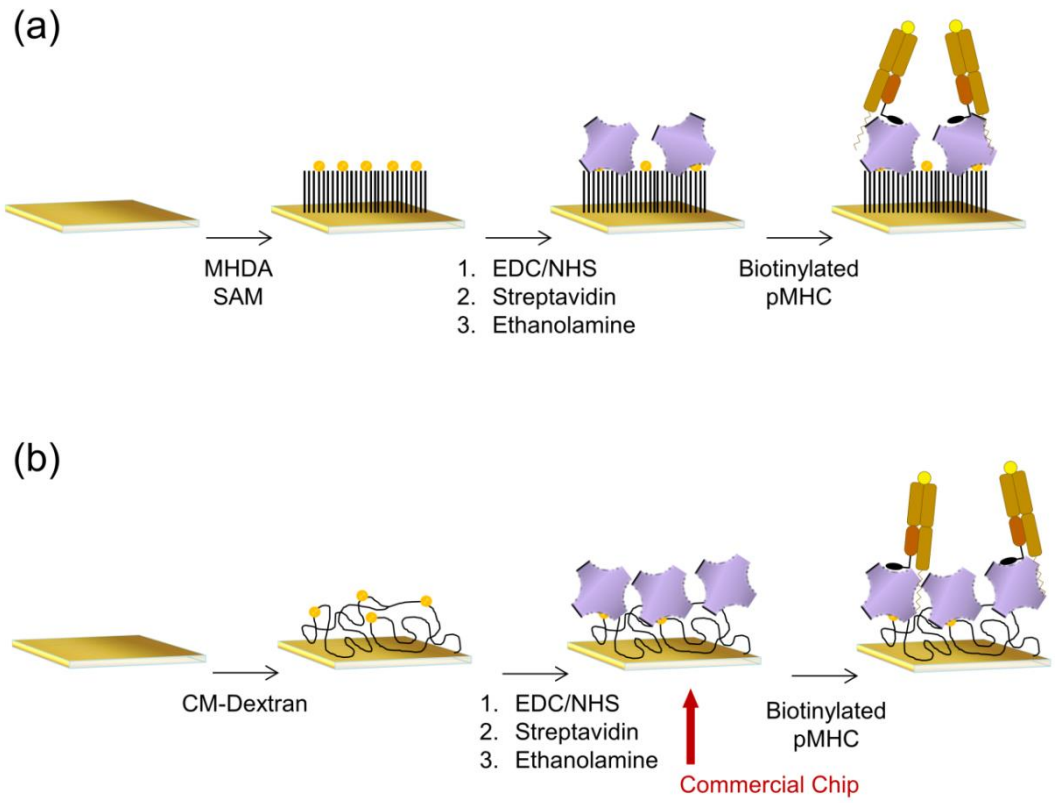

Figure A.5 SPR biosensing strategies for detection of biotinylated pMHC monomers with different streptavidin functionalization procedures: **(a)** amine-mediated covalent binding to a MHDA self-assembled monolayer, and **(b)** pre-immobilized commercial chip based on SA coated to a CM-dextran layer.

In parallel, a commercial SPR chip already coated with SA was used to compare the efficiency of the designed biofunctionalization strategy for gold substrates. We employed a carboxymethyl-dextran (CM-dextran) chips coated with SA (Sensor Chip SA) (Figure A.5b). CM-dextran chips are

often considered standard SPR chips for immobilization of any type of molecules. Gold functionalization with CM-dextran provides a hydrophylic polymeric layer containing carboxylic moieties that can be readily employed for covalent binding to the biomolecules, similarly to alkanethiol SAM procedure.

SPR assays were carried out by flowing successive biotinylated-pMHC monomer (containing 1 biotin per pMHC, MW ≈ 60 kDa) samples (1 nM in PBS buffer) over both functionalized chips and the resultant curves were plotted as the accumulated sensor signal as function of the accumulated concentration of analyte onto the receptor layer (Figure A.6). As can be observed, both curves resulted in analogous response signals leading to a similar detection capability. This demonstrated the feasibility and efficiency of the SA functionalized layer to capture the biotinylated-pMHC monomers. Furthermore, the ability to detect low concentration of pMHC molecules (< 1 nM) with elevated reliability was encouraging for the transfer of the methodology to the sensitive nanoplasmonic technology.

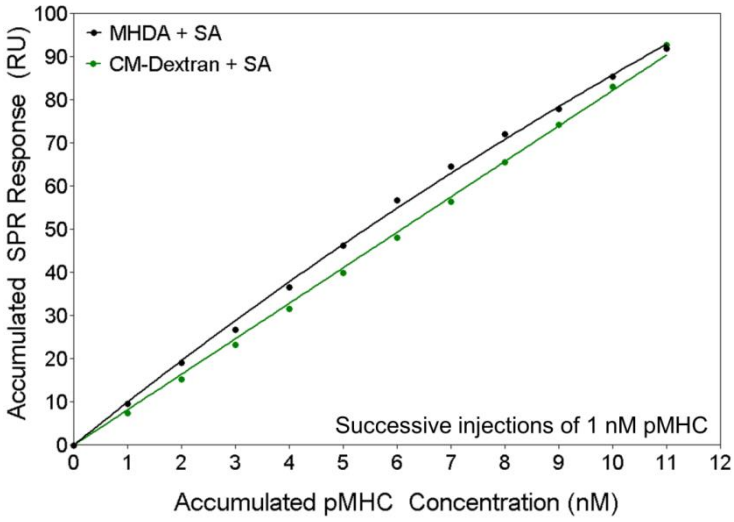

Figure A.6 SPR detection curves for additive assay of repetitive biotinylated pMHC samples (1 nM) performed with both MHDA-based (black) and CM-dextran-based (green) functionalized chips.

Nanostructured sensor chips were biofunctionalized similarly to conventional SPR gold surfaces. Since nanohole arrays are fabricated through thin gold film substrates, surface chemistry established for gold modification might lead to comparable biofunctionalization results. Thus, a carboxylic-functional SAM (500 µM MHDA) was formed onto the nanoplasmonic substrates and then SA (50 µg/mL) was immobilized by covalent binding via amine terminal groups of the protein.

In order to obtain a calibration curve, an additive assay was done but this time flowing successive dilutions of increasing concentrations of biotinylated-pMHC (0.02, 0.1, 1, 2, 10, 50 and 100 nM). Detection curve was obtained by plotting the accumulated response signals as function of accumulated pMHC concentration (Figure A.7). A LoD of 4 pM and LoQ of 36 pM were achieved, revealing the outstanding sensitivity provided by the nanoplasmonic biosensor. Moreover, specificity controls were carried out by injecting several concentrations of non-biotinylated pMHC monomers leading to negligible response of the biosensor. Results proved the excellent selectivity and reliability of the biosensing strategy to detect the pMHC complexes with high sensitivity and in a label-free manner.

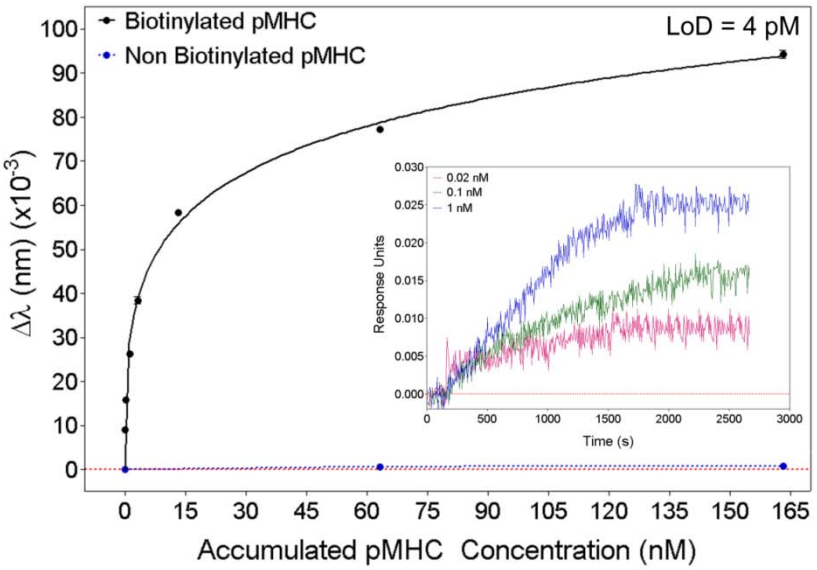

Figure A.7 Calibration curve for the detection of biotinylated pMHC monomers (black) and specificity control performed with non-biotinylated pMHC monomers (blue). Inset graph shows the nanoplasmonic sensorgrams for detection of biotinylated pMHC at 1 nM (blue), 0.1 nM (green) and 0.02 nM (pink).

A.3. Analysis of the pMHC Complex Released by Living T Cells

For the detection of the pMHC complexes liberated from T lymphocytes it was necessary to immobilize them in a cell cavity near the sensor arrays with integrated microfluidic channels that allowed the injection of the imidazole. The cavities designed for the cell immobilization consisted of transparent glass substrate surrounded by polymeric walls with volumes around 5 µL. The microfluidic chamber was built with stack polyethylene (PE) sheets designed and fabricated using a cutting plotter machine and assembled onto the glass substrate, as can be seen in Figure A.8.

This is a rapid, simple and low-cost procedure, which allows the incorporation of microfluidic tubes for in-flow measurements.

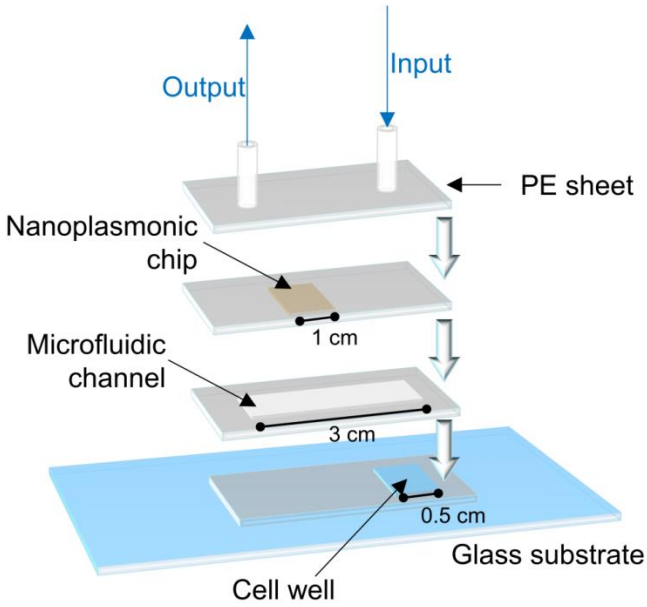

Figure A.8 Schematic representation of the assembly mechanism of PE sheets for the fabrication of the microfluidic cell onto a glass substrate.

In order to attach the cells to the microcavity, the glass substrate was covered with a poly-L-lysine (PLL) layer. This polymer presents high amount of positive charges and therefore T lymphocytes, with a negatively charged external surface, can be immobilized onto the substrate through electrostatic forces. Figure A.9 shows T cells specifically attached on the PLL-modified substrate. This immobilization strategy allowed the strong attachment of T cells to the chip without requiring any structural modification or alteration of the cell surface.

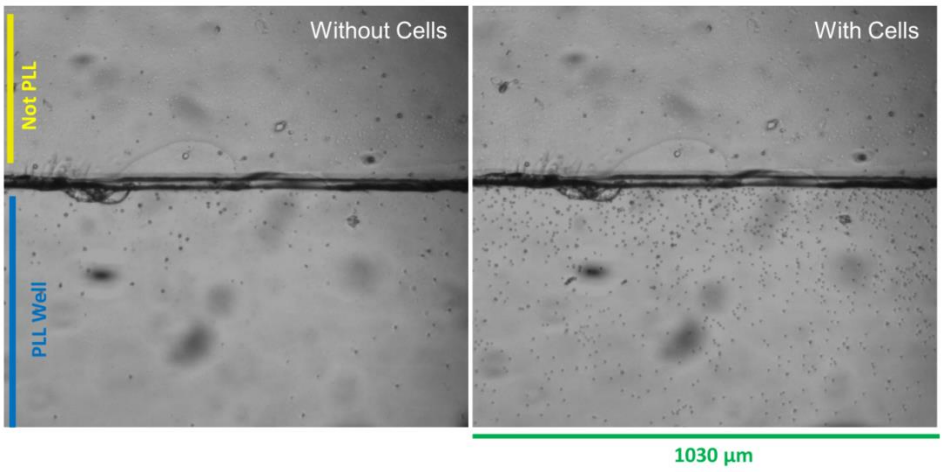

Figure A.9 Optical microscope images of a PLL-modified channel before and after T cell immobilization.

Finally, the study to assess the detection of the released biotinylated-pMHC monomers directly by living T cells was carried out. $CD8^+$ T lymphocytes specific for a common TAA peptide (NY-ESO-$I_{157-165}$) were obtained, expressing engineered TCR that allowed complete liberation of pMHC monomers in 5 minutes upon injection of imidazole in the media. T lymphocytes were stained with the NTAmers containing biotinylated-pMHC monomers by incubating them for 1 hour and they were purified by centrifugation. Prior to place the cells into the PLL-modified microfluidic chamber, a blocking solution containing 1% BSA was flowed over the cell chamber to prevent nonspecific adsorptions ensuring the cell attachment specifically onto the PLL-modified glass surface. Figure A.10a shows an image of the microcavity where stained T lymphocytes were deposited. Once cells were immobilized, the nanoplasmonic chip previously functionalized with streptavidin was integrated in the microfluidic system and the imidazole solution was injected keeping a running flow of standard PBS buffer. As the imidazole reached the cell cavity, the running flow was stopped in order to detect the released pMHC monomers by natural diffusion. Figure A.10b represents the monitoring of the released biotinylated-pMHC monomers from the cells during approximately 8 minutes. Besides, a control experiment was carried out with non-stained T lymphocytes (i.e. without biotinylated-pMHC) to ensure the accuracy and reliability of the analysis. The significant sensor response obtained for the labeled T cells compared to unlabeled ones was attributed to the efficient *in situ* capture of the dissociated pMHC complexes from living T cells.

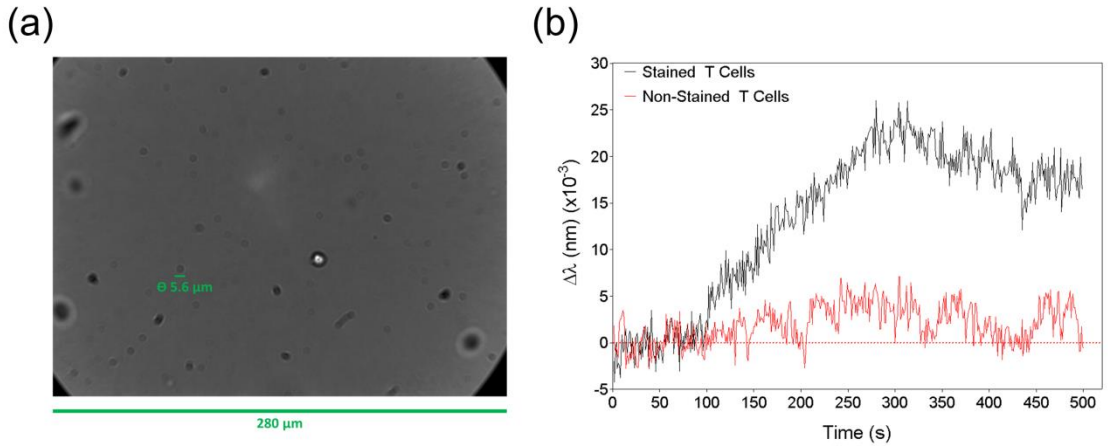

Figure A.10 (a) Optical microscope image of the inner part of the cell chamber with T lymphocytes (diameter ≈ 5 µm) immobilized at the bottom; **(b)** Nanoplasmonic sensorgrams for the detection of biotinylated pMHC monomers liberated by T lymphocytes (black) and selectivity control performed with non-stained T lymphocytes (red).

A.4. Conclusions and Future Perspectives

The main goal of this project involved the design and development of a novel biosensing methodology for the *ex vivo* analysis of T lymphocytes avidity in order to be applied for adoptive cell transfer immunotherapy. The strategy was based on the use of a highly sensitive nanoplasmonic biosensor that allows the real-time monitoring of the pMHC-TCR dissociation in a rapid and label-free manner. Optimization and assessment of the biofunctionalization procedure of the nanostructured surface enabled the reliable detection of biotinylated-pMHC monomers with outstanding sensitivity (LoD = 4 pM). On the other hand, a simple and efficient procedure was tested for the immobilization of living T lymphocytes onto a glass substrate without inducing or modifying any structural changes on the cell surface that would alter the TCR-pMHC dissociation. Besides, an integrated microfluidic system containing a compact cell chamber and the nanoplasmonic chip was designed and fabricated with an easy and low-cost technique. The overall analytical platform was finally evaluated for the detection of biotinylated-pMHC monomers directly released from living CD8+ T lymphocytes leading to promising results. On-going experiments are directed to optimize the signal monitoring, since the ultimate goal is the determination of the K_D values from the obtained signals.

The work carried out during the PhD stay represented a first proof of principle of a potential alternative for the *ex vivo* cellular analysis. Future perspectives aim to develop a multiplexed analytical platform able to perform simultaneous single-cell analysis for the rapid assessment and identification of antitumor T lymphocytes. The proposed analytical platform represents an interesting approach to improve efficiency of the adoptive cell transfer immunotherapy, being nowadays the most promising treatment for cancer.

A.5. Experimental Details

Materials. $CD8^+$ T lymphocytes, biotinylated-pMHC multimers, imidazole, poly-L-lysine (PLL) and streptavidin were provided by a collaborator research group (Dr. Luescher, Université de Lausanne – UNIL, Switzerland). Mercaptohexadecanoic acid (MHDA), reagents for carboxylate group activation and deactivation (1-ethyl-3-(3-dimethylaminopropyl)carbodiimide (EDC), N-hydroxysuccinimide (NHS) and ethanolamine 1M), standard 10 mM PBS buffer, MES buffer (0.1 M) and bovine serum albumin (BSA) were purchased to Sigma Aldrich (Germany). Commercial SPR chip SA Sensor Chip was obtained from GE Healthcare (UK) and nanoplasmonic sensor chips were fabricated in clean-room facilities of the EPFL following a reported procedure.[298]

Sensor chips functionalization. Prior to functionalization, both gold SPR chips and nanoplasmonic surfaces were subjected to a standard cleaning procedure that basically consists of successive rinse with acetone, ethanol and DI water and 20 min in a UV/O_3 generator. Rapidly, the chips were coated with 500 µM MHDA in ethanol for 5 hours at RT. Then, the surface was rinsed with ethanol and DI water and dried with a N_2 stream. For SA immobilization the chips were first coated with an EDC 0.2 M/NHS 0.05 M solution in MES buffer for 20 min at RT, rinsed with water and incubated with a 50 µg/mL solution of SA in PBS overnight at 4°C. Finally, the surface was rinsed with PBS and water, and coated with ethanolamine 1M aqueous solution for 10 min to deactivate unreacted carboxylic groups.

SPR measurements. SPR assays were carried out with a Biacore X100 (Ge Healthcare, UK) following manufacturer's instructions. The same assay protocol was applied for measurements with the commercial SPR chip and the functionalized gold chip. After conditioning steps with PBS buffer, solutions of 1 nM biotinylated-pMHC in PBS were successively injected at 15 µL/min flow rate. PBS washing steps were performed after each pMHC injection.

Nanoplasmonic measurements. After functionalization of nanoholes structured substrates, the chip was clamped in the microfluidic cell and placed on the microscope platform. The nanohole arrays were illuminated with white light and transmission spectra were collected with a spectrometer. Monitoring of the biochemical interactions was performed by tracking the EOT-wavelengths displacements using MATLAB software. Measurements of biotinylated-pMHC monomers were carried out similarly to SPR assays. After conditioning the microfluidic cell with PBS buffer, solutions of biotinylated-pMHC at different concentrations (0.02, 0.1, 1, 2, 10, 50 and 100 nM) in PBS were injected at a constant flow rate of 15 µL/min.

T cell activity analysis. Cell cavities built on glass substrates were coated with a 0.01% PLL solution for 1 hour at RT and then blocked against nonspecific adsorptions with 1% BSA in PBS. T lymphocytes were stained with NTAmers containing biotinylated-pMHC by incubating them in gentle agitation for 1 hour at 4°C. Purification of the stained cells was performed by centrifugation (5 min, 10000 rpm). Then, cells were attached to the cavity by coating the well with the cell solution for 20 min at 4°C and removal of non-attached cells was performed by rinsing with PBS buffer. The microfluidic chamber containing the nanoplasmonic chip was mounted onto the cell cavity and the system was placed on the microscope for measuring. A solution of 10 mM imidazole was injected through the microfluidic system and the running flow was stopped upon arrival of the imidazole to the chamber. The overall assay was continuously monitored.

Publications

Journal Articles:

Direct Detection of Protein Biomarkers in Human Fluids using Site-specific Antibody Immobilization Strategies
M. Soler, M.C. Estévez, M. Álvarez, M.A. Otte, B. Sepúlveda and L.M. Lechuga
2014 *Sensors* 14 (2), 2239-2258

Highly Sensitive Dendrimer-based Nanoplasmonic Biosensor for Drug Allergy Diagnosis
M. Soler, P. Mesa-Antúnez, M.C. Estévez, A.J. Ruiz-Sánchez, M.A. Otte, B. Sepúlveda, D. Collado, C. Mayorga, M.J. Torres, E. Pérez-Inestrosa and L.M. Lechuga
2015 *Biosensors and Bioelectronics* 66, 115-123

Label-free Nanoplasmonic Quantitation of Tumor-Associate Autoantibodies for Early Diagnosis of Colorectal Cancer
M. Soler, M.C. Estévez, R. Villar-Vázquez, I. Casal and L.M. Lechuga
2015 *Scientific Reports (submitted)*

Rapid and Sensitive Quantitation of Gluten in Urine for Non-Invasive Celiac Disease Follow-up
M. Soler, M.C. Estévez, M.L. Moreno, A. Cebolla and L.M. Lechuga
(in preparation)

Last Breakthroughs in Nanoplasmonic Biosensors: Applications and Lab-on-Chip Integration
G.A. López-Muñoz, M. Soler, M.C. Estévez and L.M. Lechuga
(in preparation)

Conferences:

Oriented antibody immobilization strategies to improve sensitivity of direct label-free biosensor-based immunoassays - Poster
M. Soler, M.C. Estévez, J.M. Rodríguez-Frade, M. Mellado and L.M. Lechuga
2012 *Europtrode XI Conference on Optical Chemical Sensors and Biosensors* _ Barcelona

Antibody Oriented Immobilization Strategies for Direct Label-free Detection of Protein Biomarkers in Biological Fluids - Poster
M. Soler, M.C. Estévez and L.M. Lechuga
2012 *VI Jornadas Anuales del CIBER-BBN*

Nanoplasmonic Biosensor based on Gold Nanodisks for the Direct Detection of CRP in Biological Fluids - Poster
M. Soler, M.C. Estévez, M.A. Otte, B. Sepúlveda and L.M. Lechuga
2013 *Euromat (European Congress and Exhibition on Advanced Materials and Processes)*

Nanoplasmonic Biosensor based on Gold Nanodisks for the Direct Detection of CRP in Biological Fluids - Poster
M. Soler, M.C. Estévez, M.A. Otte, B. Sepúlveda and L.M. Lechuga
2013 *Biosensors for a better environment*

Abbreviations and Acronyms

Ab	Antibody
ACT	Adoptive Cell Transfer
AFC	Anti-fouling Cocktail
APC	Antigen Presenting Cells
ATR	Attenuated Total Reflection
AX	Amoxicillin
AXO	Amoxicilloyl
BAPAD	Bis-aminoalkyl-polyamide dendrimers
BS3	Bissulfosuccinimidyl suberate
BSA	Bovine Serum Albumin
CCD	Charge-Coupled Device
CD	Celiac Disease
CRC	Colorectal Cancer
CRP	C-Reactive Protein
CV	Coefficient of Variability
DF	Dark-field
DMF	Dimethylformamide
DTT	Dithiothreitol
EDC	1-Ethyl-3-(3-dimethylaminopropyl)carbodiimide
EDIL3	EGF-like repeats and discoidin I-like domains 3
ELISA	Enzyme-Linked Immunosorbent Assay
EM	Electromagnetic
EOT	Extraordinary Optical Transmission
Fab	Fragment antigen-binding
FAK	Focal Adhesion Kinase

Fc	Fragment crystallizable
FDA	Food and Drug Administration
FEIA	Fluorescent Enzyme-labeled Immunoassay
GFD	Gluten-Free Diet
GTF2b	General Transcription Factor IIb
HBB	High-Blocking Buffer
hCG	Human Chorionic Gonadotropin
HCL	Hole-mask Colloidal Lithography
HEPES	4-(2-hydroxyethyl)-1-piperazineethanesulfonic acid
HyNic	6-Hydrazino-Nicotinamide
IC_{50}	Half Inhibitory Concentration
Ig	Immunoglobulin
IUPAC	International Union of Puer and Applied Chemistry
LoD	Limit of Detection
LoQ	Limit of Quantitation
LSPR	Localized Surface Plasmon Resonance
mAb	Monoclonal Antibody
MES	2-(N-morpholino)ethanesulfonic acid
MHDA	Mercaptohexadecanoic acid
MSR	Molar Substitution Ratio
MUOH	11-Mercaptoundecanol
NIR	Near-Infrared
NTA	Ni^{2+}-nitriloacteic acid
pAb	Polyclonal Antibody
PAMAM	Poly(amidoamine)
PBS	Phosphate Buffered Saline

PBST	Tween-containing Phosphate Buffered Saline
PCR	Polymerase Chain Reaction
PDDA	Poly(diallyldimethylammonium chloride)
PE	Polyethylene
PEG	Polyethylene Glycol
PLL	Poly-L-Lysine
pMHC	Peptide Major Histocompatibility Complex
PMMA	Poly(methyl methacrylate)
PoC	Point of Care
PSA	Prostate Specific Antigen
RAST	Radioallergosorbent Test
RCD	Refractory Celiac Disease
RI	Refractive Index
RT	Room Temperature
SA	Streptavidin
SAM	Self-Assembled Monolayer
SD	Standard Deviation
s-NHS	sulfo-N-Hydroxysuccinimide
SP	Surface Plasmon
SPP	Surface Plasmon Polariton
SPR	Surface Plasmon Resonance
TAA	Tumor-Associate Antigen
TCR	T Cell Receptor
TE	Transverse-electric
TIR	Total Internal Reflection
TM	Transverse-magnetic

List of Figures

Chapter 1. Introduction

Chapter 2. Materials and Methods

Chapter 3. Direct Immunoassay for Protein Biomarkers Detection in Biological Fluids

Chapter 4. Analysis of Gluten Immunogenic Peptide in Urine for Celiac Disease Follow-up

Chapter 6. Analysis of TAA Autoantibodies in Serum for Early Diagnosis of Colorectal Cancer

List of Tables

Bibliography

1. ESF, E.S.F. Nanomedicine: An ESF–European Medical Research Councils (EMRC) Forward Look Report. *Strasbourg cedex, France* (2005).
2. Kreuter, J. Nanoparticles—a historical perspective. *International Journal of Pharmaceutics* **331**, 1-10 (2007).
3. Albanese, A., Tang, P.S. & Chan, W.C. The effect of nanoparticle size, shape, and surface chemistry on biological systems. *Annual review of biomedical engineering* **14**, 1-16 (2012).
4. Euliss, L.E., DuPont, J.A., Gratton, S. & DeSimone, J. Imparting size, shape, and composition control of materials for nanomedicine. *Chemical Society Reviews* **35**, 1095-1104 (2006).
5. Kim, B.Y., Rutka, J.T. & Chan, W.C. Nanomedicine. *New England Journal of Medicine* **363**, 2434-2443 (2010).
6. Cheng, M.M.-C. et al. Nanotechnologies for biomolecular detection and medical diagnostics. *Current opinion in chemical biology* **10**, 11-19 (2006).
7. Vaddiraju, S., Tomazos, I., Burgess, D.J., Jain, F.C. & Papadimitrakopoulos, F. Emerging synergy between nanotechnology and implantable biosensors: a review. *Biosensors and Bioelectronics* **25**, 1553-1565 (2010).
8. Hamburg, M.A. & Collins, F.S. The path to personalized medicine. *New England Journal of Medicine* **363**, 301-304 (2010).
9. Beija, M., Salvayre, R., Lauth-de Viguerie, N. & Marty, J.-D. Colloidal systems for drug delivery: from design to therapy. *Trends in biotechnology* **30**, 485-496 (2012).
10. Allen, T.M. & Cullis, P.R. Liposomal drug delivery systems: from concept to clinical applications. *Adv Drug Deliv Rev* **65**, 36-48 (2013).
11. Bader, R.A. & Putnam, D.A. Engineering Polymer Systems for Improved Drug Delivery. (John Wiley & Sons, 2014).
12. Couvreur, P. Nanoparticles in drug delivery: past, present and future. *Adv Drug Deliv Rev* **65**, 21-23 (2013).
13. Barenholz, Y.C. Doxil®—the first FDA-approved nano-drug: lessons learned. *Journal of controlled release* **160**, 117-134 (2012).
14. Torchilin, V. Tumor delivery of macromolecular drugs based on the EPR effect. *Adv Drug Deliv Rev* **63**, 131-135 (2011).
15. Lammers, T., Kiessling, F., Hennink, W.E. & Storm, G. Drug targeting to tumors: principles, pitfalls and (pre-) clinical progress. *Journal of controlled release* **161**, 175-187 (2012).
16. Mura, S., Nicolas, J. & Couvreur, P. Stimuli-responsive nanocarriers for drug delivery. *Nature materials* **12**, 991-1003 (2013).
17. Yun, Y., Lee, B.K. & Park, K. Controlled drug delivery systems: the next 30 years. *Frontiers of Chemical Science and Engineering*, 1-4 (2014).
18. Das, M., Mohanty, C. & Sahoo, S.K. Nanotechnology for Regenerative Medicine. *Nanotechnology in Health Care*, 297 (2012).
19. Bean, A.C. & Tuan, R.S. Stem Cells and Nanotechnology in Tissue Engineering and Regenerative Medicine. *Micro and Nanotechnologies in Engineering Stem Cells and Tissues*, 1-26 (2013).
20. Johnston, H., Kermanizadeh, A. & Stone, V. Nanotoxicology: Focus on Nanomedicine. *Handbook of Safety Assessment of Nanomaterials: From Toxicological Testing to Personalized Medicine*, 43 (2014).
21. Mout, R., Moyano, D.F., Rana, S. & Rotello, V.M. Surface functionalization of nanoparticles for nanomedicine. *Chem. Soc. Rev.* **41**, 2539-2544 (2012).

22. Jokerst, J.V., Lobovkina, T., Zare, R.N. & Gambhir, S.S. Nanoparticle PEGylation for imaging and therapy. *Nanomedicine* **6**, 715-728 (2011).
23. Nazar, H. The use of nanotechnology in disease diagnosis and molecular imaging. *Gene therapy* **17**, 54 (2014).
24. Weissleder, R. & Pittet, M.J. Imaging in the era of molecular oncology. *Nature* **452**, 580-589 (2008).
25. Bipat, S. et al. Computed tomography and magnetic resonance imaging in staging of uterine cervical carcinoma: a systematic review. *Gynecologic oncology* **91**, 59-66 (2003).
26. Arvanitakis, M. et al. Computed tomography and magnetic resonance imaging in the assessment of acute pancreatitis. *Gastroenterology* **126**, 715-723 (2004).
27. Hodges, P., Pengel, L., Herbert, R. & Gandevia, S. Measurement of muscle contraction with ultrasound imaging. *Muscle & nerve* **27**, 682-692 (2003).
28. Hahn, M.A., Singh, A.K., Sharma, P., Brown, S.C. & Moudgil, B.M. Nanoparticles as contrast agents for in-vivo bioimaging: current status and future perspectives. *Anal Bioanal Chem* **399**, 3-27 (2011).
29. Byers, R.J. & Hitchman, E.R. Quantum dots brighten biological imaging. *Progress in Histochemistry and Cytochemistry* **45**, 201-237 (2011).
30. Valizadeh, A. et al. Quantum dots: synthesis, bioapplications, and toxicity. *Nanoscale research letters* **7**, 1-14 (2012).
31. Wang, Y., Hu, R., Lin, G., Roy, I. & Yong, K.-T. Functionalized quantum dots for biosensing and bioimaging and concerns on toxicity. *ACS applied materials & interfaces* **5**, 2786-2799 (2013).
32. Zheng, W. et al. Quantum Dots Encapsulated within Phospholipid Membranes: Phase-Dependent Structure, Photostability, and Site-Selective Functionalization. *Journal of the American Chemical Society* **136**, 1992-1999 (2014).
33. Rosen, J.E., Chan, L., Shieh, D.-B. & Gu, F.X. Iron oxide nanoparticles for targeted cancer imaging and diagnostics. *Nanomedicine: Nanotechnology, Biology and Medicine* **8**, 275-290 (2012).
34. Hainfeld, J., Slatkin, D., Focella, T. & Smilowitz, H. Gold nanoparticles: a new X-ray contrast agent. (2014).
35. Lee, D.-E. et al. Multifunctional nanoparticles for multimodal imaging and theragnosis. *Chemical Society Reviews* **41**, 2656-2672 (2012).
36. Muthu, M.S., Mei, L. & Feng, S.-S. Nanotheranostics: advanced nanomedicine for the integration of diagnosis and therapy. *Nanomedicine* **9**, 1277-1280 (2014).
37. Lammers, T. et al. Image-guided and passively tumour-targeted polymeric nanomedicines for radiochemotherapy. *British journal of cancer* **99**, 900-910 (2008).
38. Soundararajan, A., Bao, A., Phillips, W.T., Perez III, R. & Goins, B.A. Liposomal doxorubicin (Doxil): in vitro stability, pharmacokinetics, imaging and biodistribution in a head and neck squamous cell carcinoma xenograft model. *Nuclear medicine and biology* **36**, 515-524 (2009).
39. Southern, E.M. in DNA Arrays 1-15 (Springer, 2001).
40. Hall, D.A., Ptacek, J. & Snyder, M. Protein microarray technology. *Mechanisms of ageing and development* **128**, 161-167 (2007).
41. Heller, M.J. DNA microarray technology: devices, systems, and applications. *Annual review of biomedical engineering* **4**, 129-153 (2002).
42. Leveque, N., Renois, F. & Andreoletti, L. The microarray technology: facts and controversies. *Clinical Microbiology and Infection* **19**, 10-14 (2013).
43. Gubala, V., Harris, L.F., Ricco, A.J., Tan, M.X. & Williams, D.E. Point of care diagnostics: status and future. *Analytical Chemistry* **84**, 487-515 (2011).

44. áEric Aston, D. & áLarry Branen, A. DNA detection on lateral flow test strips: enhanced signal sensitivity using LNA-conjugated gold nanoparticles. *Chemical Communications* **48**, 7714-7716 (2012).
45. Fu, E. et al. Enhanced sensitivity of lateral flow tests using a two-dimensional paper network format. *Anal Chem* **83**, 7941-7946 (2011).
46. Sajid, M., Kawde, A.-N. & Daud, M. Designs, formats and applications of lateral flow assay: A literature review. *Journal of Saudi Chemical Society* (2014).
47. Tiwari, I. & Singh, M. Advances in Sensors' Nanotechnology. *Advanced Sensor and Detection Materials*, 1 (2014).
48. Thevenot, D.R., Tóth, K., Durst, R.A. & Wilson, G.S. in Pure and Applied Chemistry, Vol. 71 23331999).
49. Jönsson, U. in Biosensors 92 Proceedings: The Second World Congress on Biosensors (Elsevier, 2014).
50. Yoon, J.-Y. in Introduction to Biosensors 225-256 (Springer, 2013).
51. Sagadevan, S. & Periasamy, M. Recent trends in nanobiosensors and their applications - A review. *Reviews of Advanced Materia Science* **36**, 62-69 (2014).
52. Ahn, C.H. et al. Disposable smart lab on a chip for point-of-care clinical diagnostics. *Proceedings of the IEEE* **92**, 154-173 (2004).
53. Kumar, S. et al. Microfluidic-integrated biosensors: Prospects for point-of-care diagnostics. *Biotechnology journal* **8**, 1267-1279 (2013).
54. Kwong, W.K. Catalytic biosensors: novel analytical tools and their applications in sports, food and environmental monitoring. (2000).
55. Rogers, K.R. & Mulchandani, A. Affinity biosensors: techniques and protocols, Vol. 7. (Humana Press Totowa, NJ, USA:, 1998).
56. Ronkainen, N.J., Halsall, H.B. & Heineman, W.R. Electrochemical biosensors. *Chemical Society Reviews* **39**, 1747-1763 (2010).
57. Zhang, X., Ju, H. & Wang, J. Electrochemical sensors, biosensors and their biomedical applications. (Academic Press, 2011).
58. Clark, L.C. & Lyons, C. Electrode systems for continuous monitoring in cardiovascular surgery. *Annals of the New York Academy of sciences* **102**, 29-45 (1962).
59. Wang, J. Carbon-nanotube based electrochemical biosensors: A review. *Electroanalysis* **17**, 7-14 (2005).
60. Gan, T. & Hu, S. Electrochemical sensors based on graphene materials. *Microchim Acta* **175**, 1-19 (2011).
61. Justino, C.I., Rocha-Santos, T.A. & Duarte, A.C. Advances in point-of-care technologies with biosensors based on carbon nanotubes. *TrAC Trends in Analytical Chemistry* **45**, 24-36 (2013).
62. Tamayo, J., Kosaka, P.M., Ruz, J.J., San Paulo, Á. & Calleja, M. Biosensors based on nanomechanical systems. *Chemical Society Reviews* **42**, 1287-1311 (2013).
63. Ferreira, G.N., da-Silva, A.-C. & Tomé, B. Acoustic wave biosensors: physical models and biological applications of quartz crystal microbalance. *Trends in biotechnology* **27**, 689-697 (2009).
64. Carrascosa, L.G., Moreno, M., Álvarez, M. & Lechuga, L.M. Nanomechanical biosensors: a new sensing tool. *TrAC Trends in Analytical Chemistry* **25**, 196-206 (2006).
65. Arlett, J., Myers, E. & Roukes, M. Comparative advantages of mechanical biosensors. *Nature nanotechnology* **6**, 203-215 (2011).
66. Calleja, M., Kosaka, P.M., San Paulo, Á. & Tamayo, J. Challenges for nanomechanical sensors in biological detection. *Nanoscale* **4**, 4925-4938 (2012).
67. Ligler, F.S. & Taitt, C.R. Optical biosensors: today and tomorrow. (Elsevier, 2011).
68. Narayanaswamy, R. & Wolfbeis, O.S. Optical sensors: industrial, environmental and diagnostic applications, Vol. 1. (Springer, 2004).

69. Daghestani, H.N. & Day, B.W. Theory and applications of surface plasmon resonance, resonant mirror, resonant waveguide grating, and dual polarization interferometry biosensors. *Sensors* **10**, 9630-9646 (2010).
70. Passaro, V., Dell'Olio, F., Casamassima, B. & De Leonardis, F. Guided-wave optical biosensors. *Sensors* **7**, 508-536 (2007).
71. Hill, R.T. Plasmonic biosensors. *Wiley Interdisciplinary Reviews: Nanomedicine and Nanobiotechnology* (2014).
72. Long, Y.-T. & Jing, C. in Localized Surface Plasmon Resonance Based Nanobiosensors 23-37 (Springer, 2014).
73. Liedberg, B., C. Nylander, and I. Lundstrom Surface-Plasmon Resonance for Gas-Detection and Biosensing. *Sensors and Actuators B* **4**, 299-304 (1983).
74. Homola, J. Surface Plasmon Resonance Sensors for Detection of Chemical and Biological Species. *Chemical Reviews* **108**, 462-493 (2008).
75. Homola, J. Surface plasmon resonance based sensors, Vol. 4. (Springer, 2006).
76. Kretschmann, E. Die bestimmung optischer konstanten von metallen durch anregung von oberflächenplasmaschwingungen. *Zeitschrift für Physik* **241**, 313-324 (1971).
77. Raether, H. Surface plasmons on smooth surfaces. (Springer, 1988).
78. Raether, H. Surface plasmons on gratings. *Surface Plasmons on Smooth and Rough Surfaces and on Gratings*, 91-116 (1988).
79. Kashyap, R. & Nemova, G. Surface plasmon resonance-based fiber and planar waveguide sensors. *Journal of Sensors* **2009** (2009).
80. Park, S., Lee, G., Song, S.H., Oh, C.H. & Kim, P.S. Resonant coupling of surface plasmons to radiation modes by use of dielectric gratings. *Optics letters* **28**, 1870-1872 (2003).
81. Nagata, K. & Handa, H. Real-time analysis of biomolecular interactions. (Springer, 2000).
82. Willets, K.A. & Van Duyne, R.P. Localized surface plasmon resonance spectroscopy and sensing. *Annu. Rev. Phys. Chem.* **58**, 267-297 (2007).
83. Estevez, M., Otte, M.A., Sepulveda, B. & Lechuga, L.M. Trends and challenges of refractometric nanoplasmonic biosensors: A review. *Anal Chim Acta* **806**, 55-73 (2014).
84. Lu, X., Rycenga, M., Skrabalak, S.E., Wiley, B. & Xia, Y. Chemical synthesis of novel plasmonic nanoparticles. *Annual review of physical chemistry* **60**, 167-192 (2009).
85. Mayer, K.M., Hao, F., Lee, S., Nordlander, P. & Hafner, J.H. A single molecule immunoassay by localized surface plasmon resonance. *Nanotechnology* **21**, 255503 (2010).
86. Piliarik, M. et al. High-resolution biosensor based on localized surface plasmons. *Optics express* **20**, 672-680 (2012).
87. Otte, M.A., Estévez, M.C., Regatos, D., Lechuga, L.M. & Sepúlveda, B. Guiding Light in Monolayers of Sparse and Random Plasmonic Meta-atoms. *ACS Nano* **5**, 9179-9186 (2011).
88. Bolduc, O.R., Live, L.S. & Masson, J.-F. High-resolution surface plasmon resonance sensors based on a dove prism. *Talanta* **77**, 1680-1687 (2009).
89. McDonnell, J.M. Surface plasmon resonance: towards an understanding of the mechanisms of biological molecular recognition. *Current Opinion in Chemical Biology* **5**, 572-577 (2001).
90. Rich, R.L. & Myszka, D.G. Advances in surface plasmon resonance biosensor analysis. *Current opinion in biotechnology* **11**, 54-61 (2000).
91. Lofas, S., Choulier, L. & Altschuh, D. Surface Plasmon Resonance. *Biophysical Approaches Determining Ligand Binding to Biomolecular Targets: Detection, Measurement and Modelling*, 136 (2011).
92. Baird, C.L. & Myszka, D.G. Current and emerging commercial optical biosensors. *Journal of molecular recognition* **14**, 261-268 (2001).
93. www.biacore.com.

94. www.ti.com.
95. www.xantec.com.
96. www.horiba.com.
97. www.biosuplar.de.
98. www.sensia.es.
99. Rothenhäusler, B. & Knoll, W. Surface plasmon microscopy. (1988).
100. Piliarik, M., Vaisocherová, H. & Homola, J. A new surface plasmon resonance sensor for high-throughput screening applications. *Biosensors and Bioelectronics* **20**, 2104-2110 (2005).
101. Spoto, G. & Minunni, M. Surface plasmon resonance imaging: what next? *The Journal of Physical Chemistry Letters* **3**, 2682-2691 (2012).
102. Li, M., Cushing, S.K. & Wu, N. Plasmon-enhanced optical sensors: a review. *Analyst* **140**, 386-406 (2015).
103. Tokel, O., Inci, F. & Demirci, U. Advances in plasmonic technologies for point of care applications. *Chemical reviews* **114**, 5728-5752 (2014).
104. Zavaleta, C.L. et al. A Raman-based endoscopic strategy for multiplexed molecular imaging. *Proceedings of the National Academy of Sciences* **110**, E2288-E2297 (2013).
105. Lee, S. et al. Rapid and sensitive phenotypic marker detection on breast cancer cells using surface-enhanced Raman scattering (SERS) imaging. *Biosensors and Bioelectronics* **51**, 238-243 (2014).
106. Tabakman, S.M. et al. Plasmonic substrates for multiplexed protein microarrays with femtomolar sensitivity and broad dynamic range. *Nature communications* **2**, 466 (2011).
107. Zhang, B., Kumar, R.B., Dai, H. & Feldman, B.J. A plasmonic chip for biomarker discovery and diagnosis of type 1 diabetes. *Nature medicine* **20**, 948-953 (2014).
108. Im, H. et al. Label-free detection and molecular profiling of exosomes with a nano-plasmonic sensor. *Nature biotechnology* **32**, 490-495 (2014).
109. Inci, F. et al. Nanoplasmonic quantitative detection of intact viruses from unprocessed whole blood. *ACS Nano* **7**, 4733-4745 (2013).
110. Zhu, H., Isikman, S.O., Mudanyali, O., Greenbaum, A. & Ozcan, A. Optical imaging techniques for point-of-care diagnostics. *Lab on a Chip* **13**, 51-67 (2013).
111. Cetin, A.E. et al. Handheld high-throughput plasmonic biosensor using computational on-chip imaging. *Light: Science & Applications* **3**, e122 (2014).
112. www.plasmore.com.
113. www.lamdagen.com.
114. Rabe, M., Verdes, D. & Seeger, S. Understanding protein adsorption phenomena at solid surfaces. *Adv Colloid Interface Sci* **162**, 87-106 (2011).
115. Sassolas, A., Blum, L.J. & Leca-Bouvier, B.D. Immobilization strategies to develop enzymatic biosensors. *Biotechnology Advances* **30**, 489-511 (2012).
116. Goddard, J.M. & Hotchkiss, J. Polymer surface modification for the attachment of bioactive compounds. *Progress in polymer science* **32**, 698-725 (2007).
117. Wong, L.S., Khan, F. & Micklefield, J. Selective covalent protein immobilization: strategies and applications. *Chemical reviews* **109**, 4025-4053 (2009).
118. Camarero, J.A. Recent developments in the site-specific immobilization of proteins onto solid supports. *Peptide Science* **90**, 450-458 (2008).
119. YoungáJeong, J. & HyunáChung, B. Recent advances in immobilization methods of antibodies on solid supports. *Analyst* **133**, 697-701 (2008).
120. Saphire, E.O. et al. Contrasting IgG structures reveal extreme asymmetry and flexibility. *Journal of molecular biology* **319**, 9-18 (2002).
121. Stills, H.F. Polyclonal antibody production. *The laboratory rabbit, guinea pig, hamster and other rodents. Oxford, UK: Elsevier Inc*, 259-274 (2012).

122. Li, F., Shen, A. & Amanullah, A. Cell Culture Processes in Monoclonal Antibody Production. *Pharmaceutical Sciences Encyclopedia* (2010).
123. Birch, J.R. & Racher, A.J. Antibody production. *Adv Drug Deliv Rev* **58**, 671-685 (2006).
124. Jeong, K.J., Jang, S.H. & Velmurugan, N. Recombinant antibodies: engineering and production in yeast and bacterial hosts. *Biotechnology journal* **6**, 16-27 (2011).
125. Palmberger, D. et al. Insect cells for antibody production: evaluation of an efficient alternative. *Journal of biotechnology* **153**, 160-166 (2011).
126. Xu, J., Dolan, M.C., Medrano, G., Cramer, C.L. & Weathers, P.J. Green factory: plants as bioproduction platforms for recombinant proteins. *Biotechnology Advances* **30**, 1171-1184 (2012).
127. Ahmad, Z.A. et al. scFv antibody: principles and clinical application. *Clinical and Developmental Immunology* **2012** (2012).
128. Abbas, A.K., Lichtman, A.H. & Pillai, S. Basic immunology: functions and disorders of the immune system. (Elsevier Health Sciences, 2012).
129. Wide, L., Bennich, H. & Johansson, S. Diagnosis of allergy by an in-vitro test for allergen antibodies. *The Lancet* **290**, 1105-1107 (1967).
130. Wiltshire, S. et al. Detection of multiple allergen-specific IgEs on microarrays by immunoassay with rolling circle amplification. *Clinical chemistry* **46**, 1990-1993 (2000).
131. Czaja, A.J. & Freese, D.K. Diagnosis and treatment of autoimmune hepatitis. *Hepatology* **36**, 479-497 (2002).
132. Tan, E.M. Antinuclear antibodies: diagnostic markers for autoimmune diseases and probes for cell biology. *Adv Immunol* **44**, 93-151 (1989).
133. Steingart, K.R. et al. A systematic review of commercial serological antibody detection tests for the diagnosis of extrapulmonary tuberculosis. *Thorax* **62**, 911-918 (2007).
134. Anderson, K.S. et al. Protein microarray signature of autoantibody biomarkers for the early detection of breast cancer. *Journal of proteome research* **10**, 85-96 (2010).
135. Lewis, J.D. The utility of biomarkers in the diagnosis and therapy of inflammatory bowel disease. *Gastroenterology* **140**, 1817-1826. e1812 (2011).
136. Reddy, M.M. et al. Identification of candidate IgG biomarkers for Alzheimer's disease via combinatorial library screening. *Cell* **144**, 132-142 (2011).
137. Otte, M.A., Estévez, M.-C., Regatos, D., Lechuga, L.M. & Sepúlveda, B. Guiding light in monolayers of sparse and random plasmonic meta-atoms. *ACS Nano* **5**, 9179-9186 (2011).
138. Fredriksson, H. et al. Hole–mask colloidal lithography. *Adv Mater* **19**, 4297-4302 (2007).
139. Pavlickova, P., Schneider, E.M. & Hug, H. Advances in recombinant antibody microarrays. *Clinica Chimica Acta* **343**, 17-35 (2004).
140. Butler, J.E. et al. The immunochemistry of sandwich ELISAs: VI. Greater than 90 percent of monoclonal and 75 percent of polyclonal anti-fluorescyl capture antibodies (CAbs) are denatured by passive adsorption. *Molecular Immunology* **30**, 1165-1175 (1993).
141. Wink, T., J. van Zuilen, S., Bult, A. & P. van Bennekom, W. Self-assembled Monolayers for Biosensors. *Analyst* **122**, 43R-50R (1997).
142. Williams, R.A. & Blanch, H.W. Covalent immobilization of protein monolayers for biosensor applications. *Biosensors and Bioelectronics* **9**, 159-167 (1994).
143. Franco, E.J., Hofstetter, H. & Hofstetter, O. A comparative evaluation of random and site-specific immobilization techniques for the preparation of antibody-based chiral stationary phases. *Journal of Separation Science* **29**, 1458-1469 (2006).
144. Neves-Petersen, M.T., Snabe, T., Klitgaard, S., Duroux, M. & Petersen, S.B. Photonic activation of disulfide bridges achieves oriented protein immobilization on biosensor surfaces. *Protein Science* **15**, 343-351 (2006).
145. Cho, I.-H. et al. Site-directed biotinylation of antibodies for controlled immobilization on solid surfaces. *Anal Biochem* **365**, 14-23 (2007).

146. Kim, B.Y. et al. Direct immobilization of Fab ' in nanocapillaries for manipulating mass-limited samples. *Journal of the American Chemical Society* **129**, 7620-7626 (2007).
147. Steinhauer, C. et al. Improved affinity coupling for antibody microarrays: Engineering of double-(His) 6-tagged single framework recombinant antibody fragments. *Proteomics* **6**, 4227-4234 (2006).
148. Torrance, L. et al. Oriented immobilisation of engineered single-chain antibodies to develop biosensors for virus detection. *Journal of virological methods* **134**, 164-170 (2006).
149. Busse, S., Scheumann, V., Menges, B. & Mittler, S. Sensitivity studies for specific binding reactions using the biotin/streptavidin system by evanescent optical methods. *Biosensors and Bioelectronics* **17**, 704-710 (2002).
150. Boozer, C., Ladd, J., Chen, S. & Jiang, S. DNA-directed protein immobilization for simultaneous detection of multiple analytes by surface plasmon resonance biosensor. *Anal Chem* **78**, 1515-1519 (2006).
151. Bailey, R.C., Kwong, G.A., Radu, C.G., Witte, O.N. & Heath, J.R. DNA-encoded antibody libraries: a unified platform for multiplexed cell sorting and detection of genes and proteins. *Journal of the American Chemical Society* **129**, 1959-1967 (2007).
152. Evazalipour, M., Tehrani, B.S., Abolhassani, M., Morovvati, H. & Omidfar, K. Camel heavy chain antibodies against prostate-specific membrane antigen. *Hybridoma* **31**, 424-429 (2012).
153. Bürckstümmer, T. et al. An efficient tandem affinity purification procedure for interaction proteomics in mammalian cells. *Nature methods* **3**, 1013-1019 (2006).
154. Makaraviciute, A. & Ramanaviciene, A. Site-directed antibody immobilization techniques for immunosensors. *Biosensors and Bioelectronics* **50**, 460-471 (2013).
155. Vega, R.A. et al. Functional antibody arrays through metal ion-affinity templates. *Chembiochem* **7**, 1653-+ (2006).
156. Lee, Y. et al. ProteoChip: A highly sensitive protein microarray prepared by a novel method of protein immobilization for application of protein-protein interaction studies. *Proteomics* **3**, 2289-2304 (2003).
157. Chen, H., Huang, J., Lee, J., Hwang, S. & Koh, K. Surface plasmon resonance spectroscopic characterization of antibody orientation and activity on the calixarene monolayer. *Sensors and Actuators B: Chemical* **147**, 548-553 (2010).
158. Kimura-Suda, H., Petrovykh, D.Y., Tarlov, M.J. & Whitman, L.J. Base-dependent competitive adsorption of single-stranded DNA on gold. *Journal of the American Chemical Society* **125**, 9014-9015 (2003).
159. Asfari, Z. Calixarenes 2001. (2001).
160. Mokhtari, B., Pourabdollah, K. & Dalali, N. Analytical applications of calixarenes from 2005 up-to-date. *Journal of Inclusion Phenomena and Macrocyclic Chemistry* **69**, 1-55 (2011).
161. Amiri, A. & Choi, E.Y. Complexation of calix [4] crown-5-ether with-amino acids and their molecular recognition via uv/vis spectroscopy. *World Appl. Sci. J* **17**, 658-665 (2012).
162. Malmsten, M. Ellipsometry studies of protein layers adsorbed at hydrophobic surfaces. *Journal of colloid and interface science* **166**, 333-342 (1994).
163. Wu, J., Fu, Z., Yan, F. & Ju, H. Biomedical and clinical applications of immunoassays and immunosensors for tumor markers. *TrAC Trends in Analytical Chemistry* **26**, 679-688 (2007).
164. Treviño Castrillo, J. Desarrollo de un biosensor de resonancia de plasmón superficial para la determinación de hormonas pituitarias en muestras biológicas. (2009).
165. Munoz, E.M. et al. Direct surface plasmon resonance immunosensor for< i> in situ</i> detection of benzoylecgonine, the major cocaine metabolite. *Biosensors and Bioelectronics* **26**, 4423-4428 (2011).

166. Tsai, W.-C. & Lin, I. Development of a piezoelectric immunosensor for the detection of alpha-fetoprotein. *Sensors and Actuators B: Chemical* **106**, 455-460 (2005).
167. Makaraviciute, A. & Ramanaviciene, A. Site-directed antibody immobilization techniques for immunosensors. *Biosensors and Bioelectronics* **50**, 460-471 (2013).
168. Xu, H., Lu, J.R. & Williams, D.E. Effect of surface packing density of interfacially adsorbed monoclonal antibody on the binding of hormonal antigen human chorionic gonadotrophin. *The Journal of Physical Chemistry B* **110**, 1907-1914 (2006).
169. Akerström, B., Brodin, T., Reis, K. & Björck, L. Protein G: a powerful tool for binding and detection of monoclonal and polyclonal antibodies. *The Journal of Immunology* **135**, 2589-2592 (1985).
170. Huse, K., Böhme, H.-J. & Scholz, G.H. Purification of antibodies by affinity chromatography. *Journal of Biochemical and Biophysical Methods* **51**, 217-231 (2002).
171. Dostálek, J. et al. Surface plasmon resonance biosensor based on integrated optical waveguide. *Sensors and Actuators B: Chemical* **76**, 8-12 (2001).
172. Song, H.Y., Zhou, X., Hobley, J. & Su, X. Comparative Study of Random and Oriented Antibody Immobilization as Measured by Dual Polarization Interferometry and Surface Plasmon Resonance Spectroscopy. *Langmuir* **28**, 997-1004 (2011).
173. Gabarra-Niecko, V., Schaller, M. & Dunty, J. FAK regulates biological processes important for the pathogenesis of cancer. *Cancer Metastasis Rev* **22**, 359-374 (2003).
174. Prasad, K. C-Reactive Protein (CRP)-Lowering Agents. *Cardiovascular Drug Reviews* **24**, 33-50 (2006).
175. Chuang, Y.-C., Tyagi, V., Liu, R.-T., Chancellor, M.B. & Tyagi, P. Urine and Serum C-Reactive Protein Levels as Potential Biomarkers of Lower Urinary Tract Symptoms. *Urological Science (previously Journal of Taiwan Urological Association)* **21**, 132-136 (2010).
176. Medina, M.B., Van Houten, L., Cooke, P.H. & Tu, S.I. Real-time analysis of antibody binding interactions with immobilized E. coli O157:H7 cells using the BIAcore. *Biotechnology Techniques* **11**, 173-176 (1997).
177. Grogan, C. et al. Characterisation of an antibody coated microcantilever as a potential immuno-based biosensor. *Biosensors and Bioelectronics* **17**, 201-207 (2002).
178. Minhua, F., Berdugo Morales, A., Poot, A., Beugeling, T. & Bantjes, A. Effects of Tween 20 on the desorption of proteins from polymer surfaces. *Journal of Biomaterials Science, Polymer Edition* **7**, 415-424 (1996).
179. Karak, T. & Bhattacharyya, P. Human urine as a source of alternative natural fertilizer in agriculture: A flight of fancy or an achievable reality. *Resources, Conservation and Recycling* **55**, 400-408 (2011).
180. Adachi, J., Kumar, C., Zhang, Y., Olsen, J. & Mann, M. The human urinary proteome contains more than 1500 proteins, including a large proportion of membrane proteins. *Genome Biol* **7**, 1-16 (2006).
181. Krishnan, S., Weinman, C.J. & Ober, C.K. Advances in polymers for anti-biofouling surfaces. *Journal of Materials Chemistry* **18**, 3405-3413 (2008).
182. Marie, R., Dahlin, A., Tegenfeldt, J. & Höök, F. Generic surface modification strategy for sensing applications based on Au/SiO2 nanostructures. *Biointerphases* **2**, 49-55 (2007).
183. Opdahl, A., Petrovykh, D.Y., Kimura-Suda, H., Tarlov, M.J. & Whitman, L.J. Independent control of grafting density and conformation of single-stranded DNA brushes. *Proceedings of the National Academy of Sciences* **104**, 9-14 (2007).
184. Rueda, M., Prieto, F., Álvarez-Malmagro, J. & Rodes, A. Evidences of adenine–thymine Interactions at gold electrodes interfaces as provided by in-situ infrared spectroscopy. *Electrochemistry Communications* **35**, 53-56 (2013).
185. Rodes, A. et al. Adenine Adsorption at Single Crystal and Thin-Film Gold Electrodes: An In Situ Infrared Spectroscopy Study. *The Journal of Physical Chemistry C* **113**, 18784-18794 (2009).

186. Schreiner, S.M. et al. Controlled and efficient hybridization achieved with DNA probes immobilized solely through preferential DNA-substrate interactions. *Anal Chem* **82**, 2803-2810 (2010).
187. Wu, A.M. & Senter, P.D. Arming antibodies: prospects and challenges for immunoconjugates. *Nature biotechnology* **23**, 1137-1146 (2005).
188. Andersen, B.R., Abele, D.C. & Vannier, W.E. Effects of mild periodate oxidation on antibodies. *The Journal of Immunology* **97**, 913-924 (1966).
189. Wolfe, C.A. & Hage, D.S. Studies on the rate and control of antibody oxidation by periodate. *Anal Biochem* **231**, 123-130 (1995).
190. Denham, J. & Hill, I. Celiac Disease and Autoimmunity: Review and Controversies. *Curr Allergy Asthma Rep* **13**, 347-353 (2013).
191. Freeman, H.J. Celiac disease and selected long-term health issues. *Maturitas* **73**, 206-211 (2012).
192. Silvester, J. & Rashid, M. Long-term follow-up of individuals with celiac disease: An evaluation of current practice guidelines. *Canadian Journal of Gastroenterology & Hepatology* **21**, 557 - 564 (2007).
193. Hadithi, M. & Peña, A.S. Current methods to diagnose the unresponsive and complicated forms of coeliac disease. *European Journal of Internal Medicine* **21**, 247-253 (2010).
194. Walker, M.M. & Murray, J.A. An update in the diagnosis of coeliac disease. *Histopathology* **59**, 166-179 (2011).
195. Rubio-Tapia, A., Hill, I.D., Kelly, C.P., Calderwood, A.H. & Murray, J.A. ACG Clinical Guidelines: Diagnosis and Management of Celiac Disease. *Am J Gastroenterol* **108**, 656-676 (2013).
196. Duerksen, D.R., Wilhelm-Boyles, C. & Parry, D.M. Intestinal Permeability in Long-Term Follow-up of Patients with Celiac Disease on a Gluten-Free Diet. *Dig Dis Sci* **50**, 785-790 (2005).
197. Ertekin, V., Selimoglu, M.A., Turgut, A. & Bakan, N. Fecal Calprotectin Concentration in Celiac Disease. *Journal of Clinical Gastroenterology* **44**, 544-546 510.1097/MCG.1090b1013e3181cadbc1090 (2010).
198. Bethune, M.T. et al. Noninflammatory gluten peptide analogs as biomarkers for celiac sprue. *Chemistry & biology* **16**, 868-881 (2009).
199. Shan, L. et al. Structural basis for gluten intolerance in celiac sprue. *Science* **297**, 2275-2279 (2002).
200. Kagnoff, M.F. Celiac disease: pathogenesis of a model immunogenetic disease. *The Journal of Clinical Investigation* **117**, 41-49 (2007).
201. Comino, I. et al. Monitoring of gluten-free diet compliance in celiac patients by assessment of gliadin 33-mer equivalent epitopes in feces. *The American Journal of Clinical Nutrition* (2012).
202. Morón, B. et al. Sensitive detection of cereal fractions that are toxic to celiac disease patients by using monoclonal antibodies to a main immunogenic wheat peptide. *The American Journal of Clinical Nutrition* **87**, 405-414 (2008).
203. Morón, B. et al. Toward the Assessment of Food Toxicity for Celiac Patients: Characterization of Monoclonal Antibodies to a Main Immunogenic Gluten Peptide. *PLoS ONE* **3**, e2294 (2008).
204. Comino, I. et al. Immunological determination of gliadin 33-mer equivalent peptides in beers as a specific and practical analytical method to assess safety for celiac patients. *Journal of the Science of Food and Agriculture* **93**, 933-943 (2013).
205. Real, A. et al. Identification and In Vitro Reactivity of Celiac Immunoactive Peptides in an Apparent Gluten-Free Beer. *PLoS ONE* **9**, e100917 (2014).
206. Shewry, P.R. Improving the protein content and composition of cereal grain. *Journal of cereal science* **46**, 239-250 (2007).

207. Gil-Humanes, J. et al. Reduced-gliadin wheat bread: an alternative to the gluten-free diet for consumers suffering gluten-related pathologies. *PLoS ONE* **9**, e90898 (2014).
208. Van Eckert, R. et al. Towards a new gliadin reference material–isolation and characterisation. *Journal of cereal science* **43**, 331-341 (2006).
209. Buick, A., Doig, M., Jeal, S., Land, G. & McDowall, R. Method validation in the bioanalytical laboratory. *Journal of pharmaceutical and biomedical analysis* **8**, 629-637 (1990).
210. Sviridov, D. & Hortin, G.L. Urine albumin measurement: effects of urine matrix constituents. *Clinica Chimica Acta* **404**, 140-143 (2009).
211. Decramer, S. et al. Urine in clinical proteomics. *Molecular & cellular proteomics* **7**, 1850-1862 (2008).
212. Brunzel, N.A. Fundamentals of urine and body fluid analysis. (Elsevier Health Sciences, 2013).
213. Martin, C.S., MONTILLA, I.C., Calderon, A.R., ALEGRE, S.V. & Rammirez, A.C. (Google Patents, 2014).
214. Li, X., Lin, C. & O'Connor, P.B. Glutamine deamidation: differentiation of glutamic acid and γ-Glutamic Acid in peptides by electron capture dissociation. *Anal Chem* **82**, 3606-3615 (2010).
215. Joshi, A.B. & Kirsch, L.E. The relative rates of glutamine and asparagine deamidation in glucagon fragment 22–29 under acidic conditions. *Journal of pharmaceutical sciences* **91**, 2331-2345 (2002).
216. Soler, M. et al. Direct Detection of Protein Biomarkers in Human Fluids Using Site-Specific Antibody Immobilization Strategies. *Sensors* **14**, 2239-2258 (2014).
217. Soler, M. et al. Highly sensitive dendrimer-based nanoplasmonic biosensor for drug allergy diagnosis. *Biosensors and Bioelectronics* (2014).
218. Bhattacharya, S. The facts about penicillin allergy: a review. *Journal of advanced pharmaceutical technology & research* **1**, 11-17 (2010).
219. Torres, M.J. et al. Diagnosis of immediate allergic reactions to beta-lactam antibiotics. *Allergy* **58**, 961-972 (2003).
220. Aberer, W. et al. Drug provocation testing in the diagnosis of drug hypersensitivity reactions: general considerations. *Allergy* **58**, 854-863 (2003).
221. Chinoy, B., Yee, E. & Bahna, S. Skin testing versus radioallergosorbent testing for indoor allergens. *Clinical and Molecular Allergy* **3**, 4 (2005).
222. Montañez, M.I. et al. Synthetic Approach to Gain Insight into Antigenic Determinants of Cephalosporins: In Vitro Studies of Chemical Structure−IgE Molecular Recognition Relationships. *Chemical Research in Toxicology* **24**, 706-717 (2011).
223. Blanca, M. et al. Differences in serum IgE antibody activity to benzylpenicillin and amoxicillin measured by RAST in a group of penicillin allergic patients. *Allergy* **46**, 632-638 (1991).
224. Mayorga, C.S., ML; Gamboa, PM; García, BE; on behalf of the Clinical Immunology Committee of the Spanish Society of Allergology and Clinical Immunology of the SEAIC In vitro diagnosis of immediate allergic reactions to drug: an update. *J Investig Allergol Clin Immunol* **20**, 103-109 (2010).
225. Alonso, R. et al. Specific IgE determination using the CAP system: comparative evaluation with RAST. *Journal of investigational allergology & clinical immunology* **5**, 156-160 (1995).
226. Blanca, M. et al. Clinical evaluation of Pharmacia CAP System™ RAST FEIA amoxicilloyl and benzylpenicilloyl in patients with penicillin allergy. *Allergy* **56**, 862-870 (2001).
227. Blanca, M. et al. Determination of IgE antibodies to the benzyl penicilloyl determinant. A comparison between poly-l-lysine and human serum albumin as carriers. *Journal of Immunological Methods* **153**, 99-105 (1992).
228. Esfand, R. & Tomalia, D.A. Poly (amidoamine)(PAMAM) dendrimers: from biomimicry to drug delivery and biomedical applications. *Drug discovery today* **6**, 427-436 (2001).

229. Svenson, S. & Tomalia, D.A. Dendrimers in biomedical applications—reflections on the field. *Adv Drug Deliv Rev* **64, Supplement**, 102-115 (2012).
230. Kesharwani, P., Jain, K. & Jain, N.K. Dendrimer as nanocarrier for drug delivery. *Progress in Polymer Science* **39**, 268-307 (2014).
231. Astruc, D., Boisselier, E. & Ornelas, C. Dendrimers Designed for Functions: From Physical, Photophysical, and Supramolecular Properties to Applications in Sensing, Catalysis, Molecular Electronics, Photonics, and Nanomedicine. *Chemical Reviews* **110**, 1857-1959 (2010).
232. Satija, J., Sai, V. & Mukherji, S. Dendrimers in biosensors: Concept and applications. *Journal of Materials Chemistry* **21**, 14367-14386 (2011).
233. Sánchez-Sancho, F. et al. Dendrimers as Carrier Protein Mimetics for IgE Antibody Recognition. Synthesis and Characterization of Densely Penicilloylated Dendrimers. *Bioconjugate Chemistry* **13**, 647-653 (2002).
234. Montañez, M.I. et al. Dendrimerized Cellulose as a Scaffold for Artificial Antigens with Applications in Drug Allergy Diagnosis. *Biomacromolecules* **9**, 1461-1466 (2008).
235. Vida, Y. et al. Dendrimeric antigen-silica particle composites: an innovative approach for IgE quantification. *Journal of Materials Chemistry B* **1**, 3044-3050 (2013).
236. Winter, W.E., Hardt, N.S. & Fuhrman, S. Immunoglobulin E. *Archives of Pathology & Laboratory Medicine* **124**, 1382-1385 (2000).
237. Jemal, A. et al. Global cancer statistics. *CA: a cancer journal for clinicians* **61**, 69-90 (2011).
238. Haggar, F.A. & Boushey, R.P. Colorectal cancer epidemiology: incidence, mortality, survival, and risk factors. *Clinics in colon and rectal surgery* **22**, 191 (2009).
239. Kekelidze, M., D'Errico, L., Pansini, M., Tyndall, A. & Hohmann, J. Colorectal cancer: Current imaging methods and future perspectives for the diagnosis, staging and therapeutic response evaluation. *World journal of gastroenterology: WJG* **19**, 8502 (2013).
240. Hamilton, S.R., Aaltonen, L.A., Cancer, I.A.f.R.o. & Organization, W.H. Pathology and genetics of tumours of the digestive system. (IARC press Lyon, 2000).
241. Winawer, S. et al. Colorectal cancer screening and surveillance: clinical guidelines and rationale—update based on new evidence. *Gastroenterology* **124**, 544-560 (2003).
242. Adelstein, B.-A., Macaskill, P., Chan, S.F., Katelaris, P.H. & Irwig, L. Most bowel cancer symptoms do not indicate colorectal cancer and polyps: a systematic review. *BMC Gastroenterology* **11**, 65-65 (2011).
243. Duffy, M. et al. Tumour markers in colorectal cancer: European Group on Tumour Markers (EGTM) guidelines for clinical use. *European journal of cancer* **43**, 1348-1360 (2007).
244. The Cancer Genome Atlas, N. Comprehensive Molecular Characterization of Human Colon and Rectal Cancer. *Nature* **487**, 330-337 (2012).
245. Liu, W. et al. Autoantibodies to tumor-associated antigens as biomarkers in cancer immunodiagnosis. *Autoimmunity Reviews* **10**, 331-335 (2011).
246. Casiano, C.A., Mediavilla-Varela, M. & Tan, E.M. Tumor-associated antigen arrays for the serological diagnosis of cancer. *Molecular & cellular proteomics* **5**, 1745-1759 (2006).
247. Kobold, S., Lütkens, T., Cao, Y., Bokemeyer, C. & Atanackovic, D. Autoantibodies against tumor-related antigens: incidence and biologic significance. *Human immunology* **71**, 643-651 (2010).
248. Qiu, J. et al. Occurrence of autoantibodies to annexin I, 14-3-3 theta and LAMR1 in prediagnostic lung cancer sera. *Journal of Clinical Oncology* **26**, 5060-5066 (2008).
249. Boyle, P. et al. Clinical validation of an autoantibody test for lung cancer. *Annals of Oncology* **22**, 383-389 (2011).
250. Chapman, C. et al. Autoantibodies in breast cancer: their use as an aid to early diagnosis. *Annals of Oncology* (2007).

251. Cho-Chung, Y.S. Autoantibody biomarkers in the detection of cancer. *Biochimica et Biophysica Acta (BBA) - Molecular Basis of Disease* **1762**, 587-591 (2006).
252. Chen, H., Werner, S., Tao, S., Zörnig, I. & Brenner, H. Blood autoantibodies against tumor-associated antigens as biomarkers in early detection of colorectal cancer. *Cancer Letters* **346**, 178-187 (2014).
253. Barderas, R. et al. An optimized predictor panel for colorectal cancer diagnosis based on the combination of tumor-associated antigens obtained from protein and phage microarrays. *Journal of proteomics* **75**, 4647-4655 (2012).
254. Lewin, B. Oncogenic conversion by regulatory changes in transcription factors. *Cell* **64**, 303-312 (1991).
255. Shoulars, K., Rodriguez, M.A., Thompson, T. & Markaverich, B.M. Regulation of cell cycle and RNA transcription genes identified by microarray analysis of PC-3 human prostate cancer cells treated with luteolin. *The Journal of steroid biochemistry and molecular biology* **118**, 41-50 (2010).
256. Minucci, S. & Pelicci, P.G. Histone deacetylase inhibitors and the promise of epigenetic (and more) treatments for cancer. *Nature Reviews Cancer* **6**, 38-51 (2006).
257. Nguyen, D.M. et al. Molecular heterogeneity of inflammatory breast cancer: a hyperproliferative phenotype. *Clinical Cancer Research* **12**, 5047-5054 (2006).
258. Bankaitis-Davis, D.M. et al. (Google Patents, 2007).
259. Beckham, C.J. et al. Bladder cancer exosomes contain EDIL-3/Del1 and facilitate cancer progression. *The Journal of urology* (2014).
260. Watanabe, T. et al. Predicting ulcerative colitis-associated colorectal cancer using reverse-transcription polymerase chain reaction analysis. *Clinical colorectal cancer* **10**, 134-141 (2011).
261. Sun, J.-C. et al. High expression level of EDIL3 in HCC predicts poor prognosis of HCC patients. *World journal of gastroenterology: WJG* **16**, 4611 (2010).
262. Barderas, R. et al. Sporadic colon cancer murine models demonstrate the value of autoantibody detection for preclinical cancer diagnosis. *Scientific reports* **3** (2013).
263. Lu, H., Goodell, V. & Disis, M. in ASCO Ann. Meet. Proc2006).
264. Curiel, T.J. in Cancer Immunotherapy 3-15 (Springer, 2013).
265. Dougan, M. & Dranoff, G. in Innate Immune Regulation and Cancer Immunotherapy 391-414 (Springer, 2012).
266. Mahalingam, D. & Curiel, T.J. in Cancer Immunotherapy 335-376 (Springer, 2013).
267. Scott, A.M., Allison, J.P. & Wolchok, J.D. Monoclonal antibodies in cancer therapy. *Cancer immunity* **12** (2012).
268. Palucka, K., Ueno, H. & Banchereau, J. Recent developments in cancer vaccines. *The Journal of Immunology* **186**, 1325-1331 (2011).
269. Kalos, M. & June, C.H. Adoptive T cell transfer for cancer immunotherapy in the era of synthetic biology. *Immunity* **39**, 49-60 (2013).
270. Wu, R. et al. Adoptive T-cell therapy using autologous tumor-infiltrating lymphocytes for metastatic melanoma: current status and future outlook. *Cancer journal (Sudbury, Mass.)* **18**, 160 (2012).
271. Mitchison, N. Studies on the immunological response to foreign tumor transplants in the mouse I. The role of lymph node cells in conferring immunity by adoptive transfer. *The Journal of experimental medicine* **102**, 157-177 (1955).
272. Restifo, N.P., Dudley, M.E. & Rosenberg, S.A. Adoptive immunotherapy for cancer: harnessing the T cell response. *Nature Reviews Immunology* **12**, 269-281 (2012).
273. Deguine, J., Breart, B., Lemaître, F., Di Santo, J.P. & Bousso, P. Intravital Imaging Reveals Distinct Dynamics for Natural Killer and CD8+ T Cells during Tumor Regression. *Immunity* **33**, 632-644 (2010).

274. Liao, W., Lin, J.-X. & Leonard, W.J. IL-2 family cytokines: new insights into the complex roles of IL-2 as a broad regulator of T helper cell differentiation. *Current opinion in immunology* **23**, 598-604 (2011).
275. Irving, M. et al. Interplay between T cell receptor binding kinetics and the level of cognate peptide presented by major histocompatibility complexes governs CD8+ T cell responsiveness. *Journal of Biological Chemistry* **287**, 23068-23078 (2012).
276. de Visser, K.E., Schumacher, T.N. & Kruisbeek, A.M. CD8+ T cell tolerance and cancer immunotherapy. *Journal of Immunotherapy* **26**, 1-11 (2003).
277. Aleksic, M. et al. Different affinity windows for virus and cancer-specific T-cell receptors: Implications for therapeutic strategies. *European journal of immunology* **42**, 3174-3179 (2012).
278. Gallegos, A.M. & Bevan, M.J. Central tolerance: good but imperfect. *Immunological reviews* **209**, 290-296 (2006).
279. Park, T.S., Rosenberg, S.A. & Morgan, R.A. Treating cancer with genetically engineered T cells. *Trends in biotechnology* **29**, 550-557 (2011).
280. Leuci, V., Mesiano, G., Gammaitoni, L., Aglietta, M. & Sangiolo, D. Genetically Redirected T Lymphocytes for Adoptive Immunotherapy of Solid Tumors. *Current gene therapy* **14**, 52-62 (2014).
281. June, C.H., Blazar, B.R. & Riley, J.L. Engineering lymphocyte subsets: tools, trials and tribulations. *Nature Reviews Immunology* **9**, 704-716 (2009).
282. Cartellieri, M. et al. Chimeric antigen receptor-engineered T cells for immunotherapy of cancer. *BioMed Research International* **2010** (2010).
283. Stephan, M.T. et al. T cell–encoded CD80 and 4-1BBL induce auto-and transcostimulation, resulting in potent tumor rejection. *Nature medicine* **13**, 1440-1449 (2007).
284. Charo, J. et al. Bcl-2 overexpression enhances tumor-specific T-cell survival. *Cancer research* **65**, 2001-2008 (2005).
285. Laport, G.G. et al. Adoptive transfer of costimulated T cells induces lymphocytosis in patients with relapsed/refractory non-Hodgkin lymphoma following CD34+-selected hematopoietic cell transplantation. *Blood* **102**, 2004-2013 (2003).
286. Pegram, H.J. et al. Tumor-targeted T cells modified to secrete IL-12 eradicate systemic tumors without need for prior conditioning. *Blood* **119**, 4133-4141 (2012).
287. Vonderheide, R.H. & June, C.H. Engineering T cells for cancer: our synthetic future. *Immunological reviews* **257**, 7-13 (2014).
288. Rosenberg, S.A., Restifo, N.P., Yang, J.C., Morgan, R.A. & Dudley, M.E. Adoptive cell transfer: a clinical path to effective cancer immunotherapy. *Nature Reviews Cancer* **8**, 299-308 (2008).
289. Gattinoni, L. et al. Acquisition of full effector function in vitro paradoxically impairs the in vivo antitumor efficacy of adoptively transferred CD8+ T cells. *Journal of Clinical Investigation* **115**, 1616-1626 (2005).
290. Besser, M.J. et al. Clinical responses in a phase II study using adoptive transfer of short-term cultured tumor infiltration lymphocytes in metastatic melanoma patients. *Clinical Cancer Research* **16**, 2646-2655 (2010).
291. Besser, M.J. et al. Minimally cultured or selected autologous tumor-infiltrating lymphocytes after a lympho-depleting chemotherapy regimen in metastatic melanoma patients. *Journal of Immunotherapy* **32**, 415-423 (2009).
292. Dudley, M.E. et al. CD8+ enriched "young" tumor infiltrating lymphocytes can mediate regression of metastatic melanoma. *Clinical Cancer Research* **16**, 6122-6131 (2010).
293. Gordon, R., Sinton, D., Kavanagh, K.L. & Brolo, A.G. A new generation of sensors based on extraordinary optical transmission. *Acc Chem Res* **41**, 1049-1057 (2008).

294. Yanik, A.A., Wang, X., Erramilli, S., Hong, M.K. & Altug, H. Extraordinary midinfrared transmission of rectangular coaxial nanoaperture arrays. *Applied Physics Letters* **93**, 081104 (2008).
295. Martin-Moreno, L. et al. Theory of extraordinary optical transmission through subwavelength hole arrays. *Physical review letters* **86**, 1114 (2001).
296. Nauerth, M. et al. TCR-ligand koff rate correlates with the protective capacity of antigen-specific CD8+ T cells for adoptive transfer. *Science translational medicine* **5**, 192ra187-192ra187 (2013).
297. Schmidt, J. et al. Reversible major histocompatibility complex I-peptide multimers containing Ni2+-nitrilotriacetic acid peptides and histidine tags improve analysis and sorting of CD8+ T cells. *Journal of Biological Chemistry* **286**, 41723-41735 (2011).
298. Yanik, A.A., Huang, M., Artar, A., Chang, T.-Y. & Altug, H. Integrated nanoplasmonic-nanofluidic biosensors with targeted delivery of analytes. *Applied Physics Letters* **96**, 021101 (2010).